Electronic Structure of Rare Earth Based High Temperature Superconducting Systems

(X-ray spectroscopic investigations of Cuprate Superconductors)

THESIS SUBMITTED FOR THE DEGREE OF
DOCTOR OF PHILOSOPHY
IN THE FACULTY OF NATURAL SCIENCE
GOA UNIVERSITY
GOA

By
Gajanan B. Parulekar
Department of Physics
Goa University
Goa 403 206

April 1997

To

My Parents

DECLARATION

The author hereby declares that this thesis represents work which has been carried out by him and that it has not been submitted to any other University or Institution for the award of any Degree, Diploma, Associateship, Fellowship or any other such title.

Place: Taleigao-Plateau
Date: 28/4/1997

Shri G.B.Parulekar

CERTIFICATE

I hereby certify that the above Declaration of the candidate Shri Gajanan B. Parulekar is true and that this thesis represents his independent work.

Professor P.R.Sarode
Head
Department of Physics
Goa University, Goa.

CONTENTS

LIST OF FIGURES

LIST OF TABLES

CHAPTER 1

GENERAL INTRODUCTION

1.1. HISTORICAL

Since the discovery of superconductivity by Kammerlingh Onnes in 1911 in Hg at 4 K, one of the primary objectives of superconductivity research has been to raise the transition temperature T_c. By almost any criterion, progress was slow. The discovery of T_c above 10 K in NbC and NbN was one breakthrough; the discovery of the A15 compounds, with T_c finally breaking through the 20 K barrier in the late 1960s and early 1970s, represented the culmination of two decades of intense search for higher transition temperatures. This research involved extensive investigations into materials properties and gave rise to "Matthias's Rules"[1] for promoting higher values of T_c :

(1) Cubic transition metals are best.
(2) Niobium is the best transition metal.
(3) Certain values of electron/atom (e/a) ratio are special
(4) High T_c's lie in the regime of lattice instabilities.

Certain aspects of these rules have been understood on a basic level; for example, in the cubic transition metals, the transition-metal carbonitrides, and the A15 compounds, the special e/a ratio (roughly 4.7 and 6.5) corresponds to the regions of high density states $N(E_F)$ at the Fermi level E_F. Niobium not only tends to lead to e/a ratios near 4.7, but also lies near the centre of the transition metal series where the electron-phonon interaction is strongest. These trends have been reviewed by Klein and Pickett[2]. In addition, it became clear that both high T_c and lattice instabilities arise from strong electron - phonon interactions so they tend to occur together; there is no definite casual relationship between lattice instability and high T_c. Contrary to early speculations, the best estimates now seem to indicate that low phonon frequencies contribute little to high values of T_c.

The breakthrough in higher T_c's resulted from Bednorz and Müller[3] discovery in the copper oxide system. They were convinced that it was necessary to move beyond the standard high T_c classes to obtain a real breakthrough. They chose to work on transition metal oxides, both because they were different and because they often displayed polaronic effects typical of extremely strong electron-phonon interactions. In 1986 they found evidence of a superconducting transition occuring near 30 K in the La-Ba-Cu-O system, a result that was rapidly confirmed and refined by a number of laboratories in the US, Japan and Europe. It was established that T_c in the range 20-40 K occurs for $La_{2-x}M_xCuO_{4-y}$ with M = Ba, Sr, Ca and that application of pressure leads to a large pressure coefficient of T_c and drives T_c above 50 K in the M = Sr system. The crystal structure was identified and it has since become clear that high temperature superconductivity is only the most astounding of a number of unusual properties of this system.

Since pressure was so effective in increasing T_c, Wu et al.[4] simulated "chemical pressure" by replacing atoms in the La 214 system by smaller isovalent ones. The replacement of La by Y in LBCO produced in early 1987 a 90 K superconductor, later identified as $YBa_2Cu_3O_{7-y}$. Like the initial system, this material was prepared by ceramic processing techniques. High temperature annealing in an oxygen containing atmosphere was necessary to produce the oxygen content and the crystalline phase necessary to give high T_c. Although other group techniques have now been found that result in the high T_c phase, already it was clear from preparations considerations that the new copper oxides were completely different from the previous high temperature superconductors.

Although there were numerous reports of resistive and magnetic anamolies, at much higher temperatures, the next breakthrough came in early 1988 with the discovery by Maeda et al.[5] and Chu et al.[6] of $Bi_2Sr_2CaCu_2O_{8-\delta}$. This bismuth based

compound not only showed onsets around 110 K but also contained no rare earth element. It was also distinguished by its highly micaceous nature, indicating more pronounced layering than its predecessors. This breakthrough was followed rapidly by the discovery of Sheng et al.[7] of onsets at 115 K in the Tl-Sr-Ca-Cu-O system. The superconductor phase was identified as $Tl_2Ba_2CaCu_2O_{8-y}$ and this was soon improved to above 120 K by several groups. The crystal structures of this systems were identified and found to share certain features in common with the La-M-Cu-O and Y-Ba-Cu-O materials, particularly the existence of squre Cu-O layers separated by more or less ionic regions.

This period of rapid discovery may well continue for some time. While it is certainly early to review any aspects of this novel materials, intense effort has been turned towards the understanding of their electronic structures and properties, and it is useful to collect the results and contemplate their implications. Developing the clear understanding of the structure of these high T_c materials is central not only to identifying the pairing mechanism, but also to describing the host of other essential and often unusual properties displayed by these materials. Although a complete understanding of the important electronic properties would include the electronic response to perturbations of various kinds, this is an area in which little detailed work has been done.

It is far too early to draw any firm conclusions about the best way to picture, and to begin to describe the electronic structure of copper oxide high temperature superconductors. In fact, it may well be appropriate to describe the magnetic insulating state from one point of view and the metallic regime from another viewpoint. The metal insulator regime will in any case be a long time in being unraveled.

Within the metallic regime, a number of properties seem to be described rather well by the local-density version of density-functional theory. Probably the most quantitative example

is that of the calculations of the static structural properties, the lattice instability and the phonon frequencies of La_2CuO_4. To a great extent the electrical transport properties in the metallic regime look typical of quasiparticles, and the calculations appear encouraging in this respect, although many questions remain. Even many of the diverse spectral data can be interpreted in terms of the band structure density of states and corresponding characters of the states.

On the negative side, there are spectral features, particularly the valence band satellite indicating that self energy effects are strong in certain regions of the spectrum. Even for the ground state of the antiferromagnetic insulators, it is clear that there are crucial correlations that are missing from the local density treatment. How one should try to describe quantitatively the gaps in this materials is also still an open question; the local density approach does not predict them to be either antiferromagnetic or insulators. To what extent these correlations and self energy effects are important for the very-low-energy carriers and for the 0.1 - 5 eV excitations which are widely speculated to be active in these materials, is a monumental task to be addressed in the future, hopefully the near future.

1.2. THE PROCESS OF X- RAY ABSORPTION

The interaction of X-rays with matter[8,9] results in a number of interesting phenomena, such as, scattering, photoelectron absorption, radiation damage, pair production (in the case of X-rays of energy > 1.02 MeV), secondary emission, Auger emission etc. The analysis of attenuation, generally logarithmic of X-ray intensity requires, therefore, the segregation of the various processes involved, of which the photoelectric absorption is usually the most important and is referred to as the true absorption.

When an X-ray beam passes through a medium, the intensity of

the transmitted beam I is attenuated logarithmically. According to the classical absorption equation, if the incident beam of intensity I_o has traveled a distance x, then the absorption coefficient

$$\mu_l = - \frac{1}{x} \ln \frac{I}{I_o} \tag{1.1}$$

It follows from equation (1.1) that the dimensions of μ_l are reciprocal centimeters so that it represents the attenuation of the beam per unit length traveled and is called the *linear absorption coefficient*. It turns out to depend on the energy (wavelength) of the X-rays, the atomic numbers of the constituent atoms, and on their state of aggregation.

Calculation of the linear absorption coefficient is complicated by this last fact so that it is more convenient to use a *mass* absorption coefficient

$$\mu_m = \frac{\mu_l}{\rho} \tag{1.2}$$

where ρ is the density of the absorbing medium and μ_m is the absorption cross section of the mass unit.

In the analysis of the dependence of μ on wavelength and atomic number, it is most convenient to define an *atomic* absorption coefficient

$$\mu_a = \frac{A}{N_o} \mu_m \tag{1.3}$$

where A is the atomic weight of the element and N_o is Avogadro's number. A plot of μ_a against wavelength, for any element, has the general appearance of the curve shown in Figure 1.1. The

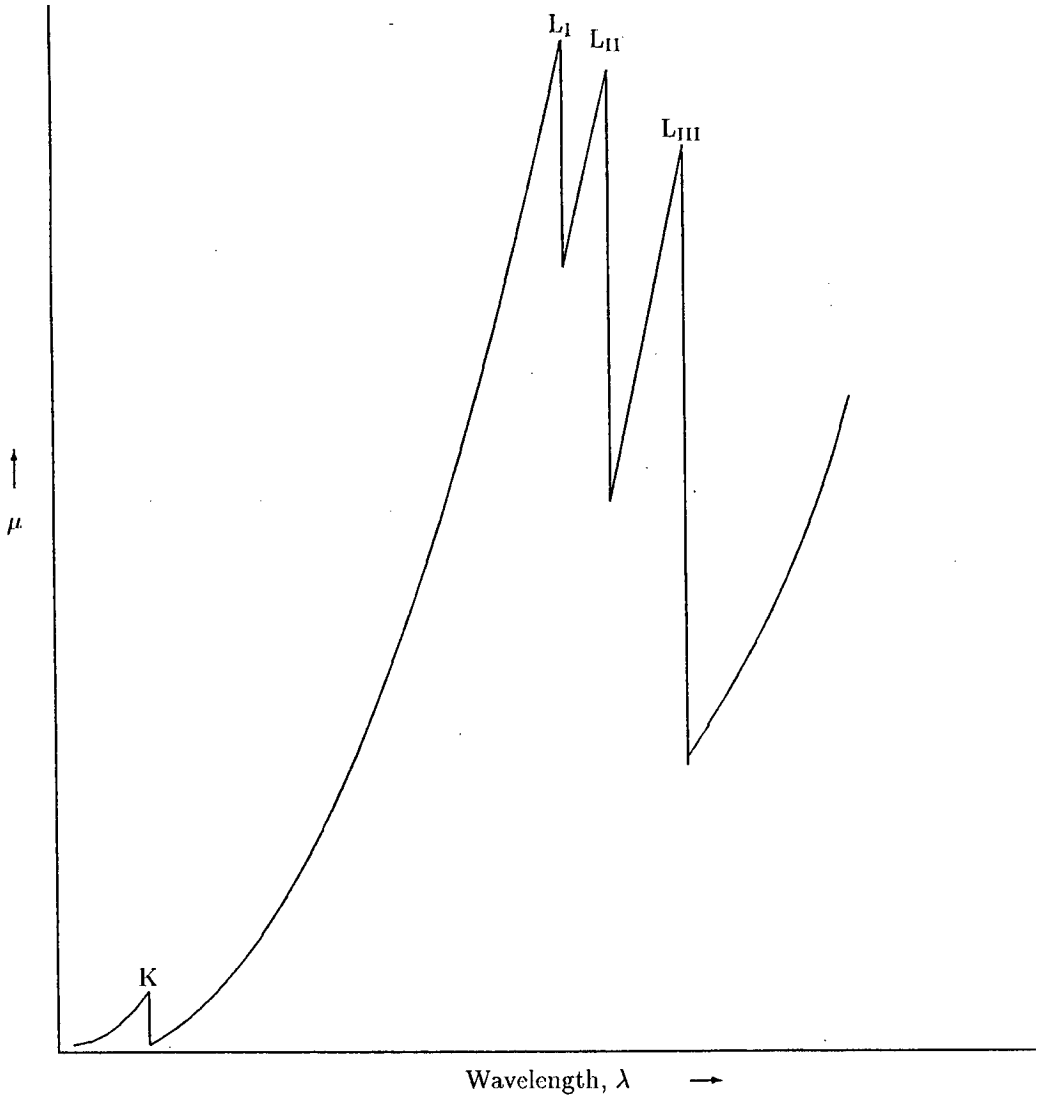

Figure 1.1: Variation of absorption coefficient of lead as a function of X-ray wavelength

absorption increases with increasing wavelength (decreasing energy of incident X-rays) until an abrupt discontinuity occurs. After this discontinuity, called an *absorption edge*, the absorption increases with wavelength until new discontinuities are encountered. An empirical study of the relation between the atomic absorption coefficient and the X-ray wavelength and atomic number of the absorbing atoms shows that curve like that in Figure 1.1 can be described by

$$\mu_a = C\ Z^m\ \lambda^n + \sigma_a(Z,\lambda) \qquad (1.4)$$

where the coeffficient C takes on different values on each side of an absorption edge and the " best " values for the two exponents are m = 4 and n = 3. The second term in equation (1.4) is called the *atomic scattering cross section* σ_a and represents the intensity lost due to the scattering in directions other than that of the incident beam. For wavelengths that are large compared to electron-electron distances in atoms ($\lambda > 0.5$), σ_a is nearly independent of wavelength and increases in proportion to Z. Since the first term in (1.4) increases with both Z and λ much more rapidly, the second term may be neglected by comparison. At shorter wavelengths, the λ dependence becomes more complex but, because of severe experimental difficulties in measuring the scattering part of (1.4), an accurate dependence has not been established. Since the second term is small (typically, $\sigma/\rho \sim$ 0.10 to 0.20 cm^2/gm), it is normally neglected in the discussion of absorption coefficients. This is an acceptable practice for all but the lightest elements, for which the total absorption coefficients may have commensurate magnitudes (For carbon $\mu_m <$ 4.0 cm^2/gm for $\lambda < 1.5\ A^o$).

The first term in (1.4) is of primary interest, not only because it is relatively much large but also because it represents the wavelength and Z dependences of the photoelectric

absorption process for X-rays. As can be seen in Figure 1.1, as the wavelength of the transmitted X-rays increases, the photoelectric absorption increases α λ^3 until a critical wavelength is reached. For wavelengths longer than that at the absorption edge, the incident X-rays have insufficient energy to knock out a particular kind of bound electron in the atom, and the photoelectric ejection of such electrons no longer contributes to the absorption process. The absorption edges in Figure 1.1 are called K, L_I, L_{II}, and L_{III} edges, respectively, according to the inner electron whose binding energy equals the energy at the absorption edge. Following the photoelectron ejection of an inner electron, the excited atom typically emits an X-ray photon, as an outer electron falls into the newly created hole, so that the first term in (1.4) is called the *fluorescence term.*

For free atoms[10], such as in the case of monoatomic gases, the processes of X- ray emission and absorption are simple and are well understood. However, these processes become rather complex when the atom is no more free, such as in solids and chemical compounds. The mechanism of X-ray emission and absorption in a solid [11,12]is shown in Figure 1.2. In a solid the valence electrons of the neighbouring atoms interact with each other and the energy levels are no longer discrete as in the case of free atoms but are broaden, the outer ones being more broad than inner ones and from quasi-continuous valence and conduction bands. The X-ray emission band spectrum results from the transition of the electrons from the valence band to a inner level. It provides information about the distribution of the occupied electron states in the valence band, since the inner level is generally sharp and well-defined. The X-ray absorption spectrum, on the other hand, corresponds to the transitions of the ejected photoelectron to empty states, bound or unbound of proper symmetry, and provides complementary information about the density of unoccupied electronic energy states.

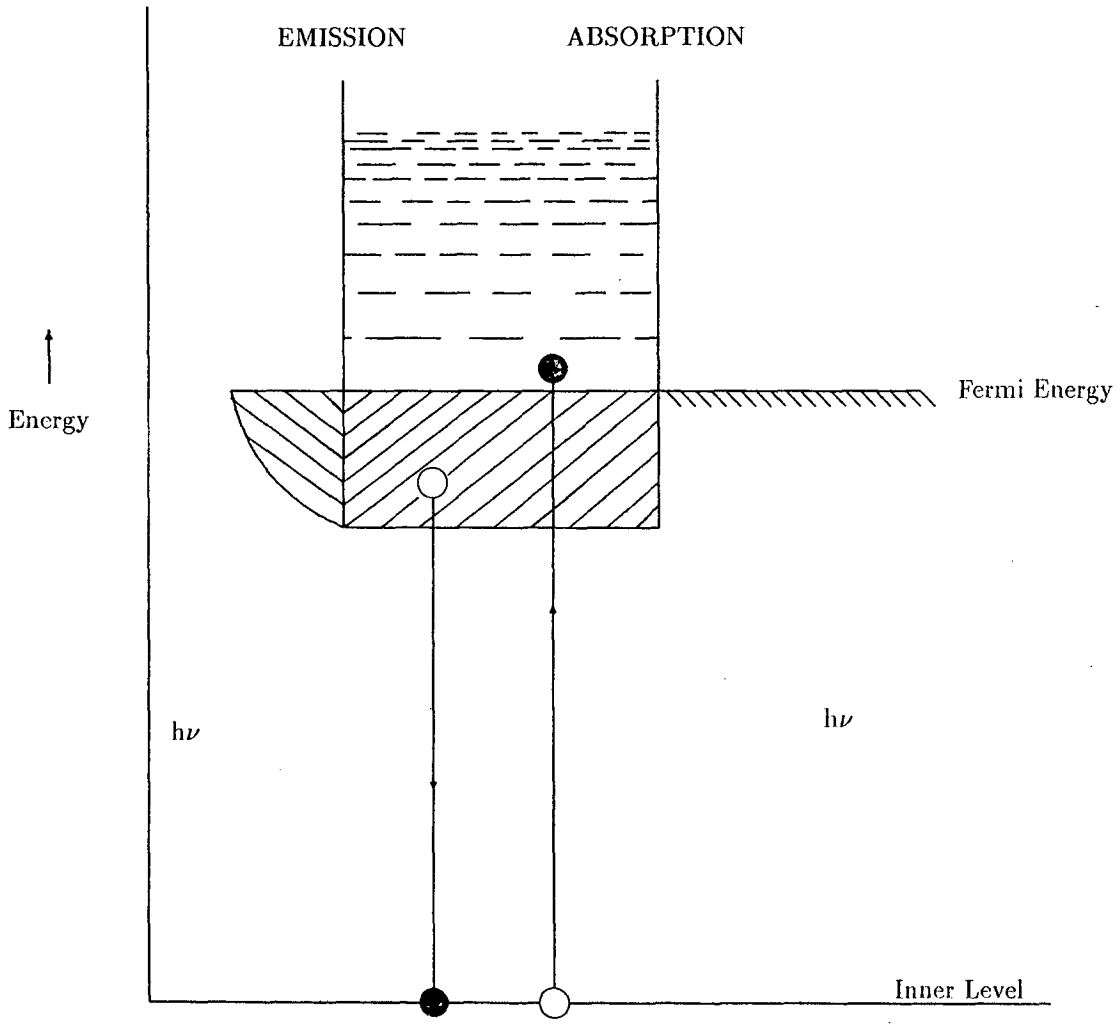

Figure 1.2: The mechanism of X-ray absroption and emission

1.3. THE POSITION, SHAPE AND FINE STRUCTURE OF AN X-RAY ABSORPTION DISCONTINUITY

In the X-ray emission process, if $I(\nu)$ denotes the intensity per unit frequency range, then $I(\nu)d\nu$ is the intensity of X-rays emitted with frequencies in the range $d\nu$ corresponding to the energy range dE and the expression for $I(\nu)$ is given[13] as

$$I(\nu) = \frac{n\ e^2\ h^3\ \Omega\ \nu^3}{3\ \pi^3\ m^2\ c^3} \int_S \frac{|M_{fi}|^2}{|\text{grad } E|}\, ds \qquad (1.5)$$

where Ω is the volume of the unit cell, n is the number of radiaters per unit volume, M_{fi} is the matrix element or the transition probability, subscript i and f correspond to the initial and the final states respectively and the integration is carried out over a constant energy surface in k-space. Equation (1.5) represents the observed frequency distribution within an emission band.

In the X-ray absorption process, if $A(\nu)d\nu$ denotes the energy absorbed per unit time by an atom in the electron transition from a sharp inner level to a band of empty states in an energy range dE and $I_o(\nu)\ d\nu$ is the incident intensity (energy per unit area per unit time), then the linear absorption coefficient (in cm^{-1}) is given by

$$\mu = \frac{n\ A(\nu)\ d\nu}{I_0(\nu)\ d\nu} \qquad (1.6)$$

where n represents the number of atoms per cm^3.

On the basis of Dirac's radiation theory, the energy absorption per second per unit frequency range by one atom may be expressed as

$$\alpha(\nu) = \frac{eh}{2\pi m^2 c\nu} \; |M_{fi}| \; I_0(\nu) \qquad (1.7)$$

Furthermore, $E = h\nu - h\nu_o$, where $h\nu$ is the energy of the incident photon and $h\nu_o$ is the energy interval between the intial X-ray level and the unoccupied state of lowest energy. Upon averaging over the three directions of the electron momentum, the power absorbed in transitions into a number of closely grouped states spread over an energy interval $hd\nu$ becomes

$$A(\nu)d\nu = \frac{e^2 h^2 \Omega \; I_o(\nu)d\nu}{6 \pi^2 m^2 c \nu} \int_s \frac{|M_{fi}|^2}{|\text{grad } E|} ds \qquad (1.8)$$

Hence by (1.8)

$$\mu(\nu) = \frac{n e^2 h^2 \Omega}{6 \pi^2 m^2 c \nu} \int_s \frac{|M_{fi}|^2}{|\text{grad } E|} ds \qquad (1.9)$$

The above expression can be approximated[14] to

$$\mu(E) \propto \upsilon \; P(E) \; N(E) \qquad (1.10)$$

where N(E) is the density of unoccupied states at energy E and P(E) is the transition probability for a transition involving the two states concerned, with the intial state being the core state (or s state) and the final state being one in which an electron is excited to a normally unoccupied level in the valence or conduction band. It is very difficult to calculate theoretically P(E) for such transitions in the case of solids. However, the selection rules often help in giving a rough estimate of the

transition probability. Assuming the dipole approximation to be valid for solids, one can assume the K, L_I, ... absorption spectra to reflect the density of unoccupied p like states in the conduction band, and the L_{II}, L_{III}, M_{III}, ... spectra to reflect the density of d and s electron states. In a given band the transition probability is generally assumed[15] to be a monotonous function of energy.

The first significant attempt towards the explanation of the shape of an X-ray absorption discontinuity in a solid was that of Richtmyer, Barnes and Ramberg[15] who described the absorption edge in terms of a series of absorption lines with equal widths and having equal transition probabilities. In their work, Richtmyer *et al.* employed the following expression for the intensity distribution function $J_{AB}(\upsilon)d\upsilon$ for an absorption line, given by Weisskoff and Wigner[16].

$$J_{AB}(\upsilon)d\upsilon = \frac{\Gamma_A + \Gamma_B}{2\pi} \cdot \frac{d\upsilon}{(\upsilon_{AB} - \upsilon)^2 + \left[\frac{\Gamma_A + \Gamma_B}{2}\right]^2} \qquad (1.11)$$

where A and B refer to the initial and final states involved in the electronic transition, υ_{AB} is the frequency corresponding to the transition and is

$$\upsilon_{AB} = \upsilon_A - \upsilon_B = (E_A - E_B)/h \qquad (1.12)$$

and Γ_A and Γ_B are related to the mean life-times τ_A and τ_B of the states A and B respectively through the relations

$$\Gamma_A = 1/2\ \pi\ \tau_A, \quad \text{and } \Gamma_B = 1/2\ \pi\ \tau_B \qquad (1.13)$$

Richtmyer *et al* have discussed using the relation (1.11) the

shape of the L_{III} absorption discontinuity of gold and have shown that the variation of the absorption coefficient in the vicinity of the absorption discontinuity follows an arc-tan curve given by the formula

$$\mu(E) = \text{Constant} \left[\frac{1}{2} - \frac{1}{\pi} \arctan \left(\frac{\upsilon_{EoA} - \upsilon}{\frac{1}{2}\Gamma_E} \right) \right] \qquad (1.14)$$

where Γ_E is the full width at the half maximum of each absorption line and υ_{EoA} is the frequency difference between the initial state in the absorption process and the first one of the final states.

It is difficult to assess the exact importance of the above formula because of the absence of experimental verification of the assumptions leading to it and the lack of the knowledge of the transition probabilities. In spite of it, it has been found that in many cases there exists rather a close similarity between the theoretical arc-tan curve and the experimentally observed curves. Whenever such a close fit exists, the calculations leading to the above formula for $\mu(E)$ show that the inflection point on the absorption curve corresponds to a transition of the inner electron to the first available empty level in the solid.

A detailed study by Parratt[17] of the K-absorption discontinuity of gaseous argon (Z=18) has led to a further step in the understanding of the X- ray absorption process. He has decomposed the observed absorption curve, duly corrected for experimental distortions, into a series of resonance absorption lines corresponding to the transitions $1s \longrightarrow np$, where $n > 3$. The wavelength positions of these absorption lines were calculated with the help of the optical terms of potassium (Z=19), since an ionised argon atom can be considered to be similar to a potassium atom. This study has been extended to the other inert gases by Brogren[18]. The approximation was further examined by Mitchell[19]

for neon who cautioned that this model may not hold for very light atoms. In a different approach, Vainshtein and Narbutt[20] have calculated the relative intensities of the various absorption lines assuming hydrogenic wavefunctions for the initial and final states for the inert gases.

Soules and Shaw[21] have studied the K - absorption spectrum of solid argon and have found that it differs very much from that obtained in the gaseous state. The absorption edge for the solid closely follows the theoretical arc-tan curve except in the region of maximum absorption. The first absorption maximum in the curve of the gas has approximately the same wavelength as the inflection point on the absorption curve of the solid. These results, together with Nilsson's[22] measurements of the absorption coefficients with different excitation voltages, confirm the view that the inflection point on an X-ray absorption discontinuity corresponds to the transition of an inner electron to the first unoccupied level in the conduction band of the solid.

Breinig et al.[23,24] have proposed a theoretical model for absorption edges and derived the following expression for absorption cross section near the edge :

$$\sigma_{nij} = \sum_{nij}' \frac{\Gamma/2}{\left[E - \left(E_{nij}' - E_{nij}\right)\right]^2 + \left(\frac{\Gamma}{2}\right)^2} + a\left(\frac{1}{2} + \frac{1}{\pi}\tan^{-1}\frac{2}{\Gamma}\left(E + E_{nij} + \epsilon'\right)\right) \qquad (1.15)$$

where E_{nij} and E_{nij}' are intial and final states in the transition, E denotes the photon energy, σ is the width of the excited state and $\epsilon(\nu-0.5$ eV) the constant energy used for inclusion with the continuum the highest bound states whoose

width exceed their separation. It is clear from this expression that the profile of the X-ray absorption discontinuity is nothing but a Lorentzian of appropriate height and width superimposed on an arc-tan curve. Breinig et al.[23,24] have studied the K-absorption edge spectrum of argon and L-absorption spectra of krypton and xenon. These workers decomposed their spectra into Lorentzians and arc-tan curve. They found a good agreement between the peak position of Lorentzian corresponding to a particular electronic transition and the optical energy obtained from experiments.

Though a rigorous calculation of the shapes of absorption discontinuity have been done by Breinig et al., for argon, krypton and xenon, these have not been to date (to our knowledge) for different absorption edges in solids. However, it has been found practical to perform numerical analysis on the absorption data in terms of the positions, widths and oscillator strengths of bound-state and resonance peaks and of an edge position, width, and height for the principal continuum edge. Cramer and Hodgson[25] have done such type of analysis by decomposing the Mo K-edge spectrum in $[Mo_7O_{24}]^{6-}$. These authors have shown that by fitting the absorption edge with several Lorentzians and an arctangent function, the positions and intensities of edge features may be quantitated. In this laboratory[26] also, the fitting of K-edge profiles of transition metal ions and L_{III}-edge profiles of tungsten ions in various compounds into Lorentzians and arctangent function has been done and it has been shown for the first time that the areas under different Lorentzians give a measure of extent of tetrahedral to octahedral clusters.

It has been often found that the position of an X-ray absorption discontinuity changes with the physicochemical environment of the absorbing atom. It was Bergengren[27] who first demonstrated the dependence of X-ray absorption discontinuities on chemical combination. He investigated the K-absorption edge of

phosphorus in its various allotropic forms and found slight variations in the wavelength of the edge. Lindh[28], who carried out a number of experiments to study the effect of chemical combination on the wavelengths of the K-absorption discontinuities of chlorine, phosphorus and sulphur in various compounds, demonstrated that the wavelength of the X-ray absorption spectrum of an atom varies with its chemical state in the compound. Stelling[29] using spectrograph with higher dispersion than that used by Lindh has studied the K-absorption limit of chlorine in various chlorides. Aoyama, Kimura and Nishina[30] have studied the K-absorption limit of chlorine in various organic compounds. Coster[31] has studied the K-absorption edges of titanium and manganese in their different oxides and lent support to the earlier observations. These investigations were soon followed by many researchers who extended the study of chemical shifts to all sorts of compounds, complexes, alloys, solutions and glasses.

Considering the various factors which may affect the energy necessary to remove an electron from an ion in a crystal, Pauling[32] has discussed the dependence of the wavelength of an absorption discontinuity on the chemical environment of the absorbing atom and has emphasized the importance of electrostatic potential seen by the absorbing ion due to its environment and the external screening caused by the valence electrons. The experimentally observed chemical shifts of the K-absorption edges of chlorine in LiCl, NaCl, KCl and RbCl seem to be in accordance with the theory proposed by Pauling, but the results obtained for some other compounds, e.g.NH_4Cl, CsCl, CuCl and AgCl do not agree with it.

Kunzl[33] made a critical examination of the experimental work concerning the displacement of the K-absorption discontinuities of atoms present in different oxidation states in their oxides. He formulated a law according to which the displacement of an absorption edge in a series of compounds depends directly upon

the valency of the element in the compound under consideration. This dependence is given by the relation $\Delta\upsilon/R \propto V$, where $\Delta\upsilon$ denotes the change in the frequency of the absorption edge for a given compound with respect to that for the pure element, R is the Rydberg constant and V is the valency of the absorbing atom. This dependence of the chemical shift on valence has been supported by the work of Zinn[34], Barton[35], Manescu[36], Glenn and Dodd[37] and many others. Assuming the dependence of the position of the K-absorption limit on valency Boehm, Faessler and Rittmayer[38] have reported the valence of cobalt in vitamin B_{12} to be three. Kirichock and Karalnik[39], Vainshtein[40], Miller[41], Mande and Chetal[42] and Sarode et al.[43] have determined the valency of transition metal ions in different compounds and complexes, making use of the Kunzl's law. However, several investigations[44-46] have pointed out the limitations of the Kunzl's law. The effect of electronegativity and character of the ligands, type of hybridization, nature of chemical bond, coordination number and the other structural parameters[47] seem to affect the chemical shift. Agarwal and Verma[48] have given an empirical rule which states that " in general, the chemical shift is towards the high energy side of the metal edge and it increases progressively with the increase in the valence of the cation, unless the shift is either suppressed by the covalent character of the bond or enhanced by the formation of metal-metal bonding." Dey and Agarwal[49] have further attempted to demonstrate a linear variation of the chemical shift with the product of the ionicity of the bond and square of the valency.

Several workers[50,51] have tried to correlate the chemical shift with effective charges on the absorbing atoms calculated by different methods. Batsanov and Ovsyannikova[52] have investigated the position of the K-absorption discontinuity of manganese in some of its compounds and have observed its dependence on the coordination charge on the absorbing ions. Barinskii and Nadzhakov[53] have attempted to determine the effective charges in

some transition metal compounds by this method. These attempts have been critically reviewed by Barinskii and Nefedow[54] in their book. Through somewhat involved reasoning Böke[55] also has tried to deduce the effective charges on the absorbing metal atoms in various complexes. Srivastava et al.[56] have also shown that the variation in the K-edge shifts of copper in some complexes involving Cu^{I} and Cu^{II} follows a parallel variation in the calculated effective nuclear charge. In 1973 Mande and Sapre[57] have shown that the absorption discontinuity in a compound shifts towards the higher or lower energy side with respect to the corresponding discontinuity in the pure element depending upon whether the absorbing atom is a cation or an anion and that the magnitude of the chemical shift depends upon the effective charge on the absorbing ion. They have determined the effective charges in the case of gallium selenide and gallium telluride using the X-spectroscopic technique. Mande and Kondawar[58] have calculated the effective charges on cobalt ions in some of its intermetalic compounds and a correlation between the X-ray absorption shifts and the effective charges has been found. Sarode[59] has investigated the L_{III}-absorption edges of bismuth in bismuth halides. He has shown that the inflection point position of the absorption discontinuity shows variation on the partial ionic charge calculated by Sanderson's method. Sarode et al.[60] have examined the K-absorption spectra of several oxides and pervoskites of manganese, iron and cobalt. These authors have found a functional relationship between chemical shifts and effective atomic charges.

It is not always easy to locate the position of the X-ray absorption discontinuities unequivocally because their shapes often appear complicated and do not always follow[61] the simple arctangent curve. Moreover, the discontinuities are frequently accompanied by[62] fluctuations in the absorption coefficient on the low as well as high energy sides. These complexities in X-ray absorption spectra can be roughly classified in the following

groups :

(i) Pre-absorption : This is the structure observed on the low energy side of the absorption edge. It is usually attributed[63,64] to the availability of localized unoccupied electronic levels below the conduction band. In the case of some rare earths and their systems one observes in the L and M spectra such preabsorption peaks corresponding to transitions to the unfilled atomic levels. Preabsorption structures in some insulators like CuO, ZnO, RbCl etc. have also been observed by Cauchois and Mott[64], who have interpreted thier results on a model suggested earlier by Frenkel[65]. According to Frenkel in the non-metallic solids the hole formed in an inner atomic level can trap the free electron in the lattice by virtue of its Coulomb field, forming a bound electron hole pair (exiton), which forms free atomic like levels in the forbidden gap. Transitions of the inner electron to these levels give rise to the preabsorption maximum on the low energy side of the absorption discontinuity.

Pre-absorption peaks have also been observed[66-72] in compounds wherein the meatal ions have tetrahedral, sqare planar and square pyramidal cordination. The intensities of these peaks are found to depend on the coordination geometry[69,70] of the metal site. For example, in compounds like Ag_3VO_4, where vanadium ion is tetrahedrally coordinated by four oxygen ligands, the intensity of pre-edge peak is large[71], whereas in $GdVO_3$, the vanadium ion being in octahedral coordination, the intensity is very small. The metal ions, which have square pyramidal coordination in compounds, give the pre-absorption peak whose intensity is slightly smaller than those observed for tetrahedrally coordinated compounds[71]. These peaks are generally attributed[67,68,72] to the core electron transition to the partially vacant conduction band. Shulman et al.[66] have explained that vibronic mixing of np and nd characters makes the low energy transitions allowed. Theoretical considerations[67,68] also support

this views.

(ii) **Splitting of the Discontinuity and the Near Edge Structure :** It has been observed[73-75] that the X-ray absorption discontinuity often splits into two or more components and that their appears some fine structure in its immediate vicinity (upto about 30eV) on its high energy side. Kossel[76] has observed this structure initially in the case of gases and had suggested a model of single electron transitions to the empty atomic states for the interpretation of such structure. This type of structure was later found[75] to appear in the liquids and solids also. This near edge structure in the case of metals, alloys and highly covalent compounds is usually attributed[62] to the distribution of unoccupied states of appropriate symmetry in the conduction band. For gaseous molecules, molecular solids and transition metal coordination complexes it is attributed[77-80] to the transitions of core electrons to the states formed due to molecular formation. In the K-absorption spectra of transition metal compounds several workers[37,58,81] have obseved a weak low energy peak at the threshold followed by a shoulder on a rising absorption that culminates in a strong peak. The occurrence of low energy peak corresponding to inner electron transition to nd state, has already been discussed above. The shoulder peak and strong absorption maxima are generally assigned to ns and np states.

The transition to the outer states created due to capture of another atom's electron[29] (cross-over transition) as well as the creation of multiple inner vacancies[82] may also give rise to some small peaks near the absorption edge.

(iii) **White Line :** The appearence of a stong peak just above the X-ray absorption edge for some elements and compounds has been an interesting subject in X-ray spectroscopy for many years. The strong peak is referred to as a "white line" (or "raie blanche"

in French), because such a little amount of radiation at certain wavelengths would penetrate the absorber relative even to the radiation transmitted above the edge, giving a white line on the photographic film used in the early experiments. For example, white lines have been observed at the K-edges of elements Ga and As, Ni in Ni_2O_3, Cu in CuO, and Zn in Zno[64], but not in the 3d transition elements[74]. White lines have also been observed at the L_{II} and L_{III} edges (but not at the L_I edge) of Fe, Co, Ni[83,84], Cu in CuO[85], Ru, Rh, Pd[86,87], Sm, Gd through Lu[88], Ta, W, Re[89-93], compounds of Hg and Tl[92], and U[93]. The list is by no means complete, in fact, with the enhanced intensity and improved resolution from synchrotron radiation sources[94,95], white lines have been obseved in a large number of substances. Although the origin of the strong absorption has not been analized in detail, it is generally believed[64] to be associated with an atomic like electric-dipole-allowed transition from an inner shell to an unoccupied level with a high density of states in the vicinity of the absorbing atom. In this regard, the white line also depends on the chemical bonding because Cu in metal or Cu_2O does not have a white line[85] while W in WO_3 exhibits a broader white line than the one in metallic W[90].

Wei and Lytle[96] have studied the L_{II} and L_{III} edges of tantalum metal. These authors have associated the white line with an atomic like allowed transition from $2p_{1/2}$ and $2p_{3/2}$ states to the vacant 5d states of a high density. However, qualitative comparison with the calculated band structure was not possible because none of the existing band structure calculations has included the effect of a core hole. In an attempt to understand the white lines, Wei and Lytle presented two least-square analysis of the Ta L_{III} edge in terms of (a) a Lorentzian profile and (b) a Breit-Wigner-Fano type formula. They found that the latter, which was first suggested by Cauchois and Mott[64], appeared to provide a better fit to the asymmetric line shape.

Brown et al.[97] have done rigorous theoretical calculations

of white lines and shown that the calculated weight of the absorption in the white line corresponding to a $2p_{3/2}$ to $5d_{5/2}$ transition is consistent with the experimentally determined value in platinum metal. However, experimental results for Ni and Ti do not fit into their theoretical framework.

(iv) **Extended X-ray Absorpption Fine Structure** : The extended X-ray absorption fine structure (EXAFS) refers to oscillations in the X-ray absorption coefficient observed on the high-energy side of an X-ray absorption edge. Such oscillations can extend up to 1000 eV above the edge and may have a magnitude of 10% or more.

The phenomenon of EXAFS has been known since 1930 and the basic physical explanation has been provided by Kronig[98], who says that these oscillations are due to modification of the final state of the photoelectron by the crystal[98] or, in the case of gaseous molecules, by atoms surrounding the excited atom[99]. Since than there have been various further attempts to theoretically understand the EXAFS, but without complete success[100-104]. The various theories can be classified into two categories, long- range order (LRO) and short range order(SRO). The LRO theories require the existence of long-range order to explain the fine structure. Because EXAFS is found expeimentally in amorphous solids and molecules the experimental evidence favours the SRO theoretical approach. For this reason during 1970 and later the theoretical interest had centered on the SRO theories. In these theories only the environment in the vicinity of the excited atom was held responsible for EXAFS. Most SRO theories of EXAFS agree on the basic Physics. The differences occur in the various approximations made in the calculations.

However, there has never been theoretical investigation of the relationship between the LRO and SRO theories although one knows that both approaches must give the same results if correctly formulated. It is shown by Stern[105] that the LRO theories as usually formulated are incorrect because they neglect

the dominant effects. In 1970, Sayers, Lytle and Stern[106] derived the first successful working theory of EXAFS. This was subsequently modified by Stern[105] to a more general form and further refined by others[107,108]. According to these theories, EXAFS is regarded as resulting from interference between the photoelectron wave propagating from the X-ray absorbing atom and the wave backscattered by neighbouring atoms. Depending on whether the scattered wave returns to the origin in phase or out of phase with the out going wave, there is an increase or decrease in absorption.

Sayers et al.[109] have shown that the structural information can be obtained most directly from EXAFS by taking the Fourier transform of EXAFS data. With highly symmetrical structures involving only a single absorber nearest neighbour distance in the first coordination sphere, one can use Fourier transform to obtain such distances to an accuracy of about 0.01 A^{O}.

Besides radial distance information, EXAFS also contains information about the type and number of scattering atoms and their motion relative to the absorber. The atom type reveals itself through the EXAFS amplitude envelope. This amplitude is also affected by the static and thermal disorder of absorber-scatterer distances. Moreover, simple theory predicts that the magnitude of the fine structure will be linearly proportional to the number of scattering atoms and inversely proportional to the square of the absorber-scatterer distances. During 1975-1977, much of the amplitude information has been discarded, but in late 1978, Cramer et al.[110] has demonstrated that using a known phase shifts and amplitude functions, one can estimate the number and identity of near-neighbours at a particular distance.

Sometimes one observes that in the extended fine structure there exists certain peaks which cannot be attributed[111] to the states created in the above fashion. There is evidence to suggest that these peaks can be attributed to plasmons, i.e. collective

electron excitations.

Since most of the experimental work presented in this thesis is done by using X-ray absorption spectroscopy, it would be appropriate here to mention briefly the special advantages of this technique that make it a versatile probe for electronic structure determination.

1.4. SOME SPECIAL ADVANTAGES OF X-RAY ABSORPTION SPECTROSCOPY

As is well known ,the surge in interest during the last two decades in X-ray absorption fine structure, which had been an obscure phenomenon for the previous fifty years, was caused by the realization that X-ray absorption spectroscopy can be used to obtain information about the local structure of the absorbing atoms[109]. Several years after this appreciation, the technique, as mentioned in section 1.1, became experimentally accessible to the general scientific community with the advent of very high intense radiation sources. Since then X-ray absorption technique has found wide applicability in many diverse areas as a tool to determine the local atomic environment in many classes of materials whose structures defied analysis by standard techniques such as diffraction or diffuse scattering[109-114]. The properties of X - ray absorption technique that make it so useful for structure determination are :

1. The local atomic arrangement can be determined about each type of atom in a sample separately. By tuning the X-rays to the absorption edge energy of an atom, only its environment is probed.

2. Since EXAFS measures only short range order, there is no fundamental distinction between crystals with long range order and samples without, such as amorphous solids, liquids, and solutions. Thus aperiodic systems can be studied with the same ease as crystals.

3. In principle, the kinds of surrounding atoms can be

distinguished by the energy depedene of their contributions to the EXAFS.

4. The numbers of atoms at a given average distance and the disorder in their location about their average can be quantified by EXAFS.

5. In unoriented samples only the radial distance between the centre atom and its neighbouring atoms is determined, but in oriented samples which have less than cubic symmetry, angular positions are discernible.

6. Structural information is obtained from EXAFS by a simple and direct analysis.

7. The X-ray absorption measurements are relatively easy and rapid.

8. Determination of the chemical state of atom is possible by determining absorption edge shift and the near edge structure.

9. Information regarding the unoccupied bound states as well as the low-lying continuum states can be obtained from the absorption spectrum by making use of a relatively narrow inner state as a scanning probe.

10. It is a non destructive technique and comparatively small quantities of materials are required in the investigations.

11. The site symmetry of the absorbing ions i.e. the geometrical distribution of atoms around the absorbing atom can be obtained simply by studying the profiles of X-ray absorption edges in the model compounds and in the unknown systems.

It is because of these properties and advantages that X-ray absorption spectroscopy occupies an important place among the different methods used for crystal structure determination.

1.5. ORIENTATION OF THE PRESENT WORK

As mentioned earlier, recent experimental and theoretical advances have made X-ray absorption spectroscopy a promising new method for the investigation of local environment around a

specific absorbing atom in simple as well as complex crystalline systems, catalysts, amorphous materials, metalloproteins and many other cases where conventional diffraction methods are not feasible. It is our intention to extend such investigations to complex oxide systems, in particular, to vanadium and thallium doped superconducting oxides and determine what correlations, if any, could be established between the changes in the different features of the X-ray absorption spectra and the changes in the electronic structures of the absorbing atom. In present thesis we report our investigations on

(i) Position and profile of vanadium K absorption edges in the model compounds viz. VO, V_2O_3, V_4O_7, VO_2, V_2O_5, $NaVO_3$, $CrVO_4$, $Zn_3(VO_4)_3$, $GdVO_4$, $Ca_3Fe_3GeVO_{12}$, $Pb_5(VO_4)_3Cl$, VOPC, VOTPP, $(NH_4)_4$[VO-tart]$_2.2H_2O$, $VO(bzac)_2$, $VO(acac)_2$, $VOMoO_4$, PbV_2O_6, $Ca_3V_{10}O_{28}.16H_2O$, $SmVO_3$, V_2S_3, VN, [VO(hshed)(acac)].$VOPO_4$, $VO(OC_3H_7)_3$, and in the superconducting oxides of composition $Tl_{1-x}V_xSr_2(Ca_{0.8}Y_{0.2})Cu_2O_Y$, $(0.2 \leq x \leq 0.5)$.

(ii) Position and profile of copper K absorption edges in model systems viz. Cu_2O, CuO, La_2CuO_4 and in the superconducting oxides viz. $YBa_2Cu_3O_{7-\delta}$, $La_{2-x}A_xCuO_4$ where A = Sr, Ba and $0 \leq x \leq 0.3$, and $Tl_{1-x}V_xSr_2(Ca_{0.8}Y_{0.2})Cu_2O_y$.

(iii) Position and profile of thallium L- absorption edges in TlCl, TlBr, TlI, Tl_2CO_3, $TlNO_3$, Tl_2SO_4, $Tl(CH_3COO)$, $Tl(C_6H_5COCHCOCH_3)$, $Tl(C_5H_7O_2)$, $Tl_2Ta_2O_6$, Tl_2O_3, $Tl(NO_3)_3.3H_2O$, $Tl(CH_3COO)_3$, $Tl(CF_3COO)_3$ and $Ba_2Tl_2O_5$ and superconducting oxides mentioned in (i).

(iv) Extended X-ray absorption fine structure at the thallium L_{III} edge in the above superconducting oxides.

Furthermore, we have also studied the X-ray photoelectron

spectra (XPS), in particular, copper - $2p_{3/2}$ core level spectra in Cu metal, Cu^{1+}, Cu^{2+}, Cu^{3+} compounds and in a few superconductors for the confirmation of results obtained from the analysis of absorption spectra of these complex oxides.

REFERENCES

1. J.K. Hulm and R.D.Blaugher, in `Superconductivity in d-and f-Band Metals, edited by D.H.Douglas (AIP, New York p1), (1972).

2. B.M. Klein and W.E. Pickett, in `Superconductivity in d-and f-Band Metals,edited by W. Buckel and W. Weber p 97,(1982).

3. J.G.Bednorz and K.A.Mûller, Z.Phys. B 64, 189 (1986).

4. M.K. Wu, J.R.Ashburn, C.J.Torang, P.H.Hor, R.L.Meng, L.Gao, Z.J.Huang, Y.Q. Wang and C.W.Chu, Phys.Rev. Lett. 58, 908 (1987).

5. H.Maeda, Y. Tanaka, M. Fukutomi and T.Asano, Jpn. J. Appl. Phys. Lett. 4 L 209, (1988).

6. C.W.Chu, J. Bechtold, L. Gao, P.H.Hor, Z.J.Huang, R.L.Meng, Y.Y.Sun, Y.Q.Wang and Y.Y.Xue, Phys. Rev. Lett. 60, 941 (1988).

7. Z.Z. Sheng, A.M. Herman, A.El Ali, C. Almasan, J. Estrada, T.Datta and R.J.Matson, Phys. Rev. Lett. 60, 937 (1988).

8. M. Siegbahn, The spectroscopy of X-rays, (Oxford University Press, London) 1925.

9. E.F.Kaelbel, Handbook of X-rays (McGraw-Hill Book Company, New York) 1967.

10. A.F.Sandström, Encyclopedia of Physics edited by S. Flûgge (Springer- Verlag, Berlin) 30, 246 (1957).

11. C.Kunz, Comments on Solid State Physics, 5, 31 (1973).

12. D.H.Tomboulian, Encyclopedia of Physics edited by S. Flûgge (Springer- Verlag, Berlin) 30, 246 (1957).

13. D.J.Fabian, L.M.Watson and C.A.W.Marshall, Rep. Prog. Phys., 34, 601 (1972).

14. G.A.Rooke, Soft X-ray Band Spectra and the Electronic Structure of Metals and Materials, edited by D.J. Fabian (Academic Press, London) p.3, (1968).

15. F.K.Ritchmayer, S.W.Barnes and R.Ramberg, Phys. Rev. 46, 843 (1934).

16. V.Weisskoff and E.Wigner, Z. Physik 63, 54 (1930).

17. L.G.Parratt, Phys. Rev. 56, 295 (1938).

18. G.Brogen, Nova Acta.Reg.Soc.Sc. Uppasala 14 (4th Series), 4 (1948).

19. G.R.Mitchell, Develop. Appl. Spectry 4, 109 (1965).

20. F.E. Vainshtein and K.I.Narbutt, Dokl. Akad.Nauk. SSSR, 105 1196 (1955).

21. J.A. Soules and C.H. Shaw, Tech. Rep. No.2, Ohio State University, Res. Found 1954.

22. A.Nilson, Ark. Physik, 6, 513 (1953).

23. M.Breinig, M.H.Chen, G.E.Ice, F.Parente and B. Crasemann, Phys.Rev. A 22, 520 (1980).

24. M. Breinig, Ph.D. thesis, University of Oregon (1979), (Unpublished).

25. S.P.Cramer and K.O.Hodgsen, Prog. of Inorg. Chem. 25, 4069 (1978).

26. P.R.Sarode and S.A.Gauns, X-ray Spectrometry (submitted).

27. J.Bergengren, Compt. Rend. 172, 1175 (1925) : Z.Physik 3, 247 (1920).

28. A.E. Lindh, Z.Physik 6, 303(1921).: Z.Physik 31, 210(1925).

29. O. Stelling, Z. Anorg. Allg. Chemie, 131, 1023 (1927).

30. S. Aoyama, K. Kimura and Y.Nishina, Zeit. f. Physik 44, 810 (1927). Zeit. f. Physik 46, 150 (1927).

31. D. Coster, Z. Physik 25, 83 (1924).

32. L.Pauling, Phys. Rev.,34, 954 (1929) .

33. V.Kunzl, Coll. Trav. Chim Techecoslovaquie 4(S), 213 (1932).

34. W.H. Zinn, Phys. Rev. 46, 659 (1934).

35. V.P.Barton, Phys.Rev. 71, 406 (1947).

36. I.Manescu Compt. Rend.255, 537 (1947).

37. G.L. Glenn and C.G.Dodd, J. Appl. Phys.39, 5372 (1968).

38. G.Boehm, A.Faessler and G. Rittmayer, Z. Naturforschung, 96,

509 (1954).

39. P.P.Kirichok and S.M.Karalink, Bull. Acad. Sci.USSR. Phys. Ser. 31, 1043 (1967).

40. E.Vainshtein, R.M.Ovrutskaya and B.I.Kotlyar, Sov. Phys. Solid State 5, 2935 (1963).

41. A.Miller, J. Phys. Chem. Solids 29, 633 (1968).

42. C.Mande and A.R.Chetal, Int. Conf. X-ray Spectra and Chem. Binding (Karl Marx University, Leipzig) 194, (1966).

43. P.R.Sarode, G.Sankar, A.srinivasan, S.Vasudevan, C.N.Rao and J.M.Thomas, Angewandte Chemie, 23, 323 (1984).

44. W.W.Beeman and J.A.Bearden, Phys. Rev. 61, 455 (1942).

45. D.Coster and S.Kiestra, Physica, 14, 175 (1948).

46. E.W. White and H.A. Mckinstry, Advances in X-ray Analysis, edited by G.R.Mallett et.al. (Plenum Press, New York) 9, 376 (1966).

47. A. Faesseler, Proc. X Colloquim Spectroscopium Internationale, University of Marylands, 307 (1962).

48. B.K. Agarwal and L.P. Verma, J.Phys. C: Solid St. Phys. 3, 535 (1970).

49. A.K. Dey and B. K. Agarwal, J. Chem. Phys. 59, 1397 (1973).

50. S. M. Karalnik, Bull. Acad. Sci. USSR Phys. Ser. 21, 1432 (1957).

51. M.V.Becker, Naturwissenscaften, 51, 633 (1964).

52. S.S.Batsanov and J.A.Ovsyannikova, Akad. Nauk. Beloruss SSR, 93 (1966).
Chemical Bonds in Semiconductors and Thermodynamics, edited by N.N.Sirota (Consultant's Bureau New York) 65 (1968).

53. R.L. Barinski and B. G.Nddzhakov, Bull. Acad. Sci.USSR Phys. Ser. 24, 419 (1960).

54. R.L.Barinski and W. I. Nefedow, Rontengenspektroskopische Bestimmung der Atomladungen in Molekulen (Akademische Verlagsgellschaft geest and Portig K.G.Leipzig).

55. K.Böke, Z.Physik Chem. Neue Folge 10, 45 (1957).

56. V.C.Shrivastava, H.L.Nigam and A.N.Vishnoi, Indian J. Pure Appl. Phys. 10, 61(1972) and refernces therein.

57. V. B. Sapre and C. Mande, J. Phys. C: Solid St.Phys. 5, 793 (1972) and J. Phys. Chem. Solids 34, 1331 (1973).

58. V.K.Kondawar and C.Mande, X-ray Spectrometry 5, 2 (1975) :J.Phys. C: Solid St.Phys.9, 1351 (1976).

59. P.R.Sarode, Z. Naturfursch (a) 33, 946 (1978).

60. P.R. Sarode, S. Ramasesha, W.H. Madhusudan and C.N.R.Rao, J. Phys. C: Solid State Phys. 12, 2439 (1979).

61. R. A. Van Nordstand, Int. Collllnf. X-ray Spectra Chem Binding (Karl Marx University Leipzig) 255 (1955).

62. L.V.Azaroff and D.M.Pease, X-ray Spectroscopy, edited by L. V.Azaroff (McGraw Hill Book Company, New York) 284 (1974).

63. P.C.Deshmukh, Ph.D. Thesis, Nagpur University, India (1975) unpublished.

64. Y. Cauchois and N.F.Mott, Phil. Mag. 40, 1260 (1949).

65. J.Frenkel, Physik z. Sowj. 9, 158 (1936).

66. R.G.Shulman, Y.Yaffet, P.Eisenberger and W.E.Blumberg, Proc. Natl. Acad. Sci. USA, 73, 1384 (1976).

67. R.A.Bair and W.A.Goddard, Phys. Rev. B 22, 2267 (1980).

68. F.W. Kutzler, C.R. Natoli, D.K. Misemer, S.Doniach and K.O. Hodgson, J.Chem. Phys. 73, 3274 (1984).

69. G.Sankar, P.R.Sarode and C.N.R.Rao Chem. Phys.76,435 (1983).

70. J.Wong, F.W.Lytle, R.P.Messmer and D.H.Maylotte, Phys. Rev. B 30, 5596 (1984).

71. B.H.Sonaye, Ph.D. Thesis, Goa University (1995).

72. L.Kau, D.J. Spira-Solomon, J.E.Penner-Hahn and K.O. Hodgson, J.Am. Chem Soc., 109, 6433 (1987).

73. C. Mande and A. R. Chetal, Int. Conf. X-ray Spectra and Chemical Binding (Karl Marx University Leipzig) p194 (1966).

74. W.W.Beeman and H. Friedman, Phys. Rev. 56, 392 (1939).

75. R.M.Levy and J.R.Van Wazer, Advances in analytical Chemistry

and Instrumentation, edited by C.N. Reilley and F.W. Mclafferty (Interscience Publishers, New York), 5, 221 (1966).

76. W.Kossel, Z.f. Physik 1, 119 (1920).

77. D. W. Fishcer, Band Structure Spectroscopy of Metals and Alloys, edited by D.J.Fabian L.M.Watson (Academic Press, London) p.669 (1973).

78. D.S. Urch, Advances in X-ray Analysis, edited by C.S.Barret (Plenum Press, New York) 14, 250 (1971).

79. D. W. Fischer, Advances in X-ray Analysis, edited by C.S. Barret *et.al.* (Plenum Press, New York) 13, 159 (1970).

80. A.V.Pendharkar and C.Mande, Chemical Analysis 7, 244 (1975).

81. W.Seka and H.P.Hanson, J.Chem. Phys. 50, 344 (1969).

82. L.G.Parratt, Rev. Mod. Phys. 31, 616 (1959).

83. Y. Cauchois and C. Bonnelle, C.R. Acad. Sci. Paris 245, 1230 (1957).

84. P.Hanzely and R.J.Liefeld, in Electronic Density of States, Natt. Bur.Stand. Spec. Publ. No.323, edited by L.H.Bennett p319 (1971).

85. C.Bonnelle, C.R. Acad. Sci. Paris 248, 2324 (1959).

86. I.G.Shveitser and M.A.Blokhin, Bull. Acad Sci. USSR 31, 962 (1967).

87. M.F.Sorokina and S.A.Nemnonov, Bull. Acad Sci. USSR 31, 1039 (1967).

88. P.R.Sarode, Ph.D. Thesis, Nagpur University (1977).

89. D.Coster and H. deLong, Physica 13, 385 (1947).

90. J.A.Bearden and T.M.Snyder, Phys.Rev. 59,1626 (1941).

91. S.N.Gupta and B.D.Padalia, J.Phys. F1, L16 (1971).

92. B.K.Agarwal and L.P.Verma, J.Phys. C2, 104 (1969).

93. Y. Cauchois and I. Manescu, C. R. Acad. Sci. Paris 210, 172 (1940).

94. B.M. Kincaid and P. Eisenberger, Phys. Rev. Lett. 34, 1361

(1979).

95. M.L.Perlman, E.M.Rowe and .E.Watson, Phys.Today 27, July 30 (1974).

96. P.S.Wei and F.W.Lytle, Phys. Rev.B 19, 679 (1979).

97. M.Brown, R.E.Peierls and E.A.Stern, Phys.Rev. B15, 738(1977)

98. R.de L.Krönig, Z. Physik 70, 317 (1931).

99. R.de L.Krönig, Z. Physik 75, 468 (1932).

100. A.Peterson, Z. Physik 80, 258 (1933).

101. A.L.Kostarev, Zh. Eksp. Teor. Fiz. 11, 60 (1941).

102. T.Hayasi, Sci.Rep.Tohoku Univ.33,123 (1949).

103. T.Shiraiwa, T.Ishimura and M. Sawadw, J. Phys. Soc.Japan 13, 847 (1958).

104. A.I. Kozlenkov, Izv.Akad. Nauk SSSR 25, 957 (1961).

105. E.A.Stern Phys. Rev. B 10 3027 (1974).

106. D.E.Sayers, F.W. Lytle and E.A.Stern, Advan. X-ray Anal. 13, 248 (1970).

107. C.Asley and S.Doniach, Phys. Rev. B 11, 1279 (1975).

108. P.A.Lee and J.B.Pendry, Phys. Rev. B 11, 2795 (1975).

109. D. E. Sayers, E. A. Stern and F. W. Lytle, Phys. Rev. Lett., 27, 1204 (1971).

110. S.P.Cramer, K.O.Hodgson, E.I.Stiefel and W.E.Newton, J.Am. Chem. Soc. 100, 2748 (1978).

111. E. A Stern, Contemp. Phys., 19, 289 (1978).

112. P.M.Eisenberger and B.M. Kincaid, Science, 200, 1441 (1978).

113. D.R. Sandström and F.W Lytle, Ann. Rev. Phys. Chem., 30, 215 (1979).

114. L. Powers, Biochem. Biophys. Acta, 683, 1 (1982).

115. P.A. Lee, P.H. Citrin, P. Eisenberger and B.M. Kincaid, Rev. Mod. Phys., 53, 769 (1981).

CHAPTER 2

EXPERIMENTAL TECHNIQUES

2.1 INTRODUCTION

To study the mechanism of superconductivity in the cuprate superconductors it is of vital importance to understand different properties of these materials. Also, it is necessary to use well characterized samples devoid of impurities for studying their electronic and structural properties. In this Chapter, we have given a brief introduction of experimental techinques employed in the work in this thesis.

In the following section, we shall first describe the methods of preparation used in this work.

2.2. PREPARATION OF MATERIALS

Copper metal, cuprous and cupric oxides, copper aluminate, barium and strontium carbonates, lanthanum and yttrium oxides were obtained from M/s Aldrich Chemical Company, USA.

La_2CuO_4 was prepared by weighing out the stoichiometric amounts of La_2O_3 and CuO. This mixture was then ground in an agate mortor. A pellet of this mixture was made and then kept in ceramic boat. It was heated to 900-950^oC in air for several hours. It was then reground and refired at 1100^oC and cooled to 900^oC before being quenched to room temperature. The final product of the solid state reaction was confirmed by X-ray diffraction to be the single phase of La_2CuO_4.

$YBa_2Cu_3O_{7-\delta}$ was prepared by starting from powders of Y_2O_3, $BaCO_3$ and CuO. The powder mixture of appropriate composition was first heated in air up to 1000^oC for 12 hours. Then it was pulverized, pressed into pellet and heated in oxygen at 950^oC for 24 hours and finally the sample was slowly cooled in oxygen atmosphere keeping it below 500^oC for 5 hours.

Sample of $La_{1.85}Sr_{0.15}CuO_4$ was synthesized from appropriate amounts of $SrCO_3$, La_2O_3 and CuO powders, each 99.99 % pure. The powders were thoroughly mixed, pressed into pellets, prefired at

950°c for 12 hrs., and then furnace cooled in air. Prefired materials were ground, pressed into pellets, sintered at 1100°c for 12 hrs. and then furnace cooled in air. Sintered materials were given the same sintering cycle again.

$Y_2Cu_2O_5$ was prepared by dissolving appropriate amounts of CuO and Y_2O_3 in nitric acid and decomposing the nitrate mixture at 1225°C.

$Ba_4NaCuO_4(CO_3)_2$, Nd_2CuO_4, $La_2Li_{0.5}Cu_{0.5}O_4$, $CaCu_3Ti_4O_{12}$, Y_2BaCuO_5, $SrCuWO_6$, $SrCuO_2$, $MgCu_2O_3$ and Ca_2CuO_3 were prepared by Dr. Bhagatsingh Sonaye and Dr. B. Chakraborti, Department of Biochemistry, Goa Medical College, Goa for us by the ceramic method by taking appropriate molar ratios of the starting materials (purity than 99.9 %) and heating them in air in the temperature range 1000 - 1200°C. Powder X-ray diffraction patterns of these compounds were recorded on a Rigaku Diffractometer (Model D/Max II-C) to ensure that a single phase of the compound was obtained.

Vanadium metal foil, VC, VN, VO, V_2O_3, V_2O_4, V_2O_5, $NaVO_3$, V_2S_3, vanadium tetraphenylporphine, vanadium phthalocyanine, vanadyl acetylacetonate were obtained commercially. Other model Vanadium compounds investigated in this work were synthesized by Anjli Chikara[1] for the study of electronic structure of complex oxides and organometallic compounds in this laboratory.

Vanadium complex of the tridentate schiff base ligand N-salicylidene-N -(2- Hydroxyethyl) ethylenediamine (designated as HSHED) studied in this work was synthesized by the method of Li et al[2] .Salicylaldehyde (2 ml, 18.8 mmol) and N- (2-Hydroxyethyl) ethylenediamine (1.9ml, 18.8 mmol) were added to 75 ml of degassed methanol and allowed to react for 1 hour. Vanadyl sulphate hydrate (3.74 gm, 18.8 mmol), dissolved in 50 ml of water, was added to this solution, and after about 3 hours the reaction solution turned blue with a small amount of blue solid precipitate. At this point, NaOH (1.5 g, 37.6 mmol) was

added to the mixture, and then the solution was kept in air, and the reaction was continued for 14 hours. At the end of this process, a yellow colour compound $[VO_2(HSHED)]_2$ was precipitated.

Superconducting samples of the composition $(Tl_{1-x}V_x)Sr_2(Ca_{0.8}Y_{0.2})Cu_2O_y$ (x = 0.2, 0.3, 0.4, 0.5) were prepared by mixing suitable amounts of Tl_2O_3, V_2O_5, SrO_2, CaO, Y_2O_3 and CuO. These mixtures were then pressed into pellets and heated in a furnace at 950^oC for 4 hours in flowing oxygen atmosphere and then cooled to room temperature.

TlCl, TlBr, TlI, Tl_2CO_3, $TlNO_3$, Tl_2SO_4, $Tl(CH_3COO)$, $Tl(C_6H_5COCHCOCH_3)$, $Tl(C_5H_7O_2)$, Tl_2O_3, $Tl(NO_3)_3.3H_2O$, $Tl(CH_3COO)_3$, $Tl(CF_3COO)_3$ were obtained from M/s Aldrich Chemical Company, USA.

$Tl_2Ta_2O_6$,and $Ba_2Tl_2O_5$ were prepared by heating the mixture of component oxides. $Tl_{0.5}Pb_{0.5}Sr_2CaCu_2O_7$ [3], $TlBa_2CaCu_2O_7$ [4-5], $Tl_2Ba_2CaCu_2O_8$ [6], and $Tl_2Ba_2Ca_2Cu_3O_{10}$ [7] were prepared by the usual ceramic process starting with the component oxides with $BaCO_3$. All the Tl- doped superconducting samples were characterized through X-ray diffraction. The unit cell parameters determined from these measurements are consistent with those reported in the literature[3-7].

The oxygen content was determined both by idometric titration and thermogravimetric studies of the reduction in hydrogen. Within experimental errors the oxygen content was the same as that expected from the nominal composition in all cases. Resistance measurements were made down to liquid nitrogen temperature using a standard D.C. four probe method.

2.3 X-RAY DIFFRACTION MEASUREMENTS

The evolution of our understanding of physics and chemistry in the solid state relied heavily upon structural information obtained from diffraction techniques. X-ray diffraction has widely been used to obtain crystal structure of different

materials. We have used Rigaku X-ray diffractometer (Model D/Max II-C) to record diffraction patterns of our superconducting powder samples. The intensity of radiation (Cu K_α) diffracted from the powder specimen was detected by a scintillation counter and recorded as a function of incident angle of X-ray (2θ). The Cu K_β radiation was suppressed using nickel filter. XRD was taken using Fe K_α radiation. Diffraction peaks were indexed and the unit cell parameters were calculated using the Powder Diffraction Package PDP1.1[8] procedure from the obtained d_{hkl} values. A typical diffraction pattern for a representative superconductiing oxide, $YBa_2Cu_3O_{7-\delta}$ is shown in Figure 2.1.

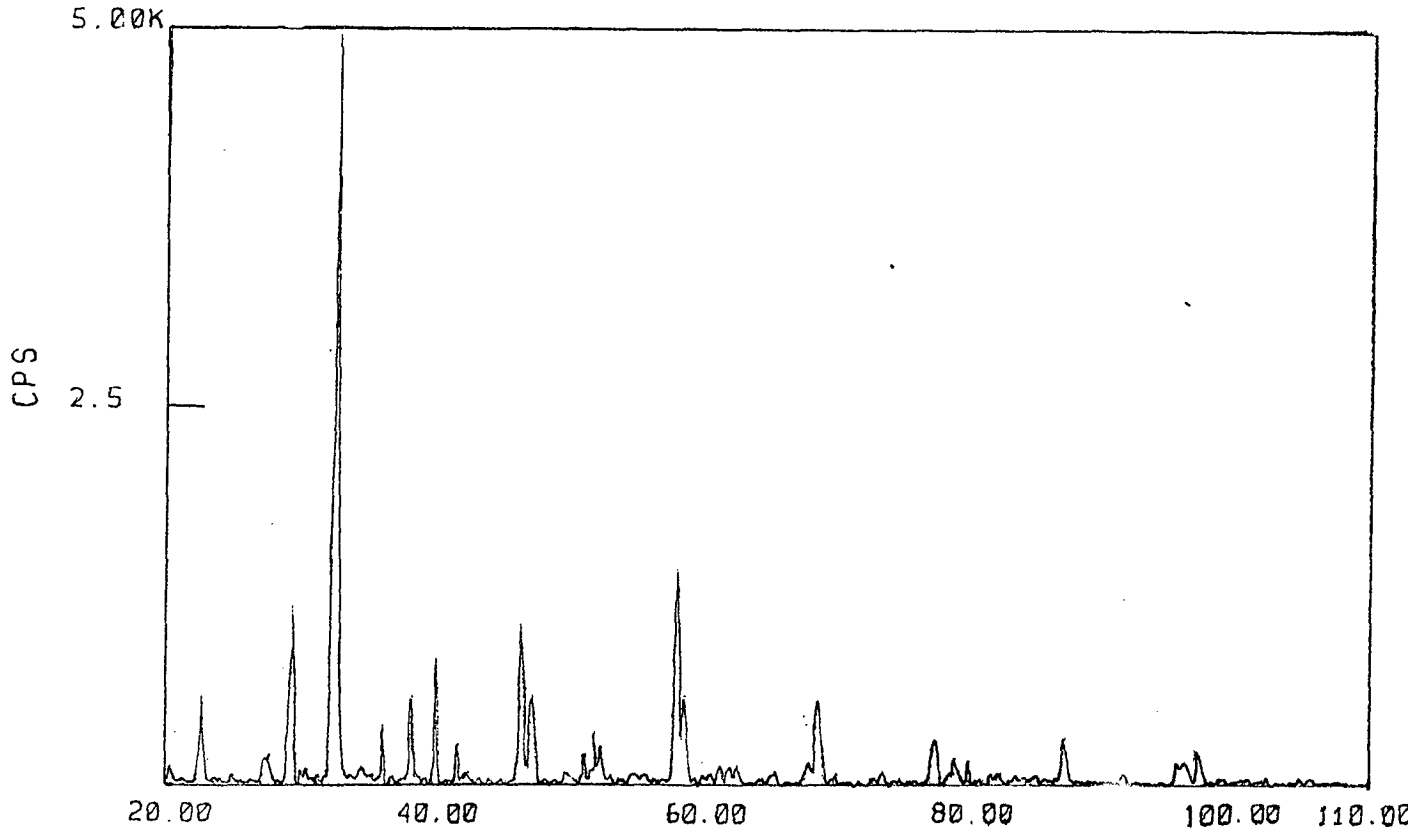

Figure 2.1: XRD pattern for $YBa_2Cu_3O_{7-\delta}$ sample

2.4 D.C. RESISTIVITY MEASUREMENTS

The restivity (ρ) in Ohm - cm of the sample is derived from Ohm's law

$$R = \rho l/A$$

$$\rho = R.A/l$$

where A is in cm^2 and l in cm.

Resistivity measurements were carried out using the four probe method Figure 2.2 shows the block diagram for d.c. resistivity experimental set up. The sample, in the form of a thin rectangular bar, is fixed on the PCB. Four thin copper wires, attached to the sample by means of a conducting silver epoxy, act as voltage and current leads. A d.c. current was sent through the outer leads from a programmable current source and the voltage developed across the inner leads was measured using a nanovoltmeter. The automated system of all the instruments was controlled by a computer. The data acquisition and on-screen plotting were performed by a computer. The resistivity was then calculated from the measured resistance using the sample dimensions. A typical resistivity plot for $YBa_2Cu_3O_{7-\delta}$ obtained in this work is shown in Figure 2.3.

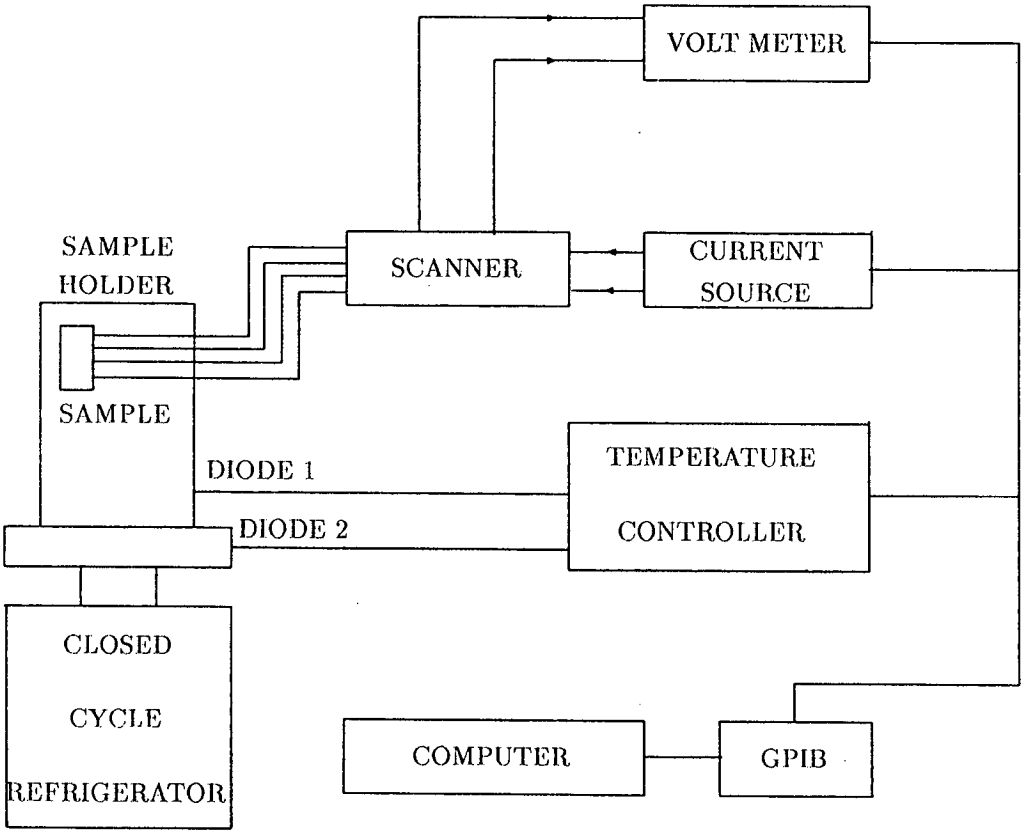

Figure 2.2: Experimental arrangement for resistivity measurement

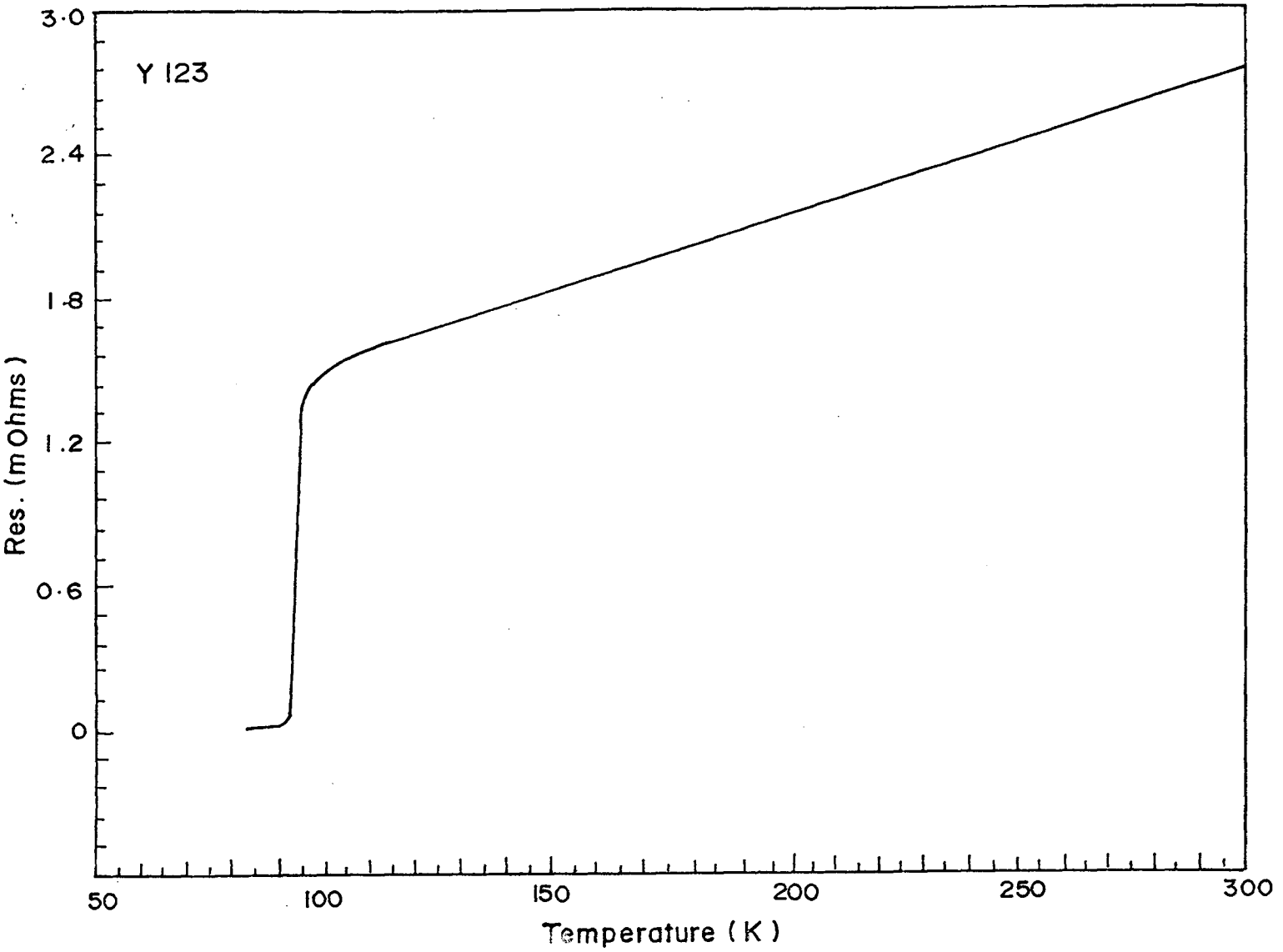

Figure 2.3: Resistivity plot for $YBa_2Cu_3O_{7-\delta}$

2.5. X - RAY ABSORPTION MEASUREMENTS

We describe below the apparatus used in this investigation to record the X - ray absorption spectra of vanadium, copper and thallium in their well-characterized compounds and in a few superconducting compounds. Since most of the work done in this thesis is in the field of X-ray absorption spectroscopy, the description of the instrument used to record the spectra and procedure is given in detail.

2.5.1 X - RAY SPECTROMETER

Our basic X-ray spectrometer is a horizontal Rigaku wide angle diffractrometer with attached tube stand. The major modification is an improved crystal (monochromator) support for optimum alignment of the diffracting crystal (Figure 2.4). This spectrometer is used with a conventional X-ray diffraction generator and X-rays tubes (W, or Cu target) chosen to provide a high intensity continuum in the region of absorption edge to be measured, while missing the intense characteristic X-ray emission lines. The spectrometer is used with a goniometer radius of 18.75 cm using simple set-back brackets and an X-ray tube takeoff angle of approximately 3^{o} (adjusted for maximum diffracted intensity). The first slit is used to limit the angular divergence of the X-ray beam, and the Bragg-Brentano parafocussing conditions and slit position require the focussing (exit) slit to be approximately of the same size. Between the two slits, a single-crystal monochromator Bragg diffracts a narrow band of the incident X-rays and adds its diffraction pattern to the divergence of the beam. The vertical divergence is limited to $\pm$ 2^{o} by a Soller slit located before the exit slit. Thus the resolution function depends primarily on the size of the slits and crystal diffraction pattern[9]. Our usual method of operation employs 0.05 mm slits (0.025^{o} divergence) in the 2θ range from 15^{o} to 45^{o} and 0.1mm (0.5^{o} divergence) slits for angles greater

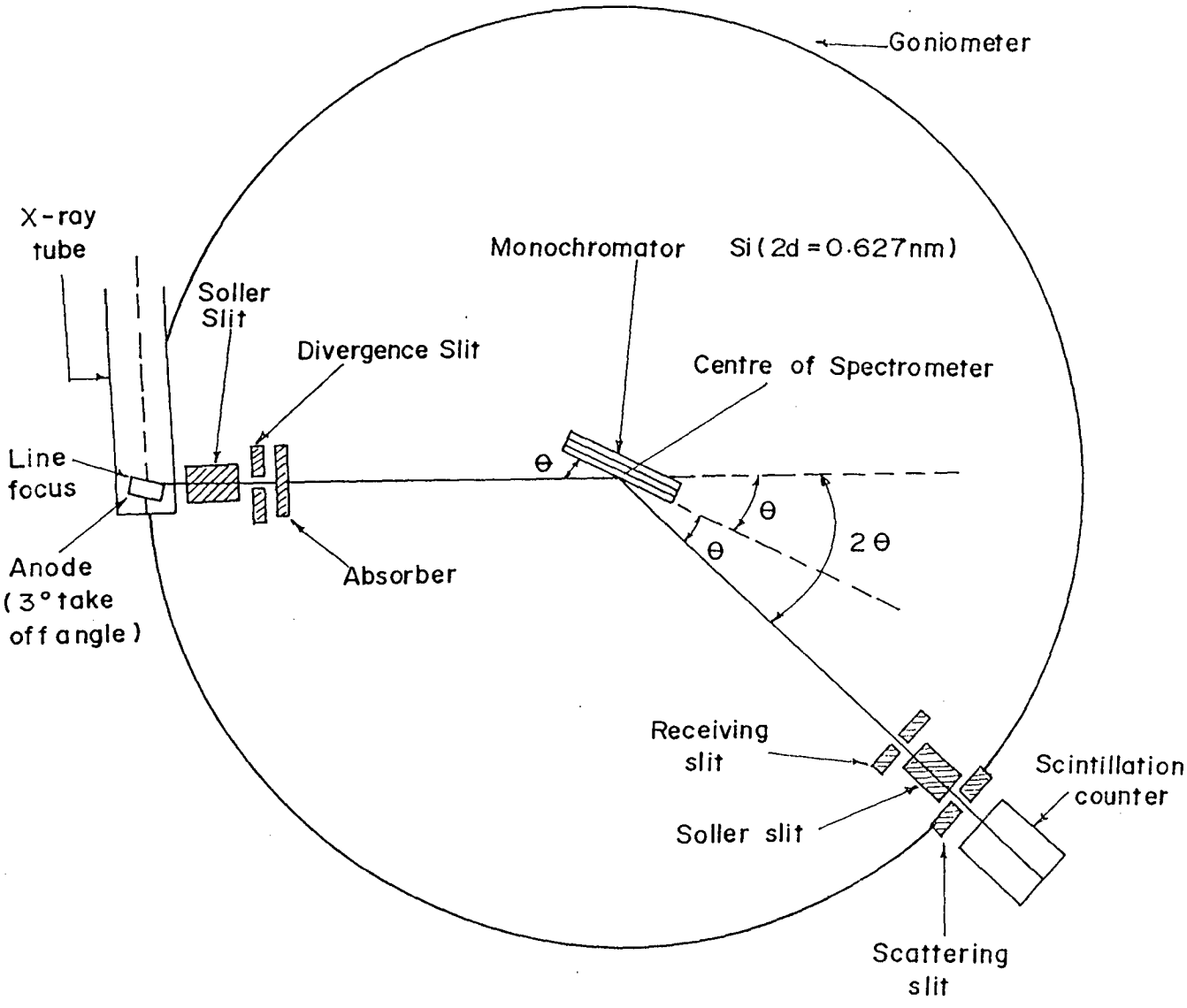

Figure 2.4: Schematic diagram of X-ray absorption spectrometer

then 45^{o} with overlap as experimentally required. Hence resolution power defined as $(\tan\theta)/\Delta\theta$ (or $\lambda/\Delta\lambda$) is approximately 1000 - 2000. The intensity from the continuum operating at full recommended tube power is typically (1-10) x 10^{3} photons per second before passing through the sample. For the case of 0.05 mm slits at $2\theta = 45^{o}$ and a LiF crystal ($2d = 4.026A^{o}$), the energy band width, assuming a rectangular response function, received at the exit slit would be ~ 4eV ($\Delta E = E \cot\theta \Delta\theta$), however, the intensity distribution of the radiation falling on the exit slit has the usual diffraction profile and the Rayleigh resolution criterion suggests that the spectrometer should be advanced in angular increments of 1/2 the angular width of the exit slit, i.e., $\Delta 2\theta = 0.01^{o}$ for 0.05 mm slits.

The mode of operation is as follows: For each spectrometer position, I, transmitted intensity through the absorber and I_o, the incident X-ray intensity are measured (preset count mode) and stored on a floppy disk, the spectrometer is advanced to the next 2θ position and the sequence is repeated. A separate scalar is used to generate a running number for each subsequent pair (I,I_o). Knowledge of the start position and the 2θ stepping increment allows calculation of X-ray wavelength for any data pair. The spectrometer stepping motor and absorber changer are activated and synchronized by the X-ray scalar print-out command. It was found that the mechanical accuracy of the absorber placement mechanism limited the precision to ~ 0.3%, thus 10^{5} photons were recorded for each I, I_o and increased precision to 0.1% was achieved by averaging multiple passes. The problem of coincidence loss in the X-ray detecting electronics was corrected using the method of Short[10] and Burbank[11]. If uncorrected, intense emission lines from X-ray tube leave an image in the data, which can be mistaken for EXAFS.

The flanged tube stand attached to the spectrometer allowed the X-ray tube to be translated, rotated and inclined with

respect to the spectrometer circle. The alignment procedure consisted of locating (by means of these adjustments) the most intense spot on the X-ray tube target so that it was directed through narrow aligned entrance and exit slits at $2\theta = 0^{o}$ as measured by a protected X-ray detector. The crystal monochromator was then inserted and a suitable characteristic line chosen for final crystal adjustment. At the calculated 2θ the translation, tilt and rotation (θ) adjustments of the crystal holder were used to obtain peak diffracted intensity of standard line which located the diffracting volume of the crystal at the centre of the spectrometer. Further refinement of the alignment was not necessary if the procedure described in the section on precision and accuracy of the energy scale was followed.

2.5.2 MONOCHROMATOR CRYSTALS

The usual discussion of monochromators for X-ray spectrometers emphasizes high resolution with narrow crystal rocking curves and multicrystal spectrometers. Our requirement stresses high X-ray intensity at moderate resolution for good statistical accuracy of measured EXAFS. Although better resolution would probably show more details particularly near the edge, there is an inherent width (~20eV) in the EXAFS due in part to temperature smearing as well as lifetime broadening[12] e.g., 1.5 eV for the Cu K edge.

Given the flat crystal geometry, this experiment is intensity limited by the inherent luminosity of X-ray tube and the diffraction efficiency of the monochromator. A given monochromator has a diffractive dispersion called its "rocking curve" which is the angular width of the diffracted beam. When the crystal is exposed to a continuum of diverging radiation, it selects from the total flux just that angular range of wavelength $\Delta\lambda$, which is its rocking curve width and diffracts a narrow band toward the exit slit, thus a crystal with very a narrow rocking

curve will diffract comparatively few photons. A crystal with a wider rocking curve than the divergence of the slit system will smear the diffracted beam over the exit slits. The optimum condition is obtained when the divergence of the slit system and rocking curve of monochromator are approximately equal.

The efficiency of diffraction and the rocking curve width of diffraction crystals may be modified by appropriate treatment. LiF(200) or Si(311) is particularly workable crystals in this respect. The integrated reflection coefficient for nonpolarised radiation, which is the area under the crystal rocking curve, has been calculated as a function of wavelength for the two extremes of the crystal perfection, a perfect crystal and an ideal mosaic crystal[13-15]. The measured values of selected cleaved and treated crystals are also shown[14,15]. This helps to increase the photons diffracted by a factor of 3. The time necessary to obtain a precision measurement was reduced proportionately. The treatment consisted of vigorous sanding on rough paper to drive dislocations into the crystal followed by successively finer paper to 600 grit to provide a smooth surface. Part of the damaged surface layer was then removed by an etching procedure[16]. After one minute in concentrated HF, a chemical polish consisting of 2-vol.% NH_4OH in H_2O at 26^{o}C with vigorous agitation was used to remove the surface at about 1μm/min. The crystal was checked repeatedly until rocking curve width narrowed to that of the desired slit size. we have used similar techniques with Si and quartz crystals with some success.

2.5.3 PREPARATION OF ABSORBERS

The absorbers were prepared in a variety of ways, malleable metals were rolled (2-5 μm); some materials were evaporated onto mylar or thin Al foil, soluble materials were dissolved and then absorbed and dried on a filter paper, many materials were ground to pass 400 mesh, mixed with a vacuum grease and then cast on a

smooth substrate. After drying, the casts were sandwiched between thin transparent adhesive tapes for support and attached to the sample holder. The optimum absorber thickness considering contrast, measurement time, and counting error problem, was attained when $I/I_o \sim 1/3$ on the high absorption side of the edge. For dilute solutions absorber thickness was kept such that $I/I_o \sim 1/10$

2.5.4 ENERGY CALIBRATION

In order to assign energy values to monochromator steps, generally the spectrum of a standard is measured which has some feature at a known energy. Often this standard is a metal foil. For EXAFS experiments on copper compounds, for example, it is convenient to do the energy calibration using copper foil whose K absorption edge comes at 8980.3 eV. In order to more easily determine the monochromator step at which various features occur in the calibration data, the first and second derivatives of spectrum in the vicinity of the edge as a function of monochromator step are calculated and plotted. From the derivatives it is easy to determine where these derivative curves cross the X - axis indicating the positions of the peaks and inflection points. To calculate the derivatives, a polynomial is fitted over a small range around each point and then differentiated at that point. Axis crossing locations are calculated by linear interpolation between two adjacent points on opposite sides of the axis.

After an energy E_p is assigned to a certain monochromator step S_p at some point of calibration, the rest of the monochromator steps in the data set can be assigned energies by the following equation

$$E = \frac{hc}{\lambda} \qquad (2.1)$$

where h is Planck's constant, c the speed of light, and λ the X-ray wavelength. λ is given by Bragg equation

$$\lambda = 2d \sin \theta \qquad (2.2)$$

where d is the distance between diffraction planes in the crystal and θ is the angle of incidence of the X-ray beam on the planes. θ_p , the angle at the point of calibration, is calculated by

$$\theta p = \arcsin \left[\frac{hc}{2dE_p} \right] \qquad (2.3)$$

Since monochromator steps are directly proportional to the angle change, the angle θ for a given monochromator step can be calculated by

$$\theta = \theta p + m (S - S_p) \qquad (2.4)$$

where m is the amount of angle change per step. Combining equations (1), (2) and (4) we obtain a relation which has energy as a function of monochromator step

$$E = \frac{hc}{2d \sin [\theta_p + m (S - S_p)]} \qquad (2.5)$$

2.5.5 PRECISION AND ACCURACY OF THE ENERGY SCALE

The kinetic energy of the ejected photoelectrons E must be established accurately in order to evaluate the natural EXAFS variable k. For every experiment, characteristic and/or impurity lines from the X-ray tube occurred and were used as standard reference points to calculate an effective lattice constant for the monochromator to establish the energy scale at the accuracy to which they were known[17]. Many elements were present as an impurities on the X- ray tube anode; W, Cu, Ni, Fe, and Mn are usually present, plus the characteristic line from the primary anode element in multiple orders of diffraction. Replicate

experiments established a precision of σ = 75 ppm ($\pm$ 0.7 eV at the Cu K edge) as compared to 40 ppm typical calibration lines. By using the calibration lines to calculate the lattice constant for every set of data, the requirement was removed for corrections involving the diffraction process in the monochromator crystal such as temperature correction, Lorentz-polarization correction, refraction and various errors due to misalignment. The value of E associated with each data pair was calculated from[18]

$$E = 12398.52/2d\sin\theta \quad eV \qquad (2.6)$$

The data collected from the EXAFS apparatus consisted of the time to collect a preset number of counts with the absorber in (T) and out (T_o) of the spectrometer.

The preliminary data processing program tabulates the initial data and calculates the X-ray energy and the absorption coefficient.

2.6 OTHER MEASUREMENTS

In addition to X-ray absorption spectroscopic technique, we have also employed technique like X-ray Photoelectron Spectroscopy (XPS) for the characterization of our superconducting compounds. A brief description is given in the following paragraph about the measurements carried out using this technique.

X-ray photoelectron spectra of powdered copper samples were recorded using an ESCA-3 Mark-II spectrometer of VG Scientific Limited, UK, fitted with a sample preparation chamber. The operating vacuum in the chamber was 10^{-10} torr. This chamber was

fitted with an argon ion gun and a quadrupole mass spectrometer. The radiation employed was Al K_{α} (1486.6 eV). The spectrometer was calibrated with reference to the binding energy of Au ($4f_{7/2}$) at 83.7 eV.

REFERENCES

1. Anjli Chikkara, Ph.D. thesis, Goa University (1996).

2. X.Lee, M.S.Lah and V.L.Pecoraro, Inorg. Chem., 27, 4657 (1988).

3. R.S.Liu and P.P.Edwards, J., Solid state Chem., 91, 407 (1991): A.K.Ganguly, K.S.Najundaswamy, C.N.R.Rao, A.Sequeira and H.Rajagopal, Z. Physik B 74, 215 (1989).

4. K.Yvon and M.Francois, Z.Phys. B 76, 413 (1989).

5. B.Morosin, D.S.Ginley, P.F.Hlava, M.J.Carr, R.J.Baughman, J.E.Schirber, E.L.Venturini and J.F.Kwak, Physica C 156, 587 (1988).

6. M.A.Subramanian, J.C.Calabrese, C.C.Toradi, J.Gopalkrishnan, T.R.Askew, R.B.Flippen, K.J.Morrissey, U.Chowdary and A.W.Sleight, Nature, 332, 420 (1988).

7. C.C.Toradi, M.A.Subramanian, J.C.Calabrese, J.Gopalkrishnan, E.M.McCarron, K.J.Morrissey, T.R.Askew, R.B.Flippen, U.Chowdary and A.W.Sleight, Science, 240, 631 (1988).

8. M.Calligaris, Powder Diffraction Package (version 1.1), Department di Scienze Chimiche, Universitat di Trieste, Italy (1989).

9. H.P. Klug and L.E. Alexander, X-ray Diffraction Procedures (John Wiley and Sons), New York 1954.

10. M.A.Short, Rev. Sci. Instrum. 31, 618 (1960).

11. R.D.Burbank, Rev. Sci. Instrum. 32, 368 (1961).

12. L.G. Parratt, Rev. Mod.Phys. 31, 616 (1959).

13. R.W.James, The Optical Principles of the Diffraction of X-rays (Bell, London) 1958.

14. J.Vierling, J.V. Gilfrich and L.S.Birks, Appl. Spectros. 23, 342 (1969).

15. F.W.Lytle, Science, 165, 416 (1969).

16. J.J.Gilman and R.Johnston, Dislocations and Mechanical Properties of Crystals (John Wiley and Sons, New York) 1957.

17. J.A.Bearden, Rev. Mod. Phys. 39, 125 (1967).

18. E.R.Cohen and B.N.Taylor, J. Phys. Chem. Ref. Data 2, 663 (1973).

TABLE 2.1. CRYSTAL AND DETECTOR ANGLES FOR VANADIUM K-ABSORPTION EDGES

Edge	Wavelength λ in A^o	Energy in eV	Crystal plane	Interplanar distance 2d in A^o	Crystal angle	Detector angle
V K	2.2691	5463.9	Si(111)	6.276	21.195^o ($21^o11'43''$)	42.391^o ($42^o23'27''$)
			Si(220)	3.825	36.386^o ($36^o23'11''$)	72.773^o ($72^o46'22''$)
			Si(311)	3.276	43.839^o ($43^o50'23''$)	87.679^o ($87^o40'46''$)
			Si(400)	2.715	56.695^o ($56^o41'43''$)	113.391^o ($113^o23'27''$)

TABLE 2.2. CRYSTAL AND DETECTOR ANGLES FOR COPPER K-ABSORPTION EDGES

Edge	Wavelength λ in A^o	Energy in eV	Crystal plane	Interplanar distance 2d in A^o	Crystal angle	Detector angle
CuK	1.38905	8980.5	Si(111)	6.276	12.787^o ($12^o47'13''$)	25.574^o ($25^o34'26''$)
			Si(220)	3.825	21.294^o ($21^o17'37''$)	42.588^o ($42^o35'15''$)
			Si(311)	3.276	25.088^o ($25^o05'16''$)	50.176^o ($50^o10'32''$)
			Si(400)	2.715	30.772^o ($30^o46'18''$)	61.544^o ($61^o32'37''$)

TABLE 2.3. CRYSTAL AND DETECTOR ANGLES FOR THALLIUM L- ABSORPTION EDGES

Edge	Wavelength λ in A^o	Energy in eV	Crystal plane	Interplanar distance 2d in A^o	Crystal angle	Detector angle
Tl L_I	0.8081	15343	Si(111)	6.276	7.398^o ($7^o23'52''$)	14.796^o ($14^o47'45''$)
			Si(220)	3.825	12.197^o ($12^o11'48''$)	24.393^o ($24^o23'36''$)
			Si(311)	3.276	14.281^o ($14^o16'50''$)	28.561^o ($28^o33'41''$)
			Si(400)	2.715	17.316^o ($17^o18'57''$)	34.632^o ($34^o37'55''$)

Edge	Wavelength λ in A^{o}	Energy in eV	Crystal plane	Interplanar distance 2d in A^{o}	Crystal angle	Detector angle
Tl L_{II}	0.8434	14699	Si(111)	6.276	7.723^{o}	15.446^{o}
					($7^{o}43'23''$)	($15^{o}26'46''$)
			Si(220)	3.825	12.738^{o}	25.476^{o}
					($12^{o}44'17''$)	($25^{o}28'35''$)
			Si(311)	3.276	14.919^{o}	29.837^{o}
					($14^{o}55'73''$)	($29^{o}50'14''$)
			Si(400)	2.715	18.098^{o}	36.196^{o}
					($18^{o}05'53''$)	($36^{o}11'46''$)

Edge	Wavelength λ in A°	Energy in eV	Crystal plane	Interplanar distance 2d in A°	Crystal angle	Detector angle
Tl L_{III}	0.9793	12660	Si(111)	6.276	8.977°	17.954°
					(8°58'37'')	(17°57'14'')
			Si(220)	3.825	14.834°	29.669°
					(14°50'38'')	(29°40'76'')
			Si(311)	3.276	17.393°	34.787°
					(17°23'36'')	(34°47'12'')
			Si(400)	2.715	21.143°	42.286°
					(21°08'25'')	(42°17'10'')

CHAPTER 3

THEORETICAL DEVELOPMENTS

3.1 THE APPROACH OF CHEMICAL BONDING

For very many years scientist have been wondering as to how atoms are held together in compounds. The clue to this problem was obtained from the stability of the electronic structure of inert gases, which led to the first modern hypothesis regarding the formation of the chemical bond. The underlying idea was that an atom combined with another in such way that both the atoms achieved an inert gas electronic structure. According to Pauling[1], a chemical bond exists between two atoms or group of atoms when the bonding force between them is of much strength as to produce an aggregate of sufficient stability to warrant its consideration as an independent molecular species.

Many factors, such as nuclear charge, radii of combining atoms, etc. influence the manner in which a chemical bond is formed. Since these factors vary from one atom to another, there arise a large number of compounds which may differ from one another to a great extent. When a bond is formed a redistribution, regrouping or reorientation of the electrons takes place in order to arrive at a stable arrangement. Pauling[1] has classified the chemical bonds in chemical systems in the following three extreme classes, viz. electrostatic bonds, covalent bonds and metallic bonds.

a) *Electrostatic bond* : When two or more atoms have the electronic configuration such that they can exists independent of each other, electrostatic interactions are set up which lead to strong attraction and the formation of a chemical bond known as an electrostatic bond. The most important electrostatic bond is the ionic bond, resulting from the Coulomb attraction of the excess electric charges of oppositely charged ions. The atoms of metallic elements lose their outer electrons easily, whereas those of nonmetallic elements tend to receive additional electrons; in this way stable cations and anions are formed, and as they approach one another a stable molecule is formed. Amongst

the simple ionic compounds, the most common structure is the rock-salt (NaCl) structure in which each ion is surrounded by six ions of opposite charge. Other electrostatic bonds, which usually occur in molecular crystals are ion-dipole bonds.

b) *Covalent bond* : A covalent bond is formed when two atoms share a pair of electrons of opposite spin. The electron density between the two atoms is large and the bonds are directional. The most common examples in which a covalent bond exists are substances having a diamond or zinc blende structure. The covalent compounds form relatively open structure because of the restriction imposed on the number of bonds that can be formed. The covalent bond is generally formed when the combining atoms have comparable ionisation energy.

c) *Metallic bond* : If all the constituent atoms in a solid have low ionisation energies, the outer electrons are completely delocalized in the lattice. The free electron gas collectively holds the ions together forming the metallic bond. The most striking characteristic of this bond that holds the atom together in a metallic aggregate is the mobility of the bonding electrons, which gives rise to the high electric and thermal conductivity of metals.

Although the properties of these extreme types of bonds are quite well defined, in nature many intermediate cases occur. Generally speaking, a substance is neither purely covalent nor purely ionic. Many physico-chemical properties of a substance are determined by the bond character. Therefore, it is necessary to know the bond character accurately. Several models based on different assumptions and approximation have been suggested to describe the electronic structure of solids and the nature of chemical bonds therein.

The purely ionic bond can be understood[2] satisfactorily on the classical electrostatic model. However, the covalent bond (as also the ionocovalent bond) arising essentially from the

superposition of electron clouds requires a quantum mechanical treatment. Generally, this problem is dealt under the variational approximation. The choice of trial wavefunctions of the system is usually based on physical intuition and the available information. The two major approaches to select the trial wavefunction are given by the valence bond theory and molecular orbital theory. These theories are discussed in brief in the following sections.

3.2 THE VALENCE BOND THEORY

The valence bond theory considers the atoms in a molecule as a set of individual atoms held together by localized covalent bonds. It is supposed that the bonding electrons spend on the average more time in between the atoms than upon the atoms themselves. In considering a molecule by the valence bond method each bond is treated separately. The orbitals of each pair of atoms participating in a bond are at first regarded as being the same as those of the isolated atoms. In order to obtain quantitative results, these orbitals are than modified to take into account the various interactions that occur[3]. The following method of constructing the interatomic orbitals was developed by Heitler and London[4] for homonuclear molecules.

Let $\psi_A(1)$ and $\psi_B(2)$ be the space wavefunctions of two unpaired electrons 1 and 2 in the valence shells of the two interacting atoms A and B. To obtain an interatomic orbital in a molecule, in which a pure covalent bonding exists, ψ_A and ψ_B are combined together in the following manner

$$\psi = \psi_A(1)\ \psi_B(2) \pm \psi_A(2)\ \psi_B(1) \qquad (3.1)$$

For combination of atomic orbitals for homonuclear atoms, the following conditions must be satisfied :

1) The combining orbitals must have approximately the same energy.

2) The combining orbitals must overlap.

3) The combining orbitals must have the same symmetry.

In this theory the energy of the interatomic orbitals is given by

$$E = 2E_o + \frac{C + A}{1 + S_{ab}}$$

where E_o = energy of the original atom in the ground state. C is the Coulomb integral and is given by

$$\iint \left[\psi_A(1)\ \psi_B(2)\right]^2 \left[\left(-\frac{e^2}{rb_1} - \frac{e^2}{ra_2} + \frac{e^2}{r_{12}} + \frac{e^2}{R} \right) d\tau_1\ d\tau_2 \right]$$

A, the exchange integral is

$$\iint \psi_A(1)\ \psi_B(2)\ \psi_A(2)\ \psi_B(1) \left[\left(-\frac{e^2}{rb_1} - \frac{e^2}{ra_2} + \frac{e^2}{r_{12}} + \frac{e^2}{R} \right) d\tau_1\ d\tau_2 \right]$$

and S_{ab}, the overlap integral is

$$\iint \psi_A(1)\ \psi_B(2)\ \psi_A(2)\ \psi_B(1)\ d\tau_1\ d\tau_2$$

In the above integrals R is the distance between the nuclei of the atoms A and B, r_{12} is the distance between the electrons 1 and 2, rb_1 and ra_2 are the distances of the two electrons 1 and 2 from the nuclei of the atoms B and A respectively, and $d\tau_1$ and $d\tau_2$ represent small elemental volumes around the atoms A and B respectively. The space wavefunctions (equation 3.1) do not take into account the difference of elecctronegativity between the combining atoms. In order to account for the ionic character of the bond, equation (3.1) is modified, assuming B to be more electronegative so that the configuration of the molecules becomes A^+ and B^-, as

$$\psi = \psi_A(1)\ \psi_B(2) \pm \psi_A(2)\ \psi_B(1) \pm \psi_B(1)\ \psi_B(2) \quad (3.2)$$

This equation is frequently written as

$$\psi = \psi_{cov} + \lambda\ \psi_{ion} \quad (3.3)$$

In the above equation λ represents the relative contribution of ψ_{ion} to that of ψ_{cov} in the formation of resultant orbital.

A major justification for the valence bond picture is that it is in accord with the observation that in a great variety of molecules the bonds between the same pairs of atoms are more or less similar. Thus the C-H bond in the hydrocarbon molecules always has almost identical properties, regardless of the particular molecule concerned. The valence bond picture seems attractive, with observed bond energies correlating nicely with the predicted number of bonds per molecule. It explains fairly well the bonding in simple systems, but in polyatomic molecules and crystalline solids the problem becomes far too complicated to be solved in any analytical way. Because of this, further development of the valence bond theory has been confined to intuitive empiricism until very recent times.

3.3 MODIFICATION OF VALENCE BOND THEORY

Several workers[1-5] have attempted to apply the valence bond formation for qualitative or semiquantitative analysis of bonding in different systems of special interest by introducing pertinent simplifying assumptions.

Pauling[1] has demonstrated that the bonds in metals are essentially covalent. He has introduced the concept of uninhibited resonance to account for metallic conduction and high coordination numbers in metals. This resonance is possible only if some of the orbitals in the valence shells of the atoms remain

empty. The metallic state is therefore characterized by covalent bonds arising from filling of the valence band of the solid.

Semiconductors are also of predominantly covalent type. Mooser and Pearson[6] and Krebs and Schottky[7] have pointed out the correspondence between the occupancy of atomic orbitals of constituting atoms and the bonds in semiconductors. They defined the semiconducting bond as follows : `The bonds in semiconductors are predominantly covalent and they form a network which runs continuously throughout the whole crystal structure. By sharing electrons in sharing electrons in forming the bonds, all atoms in the elemental semiconductors acquire filled valence subshells. In semiconducting compounds only the most electronegative atoms (i.e. the anions) need acquire filled subshells. If empty orbitals occur in the electropositive atoms (i.e. the cations) than any bonds that might form between these atoms alone must not run continuously through the lattice'.

The valence structure according to this theory are constructed by forming appropriate linear combination of atomic orbitals to obtain equivalent orbitals in different directions as demanded by the local geometry of the atom and the symmetry of the lattice. This process is referred to as hybridization. The formation of bonds many a times calls for promotion and transfer of electrons which modify the electronic configuration of the combining atoms. The relative importance of the different valence structures can be established from the interatomic distances and electronegativity differences. Resonance can occur amongst the valence structures only if they have the same number of unpaired valence electrons. For transition metal compounds magnetic properties offer[8] guidelines for arriving at the different possible structures.

3.4 MOLECULAR ORBITAL THEORY

This theory developed by Hund[9], Mulliken[10], Herzerg[11], Lennard-Jones[12] and others provides the most comprehensive treatment for studying the electronic structure of the molecule. It describes[13] any state of the molecule by a single many-electron configuration for any type of bonding. The electronic orbitals extend over the entire molecule allowing for extensive delocalization of the electrons. However, the localized bonding, characterized by the significantly large amplitudes of the wavefunctions of the electrons in between the atoms is treated as a special case. This theory clearly demonstrates the correspondence between the bonds in the compounds and the energy levels of the component atoms.

The molecular wavefunctions which describe the probability amplitude for electrons bound to the set of ions constituting the molecule look like atomic ones in the neighbourhood of the component atoms. They are formed by making suitable linear combinations of outer atomic orbitals of the individual interacting atoms. In the formation of molecular orbitals the conditions[14] concerning energy, overlapping and symmetry mentioned in the valence bond theory are also applicable.

The number of molecular orbitals formed is always the same as the total number of participating atomic orbitals. The values of the coefficients of the atomic orbitals in the expression of the wavefunctions of the molecule, are evaluated variationally and the energies of the molecular levels are obtained by solving the schrodinger equation. In the molecular orbital energy level diagram thus obtained, the electrons are distributed according to the Aufbau and exclusion principles. For degenerated levels Hund's rules are observed. The method[15] is briefly described below for a homopolar diatomic molecule, H_2.

The valence orbitals of the hydrogen atom is 1s. Hence, the wave function of an orbital for the molecule H_1-H_2 is the correct

linear combination of the two 1s wave functions and can be written as

$$\psi_{MO} = a\,(\psi_{1s}{}^{1}) + b(\psi_{1s}{}^{2}) \qquad (3.4)$$

Solving the Schrondinger equation $H\psi = E\psi$ and using the above value of ψ one gets

$$\psi^{b} = \frac{1}{\sqrt{2}}\,(\psi_{1s}{}^{1} + \psi_{1s}{}^{2})$$

$$\psi^{a} = \frac{1}{\sqrt{2}}\,(\psi_{1s}{}^{1} - \psi_{1s}{}^{2}) \qquad (3.5)$$

The energies corresponding to these molecular orbitals are

$$E^{b} = q + \beta$$

$$E^{a} = q - \beta \qquad (3.6)$$

where q is the Coulomb integral (which is equal to the energy of the electron in the ground state of the isolated atom).

$$q = \int (\psi_{1s}{}^{1})\, H\, (\psi_{1s}{}^{1})\, d\tau$$

$$= \int (\psi_{1s}{}^{2})\, H\, (\psi_{1s}{}^{2})\, d\tau \qquad (3.7)$$

and β is the exchange (resonance) integral which represents the energy of interaction between the combining orbitals and is a negative quantity.

$$\beta = \int (\psi_{1s}{}^{1})\, H\, (\psi_{1s}{}^{2})\, d\tau$$

$$= \int (\psi_{1s}{}^{2})\, H\, (\psi_{1s}{}^{1})\, d\tau \qquad (3.8)$$

The molecular orbital having energy $q + \beta$ is more stable than the individual valence atomic orbitals. Such a molecular

orbital is called a bonding orbital. The molecular orbital having energy q-β is less stable than the initial atomic orbitals and is referred to as an antibonding orbital. The molecular orbitals which are symmetric with respect to rotation about the axis connecting the two nuclei are referred to as σ orbitals, and if they posses nodal planes along the line joining the two bonded atoms they are called π orbitals. The antibonding orbitals of above type are denoted as σ^* and π^*. If Z is the interatomic axis then, s-s, s-p_z, p_z-d_{z^2} etc. will be σ orbitals and p_x-p_x, p_y-p_y etc. will be π orbitals. The angular momentum of a σ orbital about the chemical bond is zero, while that of a π orbital is unity. A few cases of bonding and antibonding (both σ and π) orbitals are illustrated in Figure 3.1.

In the case of predominantly covalent bonding the electrons in a bonding orbital are found to be most of the time in the overlap region, giving rise to attractive binding force between the nuclei. Thus, the molecular orbital theory gives a physical description of the covalent bond similar to the one given by the valence bond theory. The electron in the antibonding orbital has its density concentrated in the region farther from the nuclei than in the case of the atomic orbitals of the isolated atoms and hence it leads to an energetically unfavourable repulsive state.

In the case of hetronuclear diatomic molecules the MO's are not symmetric with respect to the plane perpendicular and bisecting the internuclear axis. The wavefunctions of the MO's are given by

$$\psi^b = \frac{1}{\sqrt{2+2S}} (\psi_A + \lambda\psi_B)$$

$$\psi^a = \frac{1}{\sqrt{2+2S}} (\psi_A - \lambda\psi_B) \qquad (3.9)$$

where S is an overlap integral and λ is the mixing coefficient. The bonding in hetronuclear molecules is generally polar in

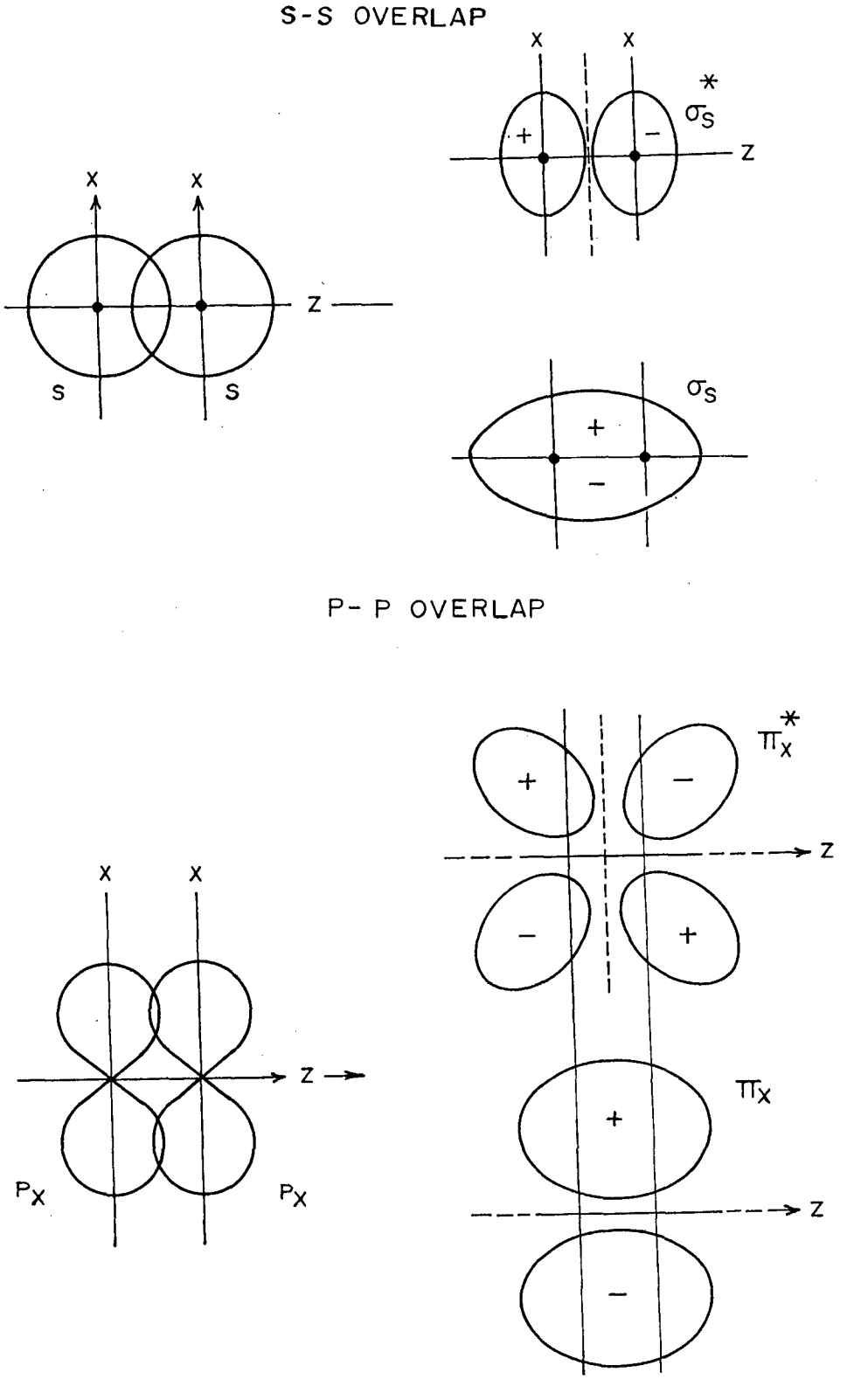

Figure 3.1: Bonding and antibonding (both σ and π) orbitals

Whenever the energies of the atomic orbitals are vastly different, their mixing is insignificant and the MO's resemble the atomic orbitals. A bonding molecular orbital has a predominant character of the atomic orbital which is energetically closer to it. The MO's then appear as if they are localized on the atoms. Such MO's are commonly found in ionic substances.

In complex molecules the molecular orbitals are very sensitive to the local symmetry of the central metal ion. Group theoretical principles are generally used[16,17] to find out the possible orbital overlaps compatible with the geometry of the surroundings in order to construct the semiempirical MO energy level diagrams. It should be noted[18] that complete MO and VB treatments always lead to same result if the same atomic orbitals are used as the starting point. In practice, however, in complicated molecules these methods cannot be carried out to completion. Since one has to take recourse to approximations which are different in the two procedures, by the two methods show only qualitative agreement.

3.5 LIGAND FIELD THEORY

Becquerel[19], Bethe[20] and Van Vleck[21] have developed the crystal field theory in order to provide a relative classification of energy levels of d electrons of transition metal ions in chemical environment of different geometries. This theory treats the interaction between the metal ion and the surrounding ions as purely electrostatic in nature. The ionic arrangement around the metal atom is represented by spatial distribution of point charges due to the neighbouring atoms and the group theoretical symmetry arguments are used to predict the electronic state of the ion. The crystal field theory has been modified by Orgel and others in order to take account of the

partial covalent character of bonding in transition metal compounds and complexes by adjusting certain parameters in accordance with experimental results. the theory is then referred to as adjusted crystal field theory. However, this theory also is successful only in the case of moderate metal-ligand orbital overlaps.

It is very well known that the MO theory can describe interatomic interactions for all types of bonding and takes into account all valence orbitals of the metal and ligand atoms. However, the calculations of the molecular orbitals become very much involved when the theory is applied to complicated structures. Therefore, a hybrid approach has been developed in order to describe the energy level distribution for coordination clusters by combining the crystal field theory and the molecular orbital theory. In this approach, called the ligand field theory, one first takes account of the splitting of the inner d orbitals of the central ion due to electrostatic field in the chemical compounds or complexes as in the crystal field theory and then the molecular orbitals are formed as given by the LCAO-MO model. In recent years the theory has been widely accepted[22-24] as it appears to explain satisfactorily most of the properties of transition metal compounds, at least qualitatively if not quantitatively.

3.6 CONCEPTS OF ELECTRONEGATIVITY, IONICITY AND EFFECTIVE CHARGES

A very useful concept in Chemistry has been that of electronegativity, which according to Pauling[25] is the power of an atom in a molecule to attract electrons to itself. When two elements, eg. A and B differ in electronegativity (denoted by X_A and X_B receptively), one finds that in general the heat of formation D_{AB} of the AB bond satisfies the relation

$$D_{AB} > \frac{(D_{AA} + D_{BB})}{2} \qquad (3.10)$$

where D_{AA} and D_{BB} represent the bond energies of the elements A and B respectively. The excess energy

$$\Delta_{AB} = D_{AB} - \frac{(D_{AA} + D_{BB})}{2} \qquad (3.11)$$

is called `ionic resonance energy' and is related to the electonegativities X_A and X_B by

$$\Delta_{AB} = 23.06 \, (X_A - X_B)^2 \qquad (3.12)$$

Making use of this relation[26] Pauling has worked out, taking bond energy values from thermodynamic data, an electronegativity scale for different elements in the periodic table.

In the more general case for a compound like AB_n the heat of formation is obtained by summing the expression over all the bonds in the molecules giving

$$\Delta_{AB} = 23.06 \, (X_A - X_B)^2 \, n \qquad (3.13)$$

where n is the chemical valence.

When two atoms with different electonegativities combine, the valence electron distribution in the bond is assymmetric. The electron density is greater near the more electronegative atom due to the charge transfer. The ionic character or the polarity of the bond is estimated by Pauling[1] with the help of the dipole moment of the molecules. He observed the correlation between the dipole moment and the electronegativity difference between the constituent atoms and derived empirically the relationship

$$I_m = 1 - \exp \left[- \frac{(X_A - X_B)^2}{4} \right] \qquad (3.14)$$

where the parameter I_m represents the ionicity of the bond in the molecule.

The values of ionicity obtained from equation 3.14 are justified for single bonds only, as in the case of isolated simple molecules in the gaseous state. Pauling has later modified this expression for multiple bonds and various coordinations existing in a crystal as

$$I = 1 - \frac{n}{c} \exp\left[- \frac{(X_A - X_B)^2}{4} \right] \qquad (3.15)$$

in which n is the valence of the cation and c its coordination number. The physical interpretation of expression 3.15 is that the total covalence n(1-I) is being shared amongst c bonds.

The formation of a chemical bond brings about a rearrangement of the outer electrons of the combining atoms, giving rise to a net charge on them. This effective charge, q, on the anion can be obtained[27] from the simple definition of bond ionicity as

$$I = \frac{q}{Q} \qquad (3.16)$$

where Q, the formal charge on the ion in a molecule or a crystal is obtained by noting the charge in the ideally ionic configuration. It has been shown that in the case of larger molecules of complicated structure the effective charge is given by the relation[28]

$$q = Q' + \Sigma I \qquad (3.17)$$

where I, the partial bond character, is summed over all the bonds, and Q' is the formal charge on the ion.

Siegbhan[28,29] and others[30] have used Pauling's method to calculate the atomic charges in the compounds. According to Siegbahn the charge on an atom in a molecule is calculated by

taking the sum of the partial ionic characters (which are obtained from the electronegativities X_A and X_B through the relation 3.14) of the bonds with the next neighbours with appropriate signs. One thus gets

$$q = \sum \left[1 - \exp \left\{ 0.25 \left(X_A - X_B \right)^2 \right\} \right] \qquad (3.18)$$

The value of this sum is dependent on the relative electronegativities of the ions under consideration.

In recent years several workers have attempted to calculate the effective charges on the atoms in molecules by more rigorous methods. Amongst these mention may be made here of the more popular methods, such as complete neglect of differential overlap (CNDO), ab intio and extended Hûckel methods. It has been found[31,32] that the empirical formulation for the atomic charges given by Pauling is in fairly good agreement with the atomic charges obtained by the more modern methods, so far as relative magnitudes are concerned. Moreover, Paulings simple formalism has the advantage that it can be easily applied to all types of molecules unlike other sophisticated methods.

Pauling's scale of electronegativity has been refined by Allred[33] using more accurate thermochemical data. However it is evident that Pauling's definition of electronegativity is independent of the valence environment and the state of hybridization of the atoms. A new scale of electronegativity proposed by Mulliken[34] gives a more exact relationship between the properties of atoms and their electronegativities. He has defined atomic electronegativity as the average of the ionization potential and the electron affinity of the neutral atom. This scale gives[35] different values of electronegativities for elements depending upon their oxidation number, coordination structure and the state of hybridization of the atom. Although

the ionization potentials can be deduced from the spectroscopic observations, there exists a shortage of information on electron affinities. In recent years, several workers have tried to evolve more refined scales of electronegativities based on attractive force constants (Gordy[36,37]), compactness of electron density distribution (Sanderson[38]), electrostatic calculations (Allred and Rochow[39]) etc. Although the trend of the values of electronegativity in all these scales is more or less the same, none of them seems to be fully satisfactory.

Finally, it may be noted that using the concepts of electronegativity, and ionicity several methods were proposed by different workers for determining ionicities and effective charges in compounds. Mention may be made here of the work of Pauling[1], Suchet[40,41], Coulson[42], Phillips[43], Levine[44] and Wemple[45]. In the X-ray spectroscopy these chemical parameters have been frequently used. By correlating some spectral features with these quantities, useful information on the nature of chemical bonding in unknown materials is obtained.

REFERENCES

1. L.Pauling, The nature of the Chemical Bond, Third Edition Oxford and IBH Publishing Co., Calcutta 1960).

2. C. Kittel, Introduction to Solid State Physics, (Wiley, New York, 1966).

3. P.J. Durrant and B. Durrant, Introduction to Advanced Inorganic Chemistry (Longmans 1962).

4. W. Heitler and F. London, Z. Phys.44, 455 (1927).

5. H.Welker, Z. Natuforsch 7a, 744 (1952).
: Z. Natuforsch 8a, 248 (1953).

6. E. Mooser and W. B. Pearson, Phys. Rev. 101, 1608 (1956).
: J. Electronics 1, 629 (1956).

7. H. Krebs and W.Schottky, Helbleiterprobleme I (Frieder Viewg and Sohn Braunschwing 1954) p.25.

8. F. Hulliger, Structure and Bonding (Springer Verlag, Berlin 4, 83 (1968).

9. F.Hund, Z. Electrochem, 34, 437 (1928).

10. R.S.Mulliken, Rev. Mod. Phys. 2, 60 (1930).

11. C. Herzberg, Z. Physik 57, 601 (1929).

12. Lennard-Jones, Trans. Farad. Soc. 25, 668 (1929).

13. H. H. Jaffe and H. Orchin, Theory and Application of Ultraviolet Spectroscopy (John Wiley and Sons Inc., New York 1962).

14. C. J. Ballhausen and H. B. Gray, Molecular Orbital Theory (Benjamin, New York 1964).

15. H.B.Gray, J.Chem. Education 41, 2 (1964).

16. F. A. Cotton, Chemical Applications of Group Theory (Wiley Interscience, New York 1963).

17. D.S. Urch, Orbitals and Symmetry (Penguin Education, London (1970).

18. A.S. Gubanov, Quantum ELectronic Theory of Amorphous

Semiconductors (Consultant's Bureau New York 1965).

19. J.Becquerel, Z. Physik 58, 205 (1929).

20. H.Bethe, Ann. Physik 3, 135 (1929).

21. J.H.Van Vleck, Theory of Magnetic and Electric Susceptibilities, Oxford University Press, Oxford (1932).

22. C.J.Ballhausen, Introduction to Ligand Field Theory, McGraw-Hill, New York (1962).

23. L.E.Orgel, An Introduction to Transition Metal Chemistry: Ligand Field Theory, Methuen and Co., London (1960).

24. B.N.Figgis, Introduction to Ligand Fields, Interscience Publishers, New York (1966).

25. L.Pauling, J.Amer. Chem.Soc. 54, 5370 (1932).

26. B.E. Douglas and D.H. Mcdaniel, Concepts and Models of Inorganic Chemistry (Oxford IBH Publishing Co. New Delhi 1965).

27. E.Mooser and W.B.Pearson, Nature, 190, 406 (1961).
:Nature, 192, 335 (1961).

28. K.Siegbahn et al, E.S.C.A., Atomic, Molecular and Solid State Structure Studies by means of Electron Spectroscopy (Almquist and Wiksells Publishing Co., Uppasala 1967 pp.108).

29. K.Siegbahn, Phil. Trans. R. Soc., A 268, 33 (1970).

30. W. L. Jolly, J. Amer. Chem. Soc., 92, 3360 (1970).

31. M.E. Schwartz, J.D. Switalski and R.F. Stronski, Electron Spectroscopy, Editor D. A. Shirley (North-Holland Publishing Co., Amsterdam, London 1972, pp.605).

32. W.L.Jolly, Electron Spectroscopy, Editor D.A.Shirley (North -Holland Publishing Co., Amsterdam, London 1972, pp.629).

33. A.L.Allred, J. Inorg. Nucl. Chem., 17, 215 (1961).

34. R.S.Mulliken, J. Chem. Phys., 2, 782 (1934).

35. J.P. Suchet, Chemical Physics of Semiconductors, (D. Van Nostrand Co. Ltd., London 1965 pp.103).

36. W.Gordy, J. Chem. Phys., 14, 305 (1946),
: Phys. Rev., 69, 604 (1946).

37. W.Gordy and W.J.O.Thomas, J. Chem. Phys., 24, 4396 (1956).

38. R.T.Sanderson, Chemical Periodicity (Reinhold Publishing Co., New York, 1960).

39. A.L. Allred and E.G. Rochow, J. Inorg. Nucl. Chem., 5, 264 (1964).

40. J. P. Suchet and P. Baily, Ann. Chem., 10, 517 (1965).

41. J.P. Suchet, Crystal Chemistry and Semiconduction in Transition Metal Compounds, Academic Press, New York and London, 1971.

42. C.A.Coulson, L.R.Redei and D.Stocker, Proc. Roy. Soc., 270, 357 (1962).

43. J.C.Phillips, Rev. Mod. Phys., 42, 317(1970); Bond and Bands in Semiconductords, Academic Press, New York and London, 1973.

44. B.F.Levine, Phys. Rev., B 7, 2591 and 2600 (1973).
: J. Chem. Phys., 59, 1463 (1973).

45. S.H.Wemple, Phys. Rev., B 7, 4007 (1973).

CHAPTER 4

VANADIUM K-ABSORPTION EDGE STRUCTURE

4.1. INTRODUCTION

X-ray absorption spectrum has traditionally been divided into a low energy region the so-called X-ray absorption near edge structure (XANES), in which the transitions are to bound states[1-3], and a high energy region, the so-called extended X-ray absorption fine structure (EXAFS), where the transitions are to free electron states[4-5]. Recently, as mentioned in Chapter 1, high intensity X-ray sources have become available whose intensities are about 10^5 times higher than those previously available. This results in improved signal to noise ratios, which allow meaningful measurements to be made even on dilute systems[5-6].

In this Chapter we present our measurements, made with X-rays from Rigaku X-ray generator, on K X-ray absorption spectra of superconducting oxides containing vanadium and several model vanadium compounds. The model compounds which we have studied in the present work are $CrVO_4$, $GdVO_4$, $BiVO_4$, $Cd_4V_2O_7$, $Ca_3Fe_3GeVO_{12}$, $Pb_5(VO_4)_3Cl$, $Zn_2(VO_4)_3$, $NaVO_3$, $VO(acac)_2$, $VO(bzac)_2$, $(NH_4)_4[VO\text{-}dd\text{-}tart]_2.2H_2O$, VOPC, VOTPP, $VOMoO_4$, V_2O_5, VO, $(NH_4)_2SO_4.VSO_4.6H_2O$, V_2O_3, $SmVO_3$, V_2S_3, VN, VO_2, V_4O_7, VC, [VO(hshed)(acac)], PbV_2O_6 and $Ca_3V_{10}O_{28}.16H_2O$. The superconducting oxides of vanadium include compounds of composition $Tl_{1-x}V_xSr_2(Ca_{0.8}V_{0.2})Cu_2O_y$, where x = 0.2, 0.3, 0.4 and 0.5. Electronic transitions from the 1*s* to 3d, 4*s* and 4p states, in the model compounds as well as in superconducting oxides have been assigned to different spectral features observed in the vanadium K-edge spectra on the basis of atomic model of Shulman et al[7] and others[8-11].

---

tart = tartrate ($C_4H_2O_6$)

acac = acetylacetonate ($C_5H_7O_2$)

bzac = benzoylacetonate ($C_{10}H_9O_2$)

Pc = phthalocyanine ($C_{32}H_{16}N_8$)

TPP = tetraphenyl porphyrin

hshed = N-salicylidene-N'-(2-hydroxyethyl)-ethylenediamine

4.2. RESULTS AND DISCUSSION

The zero of the energy scale of the XANES spectra was taken with respect to the first inflection point of the vanadium metal in the first derivative spectrum at 5465.0 eV, which, according to Bearden and Burr[12], marks the threshold or onset of photoejection of the 1s electron in vanadium metal. All the spectra were normalized by fitting a linear function to the pre-edge data and fitting cubic spline to the EXAFS region of the data upto 400 eV, extrapolating both functions to the zero of energy i.e. the inflection point energy [and taking the difference (the edge step height)], subtracting the pre-edge data function from each point in the experimental spectrum, and dividing by the step height. This procedure results in a normalization of the data to the unit step height. The energy positions of the important spectral features in all the compounds studied in this work are given in Table 4.1.

4.3. ASSIGNMENT OF ELECTRONIC TRANSITIONS

Before discussing our results on X-ray absorption measurements, it would be interesting to mention here that in the case of X-ray absorption spectra of transition metal compounds studied by various authors[13-21], the K-absorption edges exhibit a weak low-energy peak at the threshold followed by a shoulder on a rising absorption curve that culminates in a strong peak. Through an examination of a series of cubic perovskites of first-row transition metals, KMF_3 (where M = Mn, Fe, Co, Ni, and Zn), Shulman et al[7] assigned the lowest energy features in such edges

as 1s → 3d transitions, the intermediate feature as a 1s → 4s transition, and the dominant peak as 1s → 4p transition. It is observed by these authors that the experimentally measured energies of these features agree rather well with the spectroscopic energy levels of the Z+1 (where Z is an atomic number) ions. Similar assignments have been made previously by other authors[8-11].

The assignments, 1s → 3d, 1s → 4s and 1s → 4p, although useful in a qualitative sense, are unsatisfactory in one respect. They are based on an atomic model for the available orbitals that does not allow for covalent bonding. Clearly, the final orbitals for the lower energy transitions cannot be of pure d or s character, since the angular momentum selection rules forbid 1s → n d or 1s → (n+1) s transitions. Shulman et al[7] have claimed that vibronic mixing of s, p and d characters makes the low energy transitions allowed. However, in many complexes covalent interactions between metal and ligands could also cause such mixing, in which case a molecular orbital (MO) description of the electronic transitions would be more desirable. In section 4. 4, the MO scheme has therefore been used for interpretation of X-ray absorption spectra.

Most of the studies on the near-edge structure so far carried out by various authors have been primarily experimental in nature. Comparisons were made only with calculated molecular energy level spacings; no transition strengths were included. However, more quantitative calculations for the near-edge structure in transition-metal compounds have been done and few results have been published. Bair and Goddard[22] have carried out *ab initio* self-consistent field calculations on the excited states of the $CuCl_2$ molecule involving excitations of the Cu 1s orbital into bound valence and unbound virtual orbitals. These authors have calculated both the absolute excitation energies and the transition strengths, and considered the presence of a fully

relaxed core hole, in their theoretical method based on a multielectron model utilizing a Hartree-Focks configuration - interaction approach. They have found that the weak pre-edge peak is indeed due to a transition to a partially unoccupied orbital of a primarily metal 3d character, in agreement with the above discussion. The main absorption peak at 8993 eV is assigned as a transition to the orbitals that are primarily of a metal 4p character ($1s \rightarrow 4p_z$) again in agreement with some of the above studies. However, the shoulder (the lower energy feature at 8986 eV) is not assigned to any single - electron transition. The $1s \rightarrow 4s$ monopole transition strength is found to be far too weak to be observed and appears at the wrong energy to fit the shoulder peak data. Rather, this feature is reassigned by these authors to a "shake down" satellite transition involving a Cu $1s \rightarrow 4p_z$ transition simultaneous with ligand-to-metal charge transfer.

A similar interpretation has recently been proposed[23-24] for the polarised spectra of $CuCl_2.2H_2O$ and $(creat)_2CuCl_2$. Satellite peaks, which are pronounced in inner-shell XPS studies of many transition-metal complexes[25-29], are predicted to be significantly reduced in intensity in X-ray absorption edge studies due to the shielding of the valence electrons when the photoelectron is in the low-energy threshold region. A previous study[30] comparing the XPS and X-ray absorption spectra of $FeCl_2$, $MnCl_2$ and $CoCl_2$ found low intensity satellites to the high energy side of the principal absorption maxima at energies corresponding to those expected on the basis of the prominent satellite splittings found in XPS. More rigorous calculations have been reported by Kutzler et al[31] who have performed self-consistent field X_α multiple scattering wave calculations for the near-edge of iron, chromium and molybdenum compounds. Like Bair and Goddard, they calculated one-electron transition strengths into bound and continuum states including the fully relaxed core hole. The results of these numerical studies indicate that a molecular

cage defined by the first shell of ligands, which breaks the inversion symmetry at the metal atom site, can make transition from a 1s electron state to a bound state of a mainly nd character possible via admixture with p orbitals from liganding atoms. They also show that the shoulder or kink, which has been assigned by several authors to a 1s → (n+1)s transition, appears to be an inherent feature of the continuum and that the principal absorption maximum correspond to a 1s → (n+1)p transition. However, it is worth noting that the results of Kutzler et al fail to predict the various shoulder peak splittings observed in the measured spectra of transition-metal compounds[32-35]. These authors speculated that many-electron processes (such as shake-down transition considered by Bair and Goddard) may be involved but they do not attempt to incorporate such effects into their calculations.

From the above studies we see that interpretation and calculation of the near-edge structure for the transition-metal compounds is much less clear cut. Many-electron effects due to an incompletely screened core hole appear to be sufficiently important to alter the simple molecular orbital or symmetry-based transition scheme invoked by various investigators. Although it appears that we are safe in labelling the pre-edge peak and main absorption maximum as 1s → 3d and 1s → 4p transitions, respectively, more corroborating calculations are needed before a definite assignment of the shoulder peak is possible.

Vanadium K-absorption spectra in vanadium metal and typical vanadium compounds are shown in Figures 4. 1, 2, 3, 4 and 5. In Figure 4.6 are given the near-edge absorption spectra of vanadium in superconductors of the composition $Tl_{1-x}V_xSr_2(Ca_{0.8}Y_{0.2})Cu_2O_y$, where x = 0.2, 0.3, 0.4 and 0.6. These spectral curves were obtained by averaging the results of a very large number of spectra recorded for each sample. For the superconductors, 25 scans of each were recorded in order to confirm all the fine

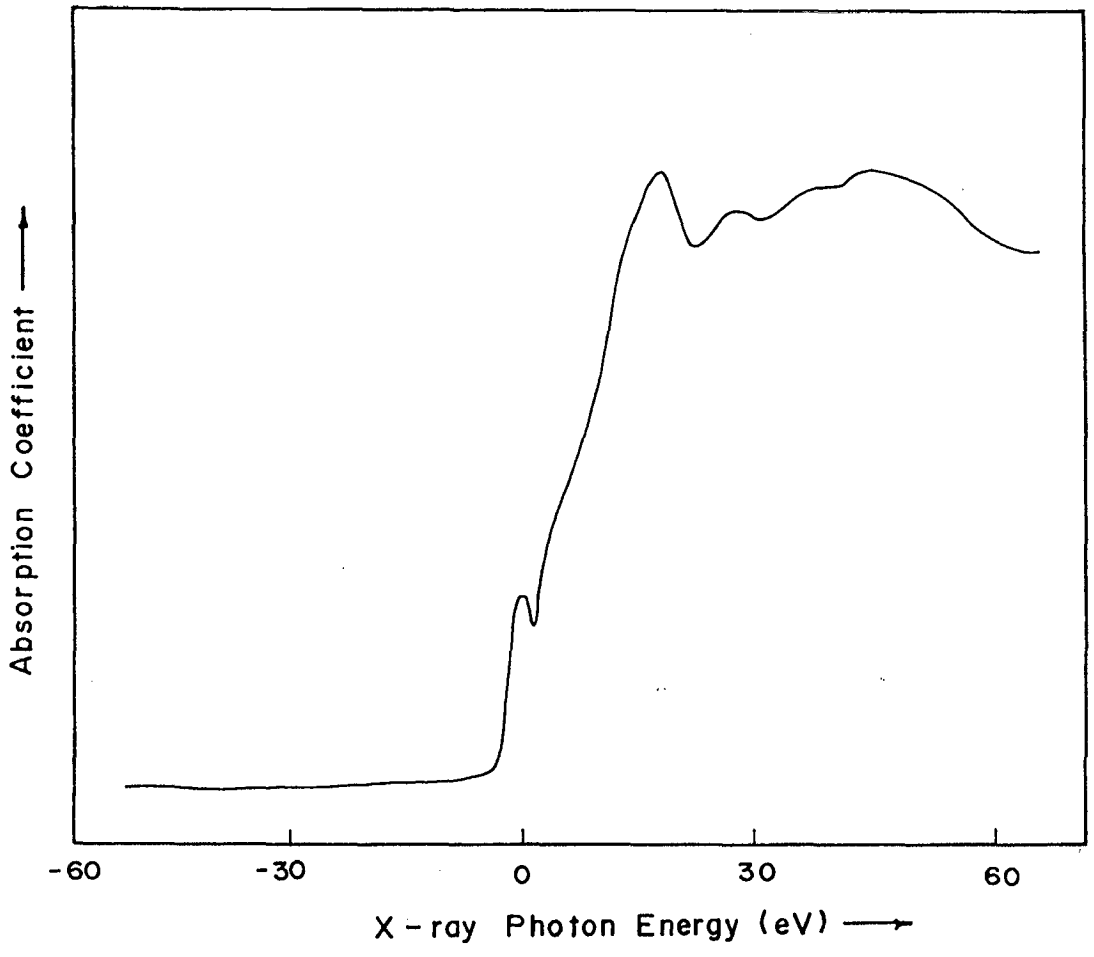

Figure 4.1: X-ray absorption spectrum of Vanadium metal

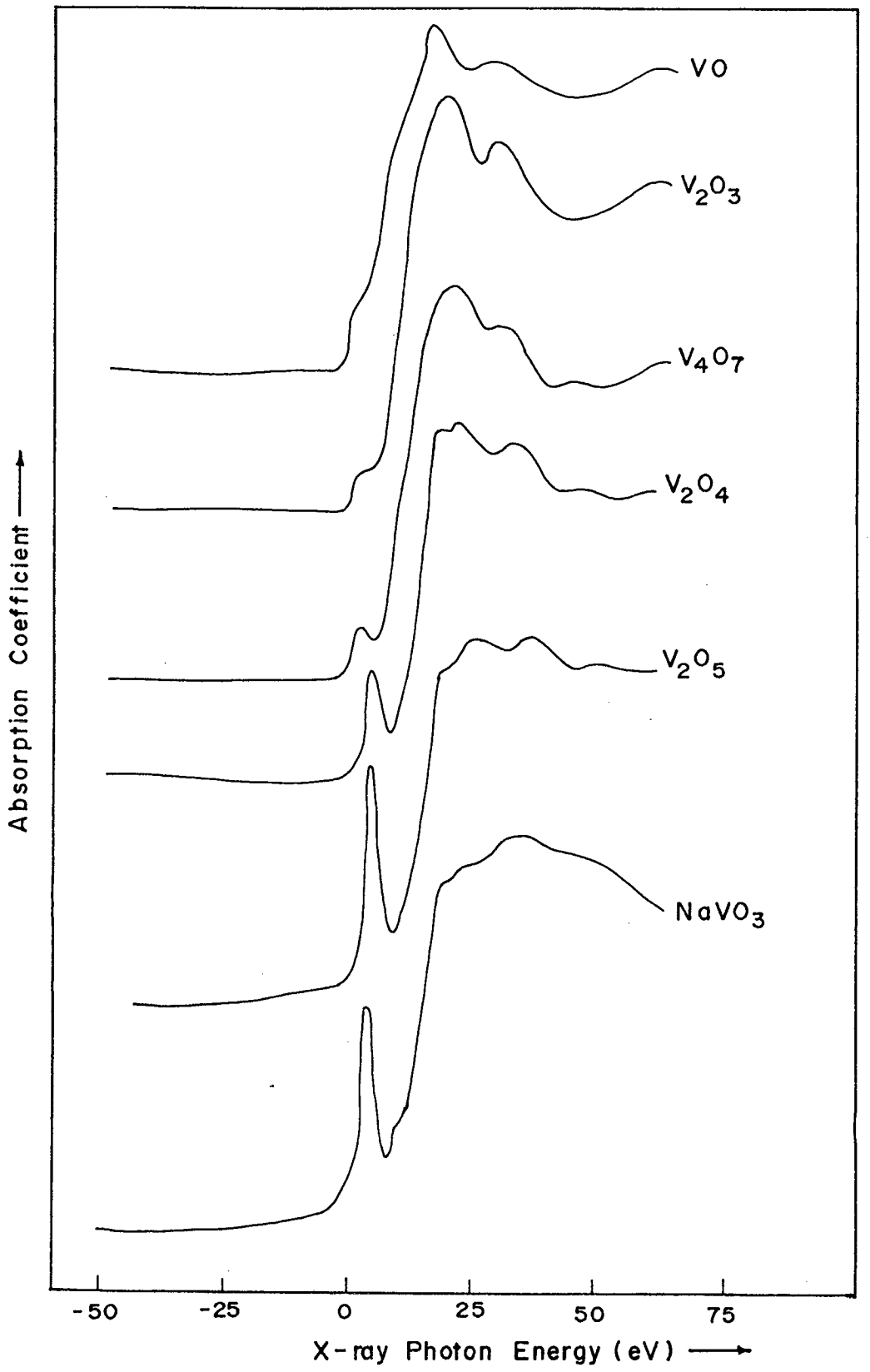

Figure 4.2: X-ray absorption spectra of VO, V_2O_3, V_4O_7, V_2O_4, V_2O_5 and $NaVO_3$

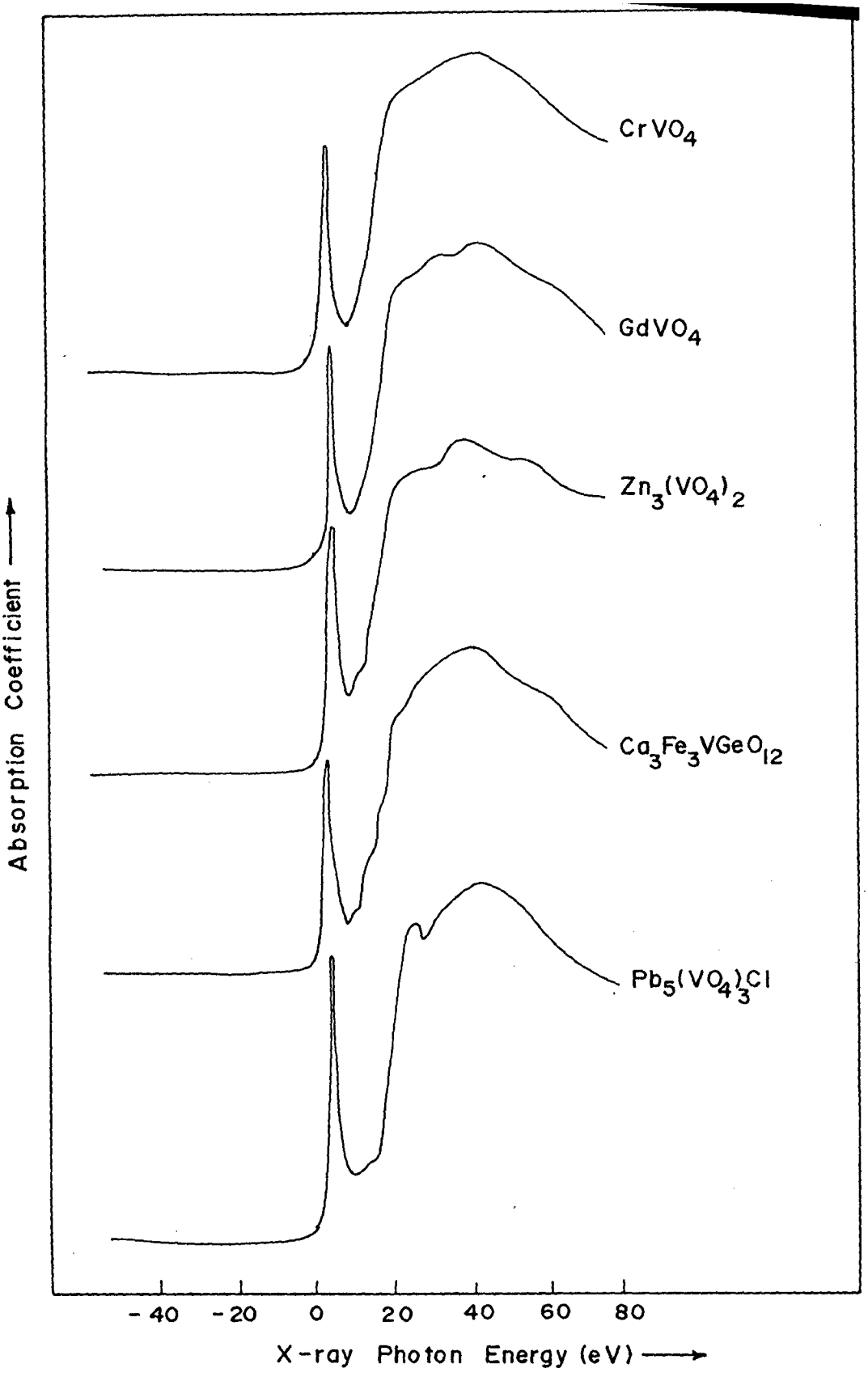

Figure 4.3: X-ray absorption spectra of $CrVO_4$, $GdVO_4$, $Zn_3(VO_4)_2$, $Ca_3Fe_3VGeO_{12}$ and $Pb_5(VO_4)_3Cl$

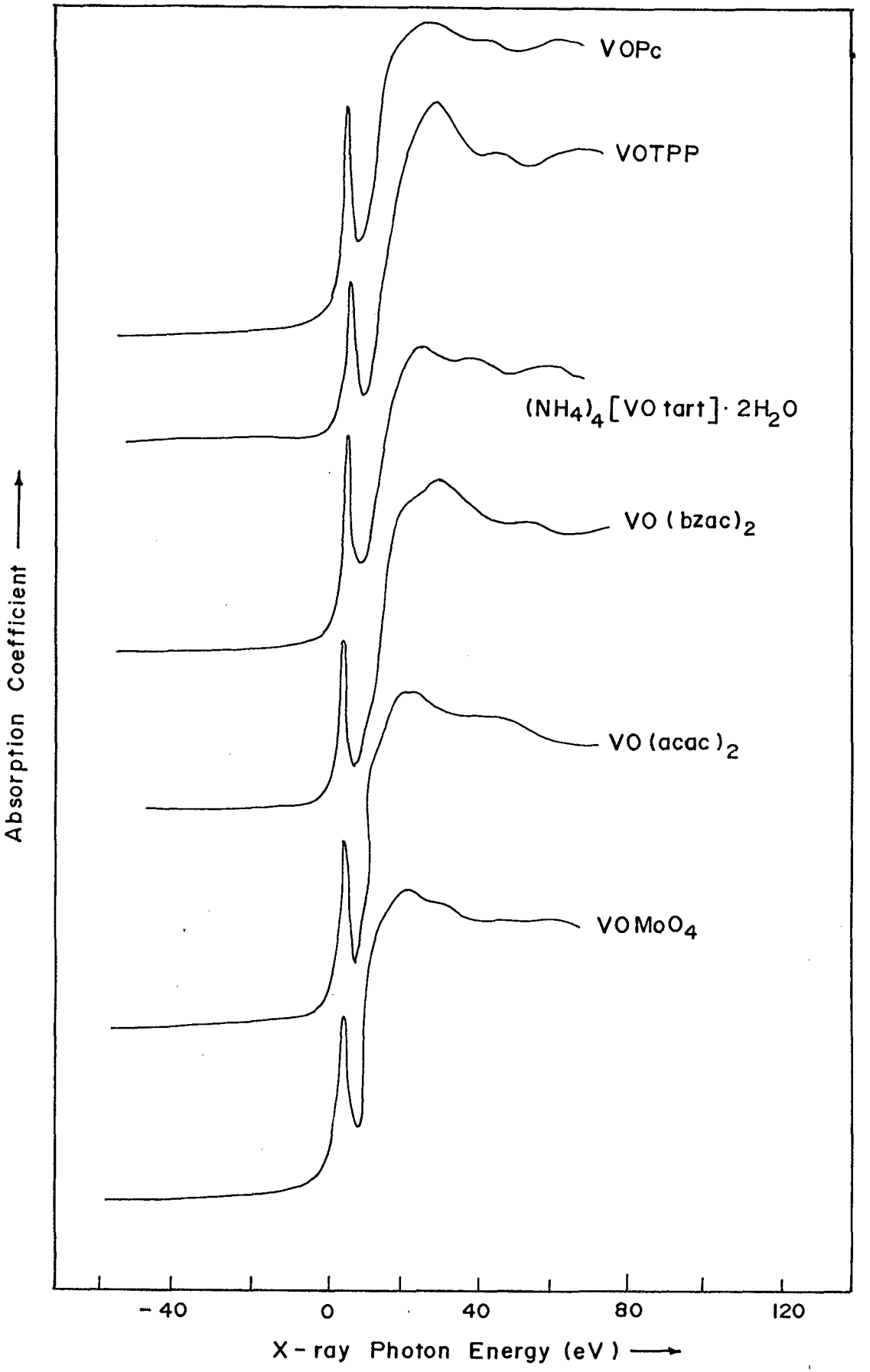

Figure 4.4: X-ray absorption spectra of VOPc, VOTPP, $(NH_4)_4$[VO tart].$2H_2O$, $VO(bzac)_2$ and $VO(acac)_2$

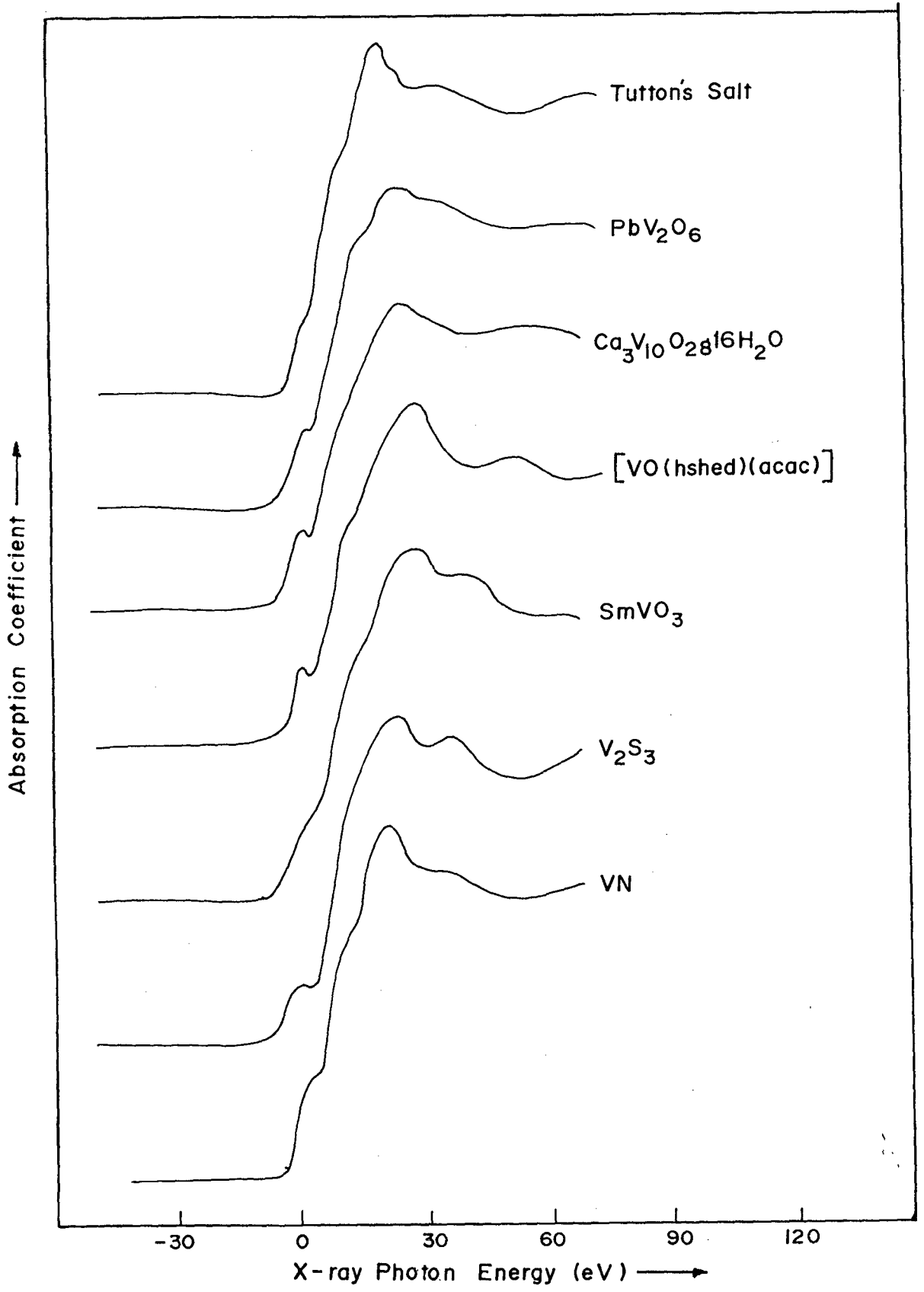

Figure 4.5: X-ray absorption spectra of Tutton's salt, PbV_2O_6, $Ca_3V_{10}O_{28}.16H_2O$, [VO(hshed)(acac)], $SmVO_3$, V_2S_3 and VN

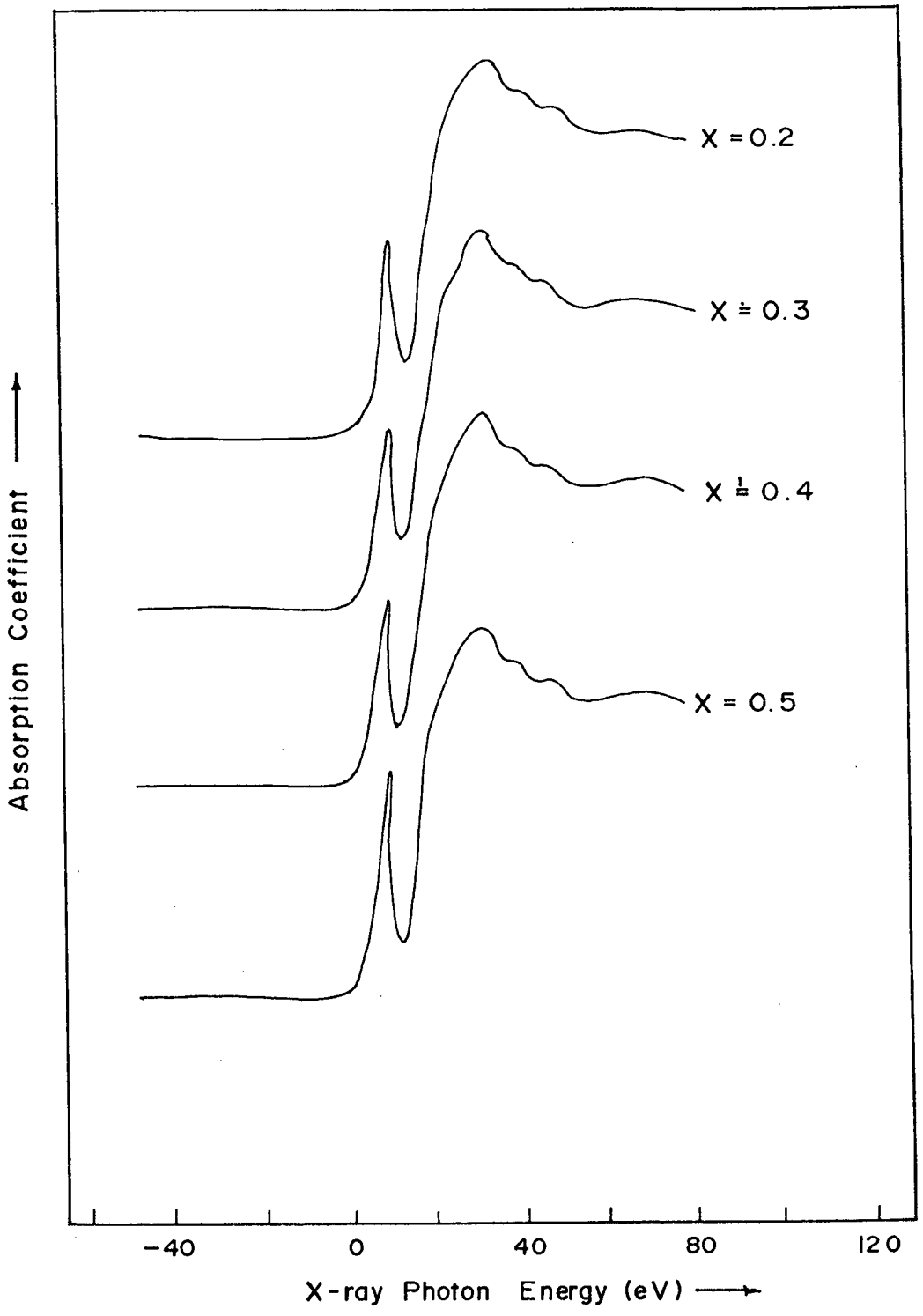

Figure 4.6: X-ray absorption spectra of $Tl_{1-x}V_xSr_2(Ca_{0.8}Y_{0.2})Cu_2O_y$, where x = 0.2, 0.3, 0.4 and 0.5

structure peaks.

It is observed from Figure 4.1 that the K absorption edge of vanadium metal splits into three components. In the case of the vanadium compounds the absorption discontinuity is seen to split into three or more components. Our results in this respect are in good agreement with those obtained by Wong et al[36] for vanadium metal and some of the compounds studied. For compounds viz. $Zn_2V_2O_7$, PbV_2O_6, $(NH_4)[VO\text{-}dd\text{-}tart]_2.2H_2O$, $Ca_3Fe_3GeVO_{12}$, $GdVO_4$, etc., no experimental data are available for comparison.

We shall first discuss our results on the near edge structure in model compounds having vanadium ions at tetrahedral, square pyramidal and octahedral sites and then we shall use these results to extract structural information in the superconducting oxides of vanadium. The relevant structural data on all the compounds are presented in Table 4.2 (Refs. 37 - 61).

4.3.1. VANADIUM K - EDGE IN MODEL COMPOUNDS

The K-absorption near edge spectra of transition metal compounds are rich in information from which details on the coordination environment can be deduced. The profiles of the vanadium K - absorption edge in Figures 4. 1, 2, 3, 4 and 5 show a pre-edge feature at the threshold followed by a shoulder on the rising absorption curve which culminates in a strong absorption peak. The pre-edge peaks are due to the transitions of the photoelectron to final states that are essentially vanadium 3d bound states. These transitions are quite sensitive to the crystal field[62-63] due to ligands around vanadium and hence the number, position, and intensity of these pre-edge peaks give information about the coordination environment of vanadium.

The main reason for this can be found in the d^0, d^1, d^2, d^3 electronic configurations of V^{5+}, V^{4+}, V^{3+} and V^{2+} ions respectively. All the d symmetry molecular levels are vacant

completely or partially depending on the oxidation state of vanadium and available to receive the photoelectron to give $(1s)^1(3d)^1$, $(1s)^1(3d)^2$, $(1s)^1(3d)^3$ and $(1s)^1(3d)^4$ excited electronic configurations. The symmetry of the final state is that of the d levels since the 1s core hole is totally symmetrical and all other shells below the valence band are filled. Taking into account only the dipole electron transitions ($\hat{O}$ dipole operator), the transition moment is given by the general Fermi golden rule[64]

$$M \propto \langle \psi_{ground} | \hat{O}_{dip} | \psi_{excitcd} \rangle^2 [N(E)] \delta(h\nu - E_{ground} + E_{excited}) \quad (4.1)$$

In this expression, N(E) is the number of vacancies in the excited states. This number is 0 or 1 or 2 in a molecular orbital description of a filled, singly occupied, or vacant orbital; δ is a Dirac function, and the matrix element is a complex quantum function quite difficult to be computed exactly in the present state of the art[22,31,65].

In a pure tetrahedral symmetry, the pre-edge absorption is an outstanding feature in the K - edge XANES spectra of vanadium compounds, as can be seen from Figure 4. 3. In every spectrum, in Figure 4.3 an intense single peak is observed. It corresponds to a dipole - allowed transition from the 1s to admixed state formed from the 3d and 4p metal orbitals and from the 2p orbitals of neighbours.

In an octahedral symmetry, a weak pre-edge feature is observed (see Figure 4.2), the intensity of which is rather low due to the presence of an inversion centre at the V site ($\Gamma_0 \equiv T_{1u}$). The weakness of the intensity is due to the absence of A_{1g} in the direct product and there is no more 3d-4p mixing. The presence of such weak transitions may be assigned[3] to some

relaxation of the Laporte selection rules, by vibronic coupling, or to the interference of a quadrupolar mechanism, as already demonstrated in a square planar $CuCl_4^{2-}$ complex[66].

The assignment of the first peak after threshold i.e. shoulder on the rising absorption curve (and other weak peaks between this shoulder and 1s → 3d peak) is still controversial[67-68]. As mentioned earlier, according to the self-consistent X_α multiple scattering wave calculations of Kutzler et al[31], this feature, which has been assigned by several authors to a 1s → 4s transition, appears to be an inherent feature of the continuum, while, according to the *ab initio* self-consistent field calculations of Bair and Goddard[22], this feature cannot be assigned to any single electron transition. Rather, this feature is reassigned by these authors as a 1s → 4p transition plus simultaneous shakedown. It appears always much below the main transition with weak intensity and it will not be discussed further. Nevertheless, its presence in the spectra of liquid samples studied by Sonaye[69] allows us to rule out any interpretation of this transition based only on 3d solid-state interactions. The remaining peak, i.e., the main absorption maximum can then be assigned to the transition of 1s electron to the 4p state. Since it is a dipole-allowed transition ($\Delta l = +1$), its intensity is expected to be more as compared to the intensities of the pre-edge and shoulder peaks.

As mentioned earlier, the profiles of the X-ray absorption spectra of tetrahedrally coordinated vanadium compounds given in Figure 4. 3 show a very intense pre-edge peak. The intensity of this pre-edge feature (in Figure 4. 4) is slightly lowered for compounds in which vanadium ion has square-pyramidal coordination and its intensity is the least for octahedrally coordinated vanadium compounds as can be seen from Figures 4. 2 and 4.

4.3.2. XANES SPECTRA AND SUPERCONDUCTING OXIDES

Since the discovery of superconductivity in the La-Ba-Cu-O and Y-Ba-Cu-O systems, there has been extensive research on the substitution of 3d transition metals. Unfortunately, the incorporation of transition elements into these superconducting oxides always has a detrimental effect on the transition temperature, T_c[70]. Recently, Doi et al[71] have synthesized a monophasic $TlSr_2CaCu_2O_7$ compound. Which has single Tl-O sheets and tetragonal symmetry (a = 3.7859 A° and c = 12.104 A°: space group p4/mmm), but the material is not superconducting for the temperatures down to 4K. These authors proposed that the introduction of lead into $TlSr_2CaCu_2O_7$ would optimize the hole concentration and lead to superconducting at high temperatures. In fact, Subramanian et al[72] synthesized the compound $(Tl_{0.5}Pb_{0.5})Sr_2CaCu_2O_7$ which is superconducting below 80K. In the case of the $TlSr_2CaCu_2O_7$ compound, the Cu valence is 2.5 +, which appears to be too high and the compound is unstable and / or difficult to prepare as a single phase. Interestingly, a large number of 3d transition metal cations have accessible valencies of four and above. This aspect leads one to suggest that high valent 3d transition metals might play the same role as lead (4+) - if they substitute for Tl (3+) sites in $TlSr_2CaCu_2O_7$, rather than substituting in the Cu-O framework. If this is possible, the substitution would reduce the overdoping of $TlSr_2CaCu_2O_7$ and give rise to a superconductor. This reasoning lead Liu et al[73-75] to synthesis of a new family of high-Tc superconductors in the system $(Tl_{1-x}M_x)Sr_2(Ca_{1-y}Y_y)Cu_2O_{7-\delta}$ (M = Ti, Zr, Hf, V, Nb, and Ta). In this work, we have studied four superconducting oxides of the composition $(Tl_{1-x}V_x)Sr_2(Ca_{0.8}Y_{0.2})Cu_2O_{7-\delta}$, (x = 0.2, 0.3, 0.4 and 0.5) in order to study atomic environment of vanadium ions.

The vanadium K-edge spectra in superconducting oxides are shown in Figure 4. 6. All the four oxides show a relatively

intense peak in the 1s → 3d region. The next peak (or a shoulder peak) in the spectra of these compounds appears ~ 10eV with respect to the inflection point on the absorption edge of vanadium metal. The main absorption peak corresponding to 1s → 4p transition in all the superconducting oxides lies in the energy region 16-18 eV. All the three pre-edge, shoulder and main absorption peaks are well within the range of quadruvalent or pentavalent compounds. There is no evidence of any transition in the spectra that would indicate the presence of V^{3+} ions. In fact, $TlSr_2CaCu_2O_7$ type structure, if Tl^{3+} ions are partially replaced by vanadium, one would expect the presence of V^{3+} ions at Tl^{3+} ion sites. Our results clearly indicate that the vanadium ions are present in quadravalent or pentavalent state but in the trivalent state. Thus a comparison of the K-edge profiles in superconductors with the vanadium K-edges of model vanadium compounds gives indication of presence of V^{4+} or V^{5+} ions. This rules out the possibility of divalent or trivalent state of vanadium in the superconducting oxides. This is because all the divalent or trivalent compounds of vanadium show a very weak pre-edge peak and this is not observed in these compounds. The coordination number of vanadium ions from the comparison of their peaks with intense peak of reference compounds appear to be five.

4.4. MOLECULAR - ORBITAL APPROACH AND V K-EDGE STRUCTURE

It is well known[2-3] that the fine structure within about 20 to 25 eV of an absorption edge in a compound is characteristic of chemical bonding. Literature survey shows that the molecular orbital theory has been successfully employed by many workers to explain fine structure observed in the absorption edges of compounds. Fischer[34-35] Pendharkar and Mande[76], Obashi[77-78], Chetal and coworkers[79-81], Sarode and Pendharkar[82] have assigned the peaks of X-ray absorption near edge structure (XANES) to the

core electron transition to the vacant molecular orbital levels of appropriate symmetry formed from interaction of ligands with central metal atoms.

In the present work, a qualitative molecular orbital diagram for octahedral compounds like VO, V_2O_3 and VO_2, adapted from the book by Ballhausen and Gray[83] is shown Figure 4. 7. This diagram takes into account the interactions of the metal 3d, 4s and 4p orbitals and the 2s and 2p (σ, π) orbitals of the ligand. In this figure, solid, half open, and fully open circles represent electron pairs, unpaired electron and fully vacant states respectively. For octahedral group such as VO_6, which exist in a compound like VO, vanadium atom contributes five electrons ($3d^3$ $4s^2$) and six oxygen ligands contribute 36 electrons ($2s^2 2p^4$) to the formation molecular orbitals. However, the VO_6 ion has ten more electrons because of its negative charge. Therefore total number of electrons of VO_6 cluster contributed to the formation of the molecular orbitals is 51. After distributing all these electrons in the various molecular orbitals as shown in Figure 4. 7, one finds that the orbitals below $2t_{2g}$ are completely filled. The antibonding orbital $2t_{2g}$ is partially vacant (half-filled) and the higher energy orbitals above $2t_{2g}$ are completely vacant. The partially vacant antibonding orbitals $2t_{2g}$ and completely vacant $3e_g$ have d symmetry and the empty antibonding orbital $3a_{1g}$ has s symmetry and the outermost empty antibonding $4t_{1u}$ level has p symmetry.

In VO, V_2O_3, VO_2 and other transition metal oxides, where transition metal ion is octahedrally coordinated to oxygen, the 3d band splitting is less than 2 eV[84]. It is difficult to see two transitions from 1s core level to $3e_g$ and $2t_{2g}$ levels as the resolution of our spectrometer is ~ 4 eV. Therefore, the ($3e_g$, $2t_{2g}$) levels. The shoulder and the main absorption maximum in Figure 4. 2 can now be assigned to the transitions of the 1s electrons of the K shell to the vacant $3a_{1g}$ and $4t_{1u}$ molecular

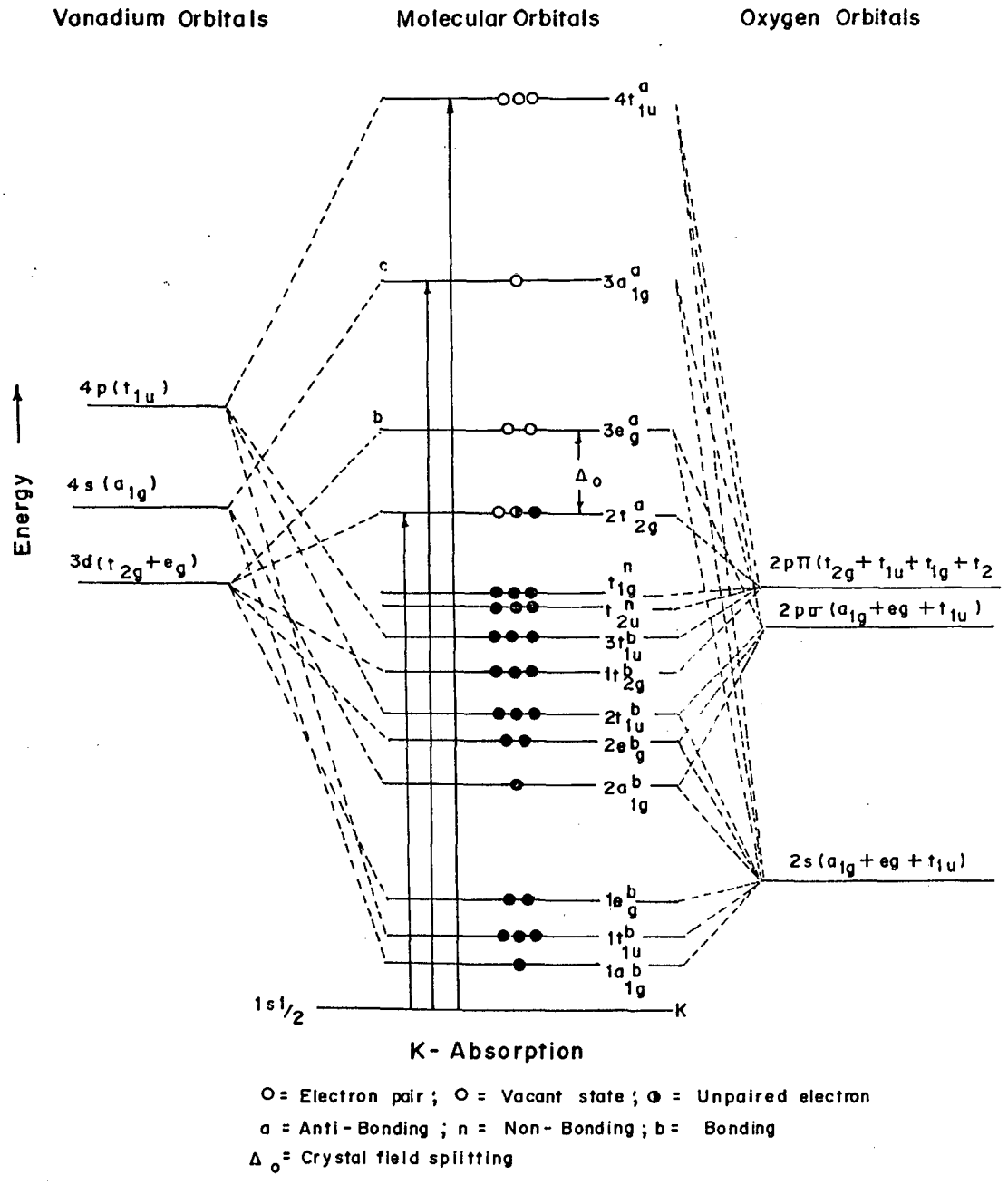

Figure 4.7: Molecular orbital energy level scheme for octahedral vanadium compounds

orbital levels respectively.

It may be noted that the 1s → ($3e_g$, $2t_{2g}$) and 1s → $3a_{1g}$ transitions are dipole forbidden. However, as can be clearly seen from the molecular orbital diagram (Figure 4. 7) some amount of the p character from oxygen orbitals mixes up with metal orbital to form these molecular orbitals, making these two electronic transitions allowed. If the liganding atom is nitrogen or carbon or sulphur instead of oxygen, the same molecular orbital picture is valid. Furthermore, in some compounds vanadium has six ligands comprising nitrogen and oxygen atoms, the molecular orbital picture in this case will remain, to the first approximation, the same. Therefore, the absorption fine structure in such compounds can be interpreted in a similar way.

For vanadium compounds like $GdVO_4$, $BiVO_4$, wherein the vanadium ion is tetrahedrally bonded to the oxygen ligand, the molecular orbital picture is shown in Figure 4. 8. It takes into account the interaction of metal 3d, 4s and 4p orbitals and 2s and 2p (σ,π) orbitals of oxygen ligands. The vanadium atom contributes 5 electrons and 4 oxygen atoms contribute 24 electrons to the formation of molecular orbitals. Taking into consideration the charge on the VO_4 cluster, the total number of electrons is 32. After distributing these electrons in various molecular orbitals of VO_4 ion as shown in Figure 4. 8, one observes that the antibonding orbital 2e and the other antibonding orbitals viz. $4t_2$, $3a_1$ and $5t_2$ are completely vacant. The 2e molecular level is formed from 3d metal orbitals and 2p orbitals of oxygen atom. The antibonding levels $4t_2$ and $5t_2$ have d+p admixture of metal character and s+p admixture of ligand. The $3a_1$ level has the s character from metal and s+p character from ligand. Hence the electrons from the K level can go, in the X-ray absorption process, to all these levels without violating the dipole selection rules. Thus, like electron transitions in octahedral compounds, the pre-edge absorption peak can be

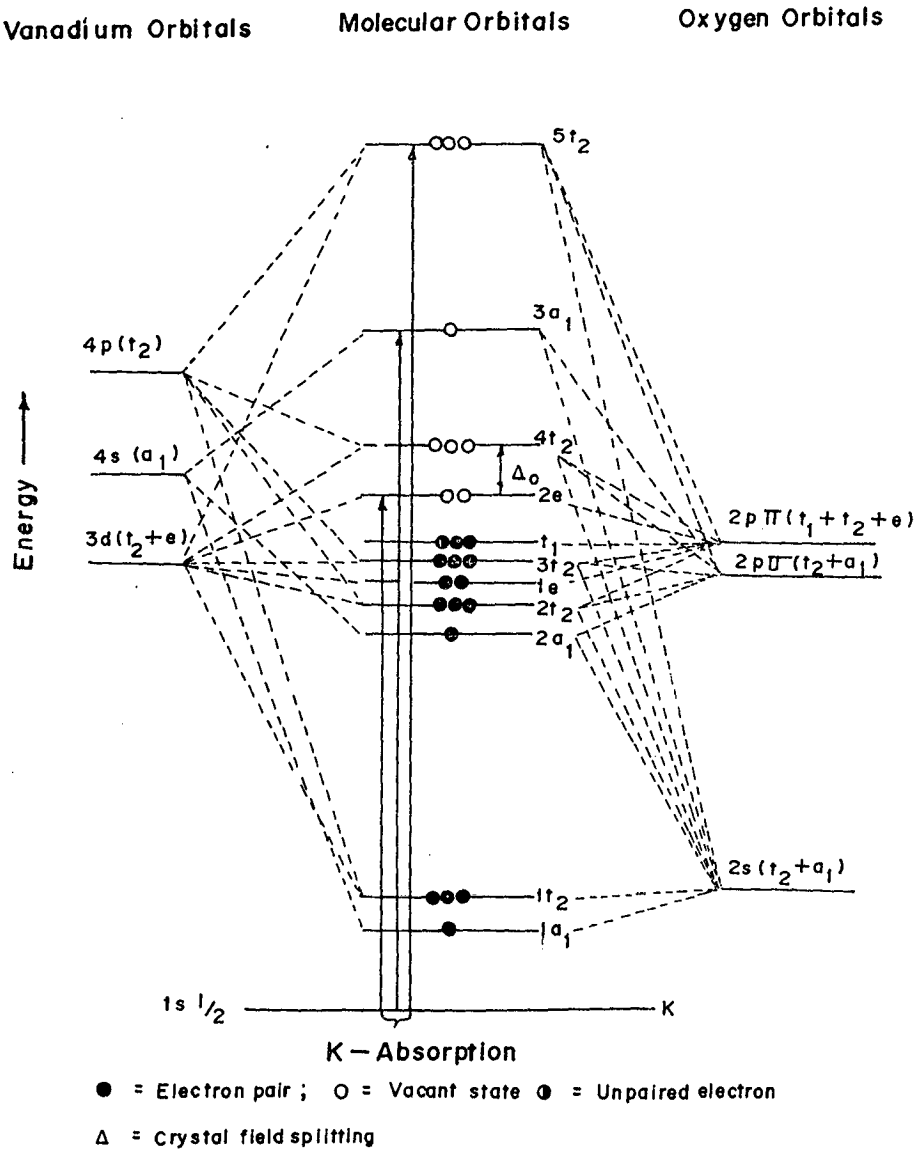

Figure 4.8: Molecular orbital energy level scheme for tetrahedral vanadium compounds

attributed to the transition of 1s electron to the (2e, $4t_2$) molecular orbitals, since the 3d level splitting is very small. The shoulder peak and the main absorption maximum can be assigned to the transition of the 1s electron to the $3a_1$ and $5t_2$ molecular levels respectively. It may be interesting to note here that the relative intensity of 1s → 3d transition in tetrahedrally coordinated vanadium ions is relatively very large as compared to that of vanadium compounds wherein vanadium ions are octahedrally coordinated. The reason is obvious, if we compare the transitions of 1s electron to ($2t_{2g}$, $3e_g$) and (2e, $4t_2$) levels in the octahedral and tetrahedral compounds respectively. The level $2t_{2g}$ or $3e_g$ has little $p(\sigma,\pi)$ contribution from oxygen and hence the intensity of 1s → ($2t_{2g}$, $3e_g$) transition is very small in octahedral compounds. However, the level $4t_2$ (or 2e) has a relatively large amount of p contribution from metal and $p(\sigma,\pi)$ contribution from ligand. It means that the $4t_2$ MO level has more p-contribution and the pre-absorption peak corresponding to the transition 1s → (2e, $4t_2$) is more intense. This is the reason why many workers[8,32,85-88] have observed a very intense 1s → 3d transition in vanadium, chromium and manganese compounds.

For square-pyramidally coordinated vanadium compounds viz. $VO(bzac)_2$, V_2O_5 the qualitative molecular orbital diagram is not available in literature. According to Figgis[87], a probable splitting pattern for the d-orbitals in a square-pyramidal complex is similar to that in a square-planar complex. Wherein the d level splits into four components. Similar thing is expected in a square-pyramidal complex. A order of increasing energy, the sequence of splitted orbitals given by Figgis[87], is $b_2(d_{xy})$, $e(d_{xz}, d_{yz})$, $a_1(d_{z^2})$, $b_1(d_{x^2-y^2})$. All these antibonding orbitals are empty if the vanadium ion is pentavalent. If it is quadruvalent, the b_2 orbital will have one electron. The next empty antibonding orbitals will be a_{1g}, a_{2u} and e_u which have

$4s+2p_\sigma$, $4p+2p_\pi$ and $4p+2p_\sigma$ characters respectively. As mentioned earlier, the d band splitting is very small, the pre-edge peak would be attributed to 1s electron transition to the empty molecular orbital (b_z, e, a_1, b_1). The shoulder of the K-edge and the principal absorption peak may be assigned to the transition of 1s electron to the vacant antibonding a_{1g} orbital and (a_{2u}, e_u) orbitals respectively. The relatively large intensity of the pre-edge peak is difficult to explain unless, a full description of MO diagram is available.

4.5. BOND LENGTH DETERMINATION FROM V K-EDGE STRUCTURE

As mentioned earlier, there is a growing interest in understanding the X-ray absorption near - edge structure (XANES) part of X-ray absorption spectra for local - structure determination in complex systems[88-90]. According to Bianconi et al[89], XANES of transition metal compounds can be separated into two parts :

(a) the discrete part below the continuum edge, where the weak features are usually called pre-edge peaks (or prepeaks), due to transitions to unoccupied bound antibonding orbitals[89] and

(b) the continuum part where the peaks are due to multiple-scattering resonances of the photoelectron, which are sensitive to both coordination geometry and interatomic distances[91-92].

The effect of the interatomic distance R has been shown to shift the multiple-scattering resonances in diatomic molecules, with a given geometry, following the rule[93] K_rR = const., where K_r is the wave vector of the photoelectron at resonance for small variation (<20%) of R. The shift of the multiple-scattering resonances with distance variation in diatomic molecules of low - Z elements has been applied in chemisorption studies[94] but the main limitation in the bond - distance determination is in the

determination of V, the average interstitial potential, which is necessary for the definition of k because k is related to V by the relation $k = \hbar\omega - E_o - \bar{V}$, where E_o is the continum threshold.

The correlation between the energy position of the multiple - scattering resonances in the continuum and the interatomic distances has been recently demonstrated by Bianconi, Natoli and others[92-96]. In the framework of the X_α - multiple - scattering theory, the absorption cross section can be shown to be determined by the multiple - scattering matrix M of the photoelectron with kinetic energy $(\hbar k)^2/2m = E = E^* - \bar{V}$ where E is the energy of the resonance above the threshold and $\bar{V}$ is the average muffin - tin interstitial potential as mentioned above. The maxima in the absorption correspond to the det (M) = 0 condition. In this formalism, Natoli derived a relation between continuum resonance energy, E_r and the first coordination shell distance,

$$(E_r - \bar{V})\ R^2 = C_r \qquad (4.2)$$

where C_r is the constant corresponding to E_r. However, C_r being unknown and $\bar{V}$ being experimentally undeterminable, the above equation was found to be of little use in practice. Natoli also obtained a similar expression for the bound state resonance energy, E_b with a different constant C_b, i.e.,

$$(E_b - \bar{V})\ R^2 = C_b \qquad (4.3)$$

Combination of the two relations (4.2) and (4.3) eliminates $\bar{V}$ and leads to the following equation

$$(E_r - E_b)\ R^2 = C_r - C_b \qquad (4.3a)$$

or

$$\Delta E_{3d-4p} \cong \frac{C_{rb}}{2R} \qquad (4.3b)$$

This is a relation containing only measurable quantities and of immediate application.

By the term "bound or excitonic resonances" we mean those spectral pre-edge features due to transition to truly bound state in molecules (e.g., the π^* transition in diatomic molecules[97] or to antibonding states of 3d character in metal oxides[94]). Both have in common the feature that they fall in an energy region where atomic resonances of the constituent atoms occur and, so to speak, are driven by them.

When applied[98] to free molecules, eqn (4.3b) states that the energy difference between the σ^* and the π^* resonance depends only on the bond length, provided initial state differences, like more or less covalent or polarity of the bond, have the same effect on the two excited states. For chemisorbed molecules one is led to the same conclusions, provided the two resonances are affected by the metal substrate shielding in the same way. Under these assumptions[98], the constant should be transferable from one phase to another. If applied to metal oxides or in general, metal compounds, eqn (4.3b), according to Natoli[98] implies that the energy separation between the pre-edge excitonic feature and the first strong absorption maximum after rising edge is a function of the bond length. The relation (4.3b) has been employed by Natoli[98] and other researchers[99-100] to determine the bond distances in the transition metal compounds.

The relation (4.3b) is an equation of straight line passing through the origin and having a slope C_{rb}. In order to determine the value of constant C_{rb}, we have plotted in Figure 4.9 the energy separations (ΔE_{3d-4p}) between the multiple - scattering resonances in the continuum (1s → 4p transition) and bound (1s →

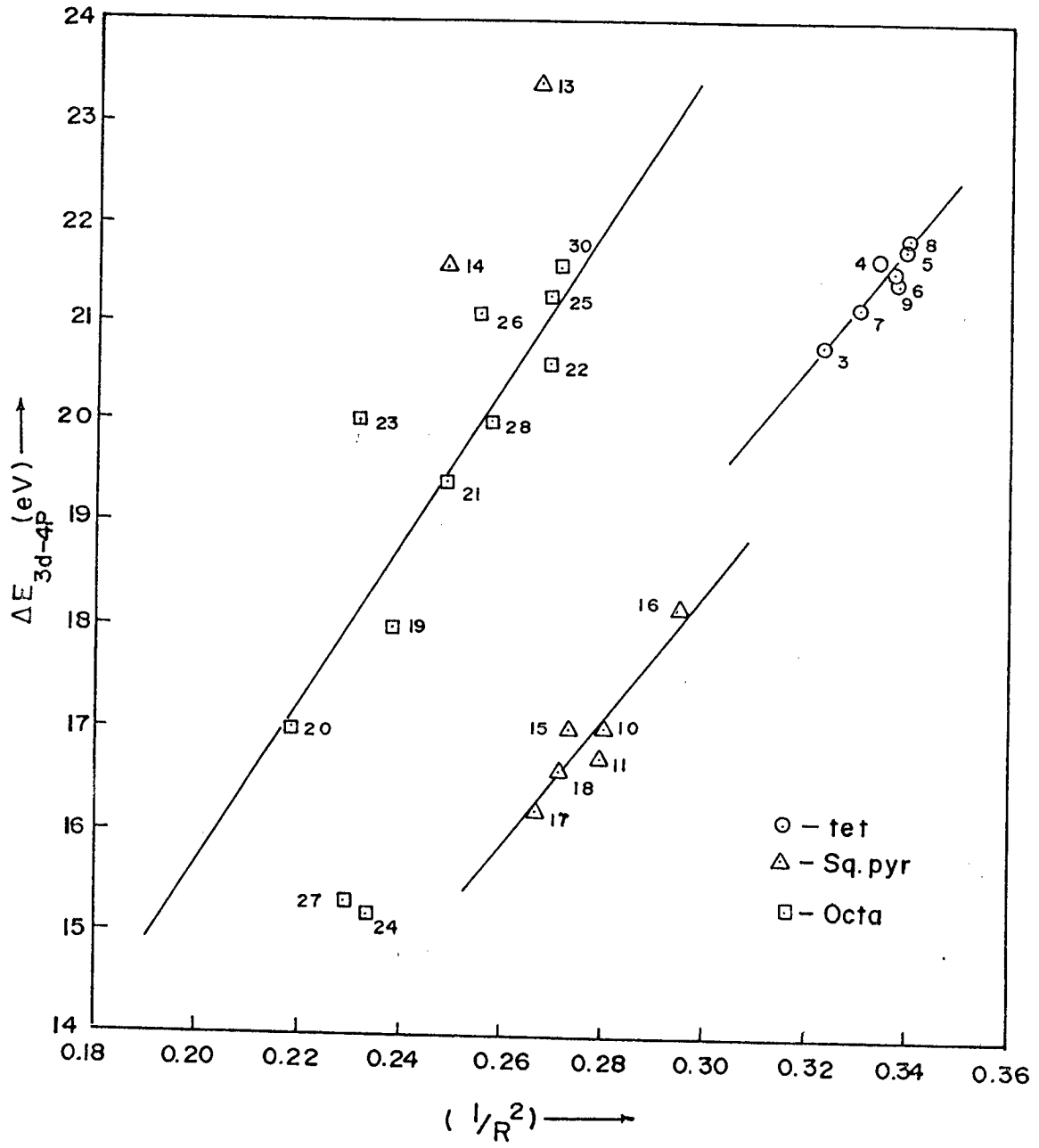

Figure 4.9: A plot of ΔE_{3d-4p} versus $1/R^2$ for vanadium compounds

3d transition) states versus the reciprocal of square of the interatomic distances (R) for a number of vanadium compounds covering a wide range of structures. The least squares analysis of the data using all the 26 points was carried out on PC-486. As can be seen from Figure 4. 9, Natoli's simple relation at first glance, does not seem to hold true for these compounds. However, when these compounds are classified according to the coordination number of vanadium and ΔE_{3d-4p} vs $1/R^2$ graphs were plotted for 4-fold, 5-fold, and 6-fold coordinated compounds separately, a fairly good linear relation was found to exist between ΔE_{3d-4p} and $1/R^2$ in each case as shown in Figure 4. 9. For tetrahedrally coordinated compounds, the correlation coefficient and standard error of estimates are found to be 0.983 and 0.095 respectively. For penta coordinated compounds, if we take into account the data for all eight compounds for regression analysis, we get the values of correlation coefficient and standard error of estimates as 0.656 and 2.994 respectively. However, for two complexes, namely VOPc and VOTPP, the deviation for the least-squares line is very large. Such large deviations for these two compounds have also been observed in the plots of intensity of pre-edge peaks versus average bond lengths of first shell ligands in various ligand geometries in the work of Wong et al[36]. If we perform the analysis excluding the data points for VOPc and VOTPP, the values of correlation coefficient and standard error of estimates obtained are 0.943 and 0.207 respectively. In the case of octahedrally coordinated compounds, the regression analysis gives the values of correlation coefficient and standard error of estimates as 0.747 and 1.405 respectively. By examining the experimental and calculated energy separations for the compounds, it is seen that the residues are large for VN, V_2S_3 and VC. That is why a relatively large value of standard error of estimates is obtained. However, the analysis carried out, excluding the data for VN, V_2S_3 and VC, yields the values of the correlation

coefficient and standard error of estimates as 0.879 and 0.692 respectively. Thus, there is a lot of improvement. Although it is difficult to give any satisfactory explanation for the large deviation observed for these three compounds, the nature of bonding seems to have some role to play in the large energy separations in the X-ray absorption spectra of these compounds. For example, the V-S and V-N bonds are strongly covalent and strongly ionic in nature respectively whereas all other compounds have mixed bond character. Barring such a few exceptions, we may conclude that Natoli's relation is valid for a series of compounds wherein the metal ions have the same coordination geometry. i.e., $\Delta E_{3d-4p} \times R^2$ = constant for a particular coordination polyhedron of ligands around metal ions. The constants for tetrahedral, square pyramidal and octahedral coordination geometries were determined from the least-squares fitting of the data to a linear equation of the form $\Delta E_{3d-4p} \times R^2 = C$, where C is the constant for each coordination geometry and are given in Table 4.3 Once the constants are known it is easy to use this formula to predict coordination geometry and bond distance from the profiles and energy positions of the XANES peaks. We have employed this method to predict the interatomic distances in superconducting compounds for which the values of ΔE have been determined from the XANES spectra.

4.5.1 TEST OF TRANSFERABILITY OF STRUCTURAL CONSTANTS

As a first test of the transferability of these constants, we have chosen three complexes. These complexes are $CrVO_4$, $(NH_4)_4$[VO-dd-tart].$2H_2O$ and PbV_2O_6, whose structures had been elucidated previously by X-ray crystallography[37,45,60]. The absorption spectra of these two vanadium compounds were recorded and the spectra are presented in Figure 4.4. To obtain structural information, the profiles of the edges of these compounds were

compared with those of the model compounds. The comparison suggests that vanadium ions are four fold coordinated in $CrVO_4$, five-fold coordinated in $(NH_4)_4$[VO-dd-tart].$2H_2O$ and six-fold coordinated in PbV_2O_6. Therefore using the constants $C_{oct.}$, C_{tetra} and C_{spyr} we have calculated the V-X (X = ligand) bond distances in the these compounds. The bond lengths 1.791 A°, 1.975 A° and 1.979 A° in $CrVO_4$, $(NH_4)_4$[VO-dd-tart].$2H_2O$ and PbV_2O_6 respectively determined in this work are in good agreement with those reported in literature[37,45,60].The close correlation of both the coordination geometry and bond distances lends confidence to our ability to predict the coordination numbers and distances in compounds of unknown structures by XANES spectroscopy.

4.5.2 DETERMINATION OF BOND DISTANCES IN SUPERCONDUCTORS

In Figure 4.6 are shown the XANES spectra of superconducting oxides containing 2, 3, 4 and 5 percent of vanadium. As already mentioned, comparison of K-edge profiles of superconducting oxides with those of model vanadium compounds such as the presence of square-pyramidally coordinated V^{4+} or V^{5+} ions in these oxides. Therefore using the constant corresponding to square-pyramidal geometry, $C_{spyr.}$, we have estimated the V-O bond distances 1.82 A°, 1.839 A°, 1.84 A° and 1.845 A° for 2, 3, 4 and 5 percent samples respectively from the energy separations 18.3, 17.9, 17.8 and 17.7 eV. Our results are in good agreement with the structural results reported by Liu and Edwards[75].

Our X-ray diffraction analysis of the samples of the series show that the structure of these oxides is similar to the $TlSr_2CaCu_2O_7$ type structure and the lattice parameter c decreases while the lattice parameter a increases with the increase of vanadium concentration. On the basis of these results we would like to suggest that the smaller V^{4+} (ionic radius 0.63 A°) or

V^{5+} (ionic radius 0.59 A°)ions partially replace the larger Tl^{3+} (ionic radius 0.95 A°) sites resulting in a decrease in the lattice parameter c. In contrast, Liu and Edwards[75] proposed that the partial substitution of vanadium for the thallium leads to a decrease of the hole concentration in the Cu-O plane and a corresponding increase in the lattice parameter a. However, for the confirmation of this, one has to take resort to the measurements of the normal state magnetic susceptibility of these high Tc -oxides. These results may also help to evaluate the valence state of the vanadium ion correctly.

4.6. XANES AND BOND VALENCE

The Pauling bond strengths (in valence units), referred to as bond orders or bond valences of the metal - non-metal bonds are useful in discussing the structural properties of compounds. The bond valence (s) reflects the relative strength of a chemical bond and shows the distribution of available valence electrons in the chemical bonding of a molecular species. Also, according to Pauling's valence sum rule[101], there is a conservation of valency associated with the metal cation. A general relationship has been developed by Brown and Wu[102-103] that relates the cation-anion bond valence s to the interatomic distance R. The empirical expression for relating a V-O bond length to its bond valence is

$$s_{V-O} \approx (R / 1.791)^{-5.1} \qquad (4.4)$$

where 1.791 A° is the estimated bond length for a V-O bond of unit valency. The empirical parameters in equation (4.3), 1.791 and -5.1, were determined by Brown and Wu from the data of 43 vanadium compounds having different environments[103]. Though this relation is given for V-O bond only, it is equally applicable for other bonds also[104].

In our work we have calculated the bond valence (s) and plotted it against ΔE_{3d-4p} for vanadium compounds in Figure 4.10. We have used few data points from the work of Sonaye[69]. It is seen that, a fairly linear relationship exists between ΔE_{3d-4p} and s for 4-fold, 5-fold and 6-fold coordinated vanadium compounds. This relationship renders the possibility of determination of bond valence in structurally unknown compounds. For example, in the superconducting oxides containing 2, 3, 4 and 5 percent vanadium, the bond valences estimated from the least-squares analysis of the data on ΔE_{3d-4p} and s are found to be and 0.892, 0.848, 0.837 and 0.826 respectively indicating that the vanadium ions are in 4^+ or 5^+ state.

It is interesting to mention here that in Raman spectroscopy correlations between vanadium-oxygen bond valence and vanadium - oxygen stretching frequencies have been shown and fruitfully used[103] for the determination of oxidation states in compounds in complicated oxide systems such as vanadium oxides supported on alumina and titania substrates. In EXAFS spectroscopy also, such correlations have been used[63] to estimate the bond valence from the distances determined from the Fourier transform analysis of the EXAFS spectra.

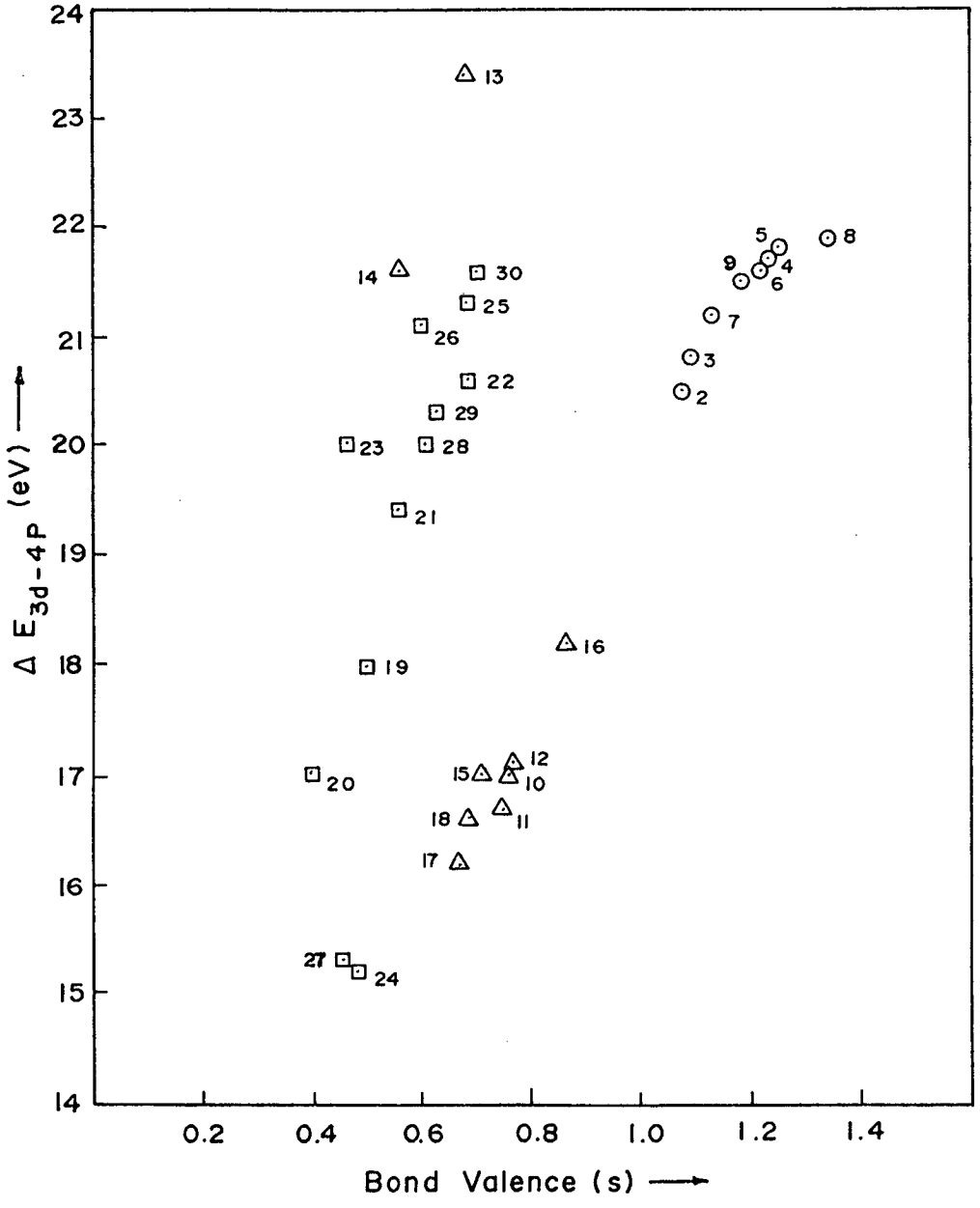

Figure 4.10: A plot of ΔE_{3d-4p} versus bond valence (s) for vanadium compounds

REFERENCES

1. W.Kossel, Z. Phys., 1, 119 (1920).

2. H.C.Yes and L.V.Azároff, J. Appl. Phys., 38, 4034 (1964).

3. L.A.Grunes, Phys. Rev., B 27, 2111 (1983).

4. D.Sayers, F.Lytle and E.A.Stern, Advan. X-ray Analysis, 13, 248 (1970).

5. R.G. Shulman, P.Eisenberger, W. Blumberg and N.A. Stombaugh, Proc. Acad. Sci. USA, 72,4003 (1975).

6. B. M. Kainkaid and P. Eisenbeger, Phys Rev. Lett., 34, 1361 (1975).

7. R.G.Shulman, Y.Yaffet, P.Eisenberger and W.E.Blumberg Proc. Natl. Acad. Sci. USA, 73, 1384 (1976).

8. G. Sankar, P.R. Sarode and C.N.R. Rao, Chem. Phys., 76, 435 (1983).

9. F.Babonneau, S.Doeuff, A.Leaustic, C.Sanchez, C.Cartier and M. Verdaguer, Inorg. Chem., 27, 3166 (1988).

10. M.Sano, Inorg. Chem., 27, 4249 (1988).

11. A.L.Roe, D.J.Schneider, R.J.Mayer, J.W.Pyrz, J.Widom and L.Que Jr., J. Am. Chem. Soc., 106, 1676 (1984).

12. J.A.Bearden and A.F.Burr, Rev. Mod. Phys., 36, 125 (1967).

13. M. Sano, S. Komorita and H.Yamatera, Inorg. Chem., 31, 459 (1992).

14. C. Sugiura, J. Chem. Phys., 80, 1047 (1984).

15. C. Sugiura and S. Nakai, Japan. J. Appl. Phys., 17 Suppl. 17-2, 190 (1978).

16. G. L. Glenn and C. G. Dodd, J. Appl. Phys., 39, 5372 (1968).

17. V.K. Kondawar and C.Mande, X- ray Spectrometry, 5, 2 (1976).

18. H. P. Hanson and W. W. Beeman, Phys. Rev., 76, 118 (1949).

19. S. A. Nemnov, Izv. Ikad. Nauk., 24, 447 (1960).

20. A. Z. Men'shikov and S. A. Nemnov, Fiz. Met. Metalloid., 10, 390 (1960).

21. H. P. Hanson and J. R. Knight, Phys. Rev., 102, 632 (1956).

22. R. A. Bair and W. A. Goddard, Phys. Rev. B, 22, 2267 (1980).

23. N. J. Kosugi, T. Yokoyama, K.Asakuna and H. Kuroda, Chem. Phys., 91, 249(1984).

24. N. J. Kosugi, T.Yokoyama, K. Asakuna and H. Kuroda, Springer Proc. Phys., 2, 55 (1984).

25. T.A. Carlson, J.C. Carver, I.J. Saethre, F.G. Santibanez and G.A. Vernon, J. Electron Spectrosc. Relat. Phonom., 5, 247 (1974).

26. Rosenawaring, G. K. Wertheim and H.J. Guggenheim, Phys. Rev. Lett., 27, 479 (1971).

27. T.A. Carlson, J.C. Carver, and G.A. Vernon, J. Chem. Phys., 62, 932 (1975).

28. G.A.Vernon, G.Stucky and T.A.Carlson, Inorg. Chem., 15, 278 (1976).

29. D.C.Frost, A.Jshitani and C.A.McDowell, Mol. Phys., 24, 861 (1972).

30. E.A.Stern, Phys. Rev. B, 10, 3027 (1974).

31. F.W. Kutzler, C.R. Natoli, D.K. Misemer, S. Doniach and K.O. Hodson, J. Chem. Phys., 73, 3274 (1980).

32. D. W. Fischer, J. Phys. Chem. Solids, 32, 2455 (1971).

33. W. Seka and H. P. Hanson, J. Chem. Phys., 50, 344 (1969).

34. D. W. Fischer, J. Appl. Phys., 41, 3561 (1970).

35. D.W. Fischer, Band Structure Spectroscopy of Metals and Alloys, eds. D.J. Fabian and L.M. Watson (Academic Press, London 1971) pp669.

36. J.Wong, F.W.Lytle, R.P.Messmer and D.H.Maylotte, Phys. Rev., B30, 5596 (1984).

37(a). C. Frazer and P. J. Brown Phys. Rev., 125, 1283 (1977).

37(b). B. I. Chamberland, Crit. Rev. Solid State Mater. Sci., 7,

1 (1977).

38. D. J. Newman et al, J. Phys. C, 5, 3101 (1972).

39. A.W.Sleight, H.Y.Chen, A.Ferretti and D.E.Cox, Mater. Res. Bull., 14, 1571 (1979).

40. P. K. L. Au and C. Calvo, Can. J. Chem., 45, 2297 (1967).

41. S.Geller, G.P. Espinosa, R.C. Sherwood and H.J. Williams, J. Appl. Phys., 36, 321 (1965).

42. J.Trotter and W.H.Barnes, Can. Mineral., 7, 161 (1958).

43. R. Gopal and C. Calvo, Can. J. Chem., 49, 3056 (1971).

44. P.K. Hon, R.L. Belford and C.E. Pfluger, J. Chem. Phys., 43, 1323 (1965).

45. J.G.Forrest and C.K.Prout, J. Chem. Soc. (A), 1312 (1967).

46. R.F. Ziolo, C.H. Griffiths and J.M. Troup, J. Chem. Soc., Dalton Trans. 2300 (1980).

47. F.S.Molinaro and J.Albers, Inorg.Chem., 15, 2278 (1976).

48. H.A.Eick and L.Kihlborg, Acta. Chem. Scand., 20, 722 (1966).

49. H.G.Bachmann, F.R.Ahamed and W.H.Barnes, Z. Krist., 115, 110 (1961).

50. N. Schönberg, Acta. Chem. Scand., 8 , 221 (1954).

51. H.Montgomery, R.V. Chastain, J.J.Natt, A.M. Witkowska and E. C. Lingafelter, Acta Cryst., 22, 775 (1967).

52. R.E,Newnham and Y.M.de Haan, Z. Krist., 117, 235 (1962).

53. S. Geller, Acta Cryst., 10, 248 (1957).

54. F. Hulliger, Structure and Bonding, 4, 83 (1968).

55. R.W.G. Wyckoff, Crystal Structures, Second edition. Wiley, New York 1963, Vol.1 pp91.

56. F.Thesbald, R.Cabala and J.Bernard, J. Solid State Chem., 17, 431 (1976).

57. M. Marezio, D.B. McWhan, P.D. Dernier and J.P. Remeika, J.,

Solid state Chem., 6, 419 (1973).

58. E.Rudy, F.Benesovsky and L.Toth, Z. Metalkd., 54, 345(1963).

59. X. Li, M.S. Lah and V.L. Pecoraro, Inorg. Chem., 27, 4657 (1988).

60. B.D. Jordan and C.Calvo, Can. J. Chem., 52, 2701 (1974).

61. A.G. Swallow, F.R. Ahmed and W.H. Barnes, Acta Cryst., 21, 397 (1966).

62. F.Babonneau, S.Doeuff, A.Leaustic, C.Sanchez, C.Cartier and M.Verdaguer, Inorg. Chem., 27, 3166 (1988).

63. R. Kozlowski, R.F. Pettifer and J.M. Thomas, J. Phys. Chem., 87, 5176 (1983).

64. H.Bethe and E. Salpeter, Quantum Mechanics of One-and-Two Electron Systems, Sections 59 and 59, Springer-Verlag, Berlin (1956).

65. P.J.Durham, J.B.Pendry and C.H.Hodges, Solid State Commun., 38, 159 (1981).

66. J.E.Hahn, R.A.Scott, K.O.Hodgson, S.Doniach, S.R.Desjardins and E.J.Solomon, Chem. Phys. Lett., 88, 595 (1982).

67. R.B.Greegor, F.W.Lytle, D.R.Sandström, J.Wong and P.Schultz, J. Non-Cryst. Solids, 55, 27 (1983).

68. B. Poumellec, F. Lagnel, J.F. Marucco and B. Touzelin, Phys. Status. Solid (b), 133, 371 (1986).

69. B.H.Sonaye, Ph.D. Thesis, Goa University, Goa (1995).

70. G.Xiao, F.H.Streitz, A.Garvin, Y.W.Du and C.L.Chien, Phys. Rev. B, 35, 8782 (1987).

71. T.Doi, K.Usami and T.Kamo, Jpn. J. Appl. Phys., 29, L57 (1990).

72. M.A.Subramanian, C.C.Torardi, J.Gopalkrishnan, P.L.Gai, J.C. Calabrase, T.R.Askew, R.B. Flippen and A.W.Slight, Science, 242, 249 (1988).

73. R.D. Liu, W. Zhou, and P.P. Edwards, Appl. Phys. Lett., 57, 2492 (1990).

74. R.S. Liu, W. Zhou, R. Janes and P.P. Edwards, Solid State

Commun., 76, 1261 (1990).

75. R.S.Liu and P.P.Edwards, J. Solid State Chem., 91 407(1991).

76. A.V.Pendharkar and C.Mande, Chem. Phys., 7, 244 (1975).

77. M.Obashi, Japanese J. Appl. Phys., 16, 167 (1977).

78. M.Obashi, Physica Fennica, 9, 148 (1974).

79. H. Hemachandran and A.R. Chetal, Phys. Stat. Sol.(b), 132, 503 (1985).

80. P.Bhattcharya and A.R.Chetal, Phys. Stat. Sol.(b), 119, 179 (1983).

81. T. Chattopadhay and A.R. Chetal, J. Phys. C: Solid State Phys., 18, 5373 (1985).

82. P.R.Sarode and A.V.Pendharkar, Chem. Phys., 28, 455 (1978).

83. C.J. Ballhausen and H.B. Gray, Molecular Orbital Theory, Benjamin, New York, 1965.

84. D. Alder, J. Feinleib, H.Brooks and W.Paul, Phys. Rev., 155, 851 (1967).

85. M. Belli, A. Scafati, A. Bianconi, S. Mobillio, L.Palladino, A. Realle and E. Burattini, Solid State Commun., 35, 335 (1980).

86. L.Kau, D.J. Spira-Solomon, J.E. Penner-Hahn and K.O.Hodgson, J. Amer. Chem. Soc., 109 6433 (1987).

87. B.N. Figgis, Introduction to Ligand Fields, Interscience Publishers, New York 1966.

88. M. Sano, S. Komorita and H. Yamatera, Inorg. Chem.,31, 459 (1992).

89. A. Bianconi, E. Fritsch, G. Calas and J.Petiau, Phys. Rev.B, 32, 4292 (1985).

90. G.Calas and J.Petiau, Solid State Commun., 48, 625 (1983).

91. A. Bianconi, in Daresbury Laboratory Report No. SERC DL/SCI/R17, 1981, eds. by C.D.Garner and S.S.Hasnain pp 13.

92. A. Bianconi, in EXAFS and Near Edge Structure eds. A.

Bianconi, L. Incoccia and S. Stipcich, Springer Series in Chemical Physics, Vol. 27 (Springer Verlag Berlin) 1983 pp 118.

93. A. Bianconi, M.Dell'Ariccia, A. Gargano and C.R. Natoli, in EXAFS and Near Edge Structure eds. A. Bianconi, L. Incoccia and S.Stipcich, Springer Series in Chemical Physics, Vol. 27 (Springer Verlag Berlin) 1983 pp 57.

94. J. Stöhr, J.L. Gland, W. Eberhardt, D. Outka, R.J. Modix, F. Sette, R.J.Koestner and W.Doebler, Phys.Rev.Lett., 51, 2414 (1983).

95. F.Sette, J.Stöhr and A.P.Hitchcock, J. Chem. Phys., 81, 4906 (1984) and references therein.

96. D.Dill and J.L.Dehmer, J. Chem. Phys., 65, 5327 (1976).

97. M.Belli, A.Scafati, A.Bianconi, S.Mobillio, L. Palladino, A. Realle and E.Burattini, Solid State Commun., 35, 355 (1980).

98. C.R. Natoli, in EXAFS and Near Edge Structure III eds. K.O. Hodgson, B. Hedman and J.E. Penner-Hahn, Springer Verlag Berlin 1984 pp 38.

99. P.Mahto and A.R.Chetal, Phsica B, 158, 415 (1991).

100. B.K.Pandey, A.R.Chetal and P.R.Sarode, Physica B, 172, 324 (1991).

101. I.D.Brown, Chem. Soc. Rev.,7, 359 (1978).

102. I.D.Brown and K.K.Wu , Acta Cryst., 32, 1957 (1976).

103. F.D. Hardcastle and I.E. Wachs, J. Phys. Chem., 95, 5031 (1991).

104. P.R.Sarode and S.A.Gauns, J. Phys. Chem. Solid (Submitted).

Table 4.1. ENERGY POSITIONS OF VARIOUS SPECTRAL FEATURES IN VANADIUM K-EDGE SPECTRA IN VANADIUM COMPOUNDS

Sr. No.	Absorber	Pre-edge peak(eV) 1s→3d	Main Absorption peak (eV) 1s→4p	Energy separation ΔE_{3d-4p}(eV)
1.	V metal	--	19.3	--
2.	$CrVO_4$*	4.3	24.8	20.5
3.	$GdVO_4$	3.9	24.7	20.8
4.	$BiVO_4$	4.7	26.4	21.7
5.	$Cd_2V_2O_7$	4.6	26.4	21.8
6.	$Ca_3Fe_3GeVO_{12}$	4.1	25.7	21.6
7.	$Pb_5(VO_4)_3Cl$	3.9	25.1	21.2
8.	$Zn_3(VO_4)_2$	3.9	25.8	21.9
9.	$NaVO_3$	4.1	25.6	21.5
10.	$VO(acac)_2$	3.9	20.9	17.0
11.	$VO(bzac)_2$	4.1	20.8	16.7
12.	$(NH_4)_4$[VO-dd-tart].$2H_2O$*	3.5	20.6	17.1
13.	VOPc	3.9	27.3	23.4
14.	VOTPP	4.0	25.6	21.6
15.	$VOMoO_4$	4.4	21.4	17.0
16.	V_2O_5	4.8	23.0	18.2
17.	$VOSO_4.3H_2O$+	4.8	21.0	16.2
18.	$VO(acen)^+$	4.0	20.6	16.6
19.	VO	3.2	21.2	18.0
20.	$(NH_4)_2SO_4VSO_4.6H_2O$	3.4	20.4	17.0
21.	V_2O_3	3.5	22.9	19.4

22. $SmVO_3$	3.3	23.9	20.6
23. V_2S_3	3.1	23.1	20.0
24. VN	4.8	20.0	15.2
25. VO_2	4.5	25.8	21.3
26. V_4O_7	4.1	25.2	21.1
27. VC	5.2	20.5	15.3
28. [VO(hshed)(acac)]	3.8	23.8	20.0
29. PbV_2O_6*	4.6	24.9	20.3
30. $Ca_3V_{10}O_{28}.16H_2O$	4.1	25.7	21.6
31. 2 % sample	3.5	23.9	20.4
32. 3 % sample	4.0	22.9	18.9
33. 4 % sample	3.8	22.8	18.0
34. 5 % sample	3.9	21.8	17.9

* Test compounds

+ Data taken from unpublished work of B. H. Sonaye

TABLE.4.2. STRUCTURAL PARAMETERS FOR VANADIUM COMPOUNDS

Sr. No.	Compound	Q^a	Bond type	No.of Bonds	R^b (Å)	s^c	Ref.
1.	V metal	--	V-V	8	2.622	--	
	Coordination Polyhedron : Tetrahedron						
2.	$CrVO_4$	5	V-O	4	1.765	1.077 &	37(a) 37(b)
3.	$GdVO_4$	5	V-O	4	1.760	1.093	38
4.	$BiVO_4$	5	V-O	4	1.730	1.229	39
5.	$Cd_2V_2O_7$	5	V-O	4	1.718	1.248	40
6.	$Ca_3Fe_3VGeO_{12}$	5	V-O	4	1.724	1.215	41
7.	$Pb_5(VO_4)_3Cl$	5	V-O	4	1.740	1.125	42
8.	$Zn_2(VO_4)_3$	5	V-O	4	1.715	1.341	43(a)
9.	$NaVO_3$	5	V-O	4	1.723	1.176	43(b)
	Coordination Polyhedron : Square pyramid						
10.	$VO(acac)_2$	4	V-O	5	1.889	0.761	44
11.	$VO(bzac)_2$	4	V-O	5	1.894	0.752	44
12.	$(NH_4)_4$[VO-dd-tart].$2H_2O$	4	V-O	5	1.886	0.768	45(a) 45(b)
13.	VOPc	4	V-O V-N	5	1.937	0.671	46
14.	VOTPP	4	V-O V-N	5	2.006	0.562	47
15.	$VOMoO_4$	5	V-O	5	1.913	0.715	48
16.	V_2O_5	5	V-O	5	1.840	0.871	49(a)
17.	$VOSO_4.3H_2O$	4	V-O	5	1.936	0.672	49(b)
18.	VO(acen)	4	V-O	5	1.922	0.698	49(c)

Coordination Polyhedron : Octahedron

19.	VO	2	V-O	6	2.050	0.502	50
20.	$(NH_4)_2SO_4VSO_4.6H_2O$	2	V-O	6	2.140	0.403	51
21.	V_2O_3	3	V-O	6	2.010	0.555	52
22.	$SmVO_3$	3	V-O	6	1.929	0.685	53
23.	V_2S_3	3	V-S	6	2.080	0.466	54
24.	VN	3	V-N	6	2.070	0.478	55
25.	VO_2	4	V-O	6	1.930	0.683	56
26.	V_4O_7	3,4	V-O	6	1.982	0.596	57
27.	VC	4	V-C	6	2.091	0.454	58
28.	[VO(hshed)(acac)]	5	V-O V-N	6	1.973	0.610	59
29.	PbV_2O_6	5	V-O	6	1.962	0.629	60
30.	$Ca_3V_{10}O_{28}.16H_2O$	5	V-O	6	1.920	0.701	61
31.	2 % sample	(5)	V-O	(5)	(1.730)	(0.892)	
32.	3 % sample	(5)	V-O	(5)	(1.798)	(0.848)	
33.	4 % sample	(5)	V-O	(5)	(1.842)	(0.837)	
34.	5 % sample	(5)	V-O	(5)	(1.847)	(0.826)	

a Q = Oxidation state

b R = Bond distance
c s = Bond valence
d Trigonal prismatic complex

TABLE 4.3. VALUES OF STRUCTURAL CONSTANTS

Coordination polyhedron	Notation for for the constant	Numerical Value of the constant
Tetrahedron	C_{tetra}	64.46
Square Pyramid	$C_{sq.pyr}$	61.08
Octahedron	C_{oct}	77.62

CHAPTER 5

COPPER K-ABSORPTION EDGE STRUCTURE

5.1. INTRODUCTION

There has been a considerable amount of work done on the X-ray absorption near-edge spectra (XANES) of the high-temperature superconductors with the hope that such measurements will provide detailed information about the electronic structure of the constituent metal ions. The most widely studied ion has been the copper ion [1-8]. Despite such wide interest in the problem and excellent reproducibility of spectra in a given system, there has been no commonly accepted interpretation of the XANES features. The major controversy is in the identification of the ubiquitous feature at about 6 eV above the main absorption peak in the XANES spectra of polycrystalline samples of all the members of the superconducting family of the copper oxides. This feature was first discussed by Alp et al[1] (peak C for example in Figure 5.1a). Considerable theoretical as well as experimental efforts have been expended in resolving this problem. One electron excitation calculations[1] (see Figure 5.1a) for La_2CuO_4 do not show the presence of this feature. Alp et al[1] have suggested that this feature must be associated with the presence of Cu^{3+} ions. Subsequent single crystal studies by Heald et al.[7] show two strong absorption features, B_1 and B_2 (shown in Figure 5.1b) which may be associated with the $1s \rightarrow 4p\pi$ and $1s \rightarrow 4p\sigma$ transitions which have energies in agreement with the calculations of Alp et al[1]. The feature C is seen as a shoulder (B_4) to the main feature B_2 for the polarization parallel to the ab plane. The origin of this feature has not been commented upon. It has been pointed out[8] that core-level spectroscopies cannot give information about the valence state when there is a strong configuration mixing between initial and final states. By including such configuration interactions in the Anderson impurity Hamiltonian model, Sarma[8] has calculated the XPS core Cu $2p_{3/2}$ as well as the Cu K-edge XANES spectra and has suggested that the feature C is to be associated with a Cu d^9

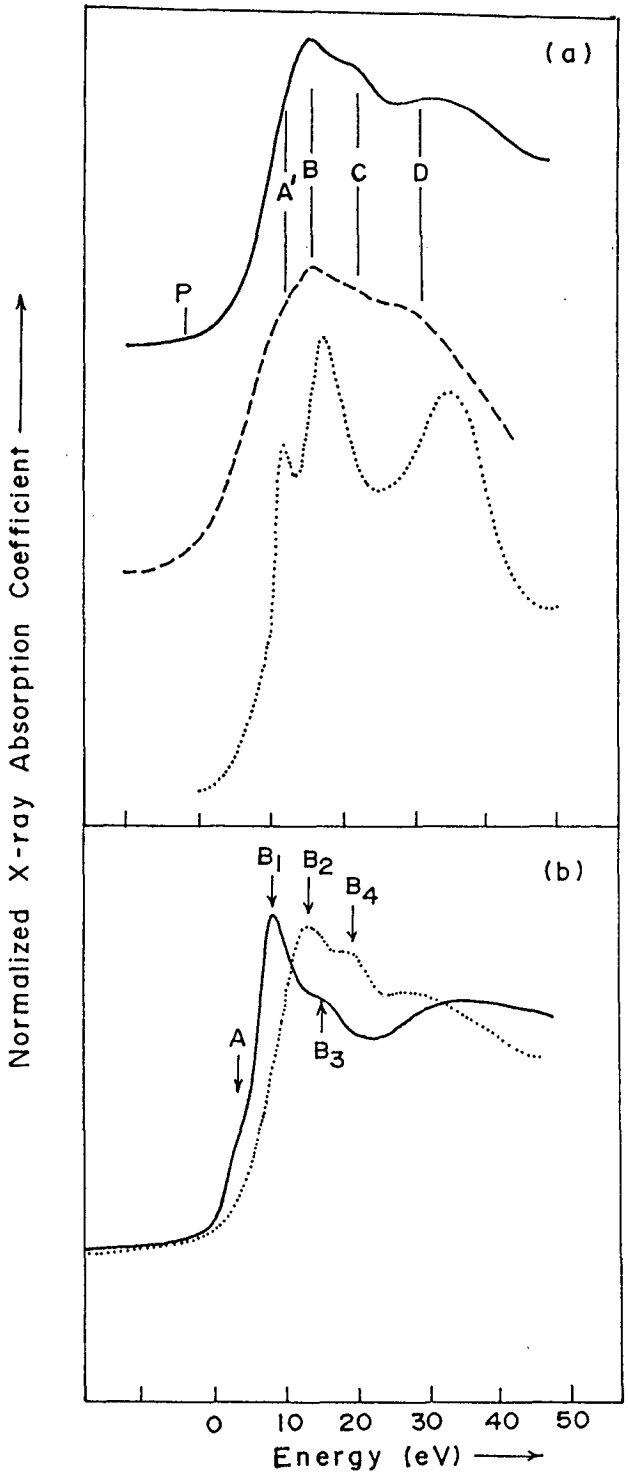

Figure 5.1: (a) Polycrystalline Cu K-edge XANES of La_2CuO_4 (from Ref. 1) showing the main features (full line); one electron theory calculation of XANES (dotted line) from Ref. 1; configuration interaction calculation of Sarma (dashed line) from Ref. 8. (b) Single crystal XANES spectra of La_2CuO_4 for $e_\pi z$ (full line) and for $e_\perp z$ (dotted line)

configuration, while the feature B is to be associated with a d^{10} configuration in much the same manner as Cu $2p_{3/2}$ 933 eV band and 942 eV satellite band in the core-level XPS studies. This study has the merit that it attempts to correlate XPS and XANES features.

The X-ray photoelectron study[9-11] of the superconducting copper oxides have been concentrated on the valence band as well as the core Cu $2p_{3/2}$ region and the oxygen 1s level. Unlike the XANES studies the XPS studies have the disadvantage that it is highly surface specific. The degree of reproducibility of XPS features have thus been entirely unsatisfactory especially with respect to those associated with oxygen ions because of the possibility of the presence of hydroxyl or carbonate groups by contamination.

A completely different approach is that followed by Lytle *et al*[4] who have interpreted the XANES region in terms of a backscattering model from nearby atoms and identified the higher energy features with different Cu-O bond distances. In this model the features at B, C and D (Figure 5.1a) are related to the distances at 3.5, 2.6 and 1.9 A^{o} respectively. The 2.6 A^{o} distance has been related to the occupation of the copper ions in the La sites in La_2CuO_4.

One of the major shortcomings in the effort to understand the XANES features is the failure to examine the obvious chemical aspect, namely the examination of other ternary copper oxides which have structural features common to the superconducting family of oxides. The family of copper oxides themselves exhibit a fascinating diversity of structures that have been very systematically studied before the discovery of superconductivity in the copper oxide system by Bednorz and Müller[12], by the pioneering efforts of Müller-Buschbaum and his coworkers[13] as well as Raveau and coworkers[14,15]. Sreedhar and Ganguly[16] and Ganguly et al[17] have carried out various studies such as magnetic

susceptibility and electron spin resonance on such oxides as part of effort to understand the properties of the non-superconducting copper oxides in relation to the properties of the superconductors. In this Chapter we present the results of our XANES as well as XPS investigations on a series of copper oxides which have structural features common to those of the superconducting family of copper oxides.

5.2 RESULTS AND DISCUSSION

The XANES from the Cu K-edge region of several compounds are shown in Figures 5.2-5. In Figure 5.2, K-edge absorption spectra of copper in Cu, Cu_2O, CuO, La_2CuO_4, $YBa_2Cu_3O_7$, $La_{1.85}Sr_{0.15}CuO_4$, $Tl_2Ba_2Ca_2Cu_3O_{10}$ and $Tl_{0.2}V_{0.8}Sr_2(Ca_{0.8}Y_{0.2})Cu_2O_y$ are presented. Some of the spectra reported here are very similar to those reported earlier in the literature[1-7].

In Figure 5.3, we show the XANES spectra of $La_2Li_{0.5}Cu_{0.5}O_4$ and $Ba_4NaCuO_4(CO_3)_9$ and in Figure 5.4 the profiles of K-edges in Nd_2CuO_4, $CuAl_2O_4$, Y_2BaCuO_5, $Y_2Cu_2O_5$ and Sr_2CuWO_4 are given. In Figure 5.5 are shown the K-edges of copper in $SrCuO_2$, $MgCu_2O_3$, Ca_2CuO_3 and $CaCu_3Ti_4O_{12}$. Nd_2CuO_4 has copper ions in a square-planar coordination with the Cu-O distance of ~ 1.98 A^o. The square-planar CuO_4 units share corners to form a two-dimensional network[21] in this structure. The main difference from La_2CuO_4 is that in this compound there are no Cu-O bonds along the c axis. Nd_2CuO_4 is therefore an ideal model for a pure square-planar array of corner linked CuO_4 units. From various studies[22-25] like X-ray and electron diffraction, magnetic susceptibility, EPR and Li NMR on $La_2Li_{0.5}B_{0.5}O_4$ with B = Co, Ni, Cu, it has been concluded that the B ions are in trivalent state including Cu. The most important result has been obtained from the magnetic susceptibility and Li NMR studies. When B = Cu or Co the system is diamagnetic; when B = Ni, the Curie constant is

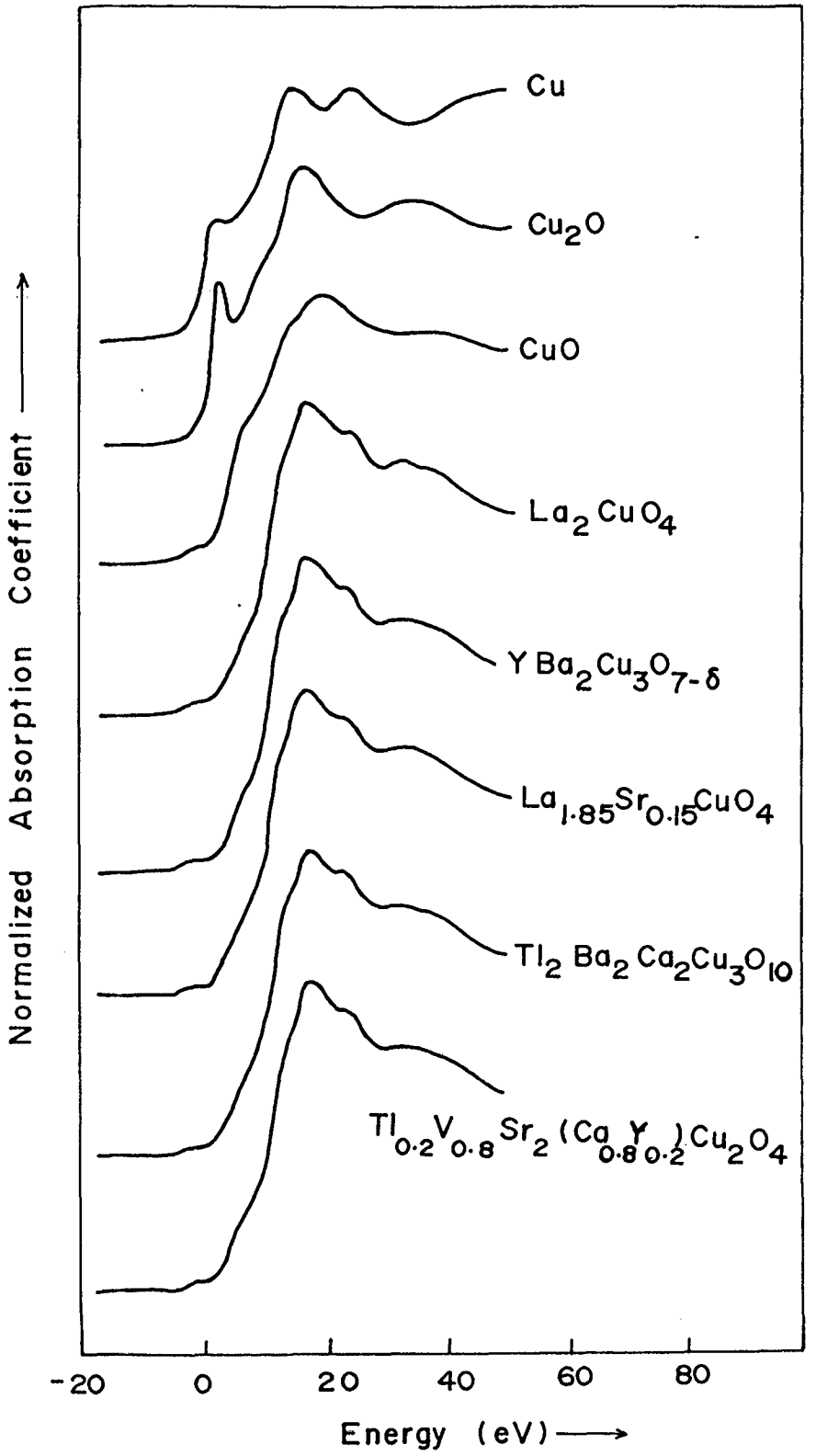

Figure 5.2: Cu K-edge spectra in copper metal, Cu_2O, CuO, La_2CuO_4, $YBa_2Cu_3O_{7-\delta}$, $La_{1.85}Sr_{0.15}CuO_4$, $Tl_2Ba_2Ca_2Cu_3O_10$ and $Tl_{0.2}V_{0.8}Sr_2(Ca_{0.8}Y_{0.2})Cu_2O_y$

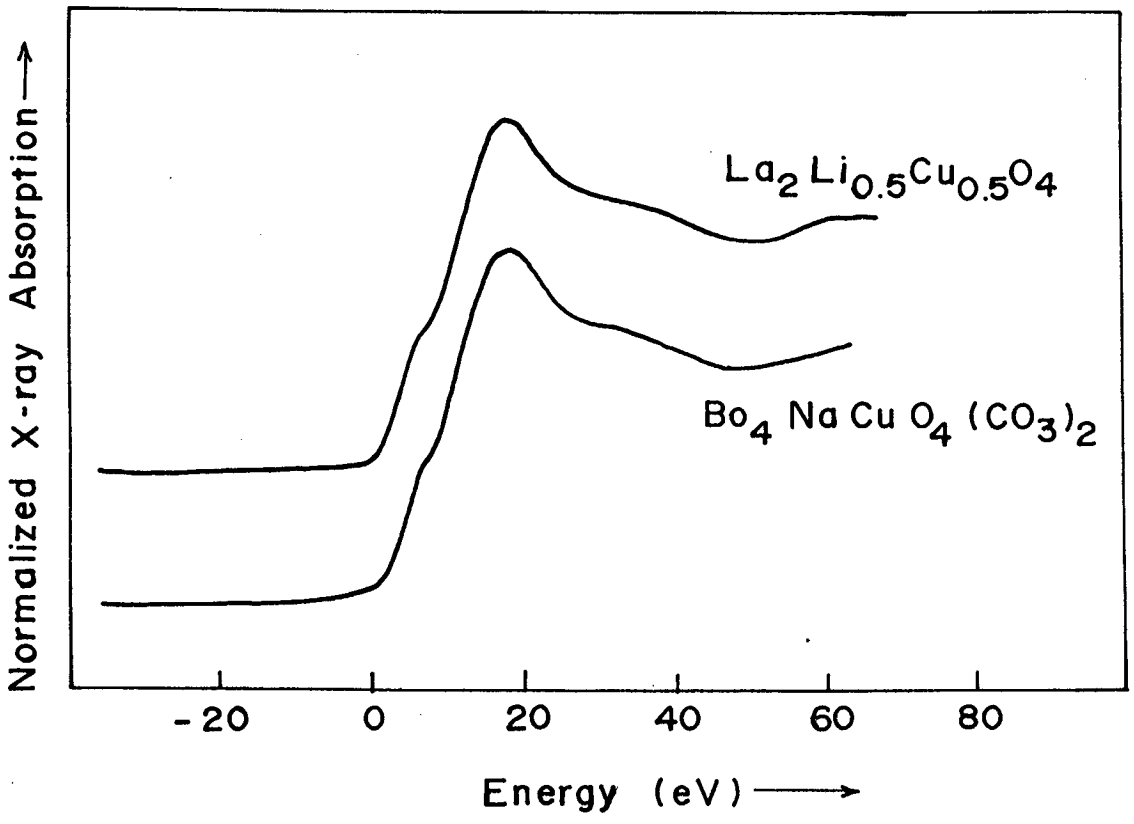

Figure 5.3: Cu K-edge spectra in $La_2Li_{0.5}Cu_{0.5}O_4$ and $Ba_4NaCuO_4(CO_3)_2$

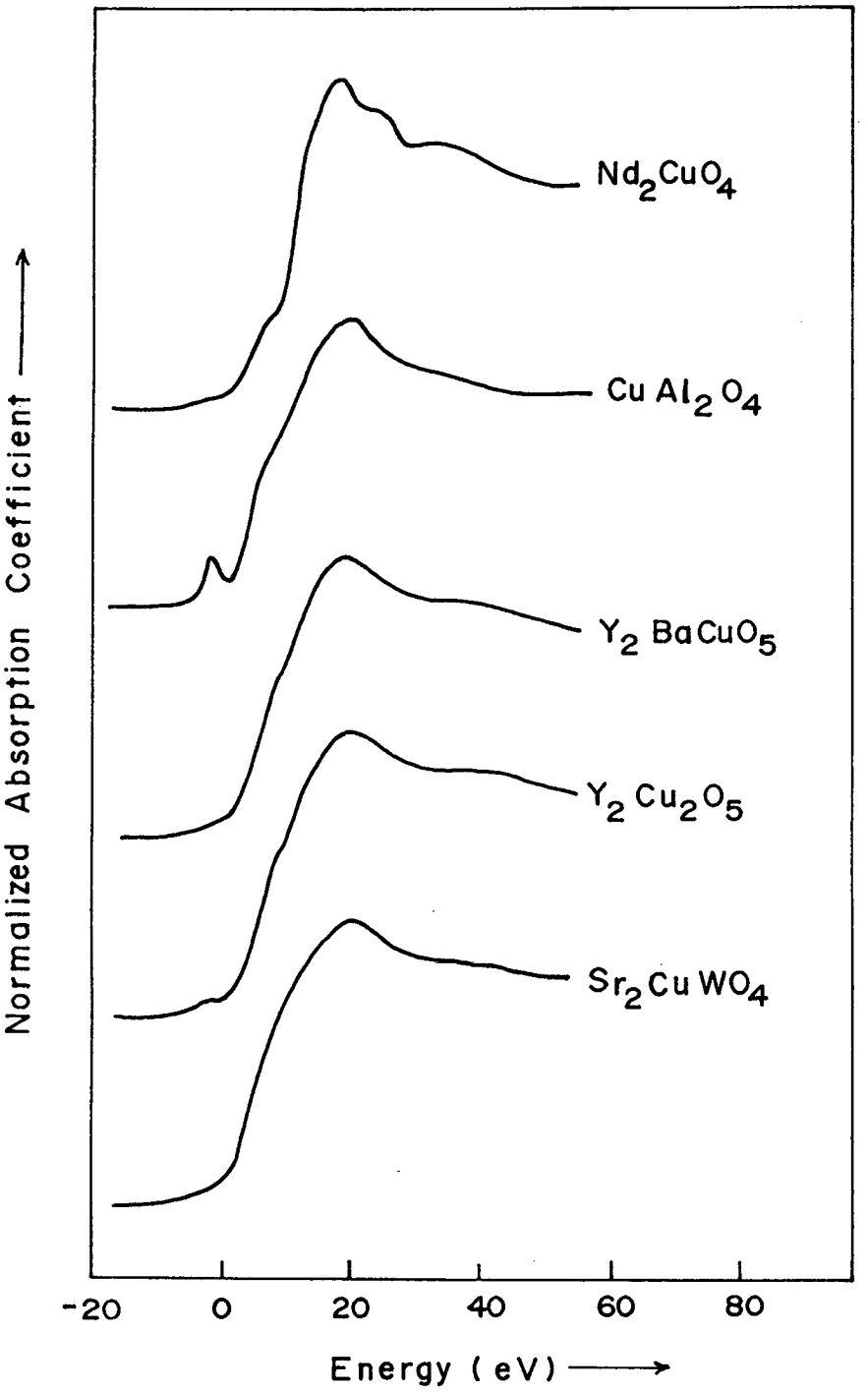

Figure 5.4: Cu K-edge spectra in Nd_2CuO_4, $CuAl_2O_4$, Y_2BaCuO_5, $Y_2Cu_2O_5$ and Sr_2CuWO_4

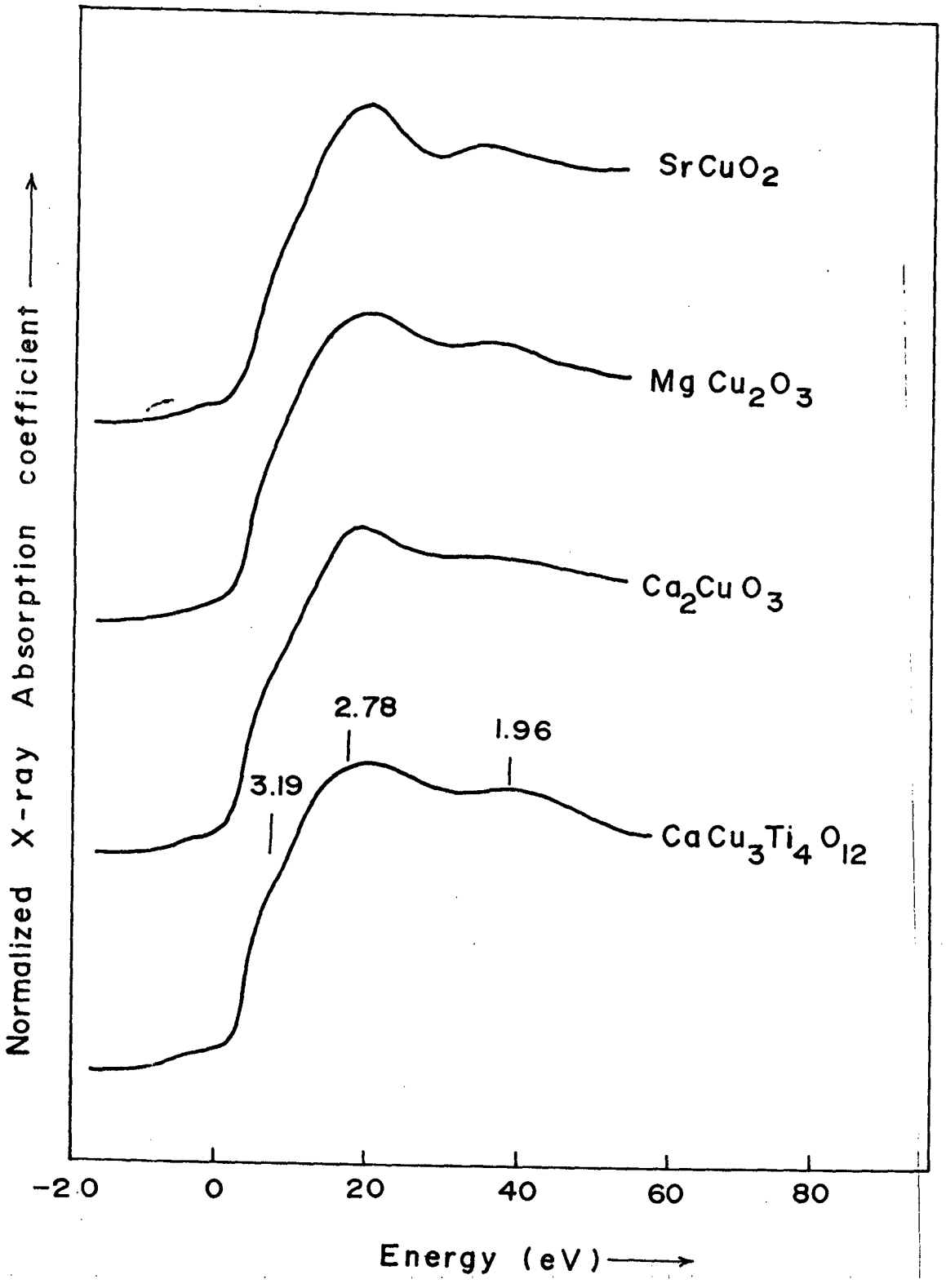

Figure 5.5: Cu K-edge spectra in $SrCuO_2$, $MgCu_2O_3$, Ca_2CuO_3 and $CaCu_3Ti_4O_{12}$

typical of one unpaired electron as expected for low-spin Ni^{3+} ions (t_{2g}^6, e_g^1) and the EPR signal characteristic of Li^{+3} ions[26] as in fluorides. The Li NMR does not show any change[25] in the chemical shift on changing B. Since electron diffraction studies show evidence for cation ordering[22], the constancy of the NMR chemical shift suggests that the Li environment is identical in all the compounds. This could only happen when there are no holes on the oxygen and all the B ions are in the trivalent state. $La_2Li_{0.5}Cu_{0.5}O_4$ is therefore a suitable model for the study of the absorption edge of isolated Cu^{3+} ions. $CaCu_3Ti_4O_{12}$ has the copper ions located at the A site with twelve oxygen neighbours[27] with three sets of Cu-O distances (1.96x4, 2.78x4 and 3.191x4 A^o) so that this compound is ideally suited for testing the model of Lytle et al[4]. The positions of the peaks expected from the ruler of Lytle et at are indicated by arrows in the Figure 5.5.

We see that the XANES of Nd_2CuO_4 is very similar to that of La_2CuO_4 and $YBa_2Cu_3O_7$ shown in Figure 5.2. The XANES of $La_2Li_{0.5}Cu_{0.5}O_4$ is very different and the main absorption peak seems to have shifted by about 3 eV relative to La_2CuO_4. The spectra of $La_2Li_{0.5}Cu_{0.5}O_4$ bears a striking similarity to the reported spectra of $KCuO_2$ in which the copper ions are expected to be in the trivalent state. In the XANES spectra of $CaCu_3Ti_4O_{12}$ we do not see any correlation between the features and those expected from the model of Lytle et al[4].

In Figure 5.4 we show the XANES spectra of $CuAl_2O_4$ in which the copper ions are in tetrahedral coordination[28]; Y_2BaCuO_5 in which the copper ions are in isolated square-pyramidal[29] coordination with the copper-oxygen distance having ~ 2.05^o; $Y_2Cu_2O_5$ in which the Cu^{2+} ions have a strong tetrahedral component of distortion[30]; and Sr_2CuWO_6 in which the copper ions are in isolated octahedral environment[31]. All these compounds have[16] a Curie constant (calculated from the temperature dependence of the magnetic susceptibility at high temperatures)

close to 1.73 μB. In all these compounds the feature C is either absent or is very weak. We note that $CuAl_2O_4$ and $Y_2Cu_2O_5$ show a relatively high intensity of the feature P indicated in Figure 5.1 which is generally associated with a 1s → 3d transition[37].

In Figure 5.5 we show the XANES spectra of $SrCuO_2$, $MgCu_2O_3$, Ca_2CuO_3 and $CaCu_3Ti_4O_{12}$. In $SrCuO_2$ there are[32] pairs of edge-shared square-planar CuO_4 units forming chains along one direction in a manner similar to that in some of the superconducting family of copper oxides[33]. In $MgCu_2O_3$ the structure[34] has features similar to that of $SrCuO_2$ except that the copper ions are in octahedral coordination with two oxygen ions at 1.94 A^o, two at 2.01 A^o and one each at 2.53 and 2.76 A^o. The Cu-O linkage along the chain involves long Cu-O distances. In Ca_2CuO_3 the square-planar CuO_4 units (two oxygen atoms at 1.89 A^o and two at 1.96 A^o) share corners along one direction to form a chain[35] just as the Cu (I) site ions in[36] $YBa_2Cu_3O_7$.

Since the relative intensities of the main and satellite features of the XPS signals from the core levels are prominent, we have recorded the $Cu_{2P_{3/2}}$ XPS spectra of some of the copper compounds studied by XANES. The results are shown in Figure 5.6.

In the forthcoming few paragraphs, we shall briefly review the interpretations of the XANES spectra as discussed in the literature. This has been done for the sake of highlighting the essential features of the various interpretations. The purpose is to focus on the possible identity of the feature C shown in Figure 5.1. As mentioned earlier we will find that not all these interpretations are consistent with one another.

The X-ray K-edge absorption spectra of copper ions show shoulders (see Figure 5.1) on the absorption edge (features B and C) as well as pre-absorption edge feature P. Also there are other features in a range within 50 eV above the absorption threshold (D). The early analysis of these features were based on the

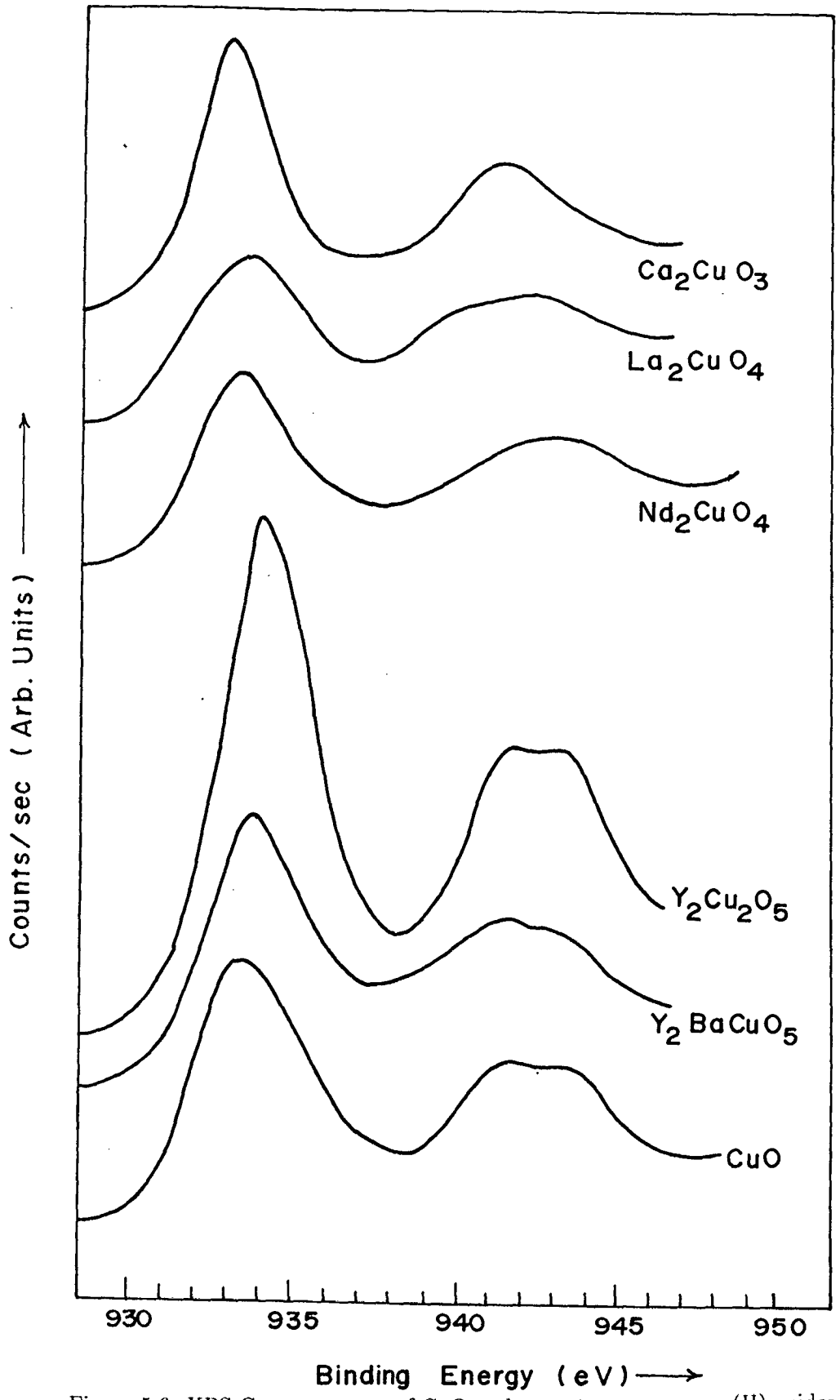

Figure 5.6: XPS $Cu_{2p_{3/2}}$ spectra of CuO and some ternary copper (II) oxides

assumption that correlation effects are negligible compared to the 1s binding energies and the state to which the 1s electron is excited is atomic in character and localized on the metal ion[38]. The final state of the ion with atomic number Z is expected to be similar to that of the corresponding (Z+1) ion with the same charge but having the 1s shell full. Thus atomic spectroscopic splittings may be used for the analyses of the XANES region. In covalent compounds the ligands, however, have a significant influence and introduce additional ligand-to-atom shakedown transitions that are not possible in atomic spectra. Thus when a 1s electron is removed the ground state of the relaxed wavefunction changes from d^9 to d^{10} with holes introduced on the ligand by a ligand-to-metal charge transfer. Such charge transfer states could have energies around 6-8 eV lower than the main transitions as demonstrated by Bair and Goddard[38]. The lowering of energy is due to the increased screening of the core hole when an electron is transferred from the ligand to the d shell of the cation.

The assignment of the features especially near the band edge seemed to have been satisfactorily resolved with the introduction of linearly polarized synchrotron radiation for the study of polarization in the XANES transitions in single crystals[39,40]. Such assignments becomes more facile in compounds of Cu^{2+} with axial symmetry. The 4p states could be spilt into $4p\sigma$ or $4p\pi$ molecular orbital states in such a symmetry and could be of the order of 4-5 eV[42,43]. The calculations of Alp *et.al.*[1] show that this splitting is of the order of 5eV in La_2CuO_4. Such splitting cannot account for the feature C. It is because of this fact that Alp *et.al.* attributed the feature at C to the presence of Cu^{3+} ions. The splitting between the $4p\pi$ and $4p\sigma$ levels are expected to decrease in clusters with tetrahedral or octahedral symmetries[38].

The pre-absorption edge features can then be assigned on the

basis of the conventional interpretation of the XANES region. The pre-absorption edge feature P in Figure 5.1 have been ascribed[20,37,38] to 1s to 3d transitions which are dipole forbidden but quadrupole allowed. The shoulder on the absorption edge around 7-10 eV relative to the 1s to 3d transition (features A in Figure 5.1 for the single crystal results of Heald *et.al.* on $La_{1.85}Sr_{0.15}CuO_4$) is likely to be due to 1s to $4p\pi$[7,38] + shakedown transition. The main peak is therefore to be associated with 1s to 4p transition and is expected to yield information on the p-type unoccupied states. The features B_1 and B_2 could relate to the direct 1s to $4p\pi$ and 1s to $4p\sigma$ transitions.

The relative intensities of the main and shakedown transitions are expected to be in the ratio

$$1:(\langle 3d \,/\, L^1\rangle)^2 \qquad (5.1)$$

where the term ($\langle 3d \,/\, L^1\rangle$) is the overlap of the ground state 3d orbital with the excited state L^1 ligand orbital with one hole. Such a ratio really implies that there are two distinct states into which transitions can be effected: The one electron excitation which involves the initial state and the other a multielectron excitation which involves the energies in the final state after the shakedown or charge-transfer process.

The main ambiguity lies in the interpretation of the features at higher energies. The next series of transitions should involve the closely spaced 5s, 4d, 5p etc. levels which should lie about 10 eV above the 1s to 4p transition or around 30 eV above the 1s to 3d transition[38].Backscattering effects due to other ions not included in the first coordination sphere of the central ion are usually dominant[1,6] in the region D. Thus an unequivocal identification becomes difficult in this region especially because the relative intensities of the 1s to 5p main and shakedown transitions are difficult to estimate.

The results of Heald et al.[7] (Figure 5.1b) support at least qualitatively the calculations of Alp et al (Figure 5.1a). In these calculations, the feature B_1 in the spectra of Heald *et.al.*[7] (Figure 5.1) is to be attributed to final states composed of Cu^{2+} axial 4p states (feature A in the calculations of Alp *et.al.*[1] in Figure 5.1a) with weak scattering from oxygen neighbours. Similarly the feature B_2 in the single crystal data may be correlated with the feature B in the calculations associated with the equatorial 4p states.

The shoulders B_3 and B_4 (Figure 5.1b) in the single crystal work of Heald et al[7] have not been commented upon. In these crystal studies of Kosugi et al[40]. such shoulders are also observed and have been attributed to 1s to 5pπ or 5pσ transitions which are expected to show the same kind of anisotropies as the 1s to 4p transitions. The relative position of these 5p energy levels have not been calculated in the case of $La_{1.85}Sr_{0.15}CuO_4$. In $CuCl_2$ molecule,Bair and Goddard[38] have calculated the 5pσ level to be about 3.1 eV above the n = 4 level and the 5pπ level to be about 1 eV above the 4pσ level. These energy differences are much smaller than that observed with the single crystal of $La_{1.85}Sr_{0.15}CuO_4$. On the other hand in the configurational-interaction calculations of Kosugi *et.al*[40] for the Cu K-shell of $[CuCl_4]^{2-}$ ions the deference in energy between the 1s → 4p and 1s → 5p transitions are ~ 7.5 eV which is roughly the separation seen in the case of single-crystal XANES spectrum of $La_{1.85}Sr_{0.15}CuO_4$.

5.3 XPS and XANES

The difference between XANES and XPS is that the first excited state to which the electron makes a transition by the absorption of a photon of energy *hv* is the first unoccupied state above the Fermi level in the case of XANES and that above the

vacuum level in the case of XPS. Both these methods enable one to locate the binding energy of the electrons as referred to the Fermi level. It is important to remember that this binding energy is the difference in energies between the final state with N-1 electrons and an initial state with n electrons : B.E. = $E_f - E_i$. Consequently it is necessary to obtain a good description of all the possible initial and final states which follow the absorption or photoemission process. The final states reflect the kind of screening processes invoked for the core hole. The binding energies should be identical in two processes provided that the same core hole is studied. Otherwise the separation in energies have to be modified by the differences in the term U_{kc} which describes the interaction between the core level c and the outer level k. In the case of Ce the configurational mixing deduced from XPS and XANES data[41] from the same core level are identical which suggests that the ratio of the intensities for the fully screened (with ligand to metal charge transfer) and poorly screened processes should be the same in the two processes[38].

The importance of multielectron excitations involving ligand-to-metal charge transfer process in core-level spectroscopies was first realized in the case of XPS studies. Larsson[42] was among the first to highlight the importance of such processes in accounting for the strong satellites in the core level XPS spectrum of transition metal ions such as Cu^{2+}. The satellite corresponds to the state assumed in crystal field theory with nine 3d electrons whereas the main peak corresponds to a state with all ten 3d electrons. In this picture the satellite becomes larger when the ligand is more electronegative. In the case of ligand admixture into the final state the relative ratios of the satellite and main peak are expected to be reduced over that in the absence of admixture. Since the ligand-to-metal charge transfer processes are the same in both XPS and XANES, it becomes necessary to assume that the relative intensities of the

shakedown or fully screened configurations as well as the main poorly screened configurations should be the same in both. This is the basic objective of the calculations of Sarma[8].

Sarma's calculations are derived from the original calculations of Alp *et.al.* As mentioned earlier, these calculations are based on one electron excitation picture[43] in which the state to which the electron is excited is the initial state. Implicit in the calculations of Sarma is the assumption that the most intense features in the calculations of Alp *et.al* are due to multielectron excitations from the 1s to the fully screened configurations 4pσ and 4pπ configurations (d^0) where the major contribution are from the final states. Sarma then adds on the satellite features of XPS at suitable energies after the normalization of intensities (see Ref.42) to the main peaks of Alp *et.al.* By including lifetime broadening Sarma has been able to reproduce fairly well the experimental features of La_2CuO_4 as shown in Figure 5.1. By doing so Sarma has completely ignored the earlier intensity calculations of say Bair and Goddard[38] or Kosugi *et.al*[40] which identify the main peak with the 1s to 4p transitions. Sarma has not commented on this discrepancy despite the fact that several papers in this area rely heavily on the calculations of Bair and Goddard. The merit of Sarma's interpretation is the remarkably good fit with realistic parameters and also the attempt to correlate XPS and XANES intensities. Another important aspect of this interpretation is that his calculations have shown that the satellite of the 1s to 4pσ main peak should be very small compared to that of the 1s to 4pπ transition. This is actually observed in the later work on single crystals (features B_3 and B_4 in Figure 5.1). However, in such an interpretation it would be difficult to account for the features at lower energies (around 7 eV) which have been attributed to 1s to 4pπ shakedown transition by polarized synchrotron radiation studies on oriented single crystals[7].

The procedure adopted by Sarma was actually first examined by Stern[44] who was among the first to propose that the structure on the higher energy side of the main absorption peak in XANES could be related to the satellite peak (what he terms as a shake-up satellite) of the main core level spectra in photoelectron spectroscopy. Stern, however, realized that XPS and XANES intensities need not be similar. The difference in the satellite strengths in XPS and XANES could be attributed to the different excitation energies of the photoelectrons involved; in the former the excitation energy is hundreds of electron volts while in the latter the photoelectron is at the threshold. The highly energetic photoelectron state in the former thus does not play an important role in shielding the core hole compared to the absorption process in which the photoelectron is still located on the metal ion and thus partially shields the core hole from the ligand. The charge transfer processes or final state effects thus become more important in photoelectron spectroscopy. It has also to be noted that at the threshold the core hole potential is turned on adiabatically while at very high energies the sudden approximation becomes valid. This could be interpreted in terms of a more overlap of the photoelectron with initial states at the threshold than at higher energies.

5.4 SCATTERING EFFECTS

As mentioned earlier a completely different interpretation is that due to Lytle et al[4] who find a simple relation between E and $1/R^2$ where R is the distance of the ligand in various coordination shells from the central cation. In this model the feature at C is to be attributed to a copper-oxygen distance of 2.6 A^{O}. This is typical of the A-O distance in ABO_3 pervoskites and from this Lytle et al[4]. suggest that the feature C is to be associated with Cu^{2+} ions at the A sites. This assumption has

been criticized by Heald *et.al.*[7] on the basis of their single crystal work since the feature C is very sensitive to the orientation although no such anisotropy is expected in the Cu-O distances if the copper ions occupy the A sites. However, such an anisotropy is anticipated if the copper ions occupy the Ba sites.

5.5 INTERPRETATION OF PRESENT RESULTS

In the interpretation of the results we resort to qualitative arguments first of all because the resolution of our measurements are not sufficient to warrant such a calculation. It has to be noted, however, that in some cases such as metals the modern techniques using intense synchrotron radiation[18] and the earlier techniques using weaker radiation[45] gave nearly identical results. The resolution obtained by us is sufficient to distinguish between the main features A',B,C and D. The main purpose of this study is to obtain information regarding the origin of the feature C in a systematic manner.

5.5.1 Scattering Models

As mentioned in section 5.4 the anisotropic behaviour of the feature C in the single crystal data of Heald *et.al*[7]. does not unambiguously refute the scattering model of Lytle *et.al*[4]. However, the features near the absorption edge B_1 and B_2 are seen at the same energies in many single crystal studies of copper complexes and for this reason cannot be simply accounted for by scattering models. We have specifically examined $CaCu_3Ti_4O_{12}$ which has Cu ions at the A sites. There three sets of four oxygen ions having Cu-O distances[27] of 3.19, 2.78 and 1.96 A^o. This is the kind of distance used by Lytle *et.al.* in accounting for spectra of the superconducting compounds. The XANES spectra of $CaCu_3Ti_4O_{12}$ should then be very similar to that of La_2CuO_4. The spectra in Figure 5.3 is, however, slightly different with the

peak positions being far from that predicted from the ruler of Lytle *et.al.* This seems to demonstrate that the model of Lytle *et.al.* is inapplicable at least in a straightforward manner. In the following discussion we shall use the scattering model in interpreting our results.

5.5.2 EVIDENCE FOR Cu^{3+} IONS

The comparison of La_2CuO_4 (Figure 5.2) with $La_2Li_{0.5}Cu_{0.5}O_4$ (Figure 5.3) shows a shift in the main absorption edge by about 4-5 eV. This the kind of shift found in $KCuO_2$ relative to that in the series $La_{2-x}Sr_xCuO_4$ and hence confirms the observation that a Cu^{3+} ion would have the maximum in the absorption edge at around 20 eV. It is important to note that L_3 XANES studies on compounds containing trivalent copper ions[49] reveal the absence of any significant amount of a d^8 configuration. It has therefore been postulated that the Cu^{3+} ion is unstable in an oxide matrix and instead a hole is created on the ligand oxygen ions. This aspect has been discussed earlier in connection with the oxidation of Ni^{2+} ions in oxide matrices by Ganguly[46]. One of the conditions for the creation of holes on oxygen seems to be that the energy level of the metal ion in the higher oxidation state should be below that of the anion levels[47]. This seems to be the case for ions such as Cu^{3+} or Ni^{3+}. Thus the $(Cu\text{-}O)^+$ unit is composed of Cu^{2+} O^- ions. Of importance to this study is our observation that the properties of $La_2Li_{0.5}Cu_{0.5}O_4$ (M = Co, Ni, Cu) are consistent with each other if the copper ions are in the low-spin trivalent Cu^{3+} state. This conclusion is based on several studies including optical spectra, Li NMR, ESR, Raman and infra-red spectra as well as systematics of lattice parameters. The most important of these perhaps, the ESR for M = Ni is typical of Ni^{3+} ion and Li NMR is identical for all M showing the identical environment of the nearest neighbour Li ions which share the same oxygen as the M ions in the ab plane. The ^{57}Co Mössbaur results of Fontcuberta *et*

al[23] with $La_2Li_{0.5}Co_{0.5}O_4$ are also consistent with the Co ion in the low spin trivalent state. The L_3 XANES results of Bianconi *et al*[49a] however show that in $La_2Li_{0.5}Co_{0.5}O_4$ the hole is on oxygen and not on copper. This apparent contradiction between our results[25] using conventional techniques and those of Bianconi *et al*[49a] using L_3 XANES technique is not clear to us yet. We note that the L_3 XANES spectra of $NaCuO_2$ as reported by Sarma *et al*[49b] is very different from that reported by Bianconi *et al*[49a]. Unlike the K-edge spectra the technique for obtaining the L_3 spectra is surface sensitive[49b] just as XPS which in the case of superconductors is very irreproducible.

5.5.3 1s → 3d Transition

The pre-absorption edge feature, P, is usually attributed to the 1s → 3d transition. Since the tetrahedral coordination does not have inversion symmetry the ligand field breaks the spherical symmetry of atom potential. As a result the dipole selection rule is relaxed and the quadrupole transition strength increases. In accordance with this the copper ions in octahedral coordination such as in $MgCu_2O_3$, Sr_2CuWO_6, or even in square-pyramidal coordination as in Y_2BaCuO_5 show very little pre-edge absorption feature. Only in $CuAl_2O_4$ or $Y_2Cu_2O_5$ where the nearest neighbour coordination shell does not have an inversion symmetry do we find a strong pre-edge absorption feature. Thus as per expectation (see section 5.2), the pre-absorption feature, P, can be truly attributed to the 1s to 3d transition.

5.5.4 COMPARISON OF XPS AND XANES

The results of Sarma highlighted the point (see section 5.3) that the XANES intensity near the feature C could be related to the intensity of the poorly screened configuration in the XPS such as the feature at 942 eV in the Cu $2p_{3/2}$ region. We find in

our studies that the compounds such as $CuAl_2O_4$, $Y_2Cu_2O_5$, Y_2BaCuO_5, Sr_2CuWO_6 in which the copper ions are either isolated or do not have strong nearest neighbour antiferromagnetic interaction strengths, do not show any feature corresponding to the feature C although these compounds show a very high satellite intensity in the XPS (Figure 5.6). The main absorption peak shows very little difference in energies in these compounds so that it is unlikely that the satellite feature has been absorbed into the main band. It is also interesting to note that the spectra obtained with Y_2BaCuO_5 in which the copper ions are in isolated five-fold square-pyramidal coordination just as the Cu (II) ions in $YBa_2Cu_3O_7$ are almost identical to those calculated for the first coordination shell for the latter ions. In these calculations only one-electron excitation is assumed. We therefore do not see any direct correlation between the intensity of the feature C in these compounds with that of the XPS intensities as suggested by the calculations of Sarma[8] and first examined by Stern[44].

From the above discussion we may come to the following conclusions regarding feature C :

i) The feature C is unlikely to be due to one-electron excitation process involving main 1s → 5pσ or 5pπ transitions since in such an one-electron picture it should be seen in both isolated copper ions (with no Cu-O-Cu interactions) as in Sr_2CuWO_6, Y_2BaCuO_5 etc., as well as in other compounds such as Ca_2CuO_3, $SrCuO_2$ etc., which have extended 180^o Cu-O-Cu interactions.

ii) Within our experimental resolution the feature C does not seem to correspond to the poorly screened configuration $3d^1L^0$ at least not in the sense suggested by Stern[44] or Sarma[8] (see section 5.2) in which the main peak corresponds to the fully screened d^0L^1 configuration. The calculations of Sarma suggest that this separation should be ~ 7 eV and should have been if it had been present with the same relative intensities as in the

XPS.

iii) As discussed earlier (section 5.2) the feature C does not seem to be due to scattering effects as proposed by Lytle *et.al*[4].

As noted earlier the feature C is to be associated with the feature B_4 in the single crystal work of Heald *et al*[7](Figure 5.1b). In order to understand the single crystal results of these authors it is necessary to understand first of all the chemical systematics in other single crystal work. To our knowledge the only work of these kind is carried out by Smith et al[39]. In this study these authors examined the X-ray absorption spectra of a series of single crystals of copper with various ligands. The important results emerging from this study is that for the polarization parallel to the plane the same two features (B_2 and B_4) are seen. The separation in energy between these two features are independent of the nature of the ligand and is close to that in Figure 5.1b. The actual energies are, however, sensitive to the nature of the ligand. For the lower energy peak (to be identified as B_2 hereafter) the energy changes from 8994 eV in the case of ionic Cl^- to 9001 eV with the more covalent trimethylimidazole in which the ligation is through nitrogen. $La_{1.85}Sr_{0.15}CuO_4$ the energy of B_2 is ~ 8997eV which would indicate that the oxygen ligand is less covalently bound than the nitrogen ligand as is to be expected. The ratio, R_2, of the intensities B_2/B_4 increases with increasing covalency. R_2 is much larger in the superconducting copper oxides.

When the beam polarization is perpendicular to the plane, Smith *et al*[39] find that there are two sharp peaks which may be attributed to highly localized electrons of copper ions. The energies of these two resonances (~ 8986 eV and ~8993 eV) are rather insensitive to the nature of the ligand. They correspond closely to the positions of the A and B_1 peaks in single crystals of $La_{1.85}Sr_{0.15}CuO_4$ (Figure 5.1b) and Nd_2CuO_4 (Figure 5.3). The low energy feature is therefore referred to as A and the higher

energy feature as B_1. The sharpness of these features increases as ligand interaction decreases. The ratio of the intensities of feature A to B_1 is rather insensitive to the nature of the ligand when the d_{z^2} electrons are localized on copper but becomes rather reduced when these electrons are delocalized over the axial ligands by π bonding[39]. We find that the feature A is quite sharply defined in the powder spectra of Nd_2CuO_4 (Figure 5.4) in which there is no axial ligation relative to that of La_2CuO_4. The feature A is barely discernible in the powder spectra of $La_{1.85}Sr_{0.15}CuO_4$. The decrease in intensity of the feature A on going from Nd_2CuO_4 to $La_{1.85}Sr_{0.15}CuO_4$ is in agreement with the increasing conductivity and hence increasing delocalization.

We may identify the conditions for observing feature C (and A) in the powder spectra if we assume that in systems with long range 180^o Cu-O-Cu interactions there is considerably more delocalization of the electrons over that in which the copper ions are isolated as in Y_2BaCuO_5 or Sr_2CuWO_6, or do not have 180^o Cu-O-Cu interactions, as in $Y_2Cu_2O_5$ or $CuAl_2O_4$. The more covalent nature of those compounds with 180^o Cu-O-Cu interactions is seen in the magnetic susceptibility studies.[16] All these compounds have a low susceptibility indicative of high antiferromagnetic ordering temperatures and hence transfer integral or covalency. Those without such interactions show well defined Curie - Weiss type of behaviour with the Curie constant being close to that of copper ions in ionic compounds[16]. From the single crystal studies of Smith *et al*[39] we would then expect B_2 feature shifted to higher energies in the more covalent compounds with delocalized 180^o Cu-O-Cu interactions (more covalent) compared to those without such interaction. The associated higher energy satellite feature B_4 (feature C in Figure 5.1a) would then become more prominent. The results of Lytle *et al* (Figure 7 of ref.4) are consistent with such an interpretation where the main peak feature is seen to shift to higher energies on going from $CuTiO_3$

to copper phthalocyanine.

The feature A is not conspicuous in powder spectra of the more ionic compounds (Figure 5.5) . In compounds such as $Y_2Cu_2O_5$ and $CuAl_2O_4$ the tetrahedral environment could completely change the nature and energies of the resonances. However in Sr_2CuWO_6 and even in Y_2BaCuO_5 the square-planar coordination around the isolated copper ions is more prominent. The distortion of the octahedra in the former (c/a ratio = 1.16) is considerably less than that in La_2CuO_4 (c/a ratio = ~ 1.26). In Y_2BaCuO_5 the axial to basal ratio in the square-pyramidal coordination is also ~1.17. This is consistent with the observation of Lytle *et al*[4] that the feature A becomes more prominent as the environment becomes more square-planar in nature (see Figure 7 of ref. 4). Thus the prominence of the feature A is to be attributed to the relatives shifts of the energies of the resonances associated with beam polarization perpendicular or parallel to the square-planar coordinated ligands.

It is difficult at this stage to assign the electronic transitions unequivocally to the features especially in the absence of high resolution data and in the absence of rigorous theoretical calculations. However, we shall make some general qualitative remarks regarding the possible assignments in the following paragraphs.

We note first of all that the calculations of Alp *et al* are in good agreement with the later single crystal work, as far as the energies are concerned. These calculations are based on the one-electron theory for the interpretation of near edge structure in which the main transition is to be associated with 1s to continuum (positive energy) p states. This corresponds to the initial state in the one-electron excitation model. Thus, the feature B_1 and B_2 would correspond to the main 1s to 4p transitions, respectively. The other features could be derived from multi- electron excitation. The lower energy feature, A,

would then correspond to the shakedown process of Bair and Goddard[38]. In the calculations of Smith *et al*[39] this is attributed to a bound-a-bound transition localized on copper which should correspond to the fully screened d^0 (hereafter the superscript will refer to the number of holes) configuration that is familiar in multielectron processes as in XPS. By the same token the feature C or B_4 should correspond to the poorly screened "shakeup" multielectron d^1 L^0 transition of the corresponding 1s to 4pσ transition. In such an interpretation the intensity of the "shakeup" feature C or B_4 is expected to decrease with increasing covalency as actually observed in the single crystal studies of Smith *et al*[39]. The shift to higher energies of the 1s to 4p transitions with increasing covalency is consistent with the antibonding nature of the unoccupied one-electron 4p level obtained from molecular orbital calculations[18].

It is not clear, however, why the "shakedown" transition should be associated only with the 1s to 4pπ transition and the "shakeup" transition only with the 1s to 4pσ transition. If both single electron and multielectron excitations were simultaneously allowed one would have expected each main transition to be accompanied by these two satellites. The later should become important at higher energies relative to the energies associated with former. The relative intensities of the satellite features cannot be obtained therefore in a straightforward manner from XPS studies using analogous of Eqn.5.1 for example. Evidence for two satellites associated with a main transition may be found in the XANES of some of the single crystals. Thus the feature B_3 on the higher energy side of B_1 in result of Heald *et al*[7] (Figure 5.1) could correspond to the "shakeup" satellite. Smith *et al*[39] find a three peak structure for the polarization parallel to the plane in some of the complexes (see Figure 3 of ref 39) and believe that there could be some real intensity (not associated with

artifacts) to the lower energy feature.

The absence or relatively lower intensities of the "shakeup" satellite for B_1 may be attributed to the weak non-bonding nature of ligation perpendicular to the plane. The dominance of the feature B_3 in $La_{1.85}Sr_{0.15}CuO_4$ (Figure 5.1b) is then consistent with either holes on the axial oxygens or with a change from $d_{x^2-y^2}$ to $d_{z^2-r^2}$ orbitals. Bianconi *et al*[50] have proposed from Cu L_3 X-ray absorption spectra of single crystals of $YBa_2Cu_3O_{7-\delta}$ that such a reordering of orbitals could take place. The calculations of Alp *et al* also show such change. Another factor that could be important is that the probability of multielectron excitations become diminished when the electrical conductivity increases. This is suggested by the results of Grunes *et al*[18] who pointed out that for most metals the one-electron excitation calculations are sufficient to account for most of the features in metals but breaks down completely when applied to insulating oxides. It is interesting to note that in $La_2Li_{0.5}Cu_{0.5}O_4$ (Figure 5.3) the feature A is rather prominent and appears at 7 eV just as in the other Cu^{2+} compounds. One would have anticipated a shift to higher energy because of the higher oxidation state. This emphasizes the non-bonding character of the axial ligands. The dominant intensity of the band at 20 eV is because of the characteristic "trivalent " character.

We find the above model attractive because of the simple manner by which we may account for all the features. All of the ingredients in the above model have been considered at one stage or another but have not been assembled together in this manner. The main difficulty with this model is that the energies separating the satellite features do not correspond to those found in XPS.

In a sense we could modify the above picture and associate the main transition as the d^1 hole (d^9 electron) configuration

and the satellites as due to d^0 (lower energy "shakedown") or d^2 (higher energy "shakeup") configurations of copper in much the same manner as the configurations included[51] in the problem of Ce. The d^0 configurations (Cu^+) is known to be stabilized in axial symmetry and dominates the axial beam polarization features while d^2 (Cu^{3+}) is known to be stabilized in square-planar geometry and therefore dominates for beam polarizations parallel to the plane. Since the feature C is close in energy to that of trivalent ions, it could support such a conjecture.

In this work, a large number of copper oxides with different structural features have been investigated through XANES studies in order to understand the XANES features reported for the superconducting compounds. The results obtained with polycrystalline samples have been compared with other single crystal work on copper complexes as well as the superconductors. The various models used so far to interpret the XANES features have been reviewed. The importance of one-electron and multi-electron excitations have been examined.

The present study has therefore been useful in delineating the conditions for the observation of the feature which is observed in all the superconducting copper oxides at about 20 ev. This feature is to be associated with the presence of extended 180^o Cu-O-Cu interactions between corner-linked square-planar CuO_4 units.

Scattering models have been specifically examined using suitable model compounds and found to be unsuccessful in explaining the XANES features. The best explanation seems to associate the features with both single-electron and multi-electron excitations picture.

REFERENCES

1. E.E.Alp, G.K.Shenoy, D.G.Hinks, D.W.Capone II, L.Soderholm, H. B. Schuttuler, J. Guo, D. E. Ellis, P. A. Montano and M. Ramanathan, Phys. Rev.B 35, 7199 (1987).

2. J.M.Tranquada, S.M.Heald and A.R.Moodenbaugh, Phys. Rev.B 36, 5263 (1987).

3. H. Oyanagi, H. Ihara, T. Matsushita, M. Tokumoto, M. Hirabayashi, N. Terada, K. Senzai, Y. Kimura and T.Yao, Jpn. J. Appl. Phys. 26, L638 (1987).

4. F.W.Lytle, R.B.Gregor and A.J.Panson, Phys. Rev.B 37, 1550 (1987).

5. J.B. boyce, F. Bridges, T. Claeson, R.S. Howland and T.H. Geballe, Phys. Rev.B 36, 5251 (1987).

6. K.B. Garg, A. Bianconi, S. Della Longa, A. Clozza and m. de Santis and A.Marcelli, Phys. Rev. B 38 244 (1988).

7. S.M. Heald, J.M. Tranquada, A.R. Moodenbaugh and Youween Xu, Phys. Rev. B 38, 761 (1988).

8. D.D. Sarma, Phys. Rev. B 37 7948 (1988).

9. (a) D.D. Sarma, K. Sreedhar, P. Ganguly and C.N.R.Rao, Phys. Rev. B 36 2371(1987); (b) D.D. Sarma and C.N.R. Rao, J. Phys. C 20 L 659 (1987).

10. A. Fujimori, E. Takayama-Muromachi, Y. Uchida and B. Okai, Phys. Rev.B 35, 8814 (1987).

11. A. Bianconi, A.Clozza, A. Congiu Castellano, S. Della Longa, M.de Santis, A. di Cicco, K. Garg, P. Delogu, A. Gargano, R. Giorgi, P.Lagarde, A.M.Flank and A.Marcelli, Intn. J. Modern Phys. B 1 853 (1987).

12. J.G.Bednorz and K.A.Mûller, Z. Physik B Condensed Matter 64, 189 (1986).

13. H. Muller Buschbaum, angew. Chem Int. Ed. Engl. 16, 674 (1977).

14. B. Raveau in Advances in Solid State Chemistry (ed. C.N.R. Rao) Proc. Ind. Nat. Sci. Acad. 67 (1986).

15. C.Michel and B.Raveau J.Solid State Chem 43, 73 (1982).

16. K.Sreedhar and P.Ganguly, Inorg. Chem. 27, 2261 (1988).

17. P. Ganguly, K. Sreedhar, A. R. Raju, G. Demazeau and P. Hagenmuller, preprint (1988).

18. L.A.Grunes, Phys. Rev B. 27, 2111 (1983).

19. L.S.Kau, D.J.Spira-Solomon, J.E.Pennar-Hahn, K.O.Hodgson and E.I.Solomon, J.Am.Chem.Soc.,109, 6433 (1987).

20. (a) P.R. Sarode, G. Sankar and C.N.R.Rao Pro.Ind. Acad. Sci. (Chem. Sci) 93, 321 (1984).
(b) G.Sankar, P.R. Sarode and C.N.R. Rao Chem.Phys. 76, 435, (1983).

21. H. Muller Buschbaum and W. Wollschlager, Z. Anorg. Allog. Chem., 414, 76 (1975).

22. G. Blasse, J. Inorg. Chem., 27, 2683 (1965).

23. (a) G. Demazeau, M. Pouchard, M. Thomas, J.F. Colombet, J.C. Grenier, L.Fouenes, J. L. Soubeyroux and P.Hagenmuller, Mat. Res. Bull., 15, 451 (1980).

23. (b) J.Fontcuberta, A.Fernandez and J.B.Goodenough, Phys. Rev. Lett., 57, 1931 (1986).

24. J.B.Goodenough, G.Demazeau, M.Pouchard and P.Hagenmuller, J. Solid State Chem., 8, 325 (1973).

25. K. Sreedhar and P. Ganguly (Unpublished results).

26. D.Reinen, C.Friebel and V.Propach, Z. Anorg. Allog. Chem., 408, 187 (1974).

27. (a). V.Propach, Z. Anorg. Allog. Chem., 433, 161 (1977).

27 (b). V. Propach, Z. Anorg. Allog. Chem., 435, 161 (1977).

27 (c). B.Bochu, M.N.Deschizeaux, J.C.Joubert, A.Collomb, J. Chenvas and M. Marezio, J. Solid State Chem., 29, 291 (1979).

28. R.F.Cooley and J.S.Reed, J. Amer. Cerm. Soc., 55, 395(1972).

29. R.M.Hazen et al., Phys. Rev., B 35, 7238 (1987).

30. H.R.Freund and H.Muller-Buschbaum, Z. Anorg. Allog. Chem., 371, 325 (1969).

31. D. Reinen and H. Weizel, Z. Anorg. Allog. Chem., 424, 31 (1976).

32. H.Muller-Buschbaum and H.Mattausch, Z. Anorg. Allog. Chem., 377, 144 (1970).

33. H.W.Zandbergen, Y.K.Huang, M.J.V.Menken, J.N.Li, K.Kadowaki, A.A.Minovsky, G. van Tendaloo and S. Amelinckx, Nature, 332, 620 (1988).

34. H. Drekhahn and H. Muller-Buschbaum, Z. Anorg. Allog. Chem., 418, 116 (1975).

35. C.Teske and H.Muller-Buschbaum, Z. Anorg. Allog. Chem., 371, 325 (1969).

36. J.D.Jorgensen, M.A.Beno, D.G.Hinks, L.Soderholm, K.J.Volin, R.L.Hitterman, J.D.Grace, I.R.Schuller, C.U.Segre, K.Zhang and M.S.Kleefisch, Phys. Rev., B 36, 3608 (1987).

37. (a). R.G.Shulman, Y.Yafet, P.Eisenberger and W.E.Blumberg, Proc. Natl. Acad. Sci., U.S.A., 73, 1384 (1976).

37. (b). U.C.Srivastava and H.L.Nigam, Coord. Chem. Rev., 9, 275 (1973).

38. R.A.Bair and W.A.Goddard, Phys. Rev., B 22, 2767 (1980).

39. A.T.Smith, M.Berding, J.E.Penner-Hahn, S.Doniach and K. O. Hodgson, J. Am. Chem. Soc., 107, 5945 (1985).

40. N.Kosugi, T.Yokoyama, K.Asakura and H.Kuroda, Chem. Phys., 91, 249 (1984).

41. J.Krill, J.P.Keppler, A.Meyer, L.Abdali and M.F.Ravett, J. Phys., F 11, 1713 (1981).

42. S.Larsson, Chem. Phys. Lett., 32, 401(1975); 40, 362 (1976).

43. F.W.Kutzler, C.R. Natoli, D.K. Misemer, S. Doniach and K. O. Hodgson, J. Chem. Phys., 73, 3274 (1980).

44. E.A.Stern, Phys. Rev. Lett., 49, 1353 (1982).

45. W.W.Beeman and H. Friedmann, Phys. Rev., 56, 392 (1939).

46. P.Ganguly, Thesis, University of Bordeaux, Bordeaux France, 1984.

47. M.S.Hegde and P.Ganguly, preprint (1988).

48. P.Ganguly and M.S.Hegde, Phys. Rev., B 37, 5107 (1988).

49 (a). A. Bianconi, J. Budnick, G. Demazeau, A. M. Flank, A. Fontaine, P.Lagarde, J.Jegoudez, A.Revcolevski, A.Marcelli and M. Verdaguer, Physica, C 153, 117 (1988).

49 (b). D.D.Sarma, O.Strbel, C.T.Simmons, U.Neukirch, G. Kindl, R. Hoppe and P. Muller, Phys. Rev., B 37, 9784 (1988).

50. A. Bianconi, M.De Santis, A. Di Cicco, A.Cloza, A. Congiu Castellano, S.Della Longa, A.Gargano, P.Delogu, T.Dikonimos Makris, R. Giorigi, A. M. Flank, A.Fontaine, P.Lagarde and A. Marcelli, Physica C 153, 115 (1988).

51. K.Schonhammer and O.Gunnarson, Solid State Communications, 23, 691 (1977).

CHAPTER 6

THALLIUM L - ABSORPTION EDGE STRUCTURE

6.1 INTRODUCTION

It is well known[1-5] that monovalent and trivalent thallium compounds have interesting chemistry as a consequence of 6s and 6p electrons present in the valence band. The nature of the bonding in these compounds also varies widely. For example, covalent contributions to the bondings[6] in thallium (I) halides reach a maximum with TlI which has a double-layered orthorhombic structure[7].

A feature of fundamental importance which influences the structure and bonding in Tl compounds is that the 6s, 6p and 6d levels are sufficiently close and hybridization of these orbitals is energetically favourable in several Tl compounds. Hybridization alters the character of the otherwise pure and vacant 6p and 6d levels of monovalent and trivalent thallium in covalently bonded compounds. In the absence of hybridization, like in ionically bonded Tl^{1+} or Tl^{3+} compounds, the same 6p and 6d levels are subject to strong crystal field effects of the coordination sphere of ligands and depending on the point group symmetry of the thallium atom, degeneracies of the p and d manifolds are lifted up. Hence it suggests that in either situation, XANES spectroscopy should prove to be a very strong informative experimental approach to study the coordination geometry and bonding relations in thallium compounds. Since the near-edge features involve the transition from some core states to allowed lowest unoccupied empty states in the valence region of a given atomic centre, XANES spectra should reveal not only the allowedness or otherwise of these transitions but also the mixing or splitting of the final state orbitals[8-9]. In this Chapter, we report XANES and EXAFS investigations of selected monovalent and trivalent thallium compounds where using the known structural data, informative deductions on structural-bonding relations have been made. Both Tl L_I and $L_{II,III}$ edge XANES spectra have been used since they probe 2s --> 6p and 2p --> 6d

transitions respectively.

Also since X-ray spectra probe dominantly the effect of local coordinations, we have extended the investigations to a new class of superconducting oxides containing thallium[10-14], which show the highest transition temperatures to-date. We may expect on reasonable grounds that the near-edge analysis of these superconductors will provide us the information on atomic environment of thallium ions.

In previous Chapter, we have studied V K-edges in $CrVO_4$, $GdVO_4$, $BiVO_4$, $Cd_2V_2O_7$, $Ca_3Fe_3GeVO_{12}$, $Pb_5(VO_4)_3Cl$, $Zn_3(VO_4)_2$, $NaVO_3$, $VO(acac)_2$, $(NH_4)_4[VO\text{-}dd\text{-}tart]_2.2H_2O$, VOPc, $VO(bzac)_2$, VOTPP, $VOMoO_4$, V_2O_5, VO, $(NH_4)_2SO_4.VSO_4.6H_2O$, V_2O_3, $SmVO_3$, V_2S_3, VN, VO_2, V_4O_7, VC, [VO(hshed)(acac)], PbV_2O_6, $Ca_3V_{10}O_{28}.16H_2O$. and the superconducting cuprate oxides of composition $Tl_{1-x}V_xSr_2(Ca_{0.8}Y_{0.2})Cu_2O_y$, where x = 0.2, 0.3, 0.4 and 0.5. Our XANES analysis has shown that the vanadium ions in these superconducting oxides are in pentavalent state. As mentioned above, thallium shows two valencies, Tl^{1+} and Tl^{3+}. It would be therefore interesting to see whether the vanadium doping on Tl ion sites in the superconducting oxides forces Tl to change its atomic environment. It is with this aim, we have undertaken the study of Tl L_I , L_{II} and L_{III} edges in some model compounds and in thallium based superconductors. In particular, we have measured the L_I, L_{II} and L_{III} absorption spectra of thallium in model compounds namely TlCl, TlBr, TlI, Tl_2CO_3, $TlNO_3$, Tl_2SO_4, $Tl(CH_3COO)$, $Tl(C_6H_5COCHCOCH_3)$, $Tl(C_5H_7O_2)$, $Tl_2Ta_2O_6$, Tl_2O_3, $Tl(NO_3)_3.3H_2O$, $Tl(CH_3COO)_3$, $Tl(CF_3COO)_3$ and $Ba_2Tl_2O_5$ and superconducting oxides of composition $Tl_{1-x}V_xSr_2(Ca_{0.8}Y_{0.2})Cu_2O_y$, where x = 0.2, 0.3, 0.4 and 0.5. In addition to these oxides, we have also examined the L_I, L_{II}, and L_{III} edge spectra in $Tl_{0.5}Pb_{0.5}Sr_2CaCu_2O_7$, $TlBa_2CaCu_2O_7$, $Tl_2Ba_2CaCu_2O_8$, and $Tl_2Ba_2Ca_2Cu_3O_{10}$.

6.2. RESULTS AND DISCUSSION

In Figures 6.1-6 are presented the normalized L_{III} and L_I absorption spectra of model thallium compounds and superconducting oxides containing thallium studied in this work. The procedure used for normalizing these XANES spectra is similar to that employed for the study of vanadium compounds.

As mentioned below, these normalized X-ray absorption spectra suggest at once that the XANES of L_{III} edge of monovalent and L_I-edges of both monovalent and trivalent compounds have far fewer features as compared to L_{III} - edge of trivalent thallium compounds. We shall first discuss the thallium L_{III}-edge spectra. It may be stated here that the L_{II}-edge spectra of thallium are very similar to L_{III}-edge spectra. Therefore, the profiles of L_{II}-edges are not given here. We could not record the L_I, L_{II} and L_{III} absorption spectra of pure thallium metal since it gets easily oxidized in air at normal temperatures[2]. The profiles of L absorption edges reported in the above figures are obtained by averaging the results of a very large number of spectra recorded in turn from each sample.

We see in Figure 6.2 that the L_{III} absorption discontinuity of thallium in trivalent thallium compounds splits into three components whereas no splitting is observed in L_{III} - edges in monovalent compounds (Figure 6.1). L_I - edge spectra of both the monovalent and trivalent thallium compounds show no splitting (Figures IV.3-4). For plotting purpose the inflection point on the L_{III} - edge in Tl_2O_3 is taken as a reference point. Its energy is found to be 12665.00 ± 0.50 eV. Energy calibration was done by assigning the energy 12654.50 eV[15] to the inflection point on the K - edge of pure selenium metal recorded for this purpose. This calibration was also checked by assigning the energy 12063.40 eV to the peak position of tungsten L_{γ_4} emission line.

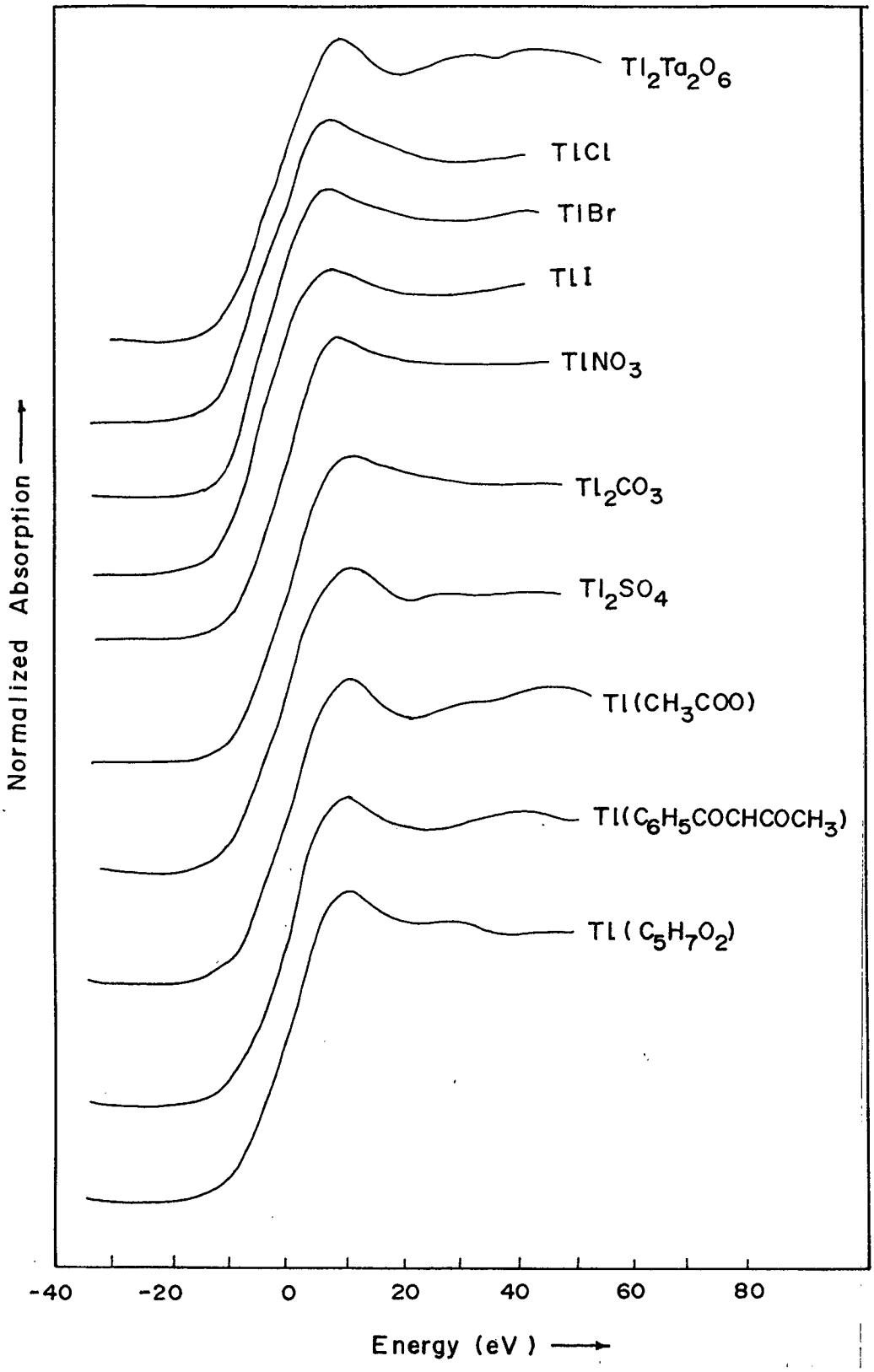

Figure 6.1: Normalized Tl L_{III} absorption spectra of $Tl_2Ta_2O_6$, TlCl, TlBr, TlI, $TlNO_3$, Tl_2CO_3, Tl_2SO_4, $Tl(CH_3COO)$, $Tl(C_6H_5COCHCOCH_3)$ and $Tl(C_5H_7O_2)$

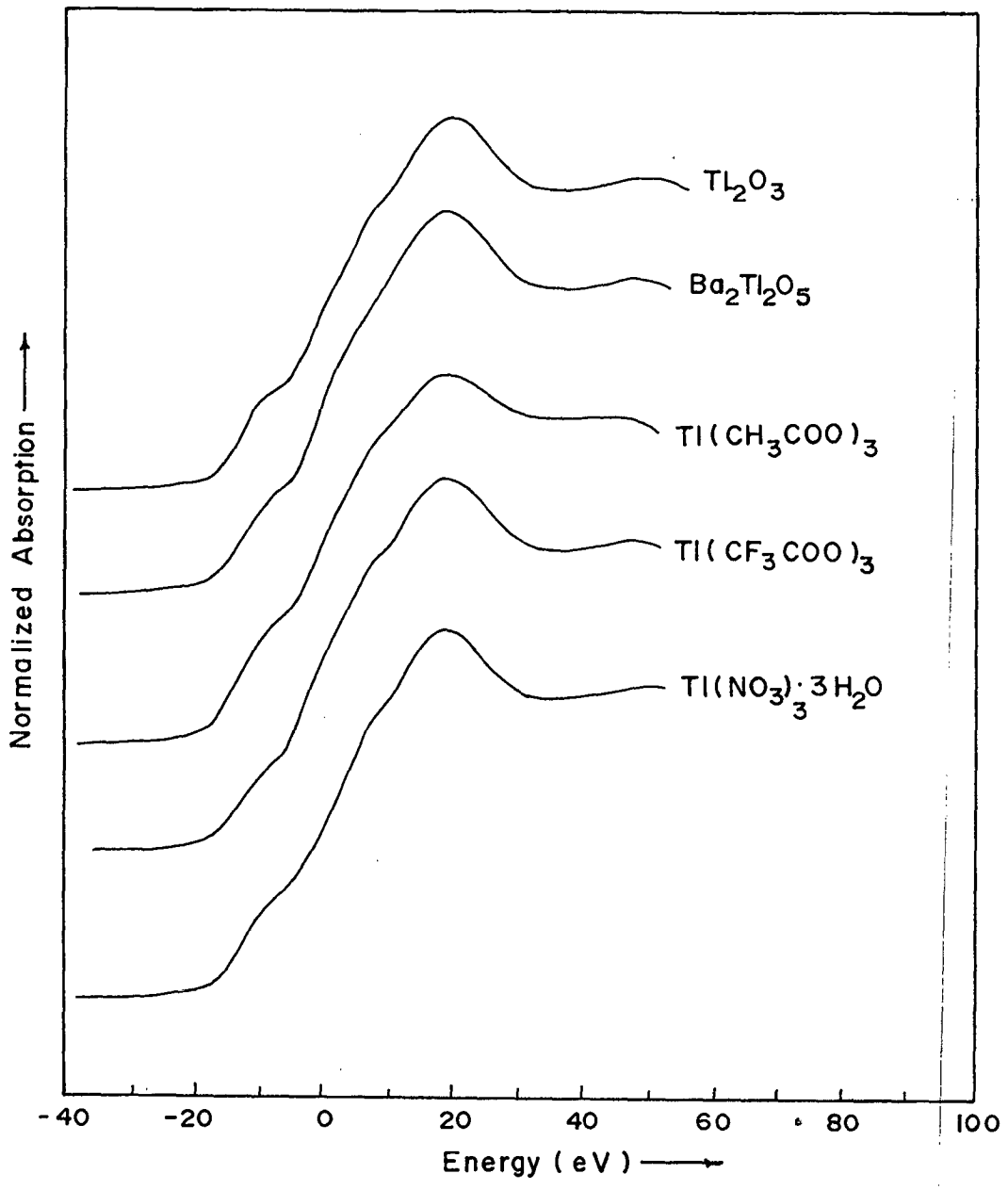

Figure 6.2: Normalized Tl L_{III} absorption spectra of Tl_2O_3, $BaTl_2O_5$, $Tl(CH_3COO)_3$, $Tl(CF_3COO)_3$ and $Tl(NO_3)_3.3H_2O$

Fig 6.2.

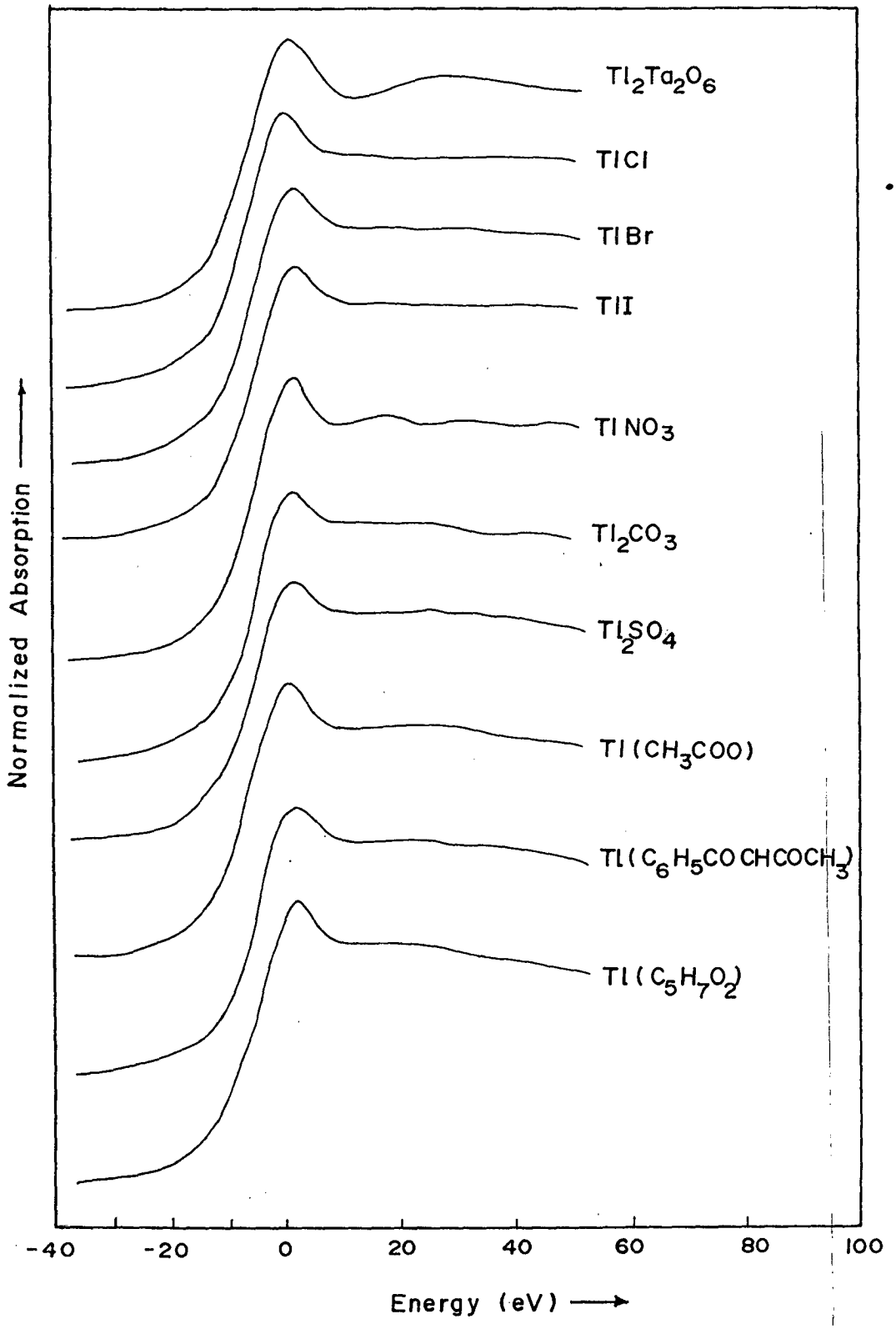

Figure 6.3: Normalized Tl L_I absorption spectra of $Tl_2Ta_2O_6$, TlCl, TlBr, TlI, $TlNO_3$, Tl_2CO_3, Tl_2SO_4, $Tl(CH_3COO)$, $Tl(C_6H_5COCHCOCH_3)$ and $Tl(C_5H_7O_2)$

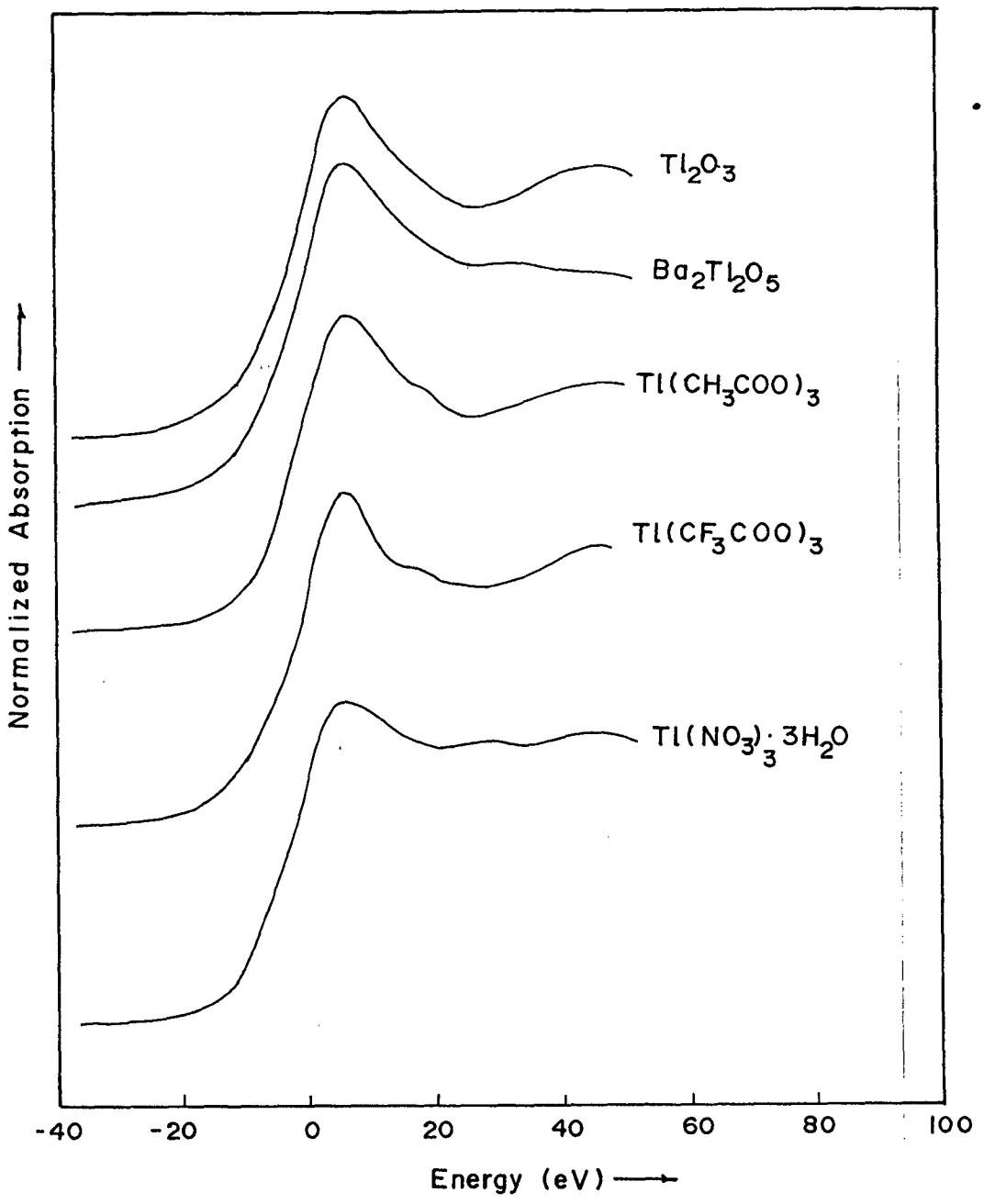

Figure 6.4: Normalized Tl L_I absorption spectra of Tl_2O_3, $BaTl_2O_5$, $Tl(CH_3COO)_3$, $Tl(CF_3COO)_3$ and $Tl(NO_3)_3.3H_2O$

Fig. 6.4

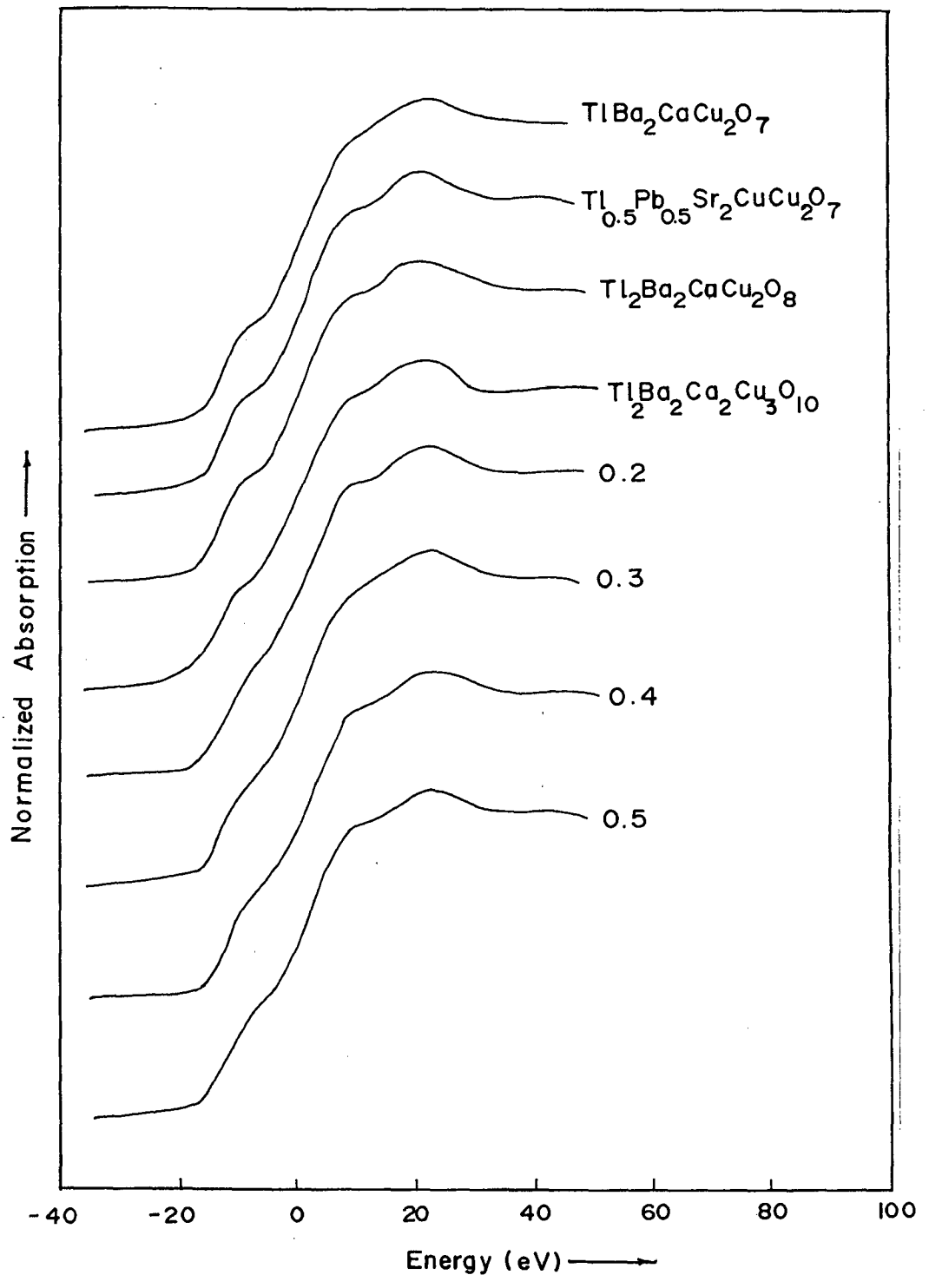

Figure 6.5: Normalized Tl L_{III} absorption spectra of $TlBa_2CaCu_2O_7$, $Tl_{0.5}Pb_{0.5}Sr_2CaCu_2O_7$, $Tl_2Ba_2CaCu_2O_8$, $TlBa_2Ca_2Cu_3O_{10}$ and $Tl_{1-x}V_xSr_2(Ca_{0.8}Y_{0.2})Cu_2O_y$, (x = 0.2, 0.3, 0.4, 0.5)

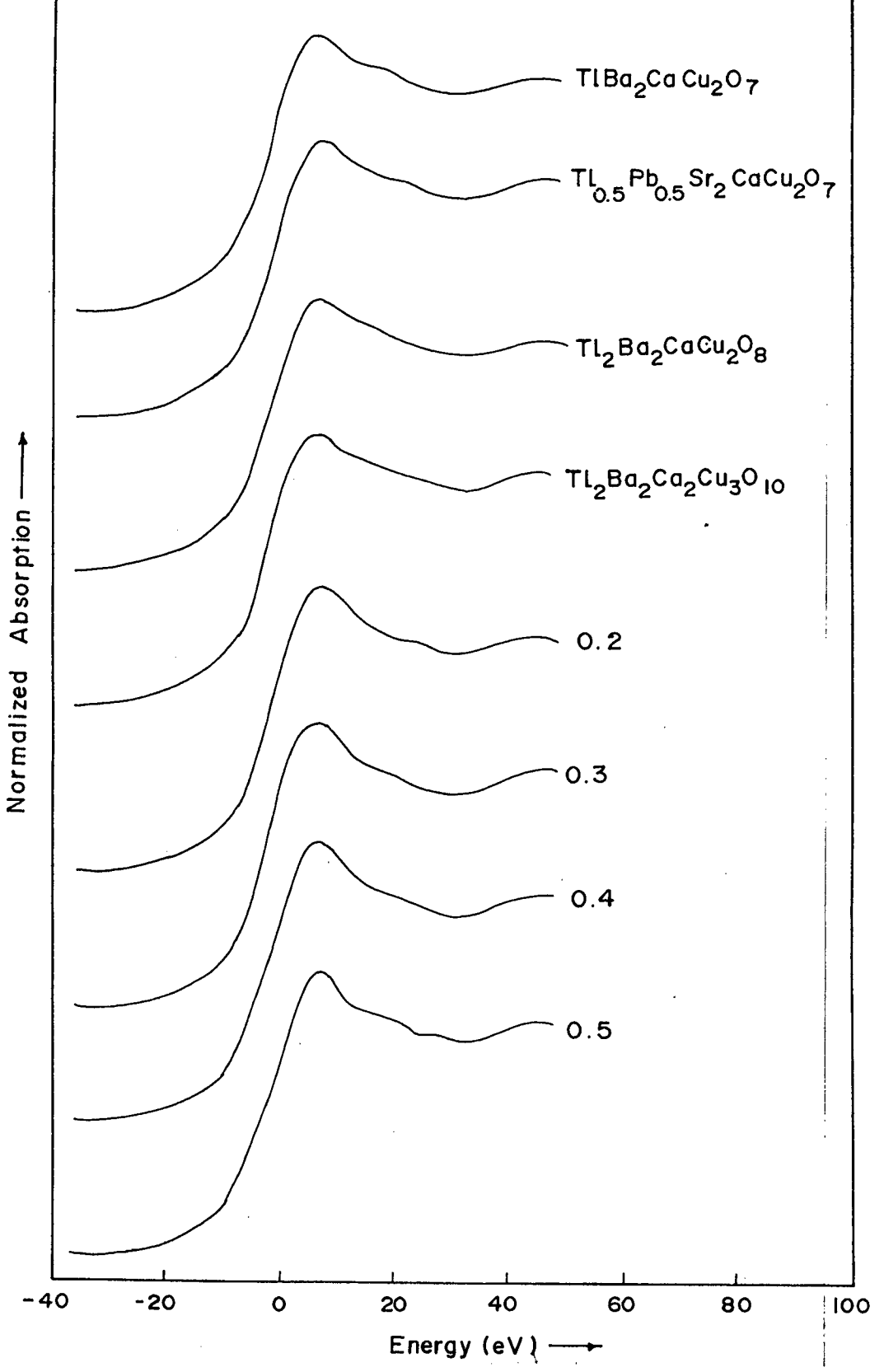

Figure 6.6: Normalized Tl L_I absorption spectra of $TlBa_2CaCu_2O_7$, $Tl_{0.5}Pb_{0.5}Sr_2CaCu_2O_7$, $Tl_2Ba_2CaCu_2O_8$, $TlBa_2Ca_2Cu_3O_{10}$ and $Tl_{1-x}V_xSr_2(Ca_{0.8}Y_{0.2})Cu_2O_y$, (x = 0.2, 0.3, 0.4, 0.5)

It may be mentioned here that the thallium L_{III} - edge spectra in Tl, TlCl, TlBr, Tl_2O_3 , $Tl(NO_3)_3$, $Tl_2(SO_4)_3$ and $Tl(CH_3COO)$ were recorded by Agarwal and Verma[16] on a Cauchois - type bent crystal X-ray spectrograph using photographic technique. These workers have given the microphotometer traces of L_{III} edges in TlCl, TlBr, and, $Tl(NO_3)_3$ only. Since these spectra are recorded on a low-resolution spectrograph and their microphotometer traces show a lot of noise in the recorded spectra it is difficult to compare our spectra with them. Studer et al[17,18] have reported X-ray absorption spectra for some thallium compounds and the profiles are given for TlBr, $Tl_2Ta_2O_6$ and Tl_2O_3. Vijayakrishnan et al[19] studied L_{III} -edge spectra in TlCl, $TlNO_3$ and Tl_2CO_3. The spectra for the compounds studied in the present investigation are similar to the spectra reported by Studer et al[17,18] and Vijayakrishnan et al[19].

6.2.1 THALLIUM L_{III} - EDGE SPECTRA

Thallium L_{III} - edge spectra for monovalent compounds are reported in Figure 6.1. In Figure 6.2 are given the L_{III} edge spectra for trivalent thallium compounds. Figure 6.1 shows a single absorption peak while the spectra in Figure 6.2 shows a weak peak followed by a shoulder on rising absorption which culminates into a strong absorption peak.

The outer electronic configuration of monovalent thallium is : $6s^2 6p^0 6d^0$ and hence the single absorption peak observed in the monovalent thallium compounds viz. TlCl, TlBr, TlI, Tl_2CO_3, $Tl(NO_3)$, $Tl_2Ta_2O_6$ corresponds to the allowed transition of $2p_{3/2}$ electron to 6p state which is admixed with 6d and 2s characters of metal and ligands respectively. On the other hand following the electronic assignment schemes invoked by Retoux et al[20] and Heald et al[21] for L_{III} absorption edge features 6s, 6p and 6d states being completely vacant in trivalent thallium compounds, the weak peak, the shoulder and the main absorption peak can be

attributed to the transitions $2p_{3/2} \rightarrow 6s$, $2p_{3/2} \rightarrow 6d\ (t_{2g})$ and $2p_{3/2} \rightarrow 6d\ (e_g)$ respectively. The final states of the latter transition are admixed with 6p from metal and 2s and 2p characters from ligand. It is interesting to note that the shoulder peak of trivalent compounds and the main absorption peak of monovalent compounds occur almost at same energy. The important difference between the spectra of monovalent and trivalent compounds is the 4 eV shift in the inflection point energy of L_{III} edges and a 12 eV energy shift of main absorption maxima is clearly seen in the figures. It is surprising that in monovalent thallium compounds, 6d being vacant, a peak corresponding to the electronic transition, $2p_{3/2} \rightarrow 6d$ is not observed. In fact, the transition probability for $p \rightarrow d$ transition is more as compared to that for $p \rightarrow s$ transition[22]. It may be mentioned here that Studer et al[19] and Rao and Wong[23] have studied L-edge spectra in thallium and lead compounds respectively and assigned such electronic transitions to the spectral features observed.

On the basis of these absorption spectra of thallium model compounds, one can distinguish between the monovalent and trivalent thallium ions in the superconducting oxides. We shall first determine the valence state of thallium ions in a well-characterized superconductors.

The L_{III}-absorption spectra of $Tl_{0.5}Pb_{0.5}Sr_2CaCu_2O_7$, $TlBa_2CaCu_2O_7$, $Tl_2Ba_2CaCu_2O_8$ and $Tl_2Ba_2Ca_2Cu_3O_{10}$ superconductors are shown in Figure 6.5. The overall profiles of these oxides are very similar to those of Tl_2O_3 and other trivalent thallium compounds suggesting octhedral environment of ligands around trivalent thallium ions. However, from a more careful examination of intensities and energies of the peaks in the L_{III}-edge region, it is found that they are slightly different from those observed for trivalent compounds. This seems to suggest that the octahedron of ligands around the thallium ions is distorted. This

sort of distortion can be studied in detail if we analyze the EXAFS spectrum associated with the L_{III}-edge. This is done in the next section of this Chapter. These observations on the whole, clearly indicate the presence of octahedrally coordinated Tl^{3+} ions in these four well-characterized superconducting oxides. Our results in this respect are in good agreement with those obtained by Studer et al[17,18] It may be interesting to mention here that on the basis of the crystal structures of these oxides Studer et al have ruled out the possibility of existence of Tl^{1+} ions. However, it is possible that the holes may be delocalized on an oxygen p-like valence band. According to the theoretical considerations of the Cu-O sheets, holes are more or less delocalized in the in-plane non-bonding oxygen p band formed by orbitals pointing towards the centre of the negative oxygen square, so that Tl(I) configuration appears to be one of the possibilities for doping. However, from the similarity of the X-ray spectra of superconducting oxides and Tl_2O_3, there is absolutely no doubt that Tl^{3+} ions exist in such oxides, as has been shown by us as well as by Studer et al[17,18].

After having confirmed the presence of Tl^{3+} ions in well characterized superconducting oxides, we will now determine the valence state of Tl ions in $Tl_{1-x}V_xSr_2(Ca_{0.8}Y_{0.2})Cu_2O_y$. The X-ray absorption spectra in Figure 6.5 show similarity with the spectra of Tl_2O_3, suggesting thereby the presence of Tl^{3+} ions in octahedral configuration in these oxides. The slight reduction of intensity and increase of energy of principal absorption maxima are also observed in these oxides. It is very difficult to give any reason for this, but it seems that the crystal structure has some relation to their absorption spectra.

Vijaykrishnan et al[19] have noted that the shoulder-like feature of Tl^{3+} compounds and the main peak in Tl^{1+} compounds are in same energy region. This observation has also been noted by us.

In order to understand the features in the spectra of Tl cuprate superconductors in the region between the pre-edge peak and the main absorption peak, Vijaykrishnan et al[19] have recorded the Tl L_{III} spectra of physical mixtures of Tl_2CO_3 and Tl_2O_3 in varying proportion. These authors observe that there is a progressive development of intensity in the region between the pre-edge peak and main absorption maximum. Furthermore, this feature shifts towards the main peak of Tl^{1+} with the increase in the proportion of Tl_2CO_3. The position of the main absorption peak due to Tl_2O_3, however seems to remain constant. On the basis of these observations, these authors have suggested that the above feature between the pre-edge and the main peak could be due to a Tl^{1-} like state different from a distinct localized Tl^{1+} species present in these cuprates. Their proposal of existence of Tl^{1+} like state in cuprate superconductors has some support from the X-ray photoemission studies of Suzuki et al[24] who have measured the Tl 4f core level binding energies in Tl_2O, Tl_2O_3 and $Tl_2Ba_2Ca_2Cu_3O_{10}$ in order to elucidate the chemical state of Tl ions in the superconducting oxides. The binding energies of Tl 4f level are found to be 118.6, 117.4 and 118.2 eV for Tl_2O, Tl_2O_3 and $Tl_2Ba_2Ca_2Cu_3O_{10}$ respectively, i.e., the binding energy of Tl $4f_{7/2}$ level in $Tl_2Ba_2Ca_2Cu_3O_{10}$ is higher than that in Tl_2O_3 but slightly lower than that in Tl_2O. These authors concluded on the basis of binding energy data that the valence of Tl in the superconducting oxide $Tl_2Ba_2Ca_2Cu_3O_{10}$ is between 3^+ and 1^+. It is not convincing that the binding energy of Tl^+ ion is greater than the binding energy of Tl^{3+} ion. Moreover, no reason has been given by Suzuki et al for this observation. In most of the compounds it is generally observed[25-28] that the higher valent metallic ions show binding energies greater than those in lower valent metallic ions. We feel that authors could have measured the binding energies in a few more monovalent and trivalent thallium compounds before arriving at the final conclusion.

Li et al[29] have also carried out X-ray absorption measurements on Tl_2CO_3, Tl_2O_3, $Tl_{1-x}Bi_xSr_2CuO_5$ (x= 0.2, 0.5) and $Tl_{0.5}Bi_{0.5}Sr_2CaCu_2O_7$. The Tl L_{III} absorption edges of $Tl_{0.8}Bi_{0.2}Sr_2CuO_5$, $Tl_{0.5}Bi_{0.5}Sr_2CuO_5$ and $Tl_{0.5}Bi_{0.5}Sr_2CaCu_2O_7$ are at the lower energy side relative to the L_{III} edge in Tl_2O_3. Although the edge shifts in these compounds are most likely due to changes in the effective charge of Tl ions, the possibility of other origins (e.g., coordination geometry related) cannot be ruled out. Interestingly, the pre-edge feature is significantly lower in Tl_2O_3 than in the other non-Tl^{1+} compounds. These authors attribute this to a combination of two effects : the edge feature in the superconducting compounds is riding higher on the edge-step which has been down-shifted by the decrease in Tl valence ; and a decrease in the width of the 6s-orbitals the pre-edge feature has occurred in these compounds. If the Tl valence in the Tl-based cuprates is less than 3^+, it would be possible for the Tl 6s level to cross the Fermi level, even though the band structure calculations show that the Tl 6s level in the single Tl-O layered compounds including $Tl_{1-x}Bi_xSr_2CuO_5$ and $Tl_{0.5}Bi_{0.5}Sr_2CaCu_2O_7$ is above the Fermi level[30-33]. However, careful examination of the L_I-edge profiles, (presented in the next section) the possibility of presence of monovalent thallium ions in these cuprate superconductors can be ruled out clearly.

Studer et al[17] reported the Tl L_{III} -edge spectra of thallium in cuprate superconductors containing thallium. They interpret the experimentally observed spectral features of L_{III}-edge in terms of the Tl-O distances in these systems using Natoli's multiple scattering approximation[34]. They find Tl-O distances similar to those in Tl^{1+}-O distances in cuprates but conclude that the Tl^{1+} state is absent within the experimental error (± 10%). It may be noted that one finds both Tl^{1+}-O and Tl^{3+}-O type distances in the cuprates since Tl has a highly distorted oxygen octahedra. It is the view of Vijayakrishnan et

al[19] that the presence of different distances can by no means be used as an argument in favour of or against the presence of Tl^{1+} or any such species. They argued that in Bi cuprates also one finds distances close to those of Bi^{3+}-O and Bi^{5+}-O although there is no Bi^{5+} in these cuprates. Furthermore, these authors have commented that Studer et al[17] have not discussed the pre-edge feature in the spectrum of Tl_2O_3 or its closeness to the main peak of Tl^{1+} compounds. However, we do find in one of the papers of Studer et al[17,18], a detailed discussion on the feature B.

Our results support the proposal of existence of Tl^{3+} state in the thallium doped cuprate superconductors. This can be clearly seen by the L_I-edge profiles, presented in the next Section. It may be noted that Vijayakrishnan et al[19] have not studied the L_I-edge profiles in these superconductors. Moreover, we feel that the L_{III}-edge profiles of physical mixture of compounds Tl_2CO_3 and Tl_2O_3 in different proportion may not give correct picture. Thus, for example the L_{III}-edge spectrum of the mixture, 60% Tl_2CO_3 (containing 60% Tl^{1+}) and 40% Tl_2O_3 (40% Tl^{3+}) will be very much different from the spectrum generated from the 60% μ vs. E curve of Tl_2CO_3 and 40% μ vs. E curve of Tl_2O_3, as has been shown by Anjli et al[35] in cuprate superconductors. A better way of doing this is to synthesize a compound wherein Tl exists in both valence states and record its L_{III} - edge spectrum. However, it is very difficult to prepare such compound in our laboratory. We therefore have not done this sort of analysis.

6.2.2 THALLIUM L_I EDGE SPECTRA

The L_I- edge spectra for the monovalent and trivalent compounds and superconducting oxides are given in Figs 6.3, 4, and 6. Here, the edge profile is simple in all the cases. Splitting of the edge is not at all observed. The only difference

in monovalent and trivalent thallium compounds is that the inflection point shift is about 4 ± 0.5 eV and main absorption peak shift is about 12 ± 0.5 eV. In monovalent compounds 6s orbital is occupied, but 6p is completely vacant. The main absorption peak observed in these monovalent compounds (Figure 6.3) corresponds to 2s → 6p transition and since 6s is being unavailable for transition to occur, no splitting of the L_I edge is visible. In trivalent compounds, the 6s and 6p orbitals being vacant, a pre-edge peak corresponding to the forbidden transition, 2s → 6s is expected to be observed. However, we have not observed such peaks. Here in this case, like the monovalent compounds, only the main absorption peak is observed. This peak corresponds to 2s → 6p (the pre-peak being absent).

The L_I edge spectra of all the superconducting oxides, $Tl_{0.5}Pb_{0.5}Sr_2CaCu_2O_7$, $TlBa_2CaCu_2O_7$, $Tl_2Ba_2CaCu_2O_8$, $Tl_2Ba_2Ca_2Cu_3O_{10}$ and $Tl_{1-x}V_xSr_2(Ca_{0.8}Y_{0.2})Cu_2O_y$ where x = 0.2, 0.3, 0.4 and 0.5 are similar to those in Tl_2O_3 and other trivalent compounds. It is also observed that the main absorption peaks are located at the same energy. The only noticeable difference is the intensity of peak corresponding to 2s → 6p transition. The intensity of this peak is slightly less in superconducting oxides as compared to that in Tl_2O_3. Similar results have been obtained by Studer et al[17,18] in 1212, 2212, 1223 and 2223 superconducting oxides. Thus, the results of L_I XANES also lead us to conclude that the octahedrally coordinated thallium ions exist in 3^+ state in superconducting oxides. In other words, it means that they are in the 6s levels.

6.2.3 SHAPE RESONANCE REGION OF ABSORPTION

A well characterized absorption peak beyond the first absorption minimum of the K-edge spectra of elements is often ascribed to shape resonances[36-38]. These absorption peaks arise as a consequence of the potential barrier created by the ligand

electrons. The presence of a potential cage forces the atomic states to exist either entirely inside or outside the cages. The inside states, better known as inner well states, are energetically capable of evolving into continuum states. However, they are compressed into the shape of the ligand cage so that they can produce sufficient overlap with the initial 1s states and hence give rise to shape resonance absorption. Extending the same arguments to L_I edge spectra, we may consider the absorption features in the region of 25-40 eV in the monovalent thallium salts as due to shape resonances arising from 2s electron excitation to quasi bound states having a p character. Our studies in this region do not suggest useful generalizations of any kind since this energy range also falls within the XANES → EXAFS transition region. This could also be due to a variety polyhedral environments around the Tl^{1+} ions in the compounds investigated. However we note that in the highly ionic thallium nitrate, in which the coordination polyhedron is both large and highly symmetrical, the shape resonance peak is relatively well defined (see Figure 6.3). The shape resonances are ill defined when covalency dominates the nature of bonding as in TlI, and when the symmetry of the coordination polyhedron is low.

L_{III} edge spectra also exhibit an absorption feature attributable to shape resonance in the same energy region. Such transitions are possible if the quasi bound states have sufficient d character in them. It is plausible because in the Xα-MSW calculations which have been used with success to simulate such spectra[37-38], the wave functions employed do include such higher angular momentum states in them.

6.3. THALLIUM L_{III} - EDGE EXAFS SPECTRA

Since no single crystal structure data are available on the superconducting oxides, $Tl_{1-x}V_xSr_2(Ca_{0.8}Y_{0.2})Cu_2O_y$ studied in this investigation, we thought it worthwhile to measure the EXAFS

at thallium L_{III} - edges and analyze the data using Fourier transform and non-linear curve fitting techniques in order to get structural information on these complex oxides.

We have used Tl_2O_3 as a model compound containing Tl-O atom pair. The Fourier transforms of L_{III} - edge EXAFS spectra for Tl_2O_3, $Tl_2Ta_2O_6$ and $Ba_2Tl_2O_5$ are shown in Figure 6.7 and in Figure 6. 8 are given the Fourier transforms of EXAFS spectra for $TlBa_2CaCu_2O_7$, $Tl_{0.5}Pb_{0.5}Sr_2CaCu_2O_7$, $Tl_2Ba_2CaCu_2O_8$, $Tl_2Ba_2Ca_2Cu_3O_{10}$ and $Tl_{1-x}V_xSr_2(Ca_{0.8}Y_{0.2})Cu_2O_y$ where x = 0.2 and 0.5.

The Fourier transform of the L_{III}-edge EXAFS data in Tl_2O_3, presented in Figure 6.7 shows three distinct peaks. The first peak is the dominant one and corresponds to Tl-O distance. Its intensity is large as compared to the others. (The small peaks on large R side (R > 4.5 A^o) in the Fourier transform are most likely resulted from an improper background removal at large k values.) This dominant peak in Tl_2O_3 was inverse Fourier transformed to yield the contribution of backscatterers about Tl^{3+} ions.

To determine the local structure of Tl^{3+} ions in the superconducting oxides, as mentioned earlier, we use Tl_2O_3 as the reference compound to model the Tl^{3+} structure in oxide environment. In the single-scattering approximation[39-41], the observed EXAFS $\chi(k)$ may be described by

$$\chi(k) = -1/k \sum_j A_j \sin [\, 2R_jk + \phi_j(k)], \qquad (6.1)$$

having oscillatory terms with frequencies $[\, 2R_jk + \phi_j(k)]$, and amplitude terms A_j is given by

$$A_j = (N_j/R_j^2)\ \ f_j(\pi,k)\ \exp(-2\sigma_j^2\, k^2). \qquad (6.2)$$

The parameters on the right hand side of equations 6.1 and 6.2 may be classified as (a) scattering parameters which include

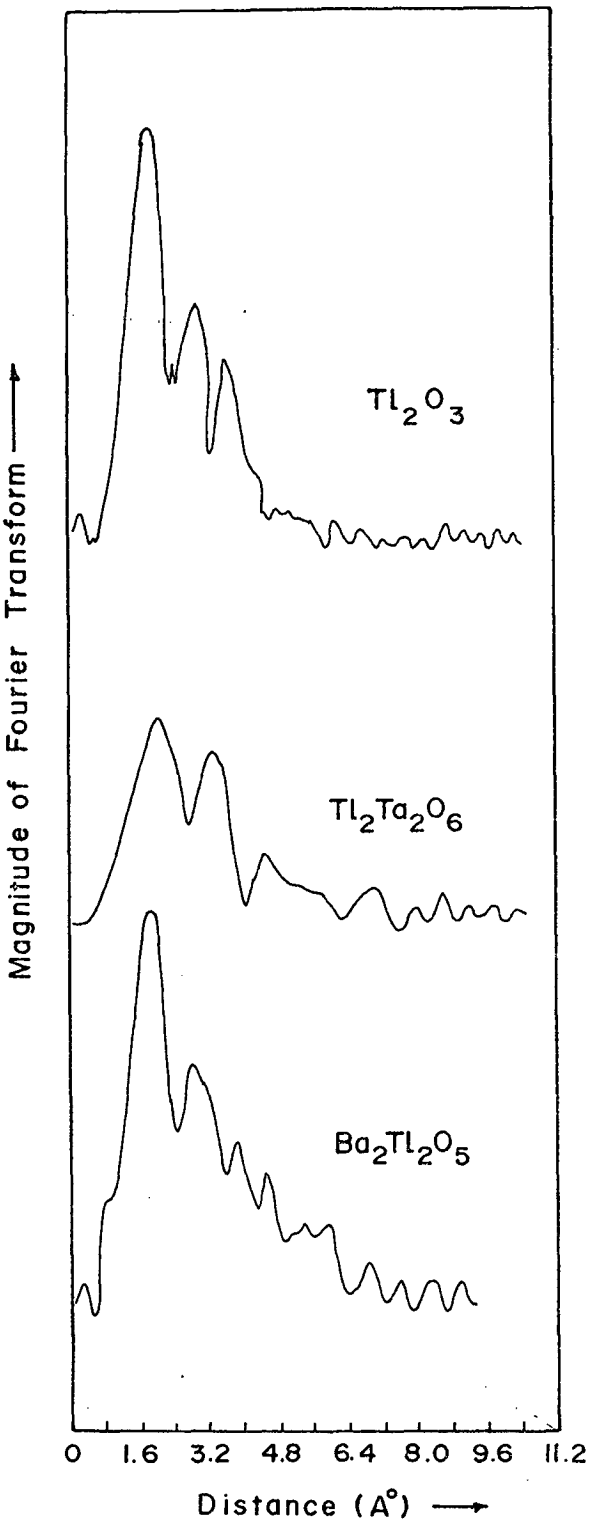

Figure 6.7: Fourier transforms of the thallium L_{III}-edge EXAFS in Tl_2O_3, $Tl_2Ta_2O_6$ and $BaTl_2O_5$

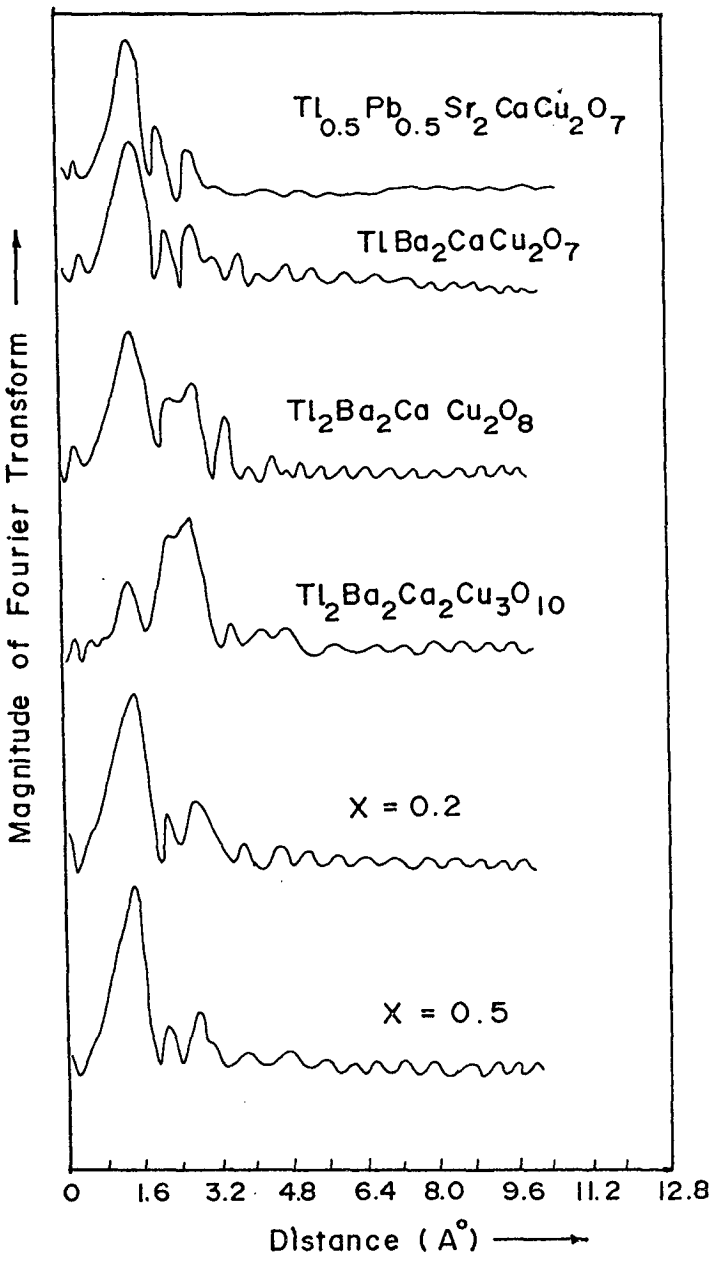

Figure 6.8: Fourier transforms of the thallium L_{III}-edge EXAFS in $Tl_{0.5}Pb_{0.5}Sr_2CaCu_2O_7$, $TlBa_2CaCu_2O_7$, $Tl_2Ba_2CaCu_2O_8$, $TlBa_2Ca_2Cu_3O_{10}$ and $Tl_{1-x}V_xSr_2(Ca_{0.8}Y_{0.2})Cu_2O_y$, x = 0.2 and 0.5

phase shift $\phi_j(k)$, backscattering amplitude $f_j(\pi,k)$ and mean free path λ and (b) structural parameters which include coordination number N_j, Debye-Waller type factor σ_j and bond distance R_j. The summation is over all coordination shells j participating in the EXAFS event. In a model system such as Tl_2O_3 for which crystallographic data are available, i.e. coordination number N_j, the interatomic distance R_j and Debye-Waller factor σ_j are known, its EXAFS spectrum may be used to generate a set of self-consistent scattering parameters, which can then be transformed to an unknown system of similar chemical nature to determine structural parameters for the unknown.

A least- squares procedure[41-42] is set up to minimize the variance S, where

$$S = \sum_{i}^{N} (\chi_i^F - \chi_i)^2 \qquad (6.3)$$

Here χ_i^F are the Fourier- filtered experimental data and χ_i is the analytical expression given in equation (6.1) which describes χ_i^F for N data points. Since $\chi(k)$ is not a linear function of the various parameters, a Taylor series expansion is used which expresses $\chi(k)$ in terms of approximate parameter values, P_j and parameter adjustments, $\Delta P_j = P_j - P_j'$. When the least -squares condition is applied, a set of simultaneous equations is obtained in terms of ΔP_j rather than P_j. The equations are solved for the adjustment ΔP_j, and the parameters were adjusted by ΔP_j to give a new set of estimates. The procedure was then reiterated with a new estimate P_j' and so on until the new solution differed from the last by less than a desired value, which is usually 1%.

6.3.1 DETERMINATION OF Tl- O PHASE SHIFT AND ENVELOPE FUNCTION FOR OXYGEN

Crystalline Tl_2O_3 is isostructural[7] with C-Mn_2O_3. It is related to that of CaF_2, from which it may be derived by removing one-quarter of the anions and the rearranging the atoms somewhat.

The six coordinated Tl atoms are of two types. Instead of 8 neighbours at the vertices of a cube, two are missing. For one quarter of the Tl atoms these two are at the ends of a body-diagonal, and for the remainder at the ends of a face-diagonal. Both coordination groups may be described as distorted octahedron. In the first coordination group, thallium is linked to six oxygen ions at a distance of 2.26 A^{o} and in the second, it is coordinated to four oxygen atoms in the range 2.13 A^{o} - 2.18 A^{o} and two at 2.47 A^{o}.

To elucidate the structural environment of thallium giving rise to the observed EXAFS in the superconducting oxides, we first use the above structural parameters for Tl_2O_3 in the curve fitting analysis of Fourier-filtered EXAFS in the region 0.8 - 2.3 A^{o}.

From the Tl L_{III}-edge EXAFS data, it is clear that the first radial peak in the region 0.8 -2.3 A^{o} of the Fourier transform for Tl_2O_3 shown in Fig 6.7, corresponds to the shell of six O atoms about the absorbing Tl atom in the C-M_2O_3 -type crystal structure. The inverse transform in Figure 6.9 indeed shows an experimental envelope characteristic of a low Z backscattering atom, i.e. oxygen. To obtain self consistent phase shifts for the Tl-O atom pair, the values of Teo and Lee [22,43-44] in the form

$$\phi_j(k) = P_0 + P_1 k + P_2 k^2 + P_3/k^3 \qquad (6.4)$$

were used as the initial inputs. The envelope function $f_j(\pi,k)\exp(-2R_j/\lambda)$ for oxygen was obtained empirically from the filtered EXAFS itself [Figure 6.9] and was fixed in the simulation. E_o, the inner potential or the threshold energy required to determine the value of photoelectron wave-vector, k, was found to be - 12659 eV. It is obtained[44] after matching the peaks in imaginary part and modulus of the Fourier transform. N = 6 and R = 2.25 A^{o} were used as fixed structural parameters. The

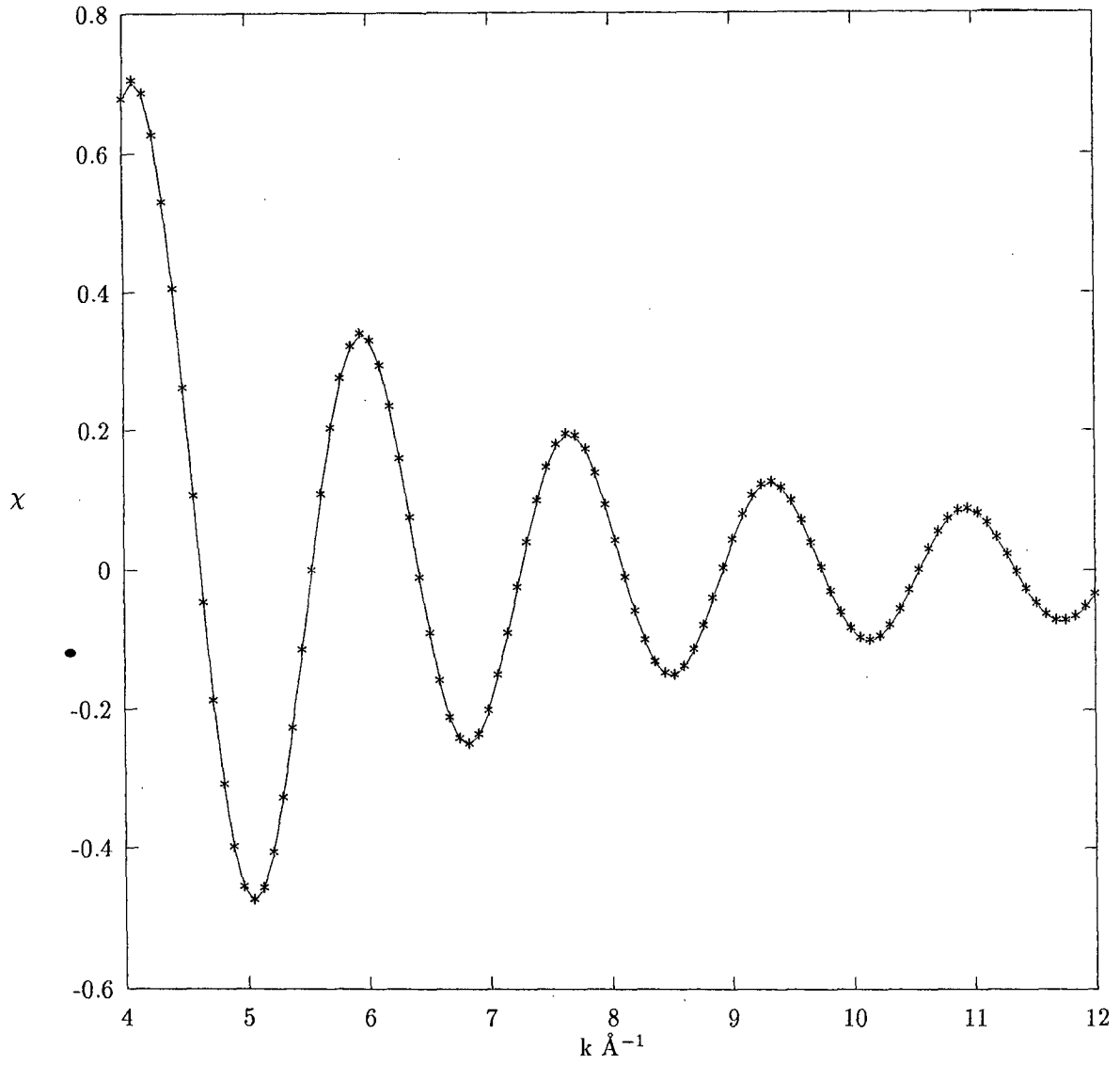

Figure 6.9: Inverse Fourier transform (* * *) and simulated EXAFS of the first FT peak (solid line) for Tl_2O_3

thermal parameter σ_j was varied. The simulation was done in k space to emphasize the backscattering contribution of oxygen at low k. The results are shown in Fig 6.9, where the curve (solid line) denotes the Fourier filtered spectrum and the points denote the simulated spectrum. The input values of N and R, the phase parameters and the thermal parameter determined in the fitting are

$$P_0 = 5.148 \quad P_1 = -1.083 \quad P_2 = 0.025 \quad P_4 = 52.03$$

$$\sigma_j = 0.002 \qquad N_j = 6 \qquad R_j = 2.25\ A^{o}$$

The computer simulation was fitted with a standard deviation of 5 % of the maximum amplitude of the experimental $\chi^F.k^3$.

The plot of experimental phase shift versus wave vector k for Tl-O atom pair obtained in the simulation is shown in Figure 6.10(a). We have plotted in Figure 6.10(b), the phase shift data of Teo and Lee[22]. Central atom phase shift for l = 2 are not given by these authors for thallium. Therefore the phase shifts for Tl were obtained by interpolation as suggested by these authors themselves. It is to be noted that in the theoretical plot, 4π has been added to the values of phase shifts for the comparison. It is seen from the Figure 6.10(a) and Fig 6.10(b) that the experimentally determined phase shift curve for Tl-O atom pair is very close to that obtained from theoretical values given by Teo and Lee[22].

6.3.2 THALLIUM ENVIRONMENT IN $Tl_2Ta_2O_6$ AND $Ba_2Tl_2O_5$

The phase shifts for Tl-O pair and envelope function for oxygen extracted from the filtered experimental L_{III}-edge EXAFS of crystalline Tl_2O_3 as described above were then transferred and used to determine N, R and σ in two well known crystalline compounds namely $Tl_2Ta_2O_6$ and $Ba_2Tl_2O_5$. Curve fitting was

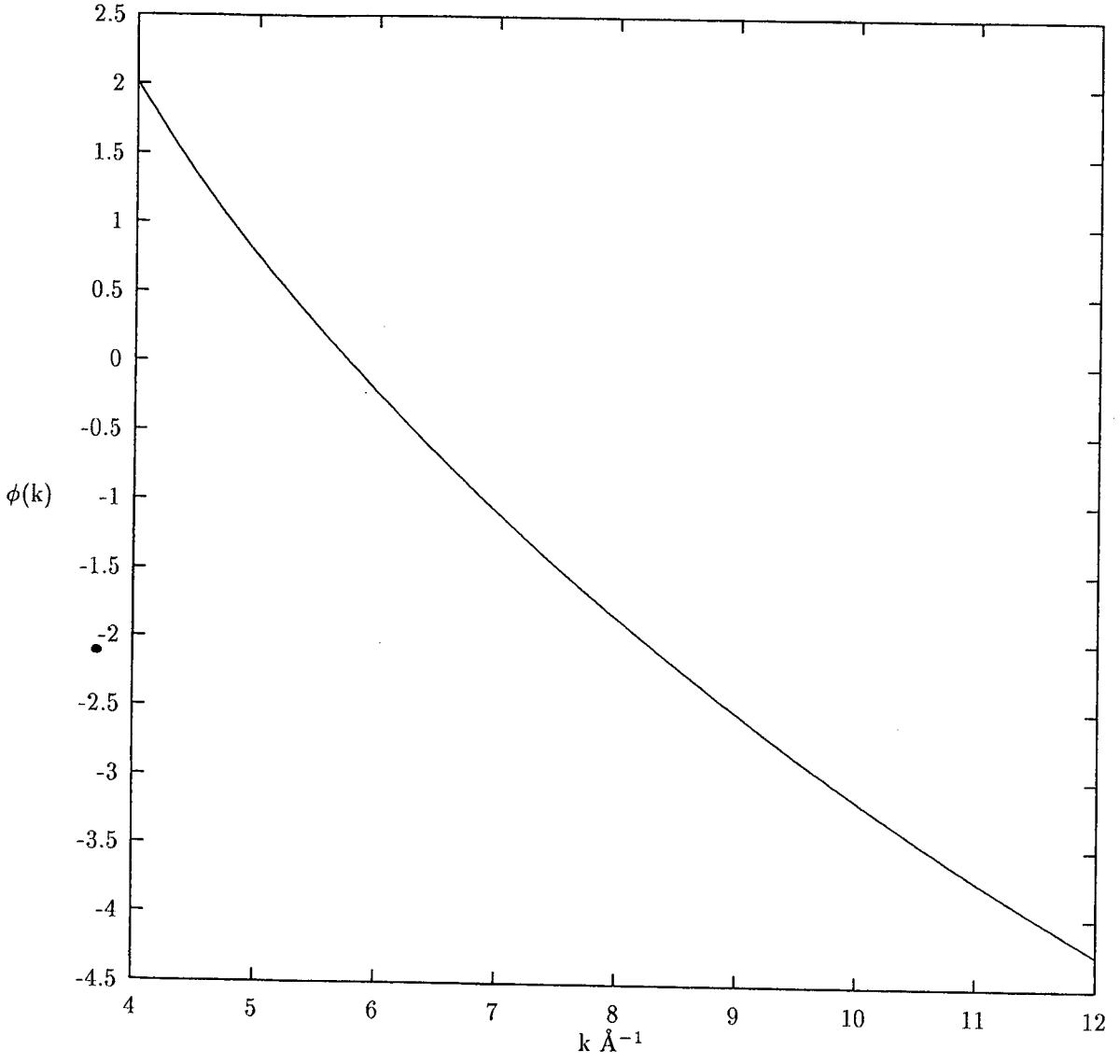

Figure 6.10: (a) Phase shifts for Tl-O atom pair : Experimental

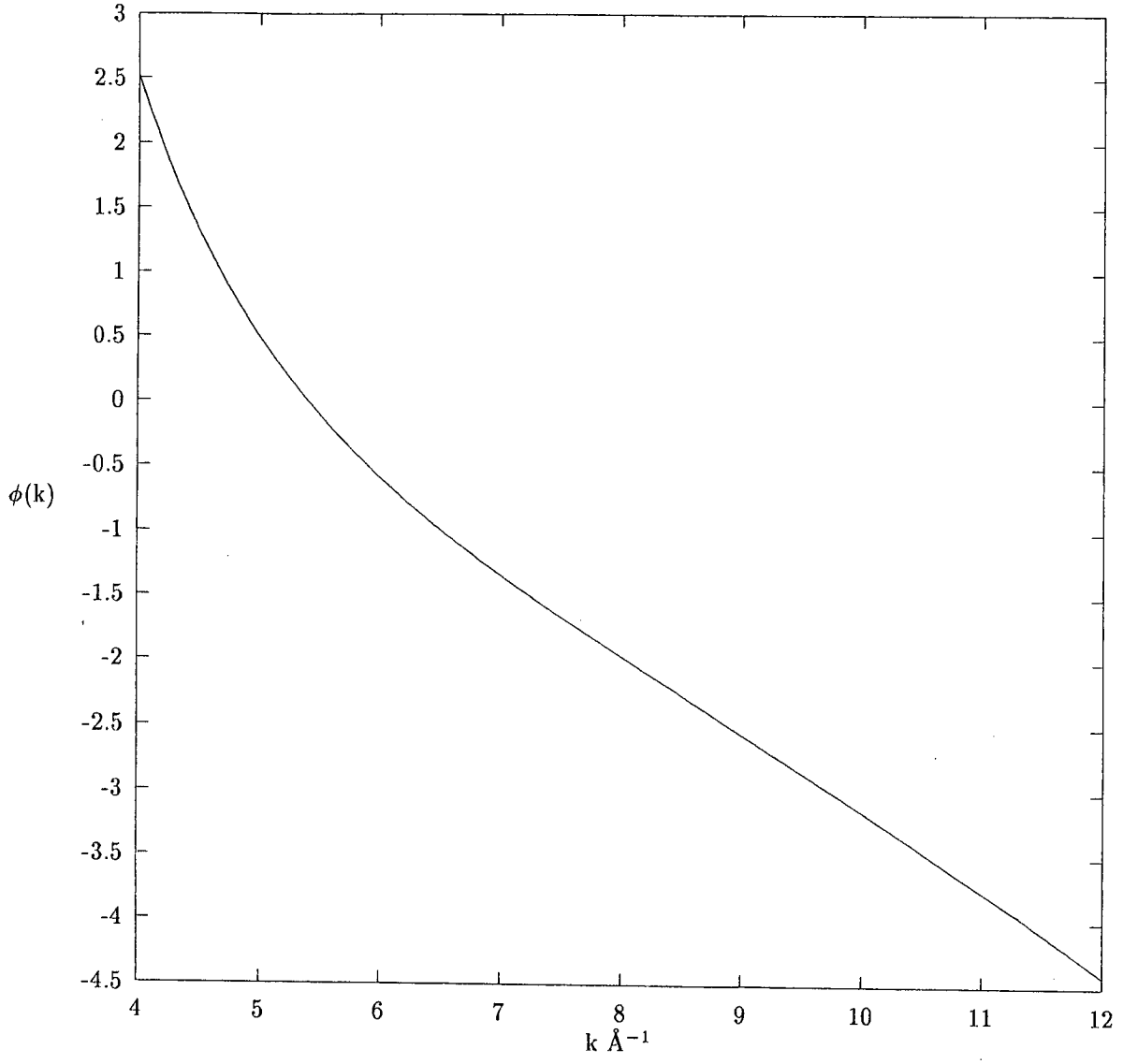

Figure 6.10: (b) Phase shifts for Tl-O atom pair : Theoretical

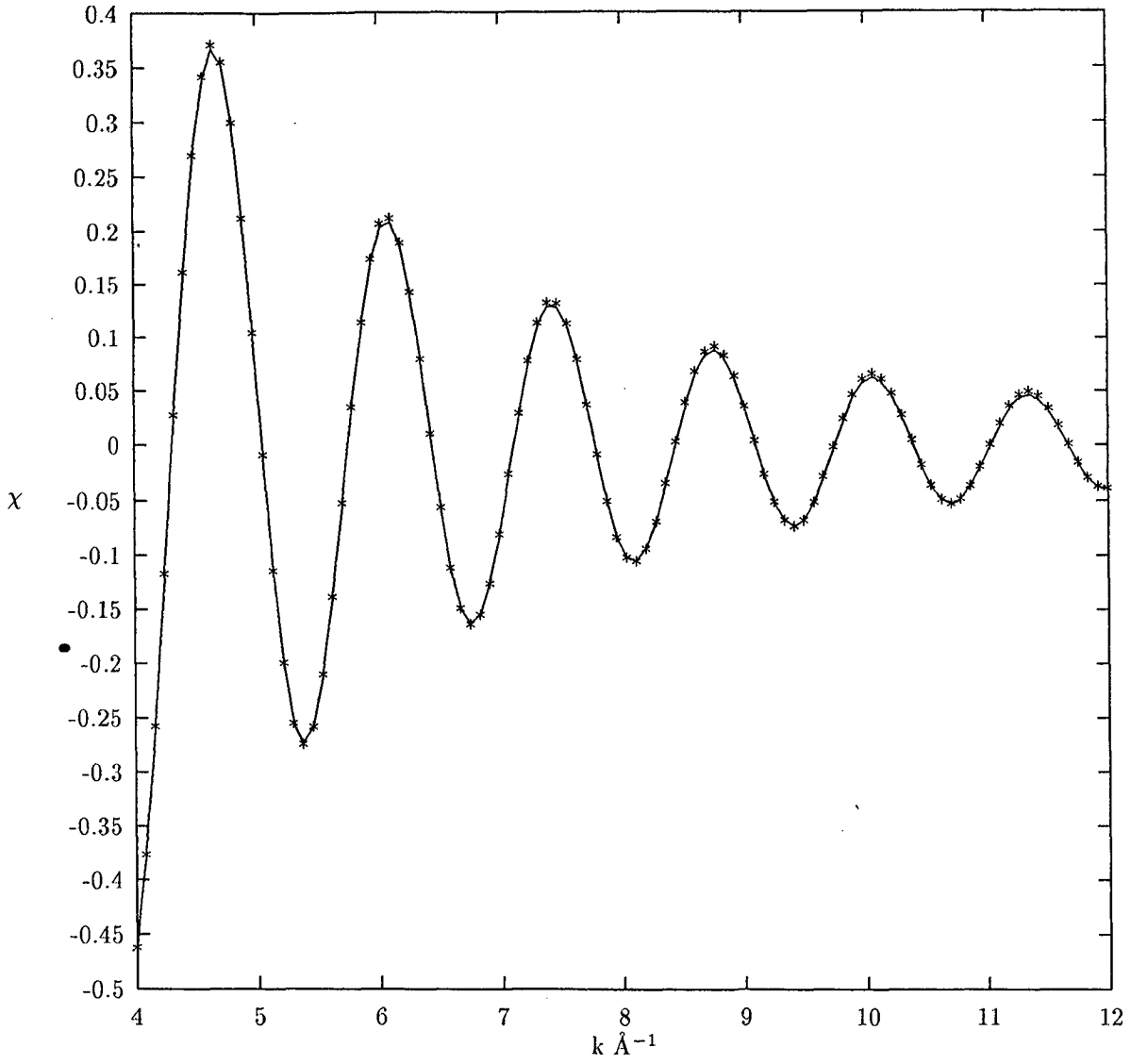

Figure 6.11: Inverse Fourier transform (* * *) and simulated EXAFS of the first FT peak (solid line) for $Tl_2Ta_2O_6$

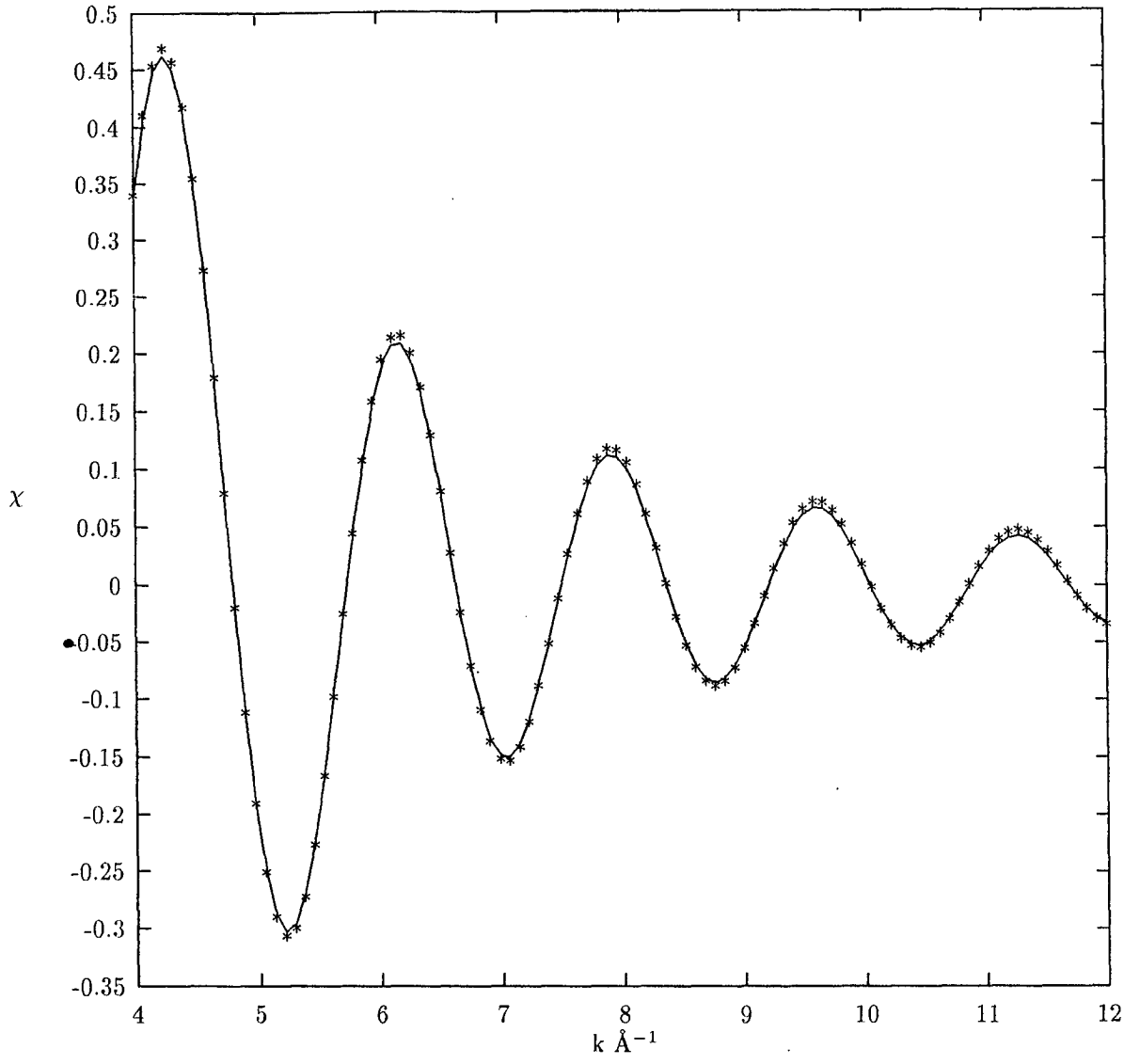

Figure 6.12: Inverse Fourier transform (* * *) and simulated EXAFS of the first FT peak (solid line) for $Ba_2Tl_2O_5$

A^{O}, there are only four oxygen atoms. This number agrees reasonably well with that determined from X-ray diffraction measurements. The two distant oxygen atoms at 2.41 A^{O} reported from diffraction measurements appear to form a second coordination shell surrounding the thallium ion.

6.3.3 THALLIUM ENVIRONMENT IN SUPERCONDUCTING OXIDES

We shall first briefly discuss the structural studies carried out on the superconducting oxides studied in this work.

The recent discovery by Sheng and Hermann[10,47] of superconductivity in the Tl-Ca-Ba-Cu-O system has sparked numerous investigations of the phases present in this system[48-53]. It is now known[51] that superconducting phases in this system can be represented as $Tl_mBa_2Ca_{n-1}Cu_nO_{m+2(n+1)}$, where m = 1,2 and n is the number of consecutive Cu-O layers. Values of n range from 1 to 3 in bulk phases but can range up to at least 5 on a microscopic level[54]. The superconducting transition temperature, T_c is about 125K for the n = 3 and m = 2 phase and appears to be about 140K for the n = 5 phase.

From X-ray single crystal data, the structures of the phases, with n = 1, 2 and 3 have been solved and refined[49,54-55]. The unit cells are tetragonal, space group I4/mmm, with a ≈ 3.85 A^{O} and c ≈ 23.2, 29.3 and 35.9 A^{O} respectively. No evidence was found for any superlattice peaks indicative of an enlarged cell (a = 5.44 A^{O}) in either the single crystal data or in X-ray powder diffraction measurements on bulk samples.

The structures are comprised of single[55], double[49] or triple[54] CuO_2 sheets, with Cu in the square planar coordination, that alternatively stack with sheets of barium ions and double sheets of Tl-O atoms. When Ca is present, it is found between the Cu-O sheets. There is considerable disorder of the oxygen atoms in the Tl-O sheets in the form of displacements of about 0.4 A^{O} from the ideal positions. (The compound with m=2 and n=3 viz.

$Tl_2Ba_2Ca_2Cu_3O_{10}$ (2223) possesses the highest known Tc of 125K). In short, these phases possess a layered structure with distorted rock salt-type layers of TlO and oxygen-deficient perovskite-type layer ($ACuO_{3-y}$) with A= Ba, Ca.

$TlBa_2CaCu_2O_7$ (also called "1212-phase") is a member of the structural series $(TlO)_mBa_2Ca_{n-1}Cu_nO_{2+2n}$, where m = 1 and n= 2, i.e.,it contains TlO single-layers and two consecutive CuO_2 layers that are separated by a Ca layer. The layer sequence Ca-CuO_2-BaO-CuO_2-Ca etc leads to a translation period perpendicular to the layers of 12.75 A^o and to a prominent low-angle reflection at 2θ = 6.94 A^o (Cu K_α) in the X-ray diffraction pattern[56]. The structure contains one thallium site with flattened octahedral oxygen coordination, one calcium site with deformed cubic, one barium site with nine-fold (capped square-antiprismatic), and one copper site with square-pyramidal oxygen coordinations and three oxygen sites. The two short Tl-O and four long Tl-O distances in this phase are 2.01 and 2.73 A^o respectively and considerable disorder in the Tl and Ba sites has been reported. Ganguli et al [57] found no such disorder in $Tl_{0.5}Pb_{0.5}CaSr_2Cu_2O_7$, and the Tl/Pb-O distances to be much shorter, being 1.98 and 2.71 A^o. Moreover, these authors commented that the introduction of Pb in the Tl layers makes the bonds considerably more covalent and that the shorter Cu-O distances obtained from neutron diffraction measurements seem to be related to the higher Tc of this cuprate superconductor.

Refined structural data on $Tl_2Ba_2CaCu_2O_8$ are reported from single-crystal X-ray diffraction by Subramanian et al[49] and Onodo et al[58] and from neutron powder diffraction by Cox et al[51]. The structure has body centerd tetragonal symmetry and shows relatively large variations in the c parameter. It contains one thallium site with deformed octahedral oxygen coordination, one barium site with nine-fold, one calcium site with nearly cubic, and one copper site with square-pyramidal oxygen coordination,

and three oxygen sites of which that constituting the Tl_2O_2 layers is shifted away from its average site 4e by about 0.5 A^O.The thallium ions are coordinated to one oxygen atom at 1.983 A^O, one at 2.022 A^O, two at 2.470 A^O and two at 3.027 A^O.

The superconducting oxide, $Tl_2Ba_2Ca_2Cu_3O_{10}$ (also called "2223 - phase") contains Tl_2O_2 double layers and three consecutive CuO_2 layers that are separated by two calcium layers. The structure of this compound has tetragonal symmetry[54] and contains one thallium site with distorted octahedral oxygen coordination, one barium site with nine fold, one calcium site with nearly cubic and two copper sites with square planar (Cu1) and square-pyramidal (Cu2) oxygen coordinations respectively and four oxygen sites. The Tl site has defects or is partially occupied by 10% calcium[51]. The bond distances within TlO single-layers at 150 K are Tl-O = 2.47 and 3.01 A^O, those between the two TlO single-layers are 2.017 A^O and those between the Tl_2O_2 and CuO_2 layers are 1.944 A^O.

The Fourier transforms for $TlBa_2CaCu_2O_7$, $Tl_{0.5}Pb_{0.5}Sr_2CaCu_2O_7$, $Tl_2Ba_2CaCu_2O_8$ and $Tl_2Ba_2Ca_2Cu_3O_{10}$ are shown in Figure 6.8. The first and the strongest peak in the transform of the first two compounds is the signal from the first coordination shell of oxygen atoms around each thallium atom. The two transforms are almost similar to each other because of similarity of their crystal structure. To interpret these data we have used the Fourier filtered data from Tl_2O_3 standard to obtain the backscattering amplitude of oxygen and Tl-O atom pair phase shift as a function of wave vector k. A non-linear least-squares fitting technique was then employed to match the calculated $\chi(k)$ to the measured one obtained from inverse Fourier transform of the first peak in Fig 6.8. The results of this first-shell fitting for the two compounds are shown in Fig 6.13 (a and b)

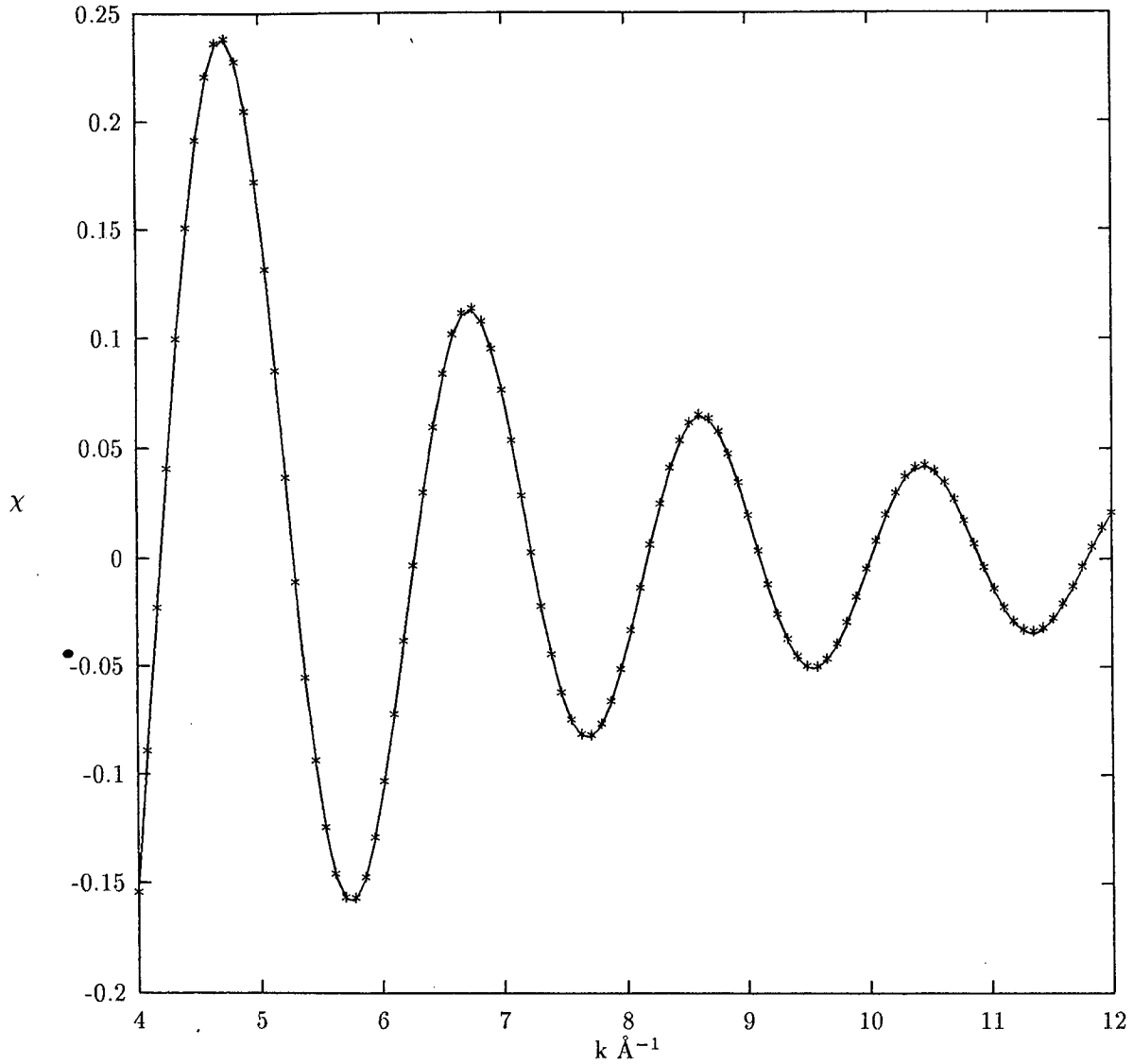

Figure 6.13: (a) Inverse Fourier transform (* * *) and simulated EXAFS of the first FT peak (solid line) for $TlBa_2CaCu_2O_7$

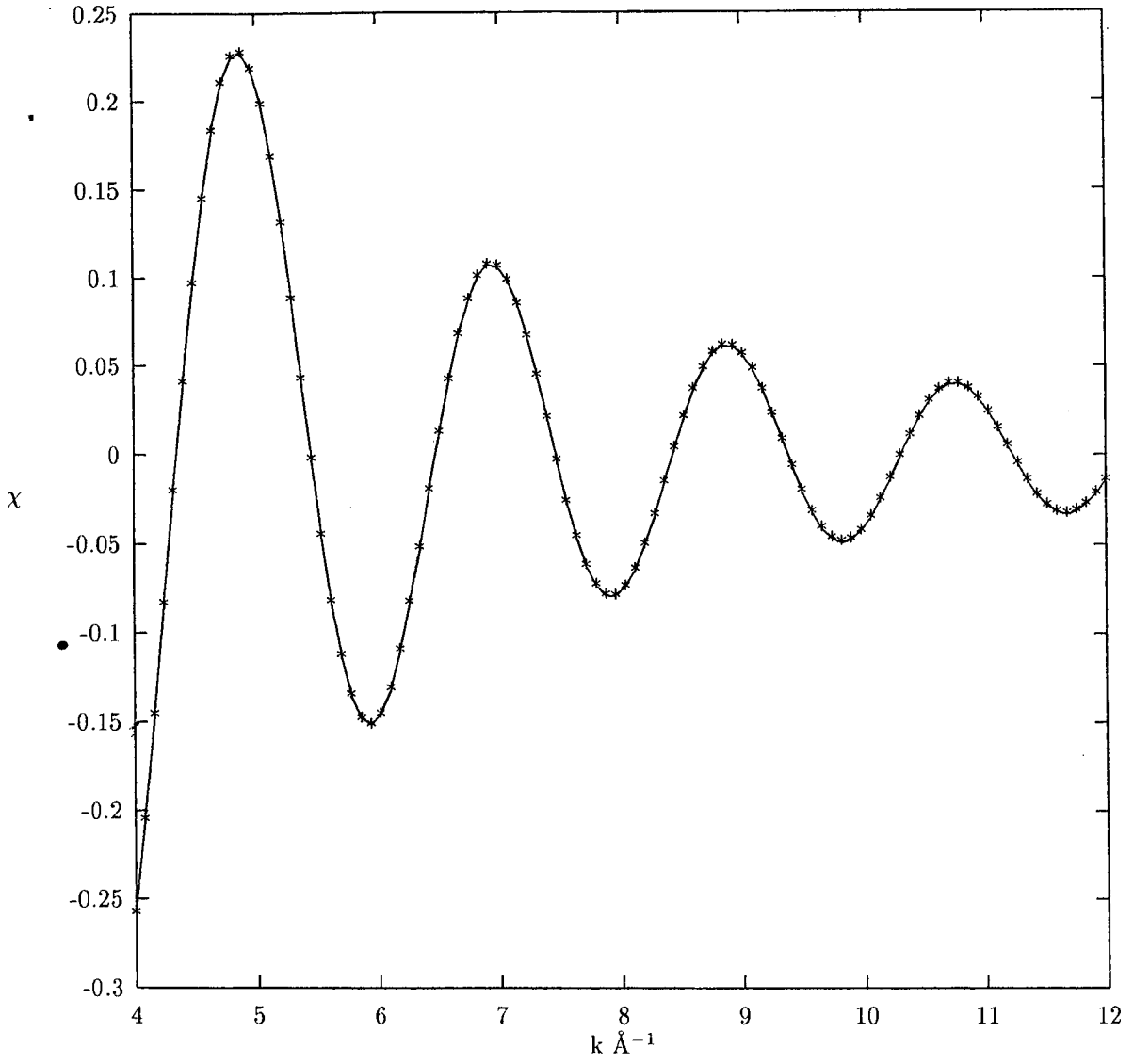

Figure 6.13: (b) Inverse Fourier transform (* * *) and simulated EXAFS of the first FT peak (solid line) for $Tl_{0.5}Pb_{0.5}Sr_2CaCu_2O_7$

and the structural parameters determined from the fitting are

	N_j	$R_j(A^o)$	$\sigma_j(A^o)$
$TlBa_2CaCu_2O_7$	2.15	2.04	0.003
$Tl_{0.5}Pb_{0.5}Sr_2CaCu_2O_7$	2.10	1.99	0.006

The validity of the fitting procedure is proven by the excellent agreement between the structural parameters obtained by the analysis of EXAFS spectra and the X-ray diffraction values for these compounds[56-57]. We have also isolated the second peak in both these compounds and by transforming the peak to k- space and by performing the non-linear least-squares analysis, we find the Tl-O bond distances of 2.72 and 2.71 A^o respectively for the above oxides. However, there is a large uncertainty in the determination of near-neighbours. These numbers are 4.7 and 4.5. This may be due to the overlapping of second oxygen shell (2.75 A^o) with other shells on higher R side as well as due to the higher Debye-Waller factor.

As can been seen from the Fourier transforms in Figure 6.8 there are four peaks in the case of $Tl_2Ba_2CaCu_2O_8$ and three peaks in $Tl_2Ba_2Ca_2Cu_3O_{10}$. The first-shell fitting results presented in Figure 6.14 (a and b) and the parameters obtained in the fitting are

	N_j	$R_j(A^o)$	$\sigma_j(A^o)$
$Tl_2Ba_2CaCu_2O_8$	1.97	2.02	0.001
$Tl_2Ba_2Ca_2Cu_3O_{10}$	1.05	2.10	0.004

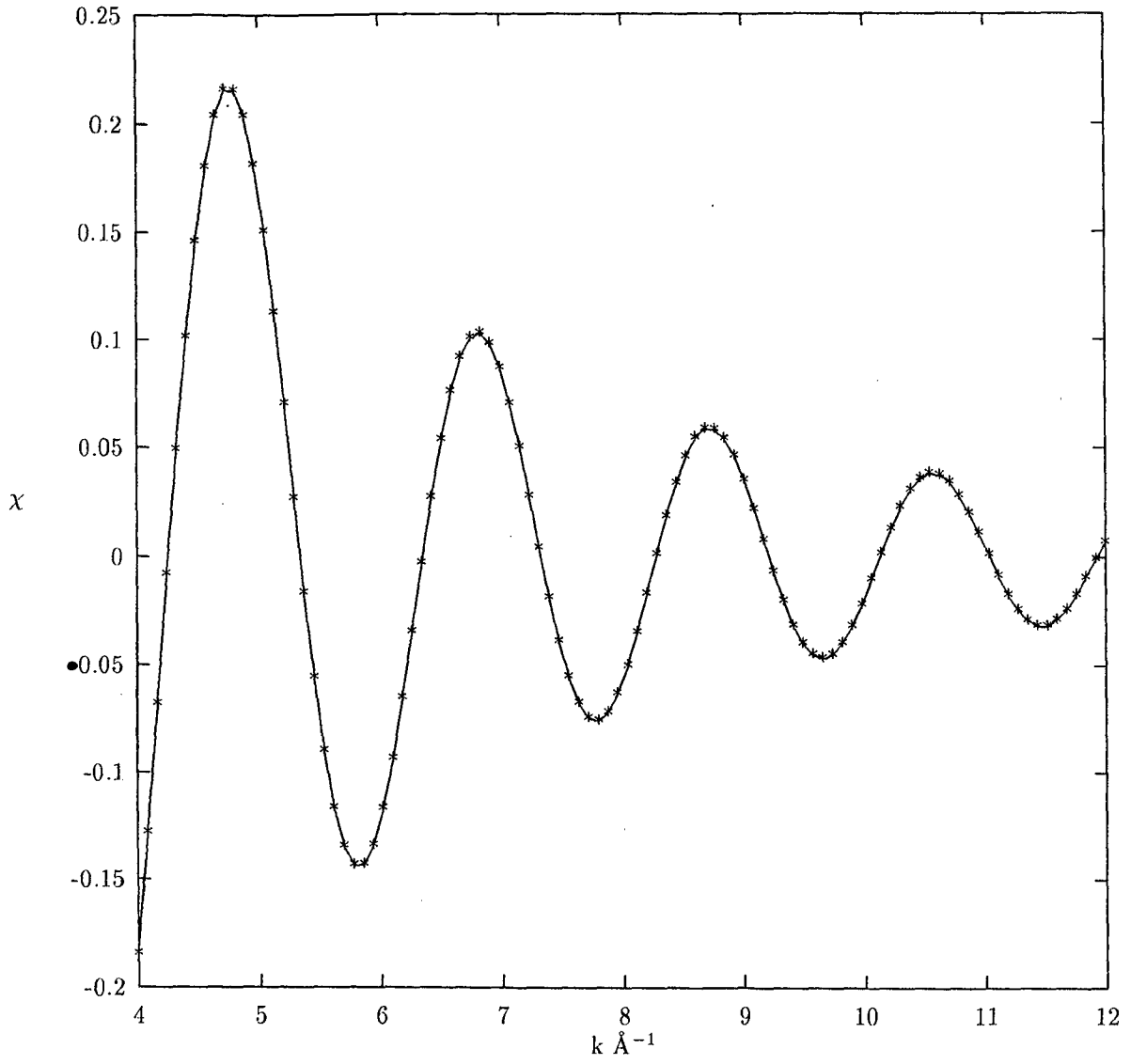

Figure 6.14: (a) Inverse Fourier transform (* * *) and simulated EXAFS of the first FT peak (solid line) for $Tl_2Ba_2CaCu_2O_8$

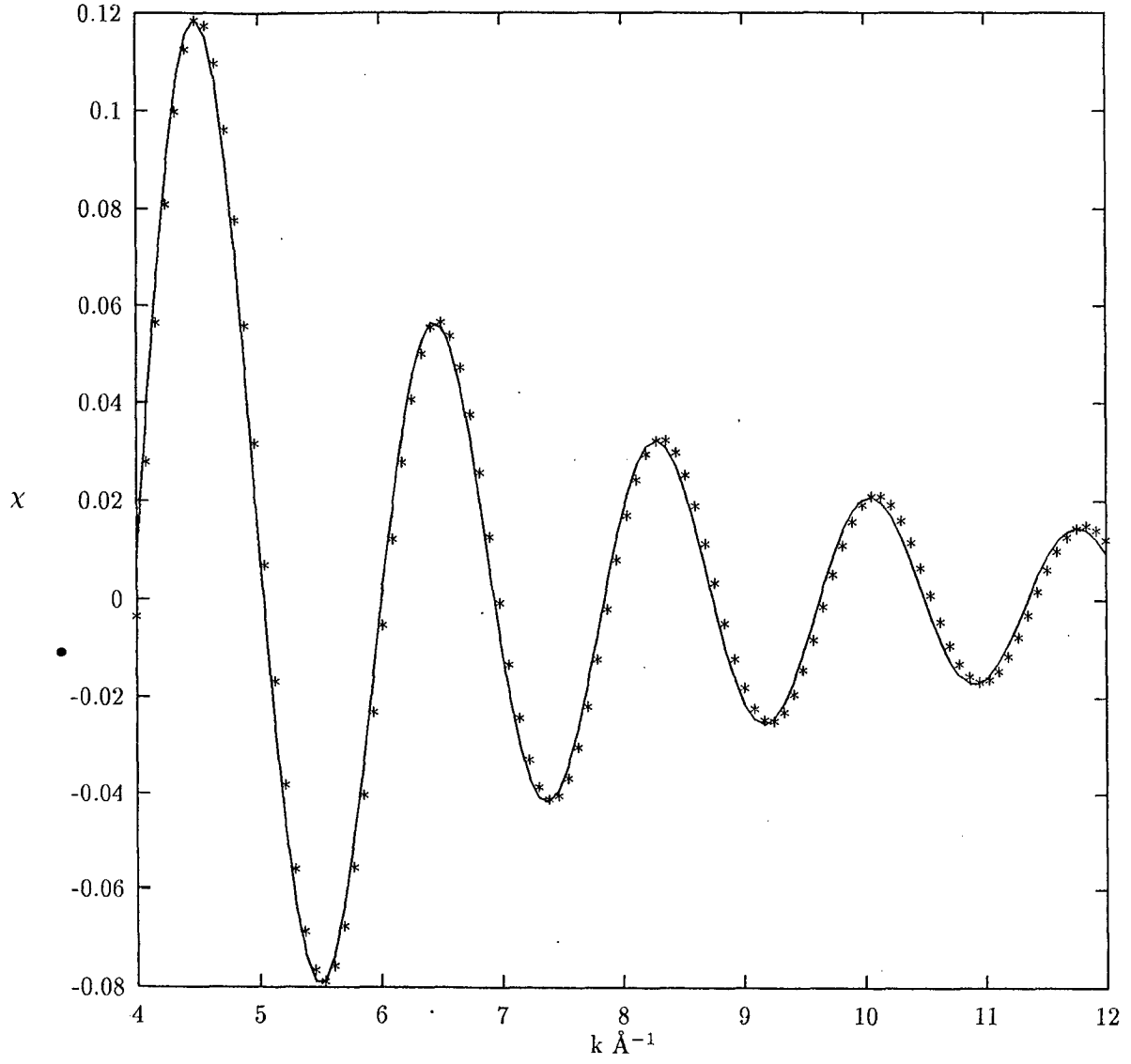

Figure 6.14: (b) Inverse Fourier transform (* * *) and simulated EXAFS of the first FT peak (solid line) for $Tl_2Ba_2Ca_2Cu_3O_{10}$

For $Tl_2Ba_2CaCu_2O_8$, the intensity of the first peak is large as compared to that in $Tl_2Ba_2Ca_2Cu_3O_{10}$. It can been seen from the values of bond distance and coordination number that there is a good agreement between our results for $Tl_2Ba_2CaCu_2O_8$ and those obtained from X-ray and neutron diffraction measurements[49,51-54]. However, for $Tl_2Ba_2Ca_2Cu_3O_{10}$,though the Tl-O distance agrees with that reported, the number of near-neighbours is found to be one. One could expect two oxygen atoms to be coordinated to thallium ion. In all the four superconducting oxides, our results show that one or two oxygen atoms appear to be closer to the central thallium ion than those found from X-ray diffraction measurements. This could perhaps be due to the lack of precision on the oxygen atomic positions deduced from X-ray or neutron powder diffraction measurements. It may be mentioned here that in the case of 2212 superconducting oxide study by neutron diffraction, Subramanian et al[49] observed two very short Tl-O distances along the c-axis of the structure, i.e., the direction of the intergrowth, again in agreement with our EXAFS distance.

From the Fourier transforms of these compounds, it is difficult to estimate the number of second-nearest neighbours of thallium because of interference between the second oxygen shell (Tl-O distances at 2.47 and 3.027 A^o) and the thallium shell (Tl-Tl distance at 3.70 A^o) and the barium and copper shells between 3.5 and 3.8 A^o. These second peaks (double-peak character) at larger distance in the above mentioned thallium bilayered compounds seem to be the characteristic of FT spectra of such compounds. It is to be noted that such double peak character in Fourier transformed spectra of monolayered compounds is absent.

The Fourier transform of $k^3\chi(k)$ of the Tl L_{III} edge EXAFS of the two superconducting oxides of composition, $Tl_{1-x}V_xSr_2(Ca_{0.8}Y_{0.2})Cu_2O_y$ where x = 0.2 and 0.5, are shown in Figure 6.8. One major peak is seen in the Fourier transforms of

both the samples followed by two peaks of less amplitude. The position of this major peak is almost the same irrespective of the vanadium doping level. It can be attributed to the oxygen atoms surrounding thallium ion. The other peaks observed on the high R side may be due to the distant neighbours of thallium.

To get quantitative information, a curve fitting analysis was performed on the inverse Fourier transform of this peak in both the compounds (Figure 6.15 (a and b)). The simulated spectra are shown in Figure 6.15 and the the Tl-O distances and coordination numbers obtained from this analysis are given below.

Sample	N_j	$R_j(A^o)$	$\sigma_j(A^o)$
x = 0.2	2.20	2.01	0.002
x = 0.5	2.10	2.03	0.0025

The predicted number of oxygen atoms in the first coordination shells around thallium ion in both the compounds agree well with that expected for $TlSr_2CaCu_2O_7$ or $TlBa_2CaCu_2O_7$ structure. The Tl-O distances 2.01 and 2.03 A^o, appear to agree with those in other superconducting oxides studied in this investigation. The distant peaks observed at 2.72 and 3.20 A^o also correspond to Tl-O interactions. Our results thus lead to the conclusion that the substitution of vanadium at Tl site does not change the local environment around thallium ion. Like $TlBa_2CaCu_2O_7$, there exists a distorted octahedron of oxygen atoms around thallium ion. It may be interesting to mention here that the single crystal data are not hitherto available on these superconducting phases. Our results will be useful to the researchers working in the field of X-ray crystallography of these phases to arrive at the accurate values of coordination numbers, bond distances and structural disorders.

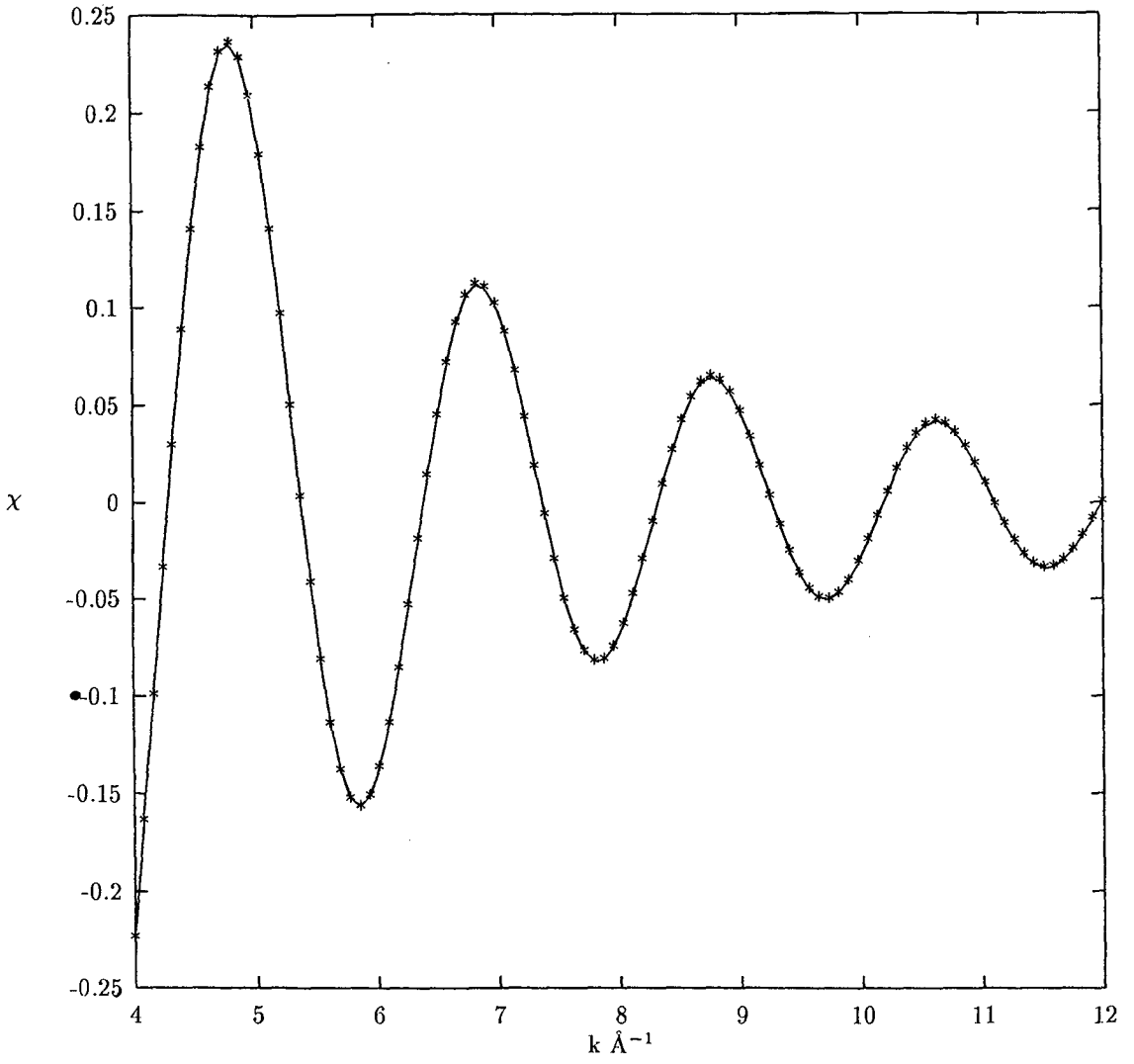

Figure 6.15: (a) Inverse Fourier transform (* * *) and simulated EXAFS of the first FT peak (solid line) for $Tl_{1-x}V_xSr_2(Ca_{0.8}Y_{0.2})Cu_2O_y$, x = 0.2

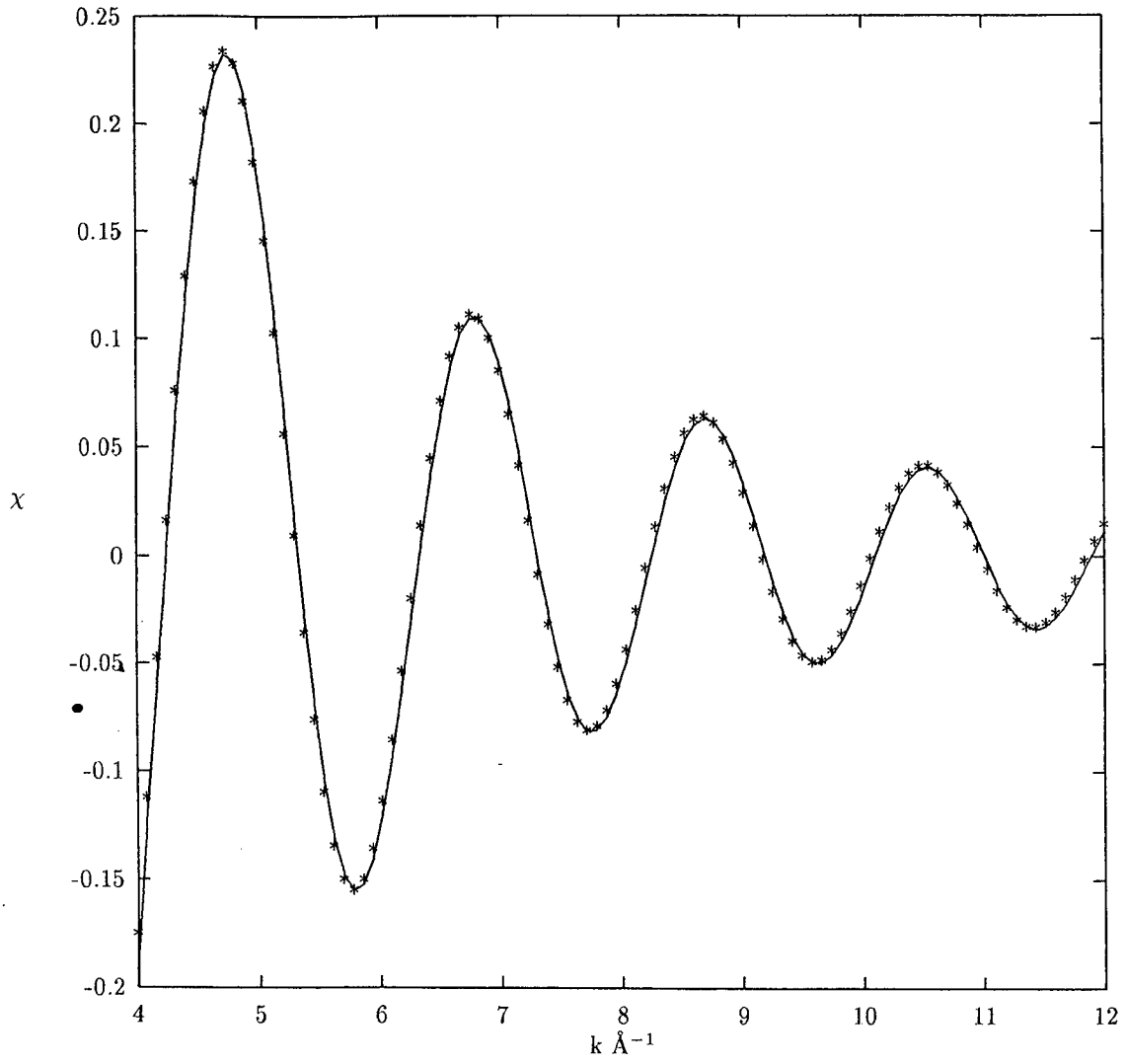

Figure 6.15: (b) Inverse Fourier transform (* * *) and simulated EXAFS of the first FT peak (solid line) for $Tl_{1-x}V_xSr_2(Ca_{0.8}Y_{0.2})Cu_2O_y$, x = 0.5

References

1. A. G. Lee, The Chemistry of Thallium, Elsevier, Amsterdam (1971).

2. K. Wade and A. J. Banister, in " Comprehensive Inorganic Chemistry", eds. J. C. Bailar et al, Vol.I, Chapter 12, Pergamon Press, New York p 993 (1993).

3. J. W. Mellor, A Comprehensive Treatise on Inorganic and Theoretical Chemistry, Vol.5, Longmans, London (1924).

4. D. F. Scriver and I. Wharf, Inorg. Chem. 8, 2167 (1969).

5. A. J. Carty, Coord. Chem. Rev. 4, 29 (1969).

6. T.C.Waddington, in "Advances in Inorganic Chemistry and Radiochemistry", H.J.Emelèus and A.G.Sharpe (Eds.), Academic Press, New York, Vol.I, pp 158-221 (1959).

7. A. F. Wells, Structural Inorganic Chemistry", Oxford University Press, London (1962).

8. D.J.Nagel and W.L.Boun, in "X-ray Spectroscopy", ed. L.V. Azároff, McGraw - Hill Book Co., New York (1974).

9. U. C. Srivastava and H. L. Nigam, Coord. Chem. Rev.,9, 275 (1972-73).

10. Z.Sheng and A.M.Hermann, Nature, 332, 55 (1988).

11. C.Politis and H.Luo, Modern Phys. Lett. B 2,793 (1988).

12. B.Domenges, M.Hervieu and B.Raveau, Solid State Commun., 68, 303(1988).

13. S.S.P. Parkin, V.Y. Lee, A.J. Nazzai, R. Savoy, R.Beyers and S.La Placa, Phys. Rev. Lett., 61, 1103(1988).

14. R.S.Liu and P.P.Edwards, J. Solid State Chem. 91, 407(1991).

15. J.A.Bearden, Rev. Mod. Phys., 39, 78 (1967).

16. B.K.Agarwal and L.P.Verma, J.Phys. C (Solid State Phys.) 2, 104(1969).

17. F. Studer, D. Bourgault, C. Martin, R. Retoux, C. Michel, B. Raveau, E.Dartyge and A.Fontaine, Physica C, 159, 609(1989).

18. F.Studer, R.Retoux, C.Martin, C.Michel, B.Raveau, E.Dartyge, A.Fontaine and G. Tourllon, Intl. J. Mod. Phys., B 3, 1085 (1989).

19. V. Vijayakrishnan, G.U. Kulkarni and C.N.R.Rao, Modern Phys. Lett. 4, 451(1990).

20. R. Retoux, F. Studer, C. Michel, B. Raveau, A. Fontaine and E.Dartyge, Phys. Rev.B 41, 193(1990).

21. S.M. Heald, D. DoDarzio, M. Croft, M.S. Hegde, S. Li, and Greenblatt, Phys.Rev. B 40, 8828(1989).

22. B.K.Teo and P.A.Lee, J.Am.Chem. Soc. 101, 2815 (1979).

23. K.J.Rao and J.Wong, J.Chem. Phys., 81, 4832 (1984).

24. T.Suzuki, M.Nagoshi, Y.Fukuda, Y.Syono, M.Kikuchi, N.Kobayashi and M.Tachki, Phys. Rev. B 40, 5184 (1989).

25. J.C.Carver, G.K.Schweitzer and T.A.Carlson J. Chem. Phys. 67, 973 (1972).

26. L.Ramquist, B.Ekstig, R.Kallne, E. Noreland and R.Manne, J. Phys. Chem. Solids 30, 1849 (1969).

27. T.A. Carlson, Photoelectron and Auger Spectroscopy Plenum Press, New York 1975.

28. G.E. McGuire, G.K. Schweitzer and T.A. Carlson, Inorg. Chem. 12, 2450(1973).

29. S. Li, M. Greenblatt, Y. Jeon, J. Chen, G.Liang and M.Croft, Physica C 173, 239(1991).

30. F.Herman and R.V.Kasowski, Physica C, in press.

31. D. Jung, M.H. Whangbo, N. Herron and C.C. Torardi, Physica C 160, 381 (1989).

32. S.V. Meshkov, S.N. Molotkov, S.S. Nazin, I.S. Smirnova and V.V.Tatarskii, Physica C 166, 476 (1990).

33. D.B.Kang, D.Jung and M.H.Whangbo, Inorg. Chem. 29, 25(1990).

34. C.R. Natoli, in " EXAFS and Near Edge Structure III", eds. K.O.Hodgson, B.Hedman and J.E.Penner-Hahn, Spinger Verlag, Berlin, p38 (1984).

35. Anjli Chikkara and P. R. Sarode, X-ray Spectrometry

(Communicated).

36. J.L.Dehmer, J.Chem.Phys., 56, 4496 (1972).

37. F.W. Kutzler, C.R. Natoli, D.K. Misemer, S. Doniach and K.O. Hodgson, J.Chem.Phys. 73 ,3274 (1980).

38. F.W. Kutzler, Ph.D. Thesis, Standford University, Standford (1981).

39. F.W.Lytle, D.E.Sayers and E.A.Stern, Phys. Rev. B 11, 4825 (1975).

40. E.A. Stern, D.E. Sayers and F.W.Lytle, Phys. Rev.B 11, 4836 (1975).

41. G.H. Via, J.H. Sinfelt and F.W. Lytle, J.Chem. Phys. 71, 690 (1979).

42. R.D.B. Fraser and E. Suzuki, Anal. Chem., 38, 1770 (1966).

43. P.A. Lee, B.K. Teo and A.L. Simons, J.Am. Chem. Soc.99, 3856 (1977).

44. P.A.Lee and G. Beni Phys. Rev. B 15, 2862 (1977).

45. C. Michel and B. Raveau, Mater. Res. Bull., 8, 451 (1973).

46. M.Arjomand and D.J.Machin J. Chem. Soc.: Delton Trans. 1061 (1975).

47. Z.Z.Sheng and A.M.Hermann, Nature,332, 138 (1988).

48. R.M. Hazen, L.W. Finger, R.J. Angel, C.T. Prewitt, N.L.Ross, C.G.Hadidiacos, P.J.Heaney, D.R.Veblen, Z.Z.Sheng, A.El Ali and A.M. Hermann, Phys.Rev.Lett., 60, 1657 (1988).

49. M. A. Subramanian, J. C. Calabrese, C. C. Torardi, J. Gopalakrishnan T. R. Askew, R. B. Flippen, K. J. Morrissey, U.Chowdhry, and A.W.Sleight, Nature, 332, 420 (1988).

50. R. Beyers, S.S.P. Parkin, V.Y. Lee, A.I. Nazzal, R. Savoy, G. Gorman, T.C. Huang and S.La Placa, Appl.Phys. Lett. 53, 432 (1988).

51. D.E.Cox, C.C.Toradi, M.A. Subramanian, J.Gopalkrishnan and A.W.Sleight, Phys. Rev. B 38, 6624 (1988).

52. C.C.Torardi, J.B.Parise, M.A.Subramanian, J. Gopalkrishnan and A.W.Sleight, Physica C 157, 115 (1989).

53. C. Martin, J. Provost, D. Bougault, B. Domenges, C. Michel, M.Hervieu and B.Raveau, Physica C, 157, 460 (1989).

54. C. C. Toradi, M. A. Subramanian, J. C. Calabrese, J. Gopalakrishnan, K. J. Morrissey, T. R. Askew, R. B. Flippen, U.Chowdhry and A.W.Sleight, Science, 240, 631 (1988).

55. C.C.Toradi,M.A.Subramanian, J.C.Calabrese, J.Gopalakrishnan, E.M. McCarron, K.J. Morrissey, T.R. Askew, R.B. Flippen, U. Chowdhry and A.W.Sleight, Phys. Rev. B 38, 225 (1988).

56. B. Morosin, D.S. Ginley, P.F.Hlava, M.J.Carr, R.J. Baughman, J.E.Schirber, E.L.Venturni and J.F.Kwak, Physica C, 152, 413 (1988).

57. A.K. Ganguli, K.S.Nanjundaswamy, C.N.R.Rao, A.Sequeira and H.Rajagopal, Z. Physik B 74, 215 (1989).

58. M.Onoda, S.Kandoh, K.Fukuda and M.Sato, Jpn. J. Phys. Lett. 27, L1234 (1988).

CHAPTER 7

Resumé

7.1 SUMMARY

The field of superconductivity fascinates us with its scientific challenges and technological promises. Many metals, alloys, binary and ternary compounds, organic solids, heavy fermions, oxides and now fullerites are found to exhibit this phenomenon. The recent breakthroughs in the field of superconductivity are the discovery of cuprates with critical transition temperature, T_c as high as 125 K and in fullerites with Tc as high as 42 K. All these superconductors invariably display three main characteristic features : *i)* the zero resistivity ; *ii)* the perfect diamagnetic behaviour i.e. magnetic flux expulsion (Meissner effect) and *iii)* the Josephson effect.

The discovery of new oxide superconductors has generated tremendous excitement among the theorists to invoke different electron pairing mechanisms. The conventional electron photon interaction appears not to be the origin of the superconductivity in these materials, leaving this fundamental Physics question open to exploration. Apart from this, it is becoming apparent that many of the properties of these new materials are unusual, and a proper understanding may now require developing and extending some concepts from many areas of Physics.

One finds that progress on genuine theoretical problems pertaining to these superconductors will require not archaic mathematics but a detailed, substantive understanding of the experimental results. In the present thesis an attempt has been made to understand the phenomenon of superconductivity by observing the changes occurring in the various spectral features of the X-ray K-absorption discontinuities of vanadium and copper and L-edges of thallium in their model compounds and cuprate superconductors on account of substitution of metallic impurities to obtain information on local environment of the excited atom species in the complex oxide superconducting systems.

The thesis is divided into seven chapters. Chapter 1 of the

thesis gives a short historical survey of the investigations regarding the electronic structure of the superconducting materials and reviews briefly the mechanism of X-ray absorption process and then describes various spectral features often observed on either side of an X-ray absorption discontinuity. It also defines the scope of the present study.

Chapter 2 gives a brief description and working principle of various experimental setups used. The experimental methods include powder X-ray diffraction, dc resistivity measurements, X-ray absorption studies and X- ray photoelectron spectroscopic measurements. The methods of preparation of materials investigated in this work are also given in this chapter.

Chapter 3 deals with the theoretical aspects of chemical bonding in compounds. In this Chapter certain theories of bonding namely the valence bond theory, molecular orbital theory and ligand field theory are discussed. We have also discussed in this Chapter the concepts of electronegativity, ionicity and effective charge in the light of approaches put forth by Pauling and some other recent workers.

Chapter 4 gives the results of our observations on the shape of K-absorption edge profile of vanadium in pure vanadium metal, in some of its model compounds and vanadium doped cuprate superconductors. It is observed that the vanadium K-absorption discontinuity in pure vanadium splits into three components, and in the compounds and complexes apart from these components, we observe an additional peak, called pre-edge, on the low energy side of the discontinuity. Electronic transitions, 1s → 3d (pre-edge), 1s → 4p (shake-down) and 1s → 4p (strong absorption) are assigned to these three peaks on the basis of simple atomic model supported by theoretical considerations. It is found that the pre-edge peak is very intense in the case of compounds and complexes having vanadium ions at tetrahedral and square pyramidal sites and very weak in compounds where octahedral symmetry prevails.

This simple observation leads us to predict the coordination geometry of ligands around vanadium ion in superconducting compounds. Thus, in $(Tl_{1-x}V_x)Sr_2(Ca_{0.8}Y_{0.2})Cu_2O_{7-\delta}$ $(0 \leq x^{\bullet} \leq 0.5)$ pyramidal VO_5 groups are found to be present.

A brief discussion of Natoli's multiple scattering approach for the interpretation of near-edge spectra is also presented in this chapter. A correlation of energy separations between pre-edge feature and the strong absorption maximum (which according to the multiple scattering formalism, correspond to the bound state and continuum resonance states respectively) with the near-neighbour distance is observed for vanadium compounds and is used to obtain interatomic distances in superconducting compounds. Comparison between the values of bond distances deduced from XANES spectra and those obtained from other diffraction techniques is fairly good, suggesting thereby the usefulness of XANES technique as a probe for the determination of bond distances in complex superconducting oxides. Furthermore, analysis of measurements of peak positions in model vanadium compounds shows that the energy separation (ΔE_{3d-4p}) in the vanadium K-edge spectra reveals another interesting correlation with the bond strength in valence unit, called bond valance. It is found that this energy separation increases with increase in bond valence. This relationship renders the possibility of determination of bond valence in superconducting oxide. For example, in $Tl_{0.8}V_{0.2}Sr_2(Ca_{0.8}Y_{0.2})Cu_2O_y$, the value of bond valence estimated from the relationship is very close to that in pentavalent vanadium oxides thereby clearly indicating that vanadium ions are in pentavalent state.

In Chapter 5 the measurements on the X-ray absorption near-edge structure (XANES) of several ternary oxides of copper having structural features common to the superconducting copper oxides are presented. The special emphasis in this investigation

is on the feature at ~ 20 eV which is present in all superconducting family of copper oxides. It is found that such a feature is present in all systems containing corner-shared square-planar CuO_4 units with 180^o Cu-O-Cu interactions. A brief review of the different interpretations of XANES by various researchers is given in this chapter including those which relate XANES features with features observed in X-ray photoelectron spectra (XPS). The XPS of the Cu $2p_{3/2}$ region of these systems are also reported in this chapter. The present data are not entirely consistent with any of the interpretations given so far in the literature. However, the data suggest the coexistence of both one electron and multielectron excitation processes responsible for appearance of XANES features.

Chapter 6 gives the results of our observations on the shapes of L_I, L_{II} and L_{III} absorption discontinuities in thallium model compounds, namely, TlCl, TlBr, TlI, Tl_2CO_3, $TlNO_3$, Tl_2SO_4, $Tl(CH_3COO)$, $Tl(C_6H_5COCHCOCH_3)$, $Tl(C_5H_7O_2)$, $Tl_2Ta_2O_6$, Tl_2O_3, $Tl(NO_3)_3.3H_2O$, $Tl(CH_3COO)_3$, $Tl(CF_3COO)_3$ and $Ba_2Tl_2O_5$ and superconducting oxides of composition $Tl_{1-x}V_xSr_2(Ca_{0.8}Y_{0.2})Cu_2O_y$, where x = 0.2, 0.3, 0.4 and 0.5. Measurements on the features of the L_I, L_{II}, and L_{III} edge spectra in $Tl_{0.5}Pb_{0.5}Sr_2CaCu_2O_7$, $TlBa_2CaCu_2O_7$, $Tl_2Ba_2CaCu_2O_8$, and $Tl_2Ba_2Ca_2Cu_3O_{10}$ are also reported in this chapter. The normalized X-ray absorption spectra suggest that the XANES at L_I and L_{III} edges of monovalent and L_I edge of trivalent compounds have far fewer features compared to L_{III} edge of trivalent thallium compounds. Thallium L_{III} edge spectra for monovalent compounds show single absorption peak whereas spectra for trivalent Tl compounds show a weak peak followed by a shoulder on rising absorption curve which culminates into a strong absorption peak. These spectral peaks have been assigned electronic transitions on the basis of assignment schemes reported in literature.

It is observed that the L_I edge profiles for monovalent and

trivalent Tl compounds are simple and splitting of the discontinuity is not at all observed. It is found that there is spectral similarity between the thallium L_I - edge profiles in superconducting oxides and those of trivalent thallium compounds indicating thereby that the trivalent thallium ions exist in the thallium doped superconductors. The data on L_{III}- edge profiles also support this conclusion.

In this Chapter our results on the thallium L_{III} edge EXAFS of model Tl compounds and two Tl doped superconductors having composition of 0.2 and 0.5 are also presented. These spectra are analyzed by a method which combines Fourier transform and curve fitting techniques. Parameterized phase shifts and amplitude function for describing Tl-O interaction were obtained from EXAFS spectra of Tl_2O_3. Application of these phase shifts and amplitude to the EXAFS spectra of two superconducting samples (x = 0.2 and x = 0.5) gives Tl-O bond distances of 2.01 and 2.03 A^o respectively with an accuracy consistently better than 0.03 A^o and predicated number of oxygen atom coordinated to the Tl ion is found to be 2 in each case with a reasonable degree of certainty.

7.2 SUGGESTIONS FOR FUTURE WORK

Our present work, which has been confined to the study of K-edges of copper and vanadium and L-edge of thallium, has shown that how the X-ray absorption spectroscopy can provide direct and fruitful information about local atomic structure of materials. This information is, however, of a limited value to a certain extent because of low intensity X-ray source and the low resolving power of the instrument used to record the spectra. The investigations of the absorption edges on a bent crystal X-ray spectrometer of high resolving power can no doubt increase the precision of observed results. However, such spectrometer usually of bigger dimensions, enhance the difficulties in recording the

spectra in air with low intensity X-ray source. In our laboratory, we are trying to design and develop two-crystal X-ray spectrometer with solid state detector and with suitable electronics to measure the transmitted intensity through the sample in order to record X-ray absorption spectra with finer details. This may probably enable us to obtain more precise and accurate information on the electronic structure of materials. It would be interesting to extend this work to more complex superconducting oxides recently reported in literature.

In our work we have studied the correlation between the energy separation between pre-edge feature and the strong absorption maximum with the near-neighbour distance and determined the bond distances in vanadium doped superconducting oxides but we do not know whether this relation is applicable to other 3d ion doped cuprate oxides. A systematic extenssion of our work to such complex materials may throw light on the validity of multiple scattering approach for the determination of bond lengths.

It will also be interesting to study the L X-ray absorption spectra of copper and vanadium in their complex oxides. These spectra come in soft X-ray regions which require vacuum and different analysing crystals. Such facilities will be available in Inter University Consortium at Indore in near future. Coupled with soft X-ray emission and absorption spectra recorded on vacuum grating spectrometer or two crystal spectrometer using synchrotron radiation source or a high power rotating anode X-ray generator in a fluorescence mode such investigation may prove to be extremely useful in obtaining more comprehensive information regarding the electronic structures of complex oxides concerned.

In the present work, we have not attempted to calculate the K-edge profile of the Cu and V and L_{III} - edge profile of thallium in complex cuprates. It would be interesting to compare the experimentally recorded profiles (background subtracted and

normalized) with those obtained theoretically using various theories recently reported in literature.

Finally it may be mentioned that it would be worthwhile to undertake the detailed investigations on the complex oxides studied in this work using various sophisticated experimental techniques such as Positron Annihilation, Ultra-Violet and X-ray Photoelectron Spectroscopy (UV and XPS), Appearance Potential Spectroscopy (APS), Bremstrahlung Isochromat Spectroscopy (BIS), IR and Raman Spectroscopy. A correlation between the findings of the different experiments with our results would indeed be very valuable for understanding the properties of the doped cuprate superconductors.

ACKNOWLEDGEMENTS

It is my previlege to express my deep sense of gratitude to Professor P.R.Sarode, Head, Department of Physics, Goa University, Goa, who has provided me all possible facilities, assistance and freedom to work in my own way. His guidance and encouragement has helped me immensely to move with this exciting field of superconductivity.

I would like to thank Professor R.B.Prabhu, the former Head of the Department of Physics, Goa University, Goa, for constant encouragement

I am thankful to the authorities of Indian Institute of Science, Bangalore, Inter University Consortium for DAE facilities, Indore, and National Institute of Oceanography, Dona-Paula, Goa for allowing us to use their sophisticated experimental facilities. I am grateful to Dr. A.V.Narlikar, Head, Superconductivity Group, National Physical Laboratory, New Delhi, for extending experimental facilities for my work.

I acknowledge the timely help of the teaching and non-teaching staff of the Physics Department throughout the course of this work. I would like to thank my colleague Mr. Kaustubh Priolkar for helping me to complete my work in time. I acknowledge with pleasure, the co-operation of my research colleagues Dr. Bhagatsingh Sonaye, Mr.Shantanu Gauns, Dr. (Ms) Anjli Chhikara, and Ms. Alka Shikerkar.

I am grateful to the Management and the Principal of Damodar Higher Secondary School, Gudi-Paroda, Goa, for the encouragement and cooperation received from them during the course of this work.

The financial assistance in the form of Research Scholarship by Goa University for the first two years is gratefully acknowledged.

Finally, I would like to acknowledge and express my deepest thanks for the immense support, encouragement and enrichment which I have experienced throughout the years from my parents, my brother and sister and my friends.

Gajanan Parulekar

LIST OF PUBLICATIONS

1. EXAFS Studies of Bi- doped Cuprate Superconductors
   G.B.Parulekar and P.R.Sarode
   Proc. National Seminar on X-ray Spectroscopy and Allied Areas, organised by Devi Ahilya Viswavidyalaya, Indore, January 9-20, 1992.

2. X-ray Absorption Near Edge Studies of $La_{2-x}Sr_xCuO_4$ and $La_{2-x}Ba_xCuO_4$
   G.B.Parulekar, and P.R.Sarode
   Proc. National Seminar on Recent Trends in Photon-Atom Interactions, held at Karnatak University, Dharwad, November 2-3, 1992.

3. K-edge X-ray Absorption Near Edge Spectrum of $Bi_{2-x}Pb_xCa_2Sr_2Cu_3O_y$
   P.R.Sarode and G.B.Parulekar
   Proc. Solid State Physics Symposium, held at S.V.University, Tirupati, Vol. 35-C, 260 (1992).

4. Structural Investigations on Vanadium Compounds by XANES
   Anjli Chhikara, G.B.Parulekar, B.H.Sonaye, S.A.Gauns and P.R.Sarode
   Proc. DAE Solid State Physics Symposium, held at University of Rajasthan, Jaipur, Vol 37-C, 113 (1994).

5. X-ray Spectroscopic Studies of $La_{2-x}Sr_xCuO_4$ and $La_{2-x}Ba_xCuO_4$
   G.B.Parulekar and P.R.Sarode
   Proc. National Seminar on X-ray Spectroscopy, organised by Department of Physics, Nagpur University, Nagpur during October 16-18, 1995 (II 19).

6. X-ray Spectroscopic Study of Vanadium Compounds
   P.R.Sarode, Anjli Chhikara, G.B.Parulekar, K.R.Priolkar, B.H.Sonaye, S.A.Gauns and R.B.Prabhu
   X-ray Spectrometry (Communicated)

7. L - Absorption Edge Studies of Tl-based Superconducting Oxides.
   P.R.Sarode and G.B.Parulekar
   Chem. Phys.(Communicated).